AD-A146 658 HANDBOOK OF PHASE TRANSITION SULFIDES SELENIDES AND 1/3
TELLURIDES(U) TACTICAL WEAPONS GUIDANCE AND CONTROL
INFORMATION ANALYSIS CE.. W J WILD ET AL. JUL 84
UNCLASSIFIED GACIAC-HB-84-02 DLA900-80-C-2853 F/G 7/4 NL

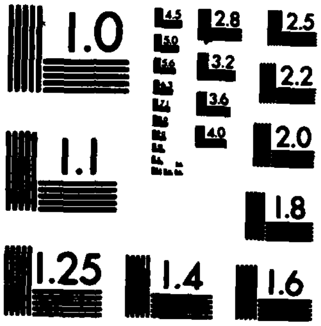

OPY RESOLUTION TEST CHART

AD-A146 658

(2)

TACTICAL WEAPON
GACIAC
GUIDANCE & CONTROL
INFORMATION ANALYSIS CENTER

HANDBOOK OF

PHASE TRANSITION SULFIDES, SELENIDES AND TELLURIDES

WALTER J. WILD
KENT J. KOGLER
MOHAMMAD NISAR
NARAYAN P. MURARKA

GACIAC HB-84-02
JULY 1984

Published by GACIAC
IIT Research Institute
10 West 35th Street
Chicago, Illinois 60616

DoD Technical Sponsor:
U.S. Army Missile Command
Redstone Arsenal, AL 35898

Approved for public release:
Distribution unlimited

84 10 10 015

NOTICES

Handbook. This Handbook has been published by the Tactical Weapon Guidance and Control Information Analysis Center (GACIAC) as part of its services to the guidance and control community. GACIAC is a DoD Information Analysis Center, administered by the Defense Technical Information Center, operated by IIT Research Institute under Contract No. DLA900-80-C-2853. GACIAC is funded by DTIC, DARPA, and U. S. Army, U. S. Navy, U. S. Air Force Laboratories/Controlling Activities having an interest in tactical weapon guidance and control. The Contracting Officer is Mrs. S. Williams, DESC, Dayton, Ohio. The Contracting Officers Technical Representative is Mr. H. C. Race, DRSMI-RN, U. S. Army Missile Command, Redstone Arsenal, Alabama 35898.

Reproduction. Permission to reproduce any material contained in this document must be requested and approved in writing by the U. S. Army Missile Command, ATTN: DRSMI-RN, Redstone Arsenal, Alabama 35898. This document is only available from GACIAC, IIT Research Institute, 10 West 35th Street, Chicago, Illinois 60616.

REPORT DOCUMENTATION PAGE

1a REPORT SECURITY CLASSIFICATION
UNCLASSIFIED

1b RESTRICTIVE MARKINGS

2a SECURITY CLASSIFICATION AUTHORITY

2b DECLASSIFICATION / DOWNGRADING SCHEDULE

3 DISTRIBUTION / AVAILABILITY OF REPORT
Approved for public release:
Distribution unlimited

4 PERFORMING ORGANIZATION REPORT NUMBER(S)
GACIAC HB-84-02

5. MONITORING ORGANIZATION REPORT NUMBER(S)

6a NAME OF PERFORMING ORGANIZATION
IIT Research Institute

6b OFFICE SYMBOL *(If applicable)*

7a. NAME OF MONITORING ORGANIZATION
U.S. Army Missile Command

6c ADDRESS *(City, State, and ZIP Code)*
10 West 35th Street
Chciago, IL 60616

7b ADDRESS *(City, State, and ZIP Code)*
ATTN: DRSMI-RN
Redstone Arsenal, AL 35898

8a NAME OF FUNDING / SPONSORING ORGANIZATION
DLA/DTIC

8b OFFICE SYMBOL *(If applicable)*
DTIC-AI

9 PROCUREMENT INSTRUMENT IDENTIFICATION NUMBER
DLA900-80-C-2853

8c ADDRESS *(City, State, and ZIP Code)*
DTIC
Cameron Station
Alexandria, VA 22314

10 SOURCE OF FUNDING NUMBERS

PROGRAM ELEMENT NO.	PROJECT NO.	TASK NO.	WORK UNIT ACCESSION NO.
65802 S	1.0		

11 TITLE *(Include Security Classification)*
Handbook of Phase Transition Sulfides, Selenides and Tellurides

12 PERSONAL AUTHOR(S) Walter Wild Mohammad Nisar Kent J. Kogler Narayan P. Murarka

13a TYPE OF REPORT
Handbook

13b TIME COVERED
FROM ________ TO ________

14 DATE OF REPORT *(Year, Month, Day)*
July 1984

15 PAGE COUNT
260

16 SUPPLEMENTARY NOTATION
This handbook is only available from GACIAC. Reproduction is not authorized except by specific permission. Cost $35.00. 410948

17 COSATI CODES

FIELD	GROUP	SUB-GROUP
II	2 & 3	
20	6	

18 SUBJECT TERMS *(Continue on reverse if necessary and identify by block number)*

Handbook	Electrical Properties	Sulfides
Coatings	Optical Properties	Selenides
Thin Films	Phase Transition Materials	Tellurides

19 ABSTRACT *(Continue on reverse if necessary and identify by block number)*

This handbook summarizes the literature review of Sulfide, Selenide and Telluride materials. In particular, the structural, chemical, electrical and optical properties of approximately 40 different materials are presented. Information is based on available unclassified published literature. References are given for all of the information presented for each of the materials described.

20 DISTRIBUTION / AVAILABILITY OF ABSTRACT
☒ UNCLASSIFIED/UNLIMITED ☐ SAME AS RPT ☐ DTIC USERS

21. ABSTRACT SECURITY CLASSIFICATION
UNCLASSIFIED

22a NAME OF RESPONSIBLE INDIVIDUAL
Howard C. Race

22b TELEPHONE *(Include Area Code)*
(205)876-5449

22c. OFFICE SYMBOL
DRSMI-RN

DD FORM 1473, 84 MAR

83 APR edition may be used until exhausted
All other editions are obsolete.

GACIAC HB-84-02 **JULY 1984**

HANDBOOK OF
PHASE TRANSITION SULFIDES, SELENIDES AND TELLURIDES

WALTER J. WILD
KENT J. KOGLER
MOHAMMAD NISAR
NARAYAN P. MURARKA

Published by GACIAC
IIT Research Institute
10 West 35th Street
Chicago, Illinois 60616

Copies available only from GACIAC. Reproduction not authorized except by specific permission.

Approved for public release. Distribution unlimited.

GACIAC- -A DoD Information Analysis Center
Operated by IIT Research Institute, 10 W. 35th St., Chicago, IL 60616
DoD Technical Sponsor - U.S. Army Missile Command, Redstone Arsenal, AL 35898

FOREWORD

This handbook was prepared for the U. S. Army Missile Command as part of a special task conducted under the Guidance and Control Information Analysis Center Contract, DLA900-80-C-2853. Because of the interest in this technology, the sponsor gave permission to publish the report as a GACIAC handbook.

The handbook summarizes the properties of sulfide, selenide, and telluride materials. In particular, the structural, chemical, electrical, and optical properties of these materials are presented. The information is based upon the available unclassified published literature, and references are provided for the data presented for each material described.

The special task was administered under the direction of Mr. J. Leonard Gibbs, DRSMI-REO, U. S. Army Missile Command, Redstone Arsenal, Alabama 35898.

TABLE OF CONTENTS

TABLE OF CONTENTS (Continued)

Page

SUMMARY

A detailed literature review of the sulfide, selenide and telluride materials was carried out by IIT Research Institute. As a result of this review, approximately 40 different materials were identified for detailed investigation. This work resulted in compilation of the structural, electrical and optical properties of these materials. Special effort was made to include those materials which undergo a phase transition as a result of applied external stimulas such as temperature, pressure or electric field. The information presented in this document is limited to available unclassified literature. Lack of experimental data in several cases was discovered during our literature review. The need for additional data have been identified. A brief summary of the characteristics of the materials is given in Table I followed by detailed description on each material.

TABLE 1
SUMMARY OF MATERIAL CHARACTERISTICS

MATERIAL	DOES IT HAVE A PHASE TRANSITION?	WHAT DOES PHASE TRANSITION DEPEND ON?	PHASE TRANSITION TEMPERATURE OR PRESSURE	TYPE OF TRANSITIONS	ASSOCIATED STRUCTURAL CHANGES
$AgGaS_2$	None indicated	---	---	• Nonlinear IR material None indicated in open literature	• Semiconductor • uniaxial, acentric crystal • no known change
AgI	YES	Stoichiometry Temperature Polytype	$\beta \rightarrow \alpha$: 147°C	Reversible	β: Hexagonal Wurtzite Cubic Sphalerite α: Disordered Cubic
Ag_2S	YES	Stoichiometry Temperature Some evidence for pressure effects also	$\beta \rightarrow \alpha$: 179°C $\alpha \rightarrow \gamma$: 585°C	Fully reversible with Hysteresis (memory) effect Semiconductor (β) → metal (α)	β: Monoclinic crystal structure a=4.23Å, b=6.91Å, c=7.87Å (Acanthite) α: a_o=4.88Å, bcc arrangement for sulphur Ag ions randomly distributed
Ag_2Se	YES	Stoichiometry Temperature	$\beta \rightarrow \alpha$: 166°C	Fully reversible with Hysteresis (memory) effect Semiconductor (β) → metal (α)	β: Orthorhombic a=7.05Å, b=4.32Å, c=7.82Å α: Body Centered Cubic a = 4.98Å
Ag_2Te	YES	Stoichiometry Temperature Polytype	$\beta \rightarrow \alpha$: 157°C	Fully reversible with Hysteresis (memory) effect Semiconductor (β) → metal (α)	β: Orthorhombic a=13.03Å, b=12.72Å, c=12.21Å α: Face Centered Cubic a = 6.58Å

TABLE 1 (Continued)
SUMMARY OF MATERIAL CHARACTERISTICS

MATERIAL	DOES IT HAVE A PHASE TRANSITION?	WHAT DOES PHASE TRANSITION DEPEND ON?	PHASE TRANSITION TEMPERATURE OR PRESSURE	TYPE OF TRANSITIONS	ASSOCIATED STRUCTURAL CHANGES
$CdGa_2S_4$ $CdGa_2Se_4$	-----	-----		• Nonlinear IR material No known transition	• Semiconductor • Structure like diamond a = 5.564 Å c = 10.05 Å
CdSe	YES	Temperature	25°K	• First-order Reversibility unknown	Zincblende to wurtzite type structural change
CoS_2	Unknown	-----	Some evidence of variation in IR reflectivity with temperature (extent of variation is not explicitly mentioned)	Temperature variations in phonon structure	• Pyrite structure (like FeS_2)
CrS	YES	Pressure Temperature	24 Kbars at 300°K 620°K at one atm (varies with x in CrS_x)	Change in electronic structure of the $3d^4$ electron configuration	Monoclinic ⟶ Hexagonal
(CrSe)	(YES)		(UNKNOWN)	(UNKNOWN)	
Cu_2S	YES	Stoichiometry Pressure	100°C for Cu_2S Changes to 108°C for $Cu_{1.8}S$	Fully reversible	Orthorhombic to mixture of hexagonal and cubic structures.

TABLE 1 (Continued)
SUMMARY OF MATERIAL CHARACTERISTICS

MATERIAL	DOES IT HAVE A PHASE TRANSITION?	WHAT DOES PHASE TRANSITION DEPEND ON?	PHASE TRANSITION TEMPERATURE OR PRESSURE	TYPE OF TRANSITIONS	ASSOCIATED STRUCTURAL CHANGES
Cu_2Se	YES	Stoichiometry Temperature	103 - 110°C	Fully reversible with Hysteresis (memory) effect The degree varying with composition	β: Tetragonal a = 11.57Å, c = 11.74Å α: Face Centered Cubic a = 5.84Å
Cu_2Te	YES	Temperature	410°C	Not fully reversible	β: Hexagonal a = 12.54Å, c/a = 1.731Å α: Face Centered Cubic a = 6.11Å
FeS	YES	Temperature Stoichiometry ($Fe_{1-x}S$) Pressure Modulation	325°C (β-transition) 140° (2.2°K/kbar pressure modification of temp.)	Ferroelectric paraelectric Reversible	Structural change unknown Phase transition is highly anisotropic (relative to $\hat{c}$ - axis)
FeS_2	YES	Temperature Polytype	673°K	Irreversible • Marcasite ⟶ pyrite; both stable at 300°K	Marcasite ⟶ Pyrite Marcasite - CaCl structure Pyrite - cubic structure
HfS_2	UNKNOWN	-----	-----	-----	CdI_2 Type hexagonal structure a = 3.635Å c = 5.837Å • Diamagnetic insulator

TABLE 1 (Continued)
SUMMARY OF MATERIAL CHARACTERISTICS

MATERIAL	DOES IT HAVE A PHASE TRANSITION?	WHAT DOES PHASE TRANSITION DEPEND ON?	PHASE TRANSITION TEMPERATURE OR PRESSURE	TYPE OF TRANSITIONS	ASSOCIATED STRUCTURAL CHANGES
HfS_3	UNKNOWN	-----	-----	-----	Monoclinic a = 5.09Å c = 8.97Å ● Anisotropic behavior
HgS	YES	Temperature Pressure	280°C - 340°C	Not reversible without pressure $\beta \longrightarrow \alpha$ β: n-type degenerate semimetal α: insulator	α-HgS: Trigonal (Cinnabar) β-HgS: Cubic (Metacinnabar) α - cinnabar structure β - cubic zinc-blende structure
In_2S_3	YES	Temperature	$\beta \longrightarrow \alpha$ at 420°C $\alpha \longrightarrow \gamma$ at 750°C	Reversible	α - *cubic* β - tetragonal γ - trigonal
MnS	YES	Temperature Pressure Polytype β α 200°C β α high pressure	$\beta + \beta$: metastable at 270°K $\beta \longrightarrow \alpha$: 200°C $\beta \longrightarrow \alpha$: high pressure	β-MnS has a reversible phase transition with a hysteresis effect. $\beta \longrightarrow \alpha$ phase transition is not reversible	α-MnS: NaCl structure 1. β-MnS: wurtzite structure 2. β-MnS: zincblende structure Lattice parameters change with temperature and pressure
MnS_2	YES	Temperature	47.93°K	Reversible Paramagnetic antiferromagnetic change at 49°K	Pyrite structure -- no known change

TABLE 1 (Continued)

SUMMARY OF MATERIAL CHARACTERISTICS

MATERIAL	DOES IT HAVE A PHASE TRANSITION?	WHAT DOES PHASE TRANSITION DEPEND ON?	PHASE TRANSITION TEMPERATURE OR PRESSURE	TYPE OF TRANSITIONS	ASSOCIATED STRUCTURAL CHANGES
MoS_2	YES	Pressure	High pressure	2H → 3R Irreversible change from one polytype to another	Hexagonal layered compound Two polytypes: 2H-MoS_2, 3R-MoS_2 • anisotropic diamagnetic semiconductor
Mo_2S_3	YES	Temperature	One at 80°K * One at 180°K (approx) * seen only for slow cooling rates	Reversible with accompanying hysteresis effect (memory) • observed in resistivity and susceptibility measurements	Possibly a stoichiometric change • space group C_{2h}^{2} • two formula units per unit cell • distorted close-packed lattice
$MoSe_2$	UNKNOWN	-----	There exists two polytropic forms of $MoSe_2$ -- a high and a low T type -- -- no evidence of a phase transition	Irreversible (between polymorphs)	No known structural phase trans. • hexagonal layer compound • Se atoms in trigonal prism coordination • Anisotropic behavior • 2D structure
$MoTe_2$	YES	Temperature	750°C (transforms to α phase) 1175°C (transforms to β phase) *β is the high temperature phase as described by the literature	Diamagnetic Semiconducting To Paramagnetic Metallic	Not given
$NbSe_3$	YES	Temperature	125°K 49°K	Reversible change in resistivity	Six Se Atoms at verticies of right triangular prisms with Nb atom at prism center. Six prisms/unit cell having dimensions of 10.006Å x 3.478Å x 15.626Å

TABLE 1 (Continued)

SUMMARY OF MATERIAL CHARACTERISTICS

MATERIAL	DOES IT HAVE A PHASE TRANSITION?	WHAT DOES PHASE TRANSITION DEPEND ON?	PHASE TRANSITION TEMPERATURE OR PRESSURE	TYPE OF TRANSITIONS	ASSOCIATED STRUCTURAL CHANGES
α-NiS	YES	Temperature Pressure	620°K	Fully reversible for phase transitions in β-NiS (264°K)	α-NiS: T>620°K • rhombohedral symmetry • hexagonal structure β-NiS: T<620°K
β-NiS	YES	Polytype	264°K	Transitions are metal-nonmetal	NiAs structure
NiS_2	YES	Temperature Pressure	40°K to 65°K 31°K Temperatures vary with pressure	Reversible paramagnetic → antiferromagnetic antiferromagnetic → weak ferromagnetic	Cubic structure of the pyrite type -- no known structural change
$NiS_{2-x}Se_x$	YES	Temperature Stoichiometry $(0.4 < X < 0.55)$	70°K - x=0.47 T < 100°K 120°K - x=0.55	Reversible change in electrical properties Semiconductor → metal transition	Solid solution x = 0: Mott insulator x = 2: Metal
SmS	YES	Pressure Radiation induced pressure wave	P inc: 6.5 kbar at 293°K P dec: 0.8 kbar	Fully reversible with hysteresis lag Semiconductor → metal	Due to 4f → 5d electron delocalization -- no structural alteration
SnS_2	UNKNOWN	Possesses a temperature dependent switching in resistivity	280°K	Reversing switching behavior for electrical properties	• Layered semiconductor • Many polytypes exist -- 1R, 4H, 2H, a_0=3.639Å CdI_2 structure c=5.884Å

TABLE 1 (Continued)

SUMMARY OF MATERIAL CHARACTERISTICS

MATERIAL	DOES IT HAVE A PHASE TRANSITION?	WHAT DOES PHASE TRANSITION DEPEND ON?	PHASE TRANSITION TEMPERATURE OR PRESSURE	TYPE OF TRANSITIONS	ASSOCIATED STRUCTURAL CHANGES
$SnSe_2$	UNKNOWN	-----	-----	----- (Little variation in electrical and optical props.)	• Anisotropic • Same as SnS_2 otherwise a_o = 3.811Å c = 6.137Å
SnS_xSe_{2-x}	UNKNOWN	Change in stoichiometry alters characteristics	-----	Continuous change in properties with temperature	• Layered structure for $0 < X < 2$ • Solid solution
TaS_2	YES	Temperature Pressure Polytype	Phase transitions between polytypes not known in detail 1T-TaS_2: 190°K and 348°K 2H-TaS_2: 70°K	Fully reversible with hysteresis (resistivity)	Four polytypes: 1T-TaS_2, 2H-TaS_2, 3R-TaS_2, 6R-TaS_2 Small crystallographic change in 2H-TaS_2 at 70°K.
TaS_3	YES	Temperature Polytype	Orthorhombic form 210°K - Peierls trans. Monoclinc form 240°K two PT's 160°K	Peierls transition due to charge density waves	Linear stacking of trigonal prisms of chalcogen atoms -- Orthorhombic structure -- Two polytypes
TiS_2	UNKNOWN	Stoichiometric variation of characteristics for $Ti_{1-x}S_2$	-----	Possesses anamolous behavior in conductivity between 40°K and 400°K.	Hexagonal CdI_2 structure a = 3.40Å, c = 5.698Å • Believed to be extrinsic semiconductor

TABLE 1 (Continued)

SUMMARY OF MATERIAL CHARACTERISTICS

MATERIAL	DOES IT HAVE A PHASE TRANSITION?	WHAT DOES PHASE TRANSITION DEPEND ON?	PHASE TRANSITION TEMPERATURE OR PRESSURE	TYPE OF TRANSITIONS	ASSOCIATED STRUCTURAL CHANGES
$ZrSe_3$	UNKNOWN	-----	-----	Peierls transition (as in TaS_3) is suspected	• *Difficult to prepare* stoichiometric samples • Monoclinic unit cell a = 5.41R, c = 9.45Å • 1D structure

APPENDIX

DESCRIPTION OF INDIVIDUAL OPTICAL MATERIALS

$AgGaS_2$

Silver Thiogallate

$AgGaS_2$, or silver thiogallate, has been reported to possess the chalcopyrite structure.[1] It is a uniaxial, acentric, nonenantiomorphous crystal. $AgGaS_2$ possesses optical activity and is birefringent. The unit cell dimensions are a = 5.74Å and c = 10.26Å.

Figure 1 shows the ordinary and extraordinary refractive indices (n_o and n_e) for $AgGaS_2$ from 4500Å to 6700Å; this is the visible part of the spectrum.[2] A fairly large literature exists concerning the nonlinear optical properties of $AgGaS_2$; these appear to be applicable for the fabrication of infrared devices.[2,3,4] In Table 1 we have a tabulation of n_o and n_e from 0.49µm to 13µm. The most noticable result of this measurement is the uniformity over the spectral range. At 10.6µm, we have

$$n_o = 2.34 \text{ and } n_e = 2.29.^4$$

Silver thiogallate absorption curves have been published from the visible to the mid-infrared spectral range. These results are given in Figure 2. To convert from the absorption coefficient (α) to the extinction coefficient (k), use the relationship:

$$\alpha = \frac{4\pi k}{\lambda} .$$

Since α is about 1 cm^{-1} at 5µm, however, it is apparent that k is indeed very small. Consequently, the reflectivity in the 0.5µm to the 12.5µm range is well approximated (at normal incidence) by:

$$R = \frac{(n-1)^2}{(n+1)^2} .$$

As a result, $AgGaS_2$ is a transparent material in this wavelength range.

Figure 3 shows the transmittance from 0.3 to about 30µm. Note that there are slight differences for each polarization. At 0.497µm, $n_o = n_e$, whereby optical activity can be studied without the added birefringence.

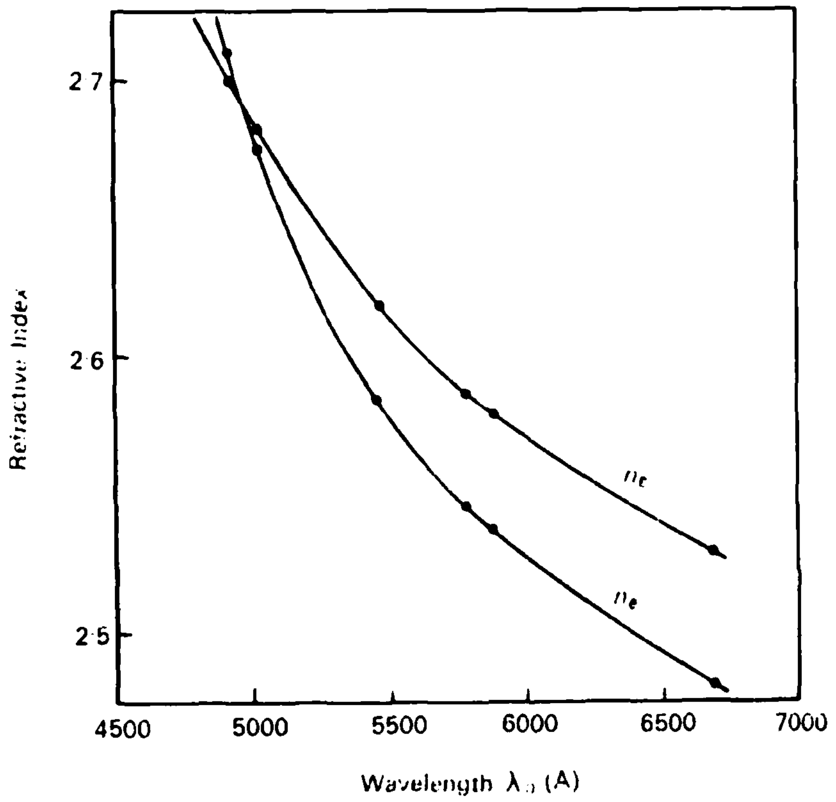

Figure 1. The refractive indices of $AgGaS_2$ at 20°C.

TABLE 1

REFRACTIVE INDEX OF $AgGaS_2$ VERSUS WAVELENGTH (μ) AND RECIPROCAL WAVELENGTH (μ^{-1})

λ μ	$\nu = \lambda^{-1}$ μ^{-1}	n^o	n^e	$n^e - n^o$
.4900	2.0408	2.7148	2.7287	.0138
.5000	2.0000	2.6916	2.6867	-.0049
.5250	1.9048	2.6503	2.6239	-.0264
.5500	1.8182	2.6190	2.5834	-.0356
.5750	1.7391	2.5944	2.5537	-.0407
.6000	1.6667	2.5748	2.5303	-.0444
.6250	1.6000	2.5577	2.5116	-.0461
.6500	1.5385	2.5437	2.4961	-.0476
.6750	1.4815	2.5310	2.4824	-.0486
.7000	1.4286	2.5205	2.4706	-.0499
.7500	1.3333	2.5049	2.4540	-.0509
.8000	1.2500	2.4909	2.4395	-.0514
.8500	1.1765	2.4802	2.4279	-.0522
.9000	1.1111	2.4716	2.4192	-.0525
.9500	1.0526	2.4644	2.4118	-.0526
1.0000	1.0000	2.4582	2.4853	-.0529
1.1000	.9091	2.4486	2.3954	-.0532
1.2000	.8333	2.4414	2.3881	-.0533
1.3000	.7692	2.4359	2.3819	-.0540
1.4000	.7143	2.4315	2.3781	-.0534
1.5000	.6667	2.4280	2.3745	-.0535
1.6000	.6250	2.4252	2.3716	-.0535
1.8000	.5556	2.4206	2.3670	-.0536
2.0000	.5000	2.4164	2.3637	-.0527
2.2000	.4545	2.4142	2.3604	-.0537
2.4000	.4167	2.4119	2.3583	-.0535
2.6000	.3846	2.4102	2.3567	-.0535
2.8000	.3571	2.4094	2.3559	-.0535
3.0000	.3333	2.4080	2.3545	-.0535

TABLE I (CONT.)

λ μ	$\nu = \lambda^{-1}$ μ^{-1}	n^o	n^e	$n^e - n^o$
3.2000	.3125	2.4068	2.3534	-.0534
3.4000	.2941	2.4062	2.3522	-.0548
3.6000	.2778	2.4046	2.3511	-.0535
3.8000	.2632	2.4024	2.3491	-.0533
4.0000	.2500	2.4024	2.3488	-.0536
4.5000	.2222	2.4003	2.3461	-.0542
5.0000	.2000	2.3955	2.3419	-.0536
5.5000	.1818	2.3908	2.3401	-.0537
6.0000	.1667	2.3988	2.3369	-.0539
6.5000	.1538	2.3874	2.3334	-.0540
7.0000	.1429	2.3827	2.3291	-.0536
7.5000	.1333	2.3787	2.3252	-.0535
8.0000	.1250	2.3757	2.3219	-.0538
8.5000	.1176	2.3699	2.3163	-.0536
9.0000	.1111	2.3663	2.3121	-.0542
9.5000	.1053	2.3606	2.3064	-.0542
10.0000	.1000	2.3548	2.3012	-.0536
10.5000	.0952	2.3486	2.2948	-.0538
11.0000	.0909	2.3417	2.2888	-.0537
11.5000	.0870	2.3329	2.2789	-.0540
12.0000	.0833	2.3266	2.2716	-.0550
12.5000	.0800	2.3177		
13.0000	.0769	2.3076		

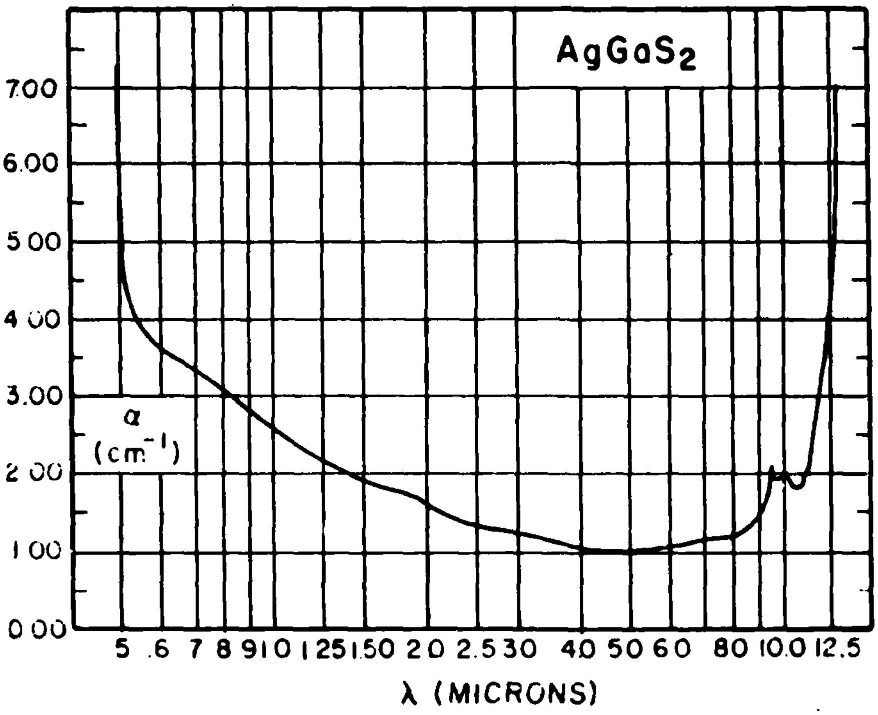

Figure 2. Room temperature absorption coefficient $\alpha(cm^{-1})$ versus wavelength (λ) for $AgGaS_2$

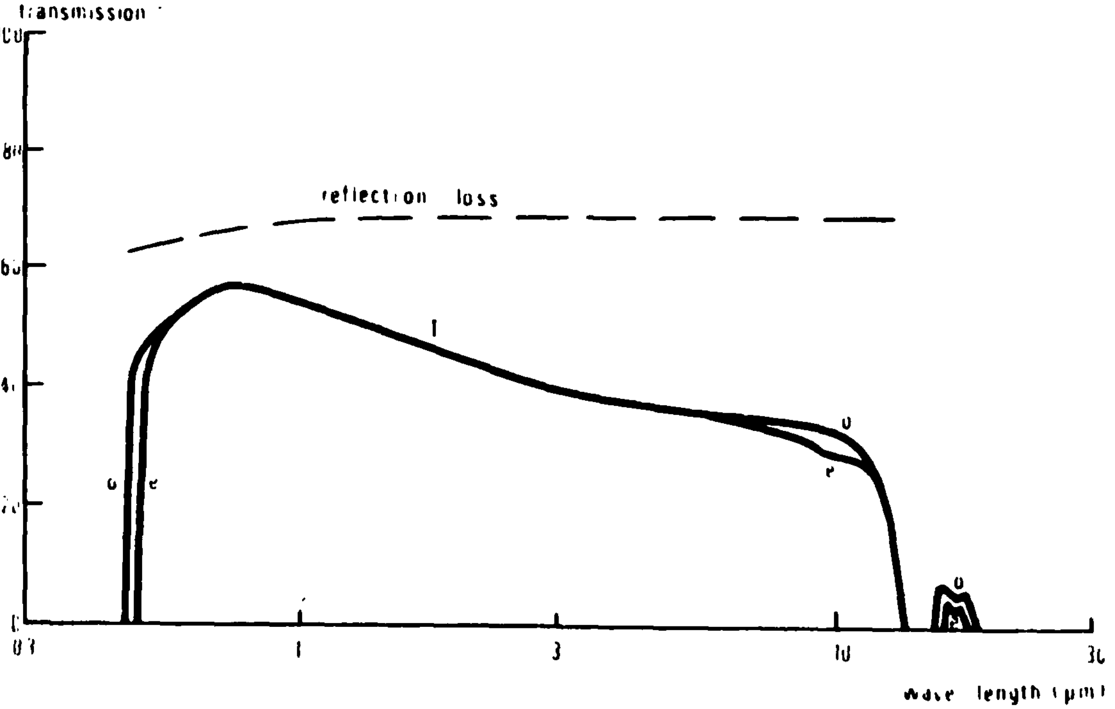

Figure 3. Transmission of a 1.2mm plate of $AgGaS_2$. The optic axis was at 40^o to the plate.

The dispersion curves for n_o and n_e can be fitted for infrared wavelengths by the equations:

$$n_o = 5.728 + \left[\frac{0.2410}{\lambda^2 - 0.0870} - 0.00210\,\lambda^2\right]^{1/2} .$$

$$n_e = 5.497 + \left[\frac{0.2026}{\lambda^2 - 0.1307} - 0.00233\,\lambda^2\right]^{1/2} .$$

Here λ is in microns. Therefore:

$$R_o = \left[\frac{n_o - 1}{n_o + 1}\right]^2 , \qquad R_e = \left[\frac{n_e - 1}{n_e + 1}\right]^2 .$$

Phase matched second harmonic generation in $AgGaS_2$ at 10.6 µm radiation has been observed.[3] The result of this experiment is shown in Figure 4.

$AgGaS_2$ is a ternary chalcopyrite semiconductor. Its melting point is near 1000°C. There does not appear to be a phase transition at temperatures above room temperature, although a phase transition near 100°K has been reported. We have been unable to determine the nature of this transition or any accompanying change in electrical or optical properties. At 10.6 µm (or 943 cm^{-1}), the reflectivity at room temperature is near 18% for both field polarizations (Figure 5).[6] Possibly the low temperature phase will possess a different value of R at 10.6 µm. Although any such phase must be insulating, it would then appear that R would probably be the same or even less. That is, no significant change is expected unless there exists a higher temperature phase change where $AgGaS_2$ becomes metallic.

REFERENCES ($AgGaS_2$)

1. H. Hahn, et.al., Z. Anorg. Chem., 271, 153 (1953).
2. M.V. Hobden, Acta Cryst., A24, 676 (1968).
3. D.S. Chemla, et.al., Optics Commun. 3, 29 (1971).
4. G.D. Boyd, et.al., J. Quan. Elec., QE-7, 563 (1971).
5. B. Tell, et.al., Phys. Rev. B6, 3008 (1972).
6. J.L. Shay and J.H. Wernick, "Ternary Chalcopyrite Semiconductors: Growth, Electronic Properties, and Applications", Pergamon Press, Oxford, 1975.

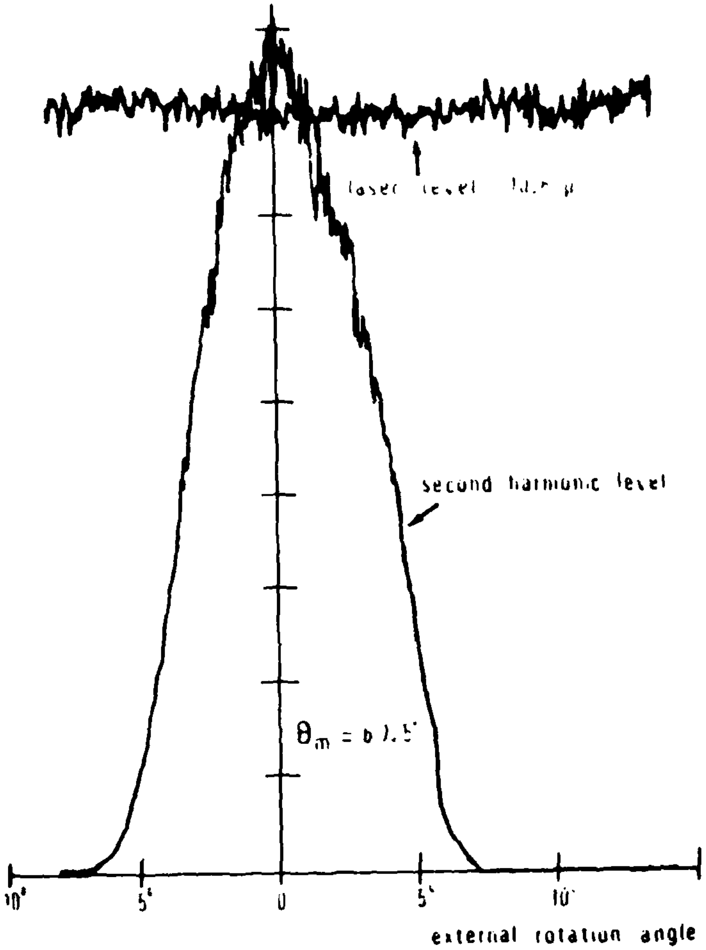

Figure 4. Phase matched SHG in $AgGaS_2$ from 10.6μm radiation.

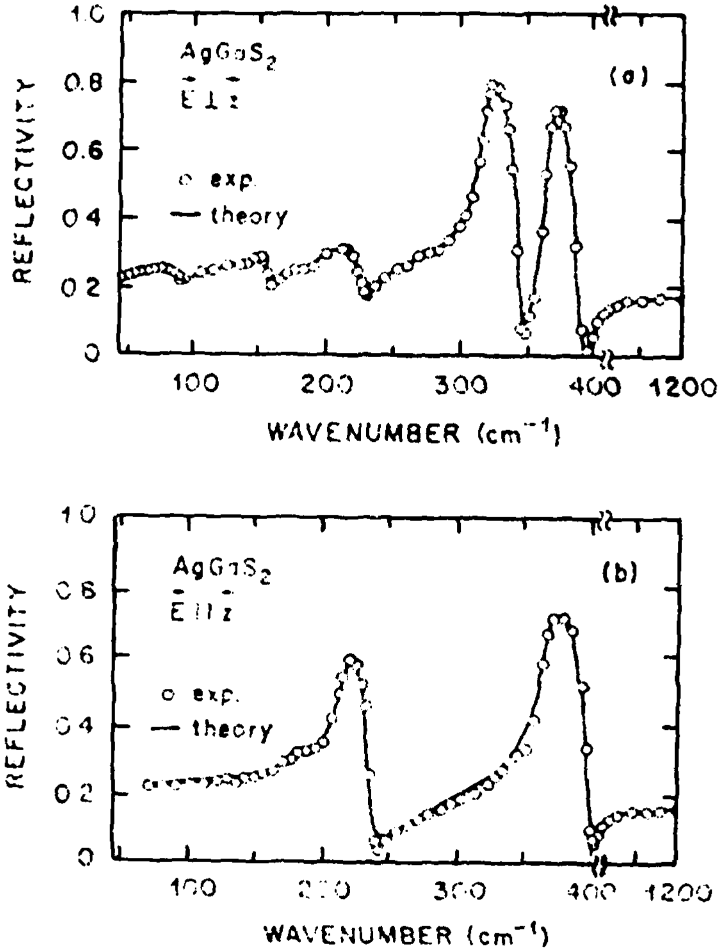

Figure 5. Reflectivity curves for $AgGaS_2$.

AgI

Silver Iodide

Thin films of AgI have been prepared by thermally evaporating Ag in iodine vapor or iodizing films of silver sequentially to build up thick layers.[1] Direct evaporation of molten AgI has been found to produce nonstoichiometric films due to evolution of iodine. Films have been deposited on glass,[2] quartz,[3] mica,[4] polyethyline,[5] celluloid,[6] and sodium chloride[7] substrates.

Silver iodide undergoes a phase transition at 147°C. In the low temperature phase it has two polymorphs, namely a hexagonal wurtzite-type structure and a cubic sphalerite structure. The structure achieved in thermally evaporated films seems to be dependent on substrate temperature during depositions and may be dictated by stoichiometry, ie., the amount of iodine in the film.[5,6] There is also some evidence that the cubic form is stable from room temperature to 137°C and the hexagonal form exists from 137° to 146°C. Above the phase transition temperature, a disordered cubic structure exists.

AgI exhibits an especially large increase in ionic conductivity (six orders of magnitude) when undergoing the phase transition. The high temperature phase corresponds to a "quasi molten" or "liquid like" state of silver ions which are almost free to move. The mobility of the silver ions contributes to the total conductivity of the material. Electrical conductivity is shown as a function of temperature in Figure 1 compared to varying degrees of mixture with Ag_2WO_4. The phase transition of pure AgI is apparent by the better than three order of magnitude increase in conductivity. Since the high temperature phase has a conductivity on the order of 1 ohm-cm and the slope does not reverse, the material does not become metal-like and the alteration in optical properties may not be large.

No data on the optical properties of AgI was found in the literature.

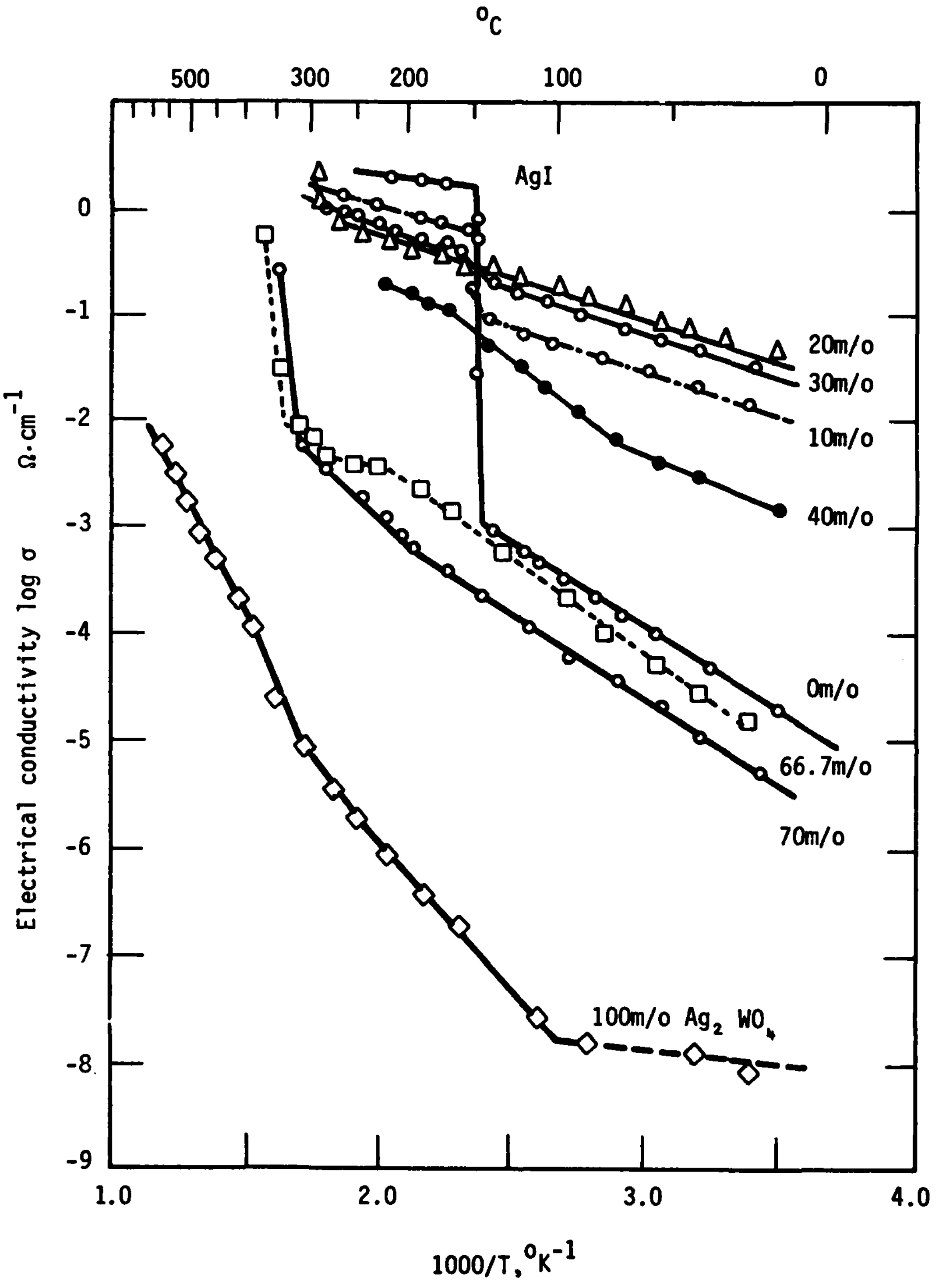

Figure 1. Electrical Conductivity vs. Temperature.

REFERENCES (AgI)

1. C. Cochrane, J. Crys. Growth, 7, (1970), 109.
2. I.A. Akinov, Zh. Fiz. Khim. 30 (1956), 1007.
3. S. Fitihasi, Phys. Rev. 105 (1957), 882.
4. D.W. Pashley, Phil. Mag., 43, (1952), 1028.
5. G.L. Bottger, et.al., J. Chem. Phys., 46 (1963), 3000.
6. R.N. Kurdyumova, Sov. Phys. - Cryst., 10 (1965), 36.
7. R. Block, et.al., Z. Phys. Chem., A152 (1930), 245.

Ag_2S

Silver Sulfide

Silver sulfide is a chalcogenide which displays a dramatic first-order crystallographic phase transformation with an accompanying change in its electrical, thermal, and optical properties. It can exist in a variety of stoichiometries of the form $Ag_{2+\delta}S$ where δ can range from -0.000035 to 0.000018 in the low temperature state and from 0.0 to 0.0022 in the high temperature state. The low temperature phase is referred to as acanthite or the β-phase and possesses a monoclinic crystal structure. The cell constants for the β-phase are $a = 4.23$ Å, $b = 6.91$ Å, $c = 7.87$ Å and $\beta = 99° 35'$.[1] There are four units of Ag_2S per unit cell. At 450°K (179°C) the β-phase undergoes a reversible phase change to the high temperature α-phase (known as argentite). A small volume expansion of about 1% accompanies this phase transition. The transition is first-order due to the changes in the thermal properties across the temperature boundary. Both the β- and α-phases have in common a body centered cubic arrangement of the sulfur atoms though the silver sublattice is quite different in each case. For the β-phase the silver atoms are well ordered whereas in the α-phase the four silver atoms (ions) are randomly distributed on the 42 positions given in Reference 2. For the α-phase the lattice constant is $a_0 = 4.88$ Å. There exists yet another phase transformation at 585°C to the γ-phase.[3] The lattice dynamics of silver sulfide is not known.[4]

Silver sulfide exhibits a marked increase in the electrical conductivity at the transition temerature. Figure 1 shows that the change is about three orders of magnitude.[5] The extent of the change in the conductivity will depend on the stoichiometry. Ag_2S is a mixed conductor, there being an ionic and an electronic component. The ionic conduction is due to the motion of Ag^+ ions in both phases.[6,7] (It should be pointed out that β-Ag_2S is an n-type semiconductor.)

Concerning the thermal properties there is a change in the heat capacity from the low temperature phase to the high temperature phase (as may be expected, intuitively, in a semiconductor to a metal phase transformation). However, it is still not known if there is such a change for the thermal conductivity across the transition temperature. According to the Franz-

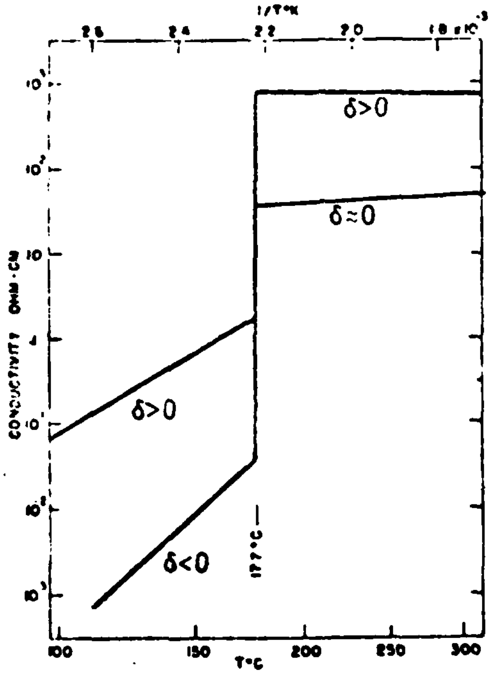

Figure 1. Electrical Conductivity of $Ag_{2+\delta}S$ vs. T

Wiedermann law for a Drude material we might expect a change in the thermal conductivity to be the same (quantitatively) as the change in the electrical conductivity. This, however, may not take place for a variety of reasons - for example, one may expect a similar effect to occur for VO_2, though none is observed.[8] No definite measurement of the thermal conductivity for α-Ag_2S is known, though there are measurements reported in the literature for Ag_2Se.[9]

The optical properties of Ag_2S are well studied in the infrared part of the spectrum. For the β-phase there is little extinction up to about 30 μm when the reststrahlen bands are reached. As seen in Figure 2, there is considerable structure in the far-infrared which characterizes the lattice vibrations. From a Kramers-Kronig analysis, an index of refraction of 3.0 is arrived at for the flat portion of the reflectivity curve. The α-phase is a good Drude metal (in the sense of the free carriers being modeled as a Fermi gas). The carrier concentration is a function of stoichiometry, and can vary from 1.2×10^{18} cm^{-3} to 3.6×10^{19} cm^{-3}.[10] Here the value of the long wavelength dielectric constant has been determined to be $\varepsilon_0 = 8.8$. The effective carrier (electron) mass is $0.24\ m_0$, and the relaxation time is $\tau = 2.2 \times 10^{-14}$ second.[11]

From the three parameter free carrier Drude theory we have

$$\varepsilon' = n^2 - k^2 = \varepsilon_0 - \frac{n_e e^2}{\varepsilon_0 m^*} \frac{\tau^2}{1 + \omega^2 \tau^2} ,$$

$$\varepsilon'' = 2nk = \frac{n_e e^2}{\varepsilon_0 m^* \omega} \frac{\tau}{1 + \omega^2 \tau^2} ,$$

where $\varepsilon(\omega) = \varepsilon'(\omega) + i\ \varepsilon''(\omega)$ is the complex dielectric constant and n_e the carrier concentration. From these expressions the normally incident reflectivity is given by the well known formula (as derived from the Fresnel equations):

$$R = \frac{(n - 1)^2 + k^2}{(n + 1)^2 + k^2}$$

Figure 3 shows the index of refraction (n) and the extinction coefficient (k) as calculated from the reflectivity curve using the Kramers-Kronig method. This is for the low temperature (β) phase of the material. The

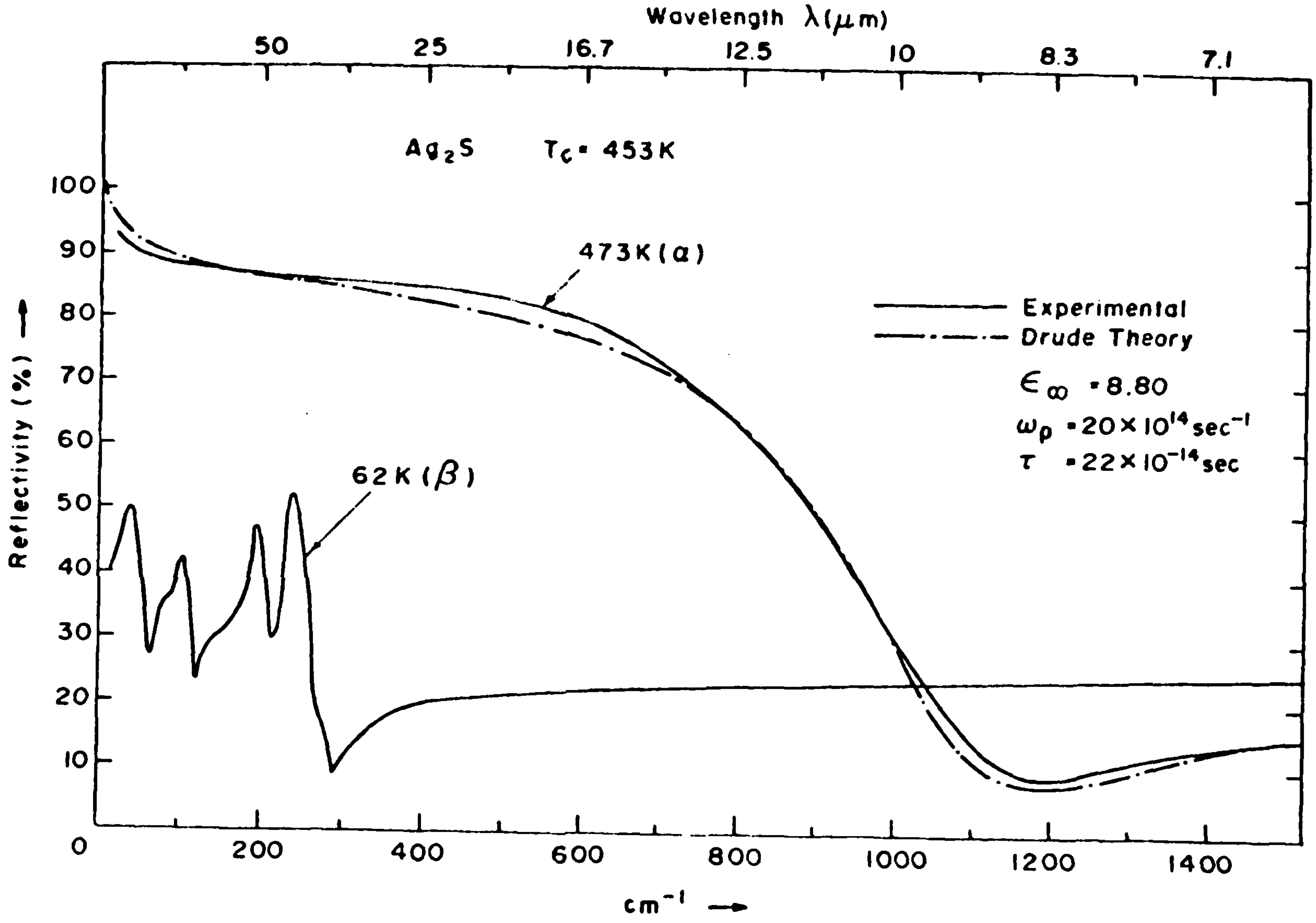

Figure 2. Reflectivity of β-Ag_2S at 62K and of α-Ag_2S at 473K

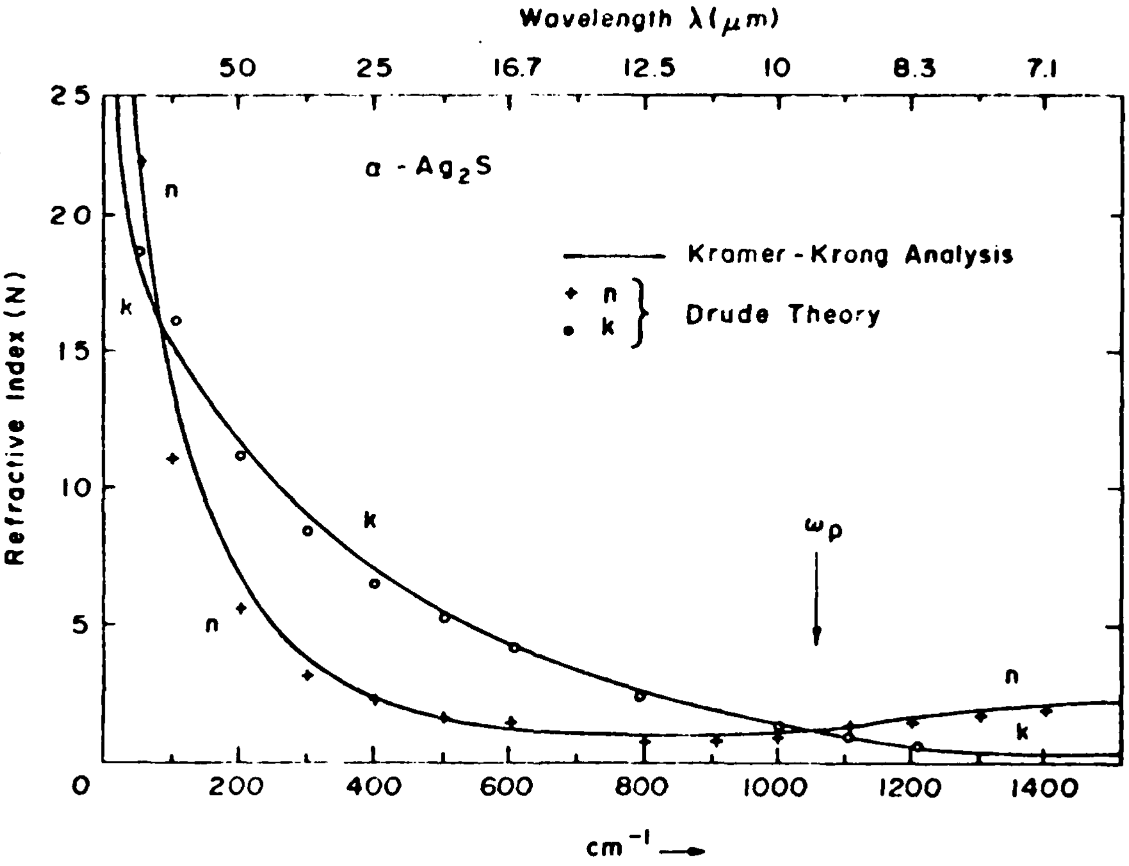

Figure 3. Dispersion of the complex refractive index N = n + ik of α - Ag_2S.

experimental curves are compared directly with the predicted curves obtained from the Drude model. In Figure 4 are shown the reflectivity curves for the α-phase for various values of the carrier concentration; these curves have also been generated from the Drude model; though there is close agreement with the measured values.[12]

REFERENCES (Ag_2S)

1. A.J. Frueh, Z. Kristallogr., Vol. 110, 2 (1958).
2. P. Rahlfs, Z. Phys. Chem., Vol. B31, 157 (1936).
3. T. Smit, E. Venema, J. Wiersma, and G.A. Wieglas, J. Solid State Chem., Vol. 2, 309 (1970).
4. W. Andreoni, Solid State Commun., Vol. 38, 837 (1981).
5. M.H. Hebb, J. Phys. Chem., Vol. 20, 185 (1952).
6. C. Wagner, Z. Physik Chem., Vol. B21, 25 (1933).
7. C. Tubandt, et.al., Z. Anorg. U. Allsem. Chem., Vol. 117, 1 (1921).
8. The lack of a change in the thermal conductivity, in so far as the Franz-Wiedemann law is concerned, has been attributed to imperfections in the crystal sample, or a breakdown in the theory due to the carriers scattering inelastically within the lattice.
9. S. Miyatani and Y. Toyota, J. Phys. Soc. Japan, Vol. 23, 37 (1967).
10. H.H. Dorner, H.P. Geserich, and H. Rickert, Phys. Stat. Sol. (a), Vol. 37, K85 (1970).
11. P. Bruesch and J. Wullschleger, Solid State Commun., Vol. 13, 9 (1973).
12. The IIT Research Institute has been doing research on Ag_2S for use as a rejection filter for over four years; to date this work has been considered to be quite successful.

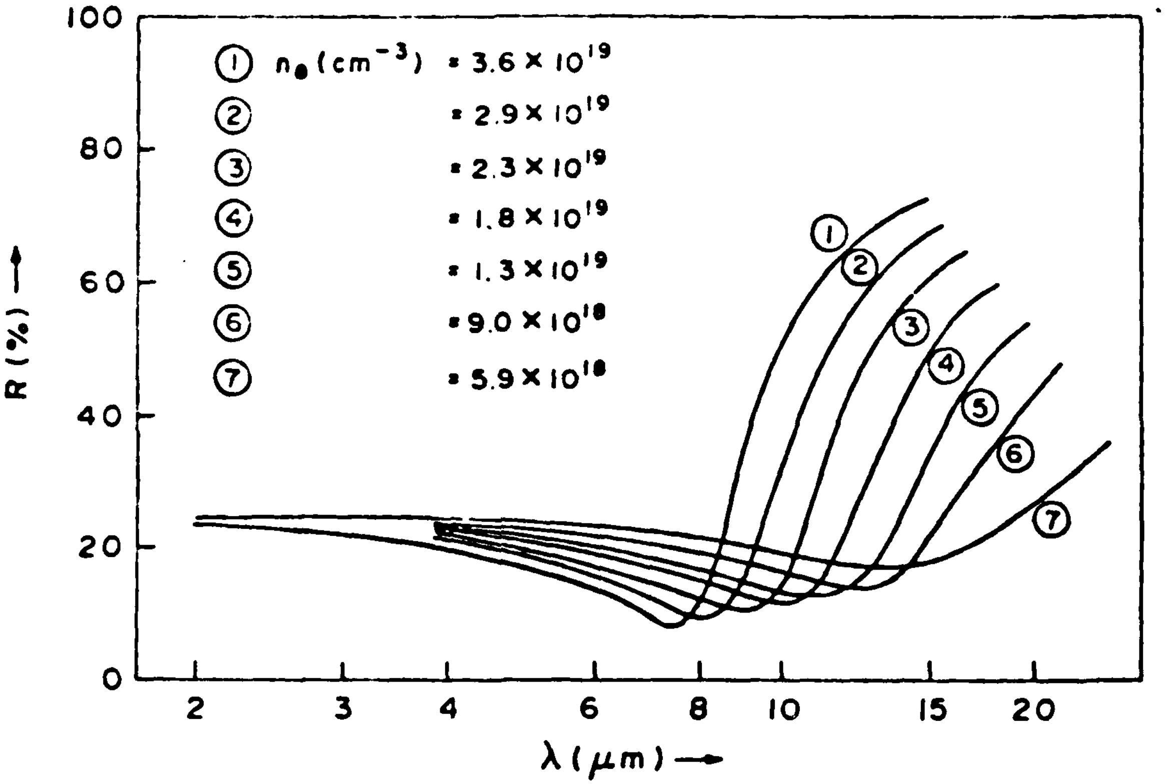

Figure 4. Reflectivity R(λ) of α-Ag_2S with different electron concentrations, T = 200°C.

Ag_2Se
Silver Selenide

Thin films of Ag_2Se have been prepared by thermal evaporation of the compound synthesized by reacting components in quartz ampules and by evaporating the constituents in stoichiometric proportions from the same boat.[1] Films have been deposited on glass substrates and freshly cleared single crystals of KCl maintained at room temperature. Post annealing at different temperatures homogenized the films. Films annealed at 120°C revealed polycrystalline growth when examined by electron diffraction. The low temperature phase is orthorhombic with lattice parameters a = 7.05Å; b = 4.32Å; c = 7.82Å. Films annealed at 140°C exhibited oriented growth and those annealed at 150°C showed a mosaic single crystal structure.[2,3]

A phase transformation from orthorhombic to body centered cubic with a = 4.98Å occurs at 166°C.[4] Significant hysteresis is apparent since on cooling, films of all thicknesses showed a transformation in structure at 107 ± 2°C. Structural transformations in the bulk state have been reported at lower temperatures ranging between 122°C and 133°C.[5-10] The phase transition is associated with a volume expansion of 5%. The high temperature phase α-Ag_2Se presents the same characteristic disorder of silver atoms as does α-AgI and α-Ag_2S.

Ag_2Se like Ag_2S exhibits ionic as well as electronic conductivity. The exact amount of the Ag/Se ratio determines the relative magnitudes of ionic to electronic conduction according to the electrochemical studies of Wagner,[10] and Valverde;[11] the Ag/Se ratio is variable and therefore the ratio of ionic to electronic conductivity can be controlled stoichiometrically. The homogeneity range determined by Valverde is compared with that of Ag_2S in Table 1.

TABLE 1

HOMOGENEITY RANGE (MOLAR CONCENTRATIONS)

Phase	Temperature (°C)	$\delta \times 10^4$ in $Ag_{2+\delta}X$
α-Ag_2S	200	0 to + 22
β-Ag_2S	150	-0.35 to + 0.18
α-Ag_2Se	150	0 to + 36.5
β-Ag_2Se	100	-2.0 to + 6.5

Both phases α-Ag_2S and α-Ag_2Se have in the whole homogeneity range comparable amounts of excess silver. The low temperature phases may be silver rich or silver deficient; however the homogeneity range, especially for the low temperature phase of Ag_2S, is narrow compared with the corresponding value for the disordered high temperature phase.

The value of conductivity at the transition temperature varies between 1000 and 3000 ohm-cm.[1] The conductivity as a function of temperature is shown in Figure 1.[12] Below the transition temperature Ag_2Se behaves as a semiconductor and above this temperature it behaves as a metal.

Optical absorption in Ag_2Se as a function of photon energy is shown in Figure 2 for temperatures ranging from 20° to 160°C.[12] A gradual decrease in absorption over all wavelengths is evident as the temperature is increased. No abrupt increase in absorption is evident at the phase transition. A shift of the plasma edge to shorter wavelengths is apparent as the temperature is increased and the edge appears to be located at about 15 microns (0.08 ev) at the phase transition temperature. This leads to an anticipation of high reflectivity at wavelengths in this vicinity.

REFERENCES (Ag_2Se)

1. S.K. Sharma, J. Matls. Sci., 4, (1969), 189.
2. J. Appl, Z.F. Naturforsch., (1955), 10a, 530.
3. P.J. Busch, Helv. Phys. Acta, (1957), 30, 6, 70.
4. S.K. Sharma, et.al., Phys. Lett., 9, (1964), 217.
5. B. Rehles, Z. Phys. Chem., 31B, (1936), 157.
6. M. Bellati, et.al., Z. Phys. Chem 5, (1890), 282.
7. G. Pellini, Gazz. Chim. Ital., 45 (1955), 533.
8. U. Zorll, Ann. PHysik, 16, (1955), 27.
9. Chou Ching Liang, et.al., Phys. Crystallog, 7, (1962), 52.
10. Wagner, C., J. Chem. Phys. 21, 1819, (1953).
11. Valverde, N., Z., Phys. Chem. NF, 70, 113, 138 (1970).
12. Junod, P., et.al., Phil. Mag. 36, 4, 941 (1977).

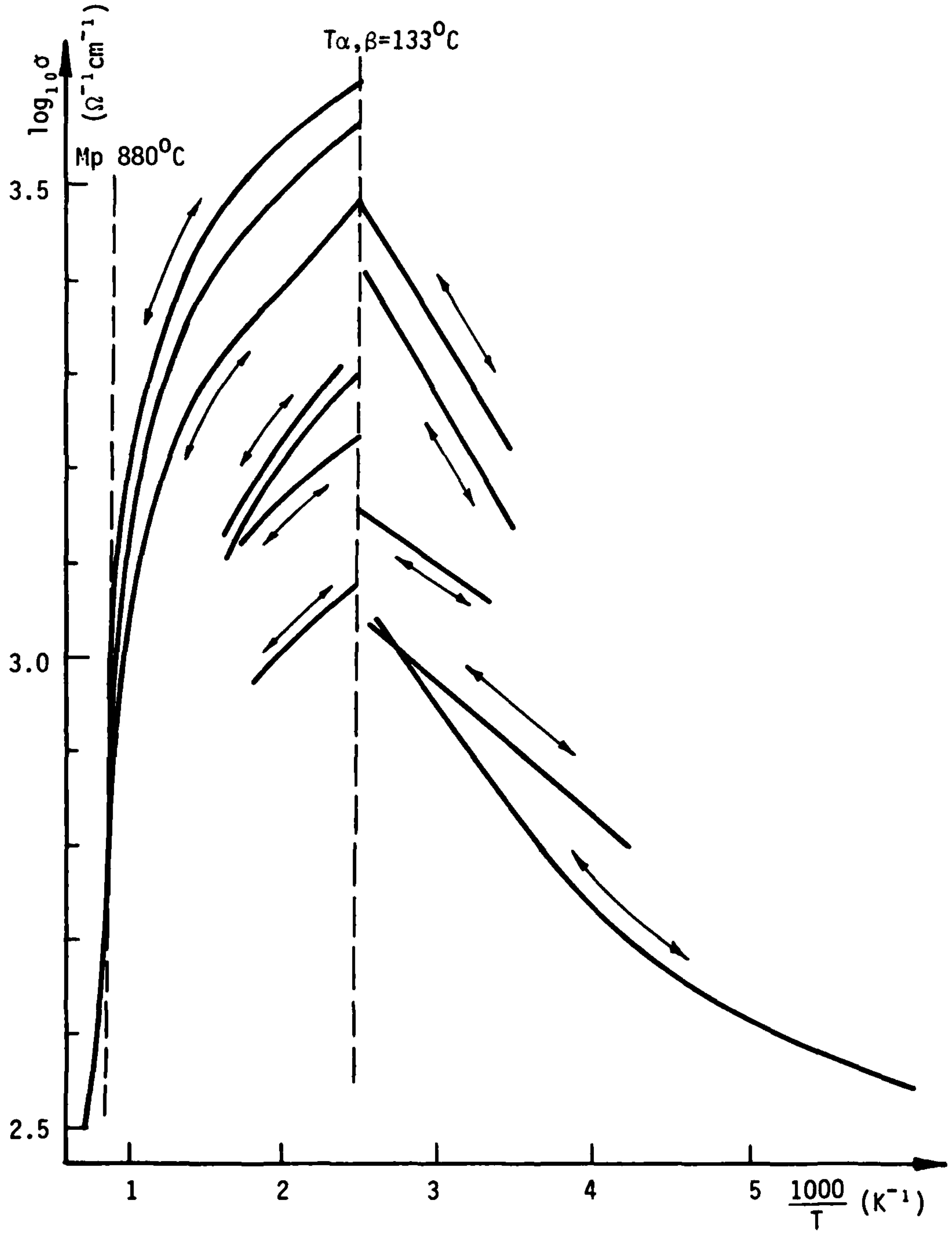

Figure 1. Electrical conductivity of Ag_2Se. For $T < T_{\alpha,\beta}$ = 133°C, all the measured samples demonstrate semiconducting properties. For $T > T_{\alpha,\beta}$ the coefficient $d\sigma/dT$ is always <0. The different curves, corresponding all to nominally pure and stoichiometric samples, demonstrate the influence of thermal history on the electrical conductivity of Ag_2Se.

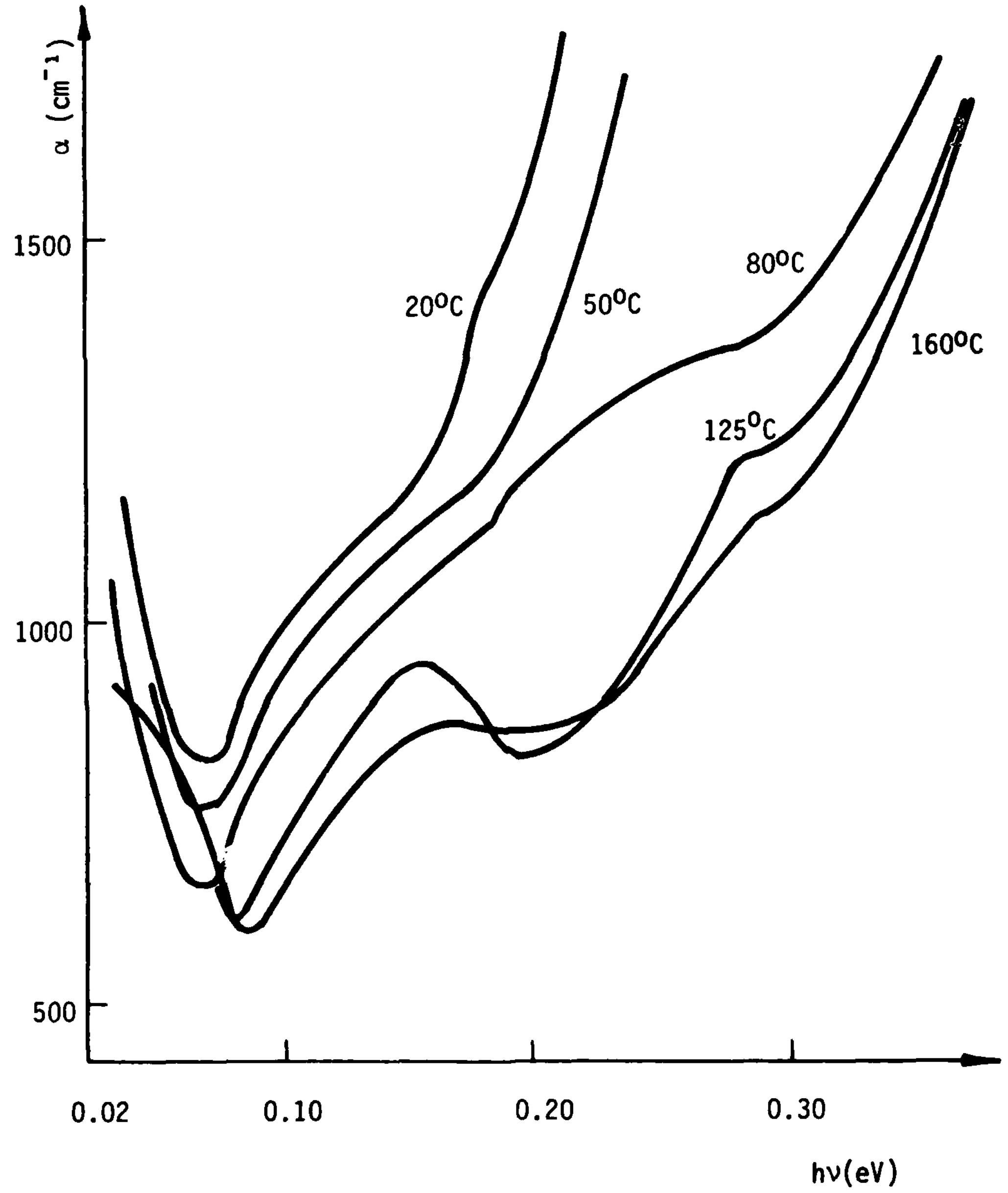

Figure 2. Optical absorption of Ag_2Se at various temperatures. This figure demonstrates the presence of two different absorption mechanisms: (*a*) For photon energies lower than about 0·05 eV, free-carrier absorption is predominant; (*b*) for photon energies larger than about 0·1 eV, absorption is due to interband transitions.

Ag_2Te
Silver Telluride

Ag_2Te films have been prepared by thermal evaporation by synthesizing the starting material in bulk by reacting the components in quartz ampules and by evaporating the constituents from separate boats or the same boat. Films have been deposited in glass, formvar and KCl substrates.[1] When constituents were evaporated from the same boat annealing was necessary to attain compound formation. The films deposited on KCl at 300°C and annealed at the same temperature showed oriented growth.

Electron diffraction patterns in the low temperature phase showed an orthorhombic structure with the lattice parameters a = 13.03Å; b = 12.72Å; c = 12.21Å. At 157°C a phase transformation to the face centered cubic structure occurs with a = 6.58Å. Both oriented and polycrystalline samples showed the same transformation temperature within ±2°C over the entire thickness range investigated. Cycling the film through the phase transformation exhibited hysteresis, the original phase being regained below 115°C.

The specific electrical conductivity of the films was found to be 38 $ohm^{-1}cm^{-1}$ which is one order lower than the specific electrical conductivity measured for bulk samples.[2,3] This is explained by the mobility of charge carriers decreasing due to the transitional resistance between grains in the film. The electrical conductivity as a function of temperature for silver telluride is shown in Figure 1, where the jump in conductivity is attributed to the polymorphic phase transformation. The conductivity curves indicate that Ag_2Te is a semiconductor below the phase transition and a metal above the transition. The transformation is accompanied by a change in the character of the chemical bonds.[2,3] In the low temperature phase, the bonds are covalent and in the high temperature phase they are polar with a considerable degree of ionic conductivity.

Figure 2 illustrates the temperature dependance of the heat conductivity of Ag_2Te. The phase transformation is again evidenced by the minima occuring at 140°C and 150°C. The coefficients of heat conductivity of Ag_2Te varies from 7.8×10^{-3} to 3.9×10^{-3}.

No data has been found on the optical properties of Ag_2Te.

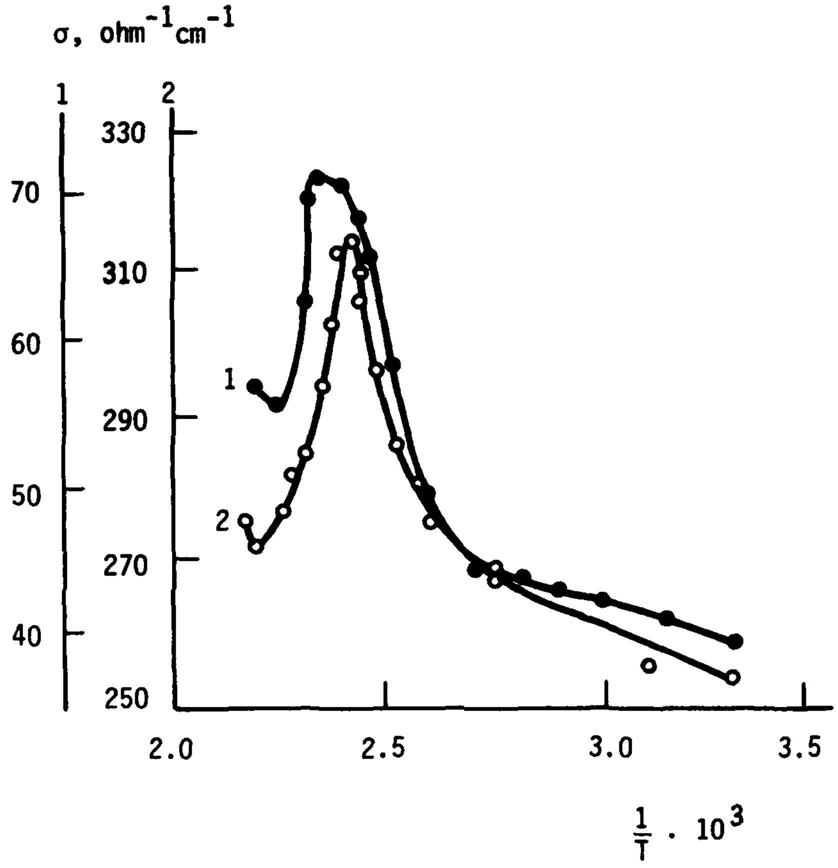

Figure 1. Effect of temperature on the electrical conductivity of Ag_2Te (1), and Ag_2Se (2).

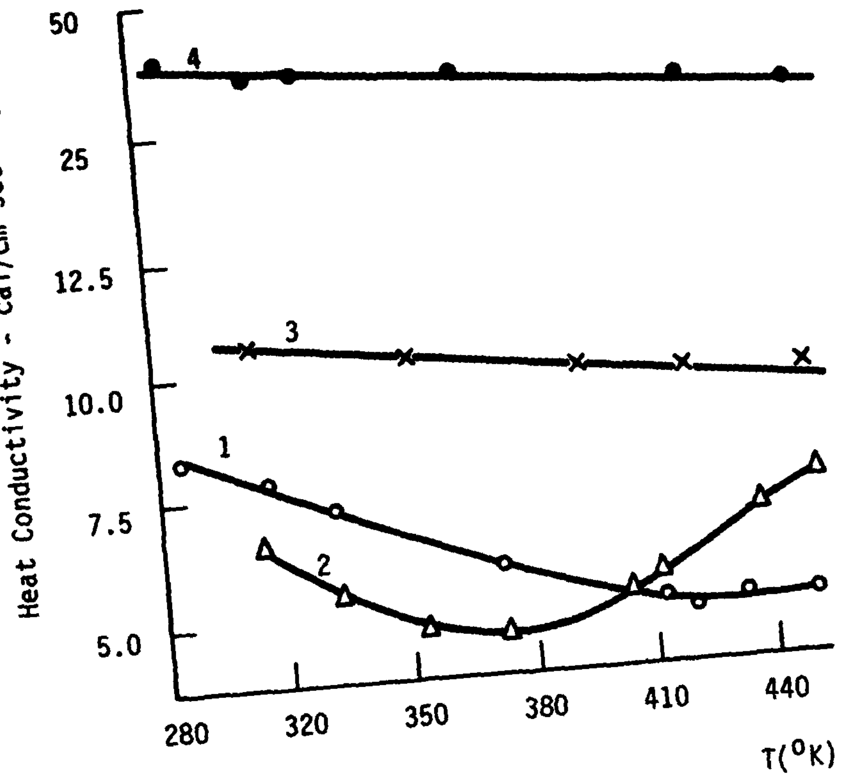

Figure 2. Effect of temperature on the heat conductivity of Ag_2Te (1), Ag_2Se (2), SnTe (3), and CdTe (4).

REFERENCES (Ag_2Te)

1. S.K. Sharma, J. Mat. Sci., 4 (1969), 189.
2. J. Appl, Z.F. Naturforsch., (1955), 10a, 530.
3. P.J. Busch, Helv. Phys. Acta, (1957), 30, 6, 70.

$CdGa_2S_4$
Cadmium Thiogallate
$CdGa_2Se_4$
Cadmium Chalcopyrite

$CdGa_2S_4$, cadmium thiogallate, belongs to the class of defect ternary diamond-like semiconductors in the $A^{II}\ B_2^{III}\ C_4^{VI}$ class. $CdGa_2Se_4$ is also known as cadmium chalcopyrite. Both of these can be prepared as single crystals via the method of chemical transport reaction. Their structure is characterized by a tetrahedral atomic configuration corresponding to the structure of the space group $S_4^2 - I\bar{4}$ (tetragonal unit cell with two formula units). Two sites of the cationic lattice are free (cadmium vacancies). Figure 1 shows the structure for $CdGa_2S_4$. On the basis of the experimentally determined lattice periods of the compound $CdGa_2S_4$, the calculated lengths of its interatomic bonds are as follows: Cd-S, 2.52Å; Ga^2-S, 2.29Å; Ga^1-S, 2.32Å; also the fundamental lattice parameters are a = 5.564 ± 0.005 A and c = 10.05 ± 0.01Å.[1] It should be noted if the vacancies of cadmium are treated as atoms of zero valence, in accordance with what is known as the Grimms-Sommerfeld rule for tetrahedral phases, the number of valence electrons per atom of this compound is four.[1]

$CdGa_2S_4$ and $CdGa_2Se_4$ are of interest primarily because of their anisotropic (birefringent) behavior. For both polarizations ($\vec{E} \parallel \vec{C}$ and $\vec{E} \perp \vec{C}$), both materials show reflection peaks at 3.58 and 2.55 eV (near UV and visible). Further, $CdGa_2S_4$ possesses a reflection peak at 4.76 eV and $CdGa_2Se_4$ has two, one at 3.87 eV and one at 4.19 eV (which distinguishes each material). These peaks are due to transitions allowed due to the nature of the spin-orbit interaction.[2,3] Figures 2 and 3 show the reflection spectra for both polarizations for both substances.[4]

Reference 1 presents a discussion of the infrared reflection spectra for $CdGa_2S_4$. There are five vibrations for each polarization. Figure 4 shows the infrared reflectance from about $50cm^{-1}$ to $1000cm^{-1}$ (10µm). From this data it is possible to determine the complex dielectric function $\epsilon(\omega) = \epsilon_1(\omega) + i\epsilon_2(\omega)$ using the well known Kramers-Kronig method. From $\epsilon(\omega)$ it is possible to determine the frequencies of the TO and LO vibration modes in the crystal lattice. For $\vec{E} \parallel \vec{C}$ polarization, the greatest oscillator strengths (for this

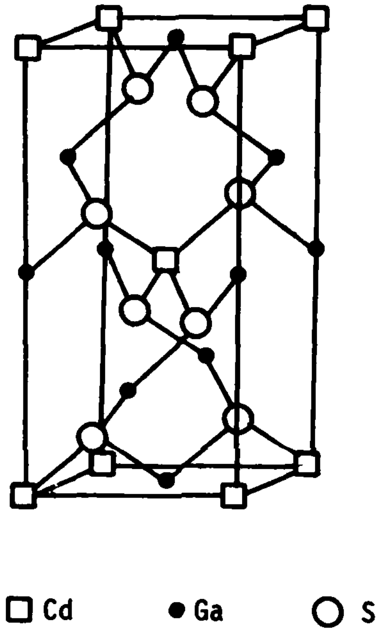

Figure 1. Structure of $CdGa_2S_4$.

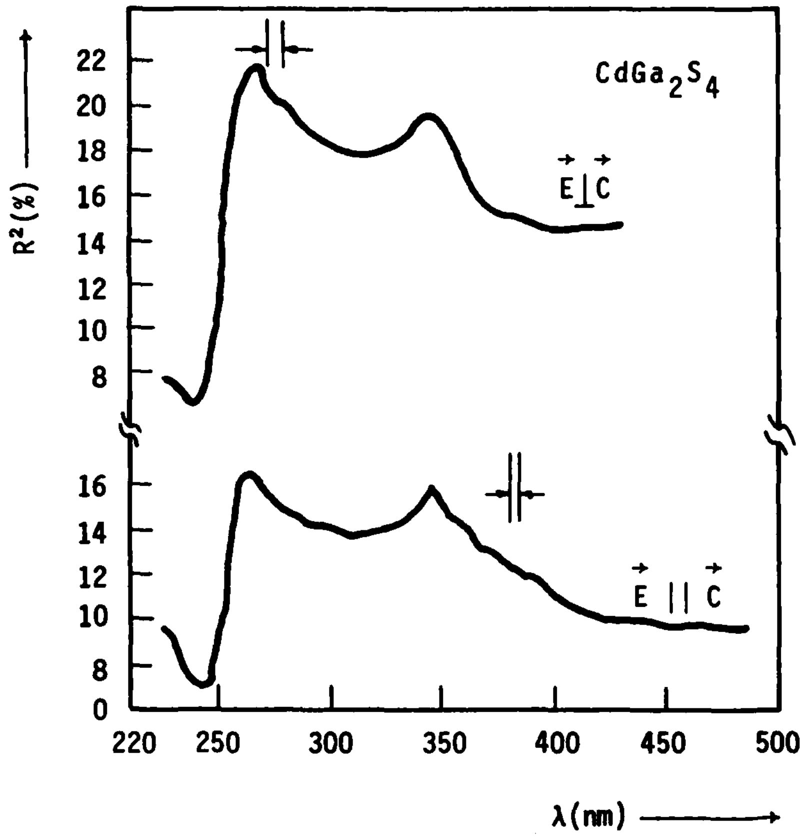

Figure 2. Spectrum of twofold reflection for CdGa$_2$S$_4$ in polarized light.

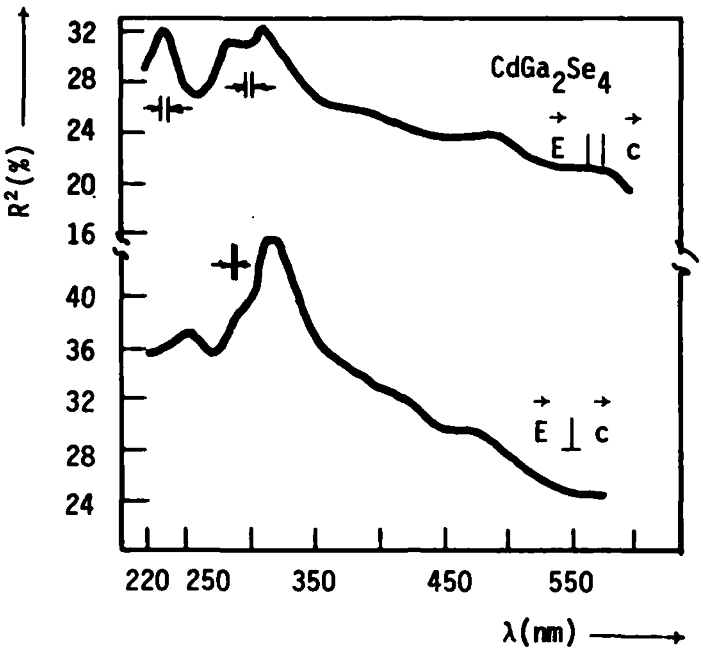

Figure 3. Spectrum of twofold reflection of $CdGa_2Se_4$ in polarized light.

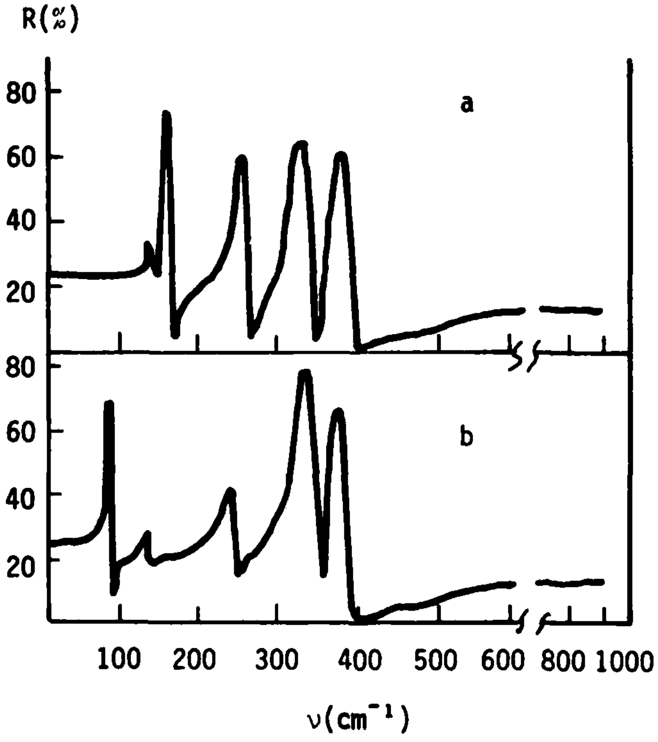

Figure 4. Infrared reflection spectra of $CdGa_2S_4$: (a) $\vec{E} \parallel \vec{c}$; (b) $\vec{E} \perp \vec{c}$.

lattice vibration) are at 162, 254, and 323 cm^{-1}. These can be used to calculate the static permittivity value for the substance. For $\vec{E} \perp \vec{C}$ polarization, the strongest oscillators are at 84 and 324 cm^{-1}.[5]

The Lydane-Sachs-Teller relation:

$$\frac{\varepsilon_0}{\varepsilon_\infty} = \sum_{i=1}^{n} \frac{\nu_{LO}}{\nu_{TO}}^{2}$$

can be used to verify the values of ε_0 and ε_∞ which for $CdGa_2S_4$ are $\varepsilon_0 = 8.76$, $\varepsilon_\infty = 1.04$ for $E \parallel c$, and are $\varepsilon_0 = 8.54$, $\varepsilon_\infty = 4.64$ for $\vec{E} \perp \vec{c}$.[1]

Figure 5 shows the permittivity dispersion of $CdGa_2S_4$ for each polarization.[1] We have been unable to find any literature on the behavior of either material in the infrared from about 10μm to the visible. However, from Figure 4 it may be inferred that there are no Restrahlen bands beyond 400 cm^{-1} (25μm). The reflectivity for both polarizations appears to be flat; this is very similar to other semiconductors such as silver sulfide in the low temperature phase (as well as MnS). We have been unable to locate significant information alluding to temperature dependence of the optical properties or even the presence of a phase transition to a metallic state.

REFERENCES ($CdGa_2S_4$)

1. L.M. Suslikov. et.al., Opt. Spectrosc (USSR), 48, (4), 436 (1980).
2. G.B. Abdullaev, et.al., Phys. Stat. Sol. (b) 54, K115 (1972).
3. G.B. Abdullaev, et.al., Fiz. Tekh. Poluprov, 23, 235 (1973).
4. A.S. Poplavnoi, et.al., Izv. Vuzov. Ser. Fiz. 11, (1969).
5. E.A. Vinogradov and L.K Vodopyanov., Fiz. Tverd. Tela. (Leningrad) 17, 3161 (1975) (Sov. Phys. Solid State 17, 2088 (1975).

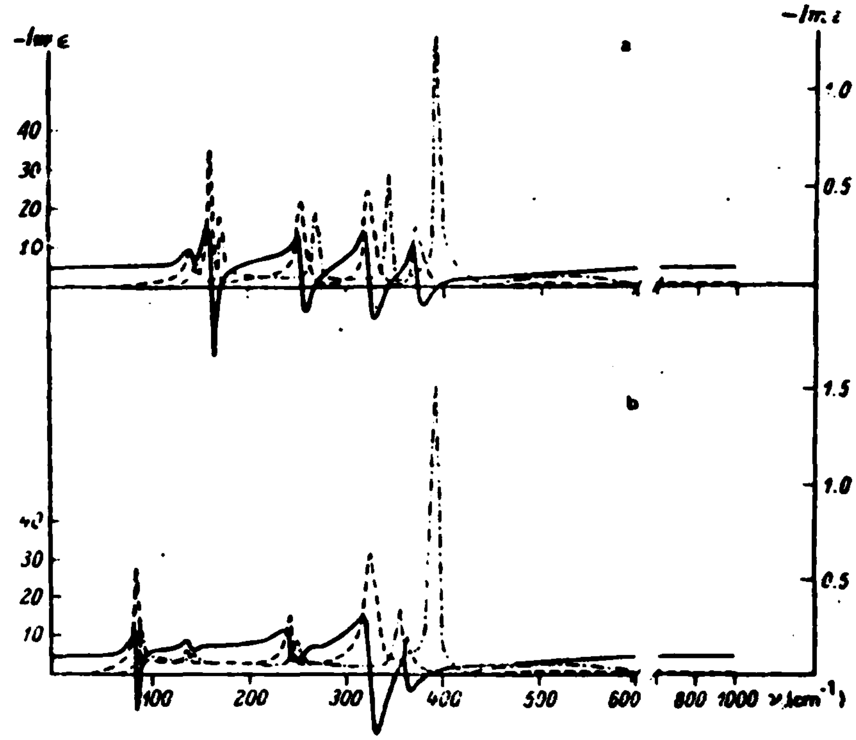

Figure 5. Permittivity dispersion of $CdGa_2S_4$ for E || c (a) and E ⊥ c (b). Solid line — $\varepsilon_\perp(\nu)$; dashed line --- $\varepsilon_2(\nu)$; dot-dash line -·- $\mathrm{Im}\left[-\varepsilon^{-1}(\nu)\right]$.

CdSe

Cadmium Monoselenide

Cadmium selenide is a metal-nonmetal phase transition material; it is a II-VI compound. Single crystals of CdSe with a chromium impurity can be prepared via the well known Bridgman technique. The chromium density can be determined using Hall effect measurements.[1]

Both zincblende and wurtzite forms of CdSe are known. Crystals grown at high temperature possess the wurtzite structure; the zincblende structure is obtained from room temperature growing methods. For the former case, there appears to be considerable variation in the measured lattice constants which suggests that there may be impurities due to contamination or stacking faults within the material. It has been determined that $a = 6.052Å$ for the zincblende form of CdSe.[2] The cubic form of CdSe is metastable and partial conversion to a hexagonal form takes place upon heating at 130°C; the transformation is complete by 700°C over a span of 18 hours.[3]

Very little is known about the electrical properties of CdSe. It is similar in behavior to CdS with a smaller electron effective mass, larger mobility, and smaller piezoelectric coupling.[4] The electron effective mass has been determined from the Zeeman splitting of exciton lines, and it is $m^* = 0.13\ m_0$ where m_0 is the electron rest mass.[5] This value was subsequently confirmed by Dolega who measured the dependence of the thermoelectric power on carrier concentration.[6] Optical reflectivity measurements in the infrared suggest that $m^* = 0.15 \pm 0.01\ m_0$ (this is due to free carriers).[7] The optical measurements seem to indicate that m^* possesses an anisotropic behavior. CdSe is like CdS in that it is always n-type.[4]

The room temperatures carrier concentration is quite low, around $2 \times 10^{16}\ cm^{-3}$.[8] By heat treating CdSe in a selenium vapor and obtaining single crystals, this figure has been increased to around $3.6 \times 10^{-17}\ cm^{-3}$ with a mobility of 580 cm^2/V-sec. For holes, it was found that $\mu_H = 50\ cm^2/V$-sec (hole mobility), and there is a trap density of $10^{11}\ cm^{-3}$.

A first-order phase transition has been reported for CdSe (first-order because of symmetry requirements that must be met if the phase transition is to be of second-order).[4] This transition is from the zincblende to the wurtzite type structure. It is still not known if this phase transition is reversible. For CdSe, there is an additional metal-nonmetal transition at very low temperature, around 25°K.[1] This phase transition is deduced from low temperature resistivity and Hall coefficient studies.

Figure 1 shows the room temperature reflectivity of CdSe.[9] Table 1 gives various parameters for CdSe. Further details concerning these data can be found in reference 1.

TABLE 1
PARAMETERS OF CdSe

$m^* = 0.13\ m_0$

$\varepsilon_0 = 9.4$

$C_1 = 7.4 \times 10^{11}$ cgs units

$E_1 = 3.7\text{eV}$

$\rho = 5.8\ \text{gm cm}^{-3}$

$\varepsilon_\infty = 6.1$

$h\omega_1 = 0.027\text{eV}$

The nature of the phase transition of CdSe is not well understood; we have been unable to find literature discussing how the optical properties change across this boundary, which is nevertheless at a very low temperature.

REFERENCES (CdSe)

1. D.M. Finlayson, et.al., Phil. Mag., Vol. **B39**, No. 3, 253 (1979).
2. A.D. Stuckes and G. Farrell, J. Phys. Chem. Solids, **25**, 477 (1964).
3. A. Pashinkin and L. Kovba, Soviet Phys. - Cryst. **7**, 247 (1962).
4. M. Aven and J.S. Preuer, eds. *Physics and Chemistry of II-VI Compounds*, North-Hollard, Amsterdam, 1967.
5. R. Wheeler and J. Dimmock, Phys. Rev. **125**, 1805 (1962).
6. U. Dolega and Z. Naturf, **18a**, 809 (1963).
7. S. Kubo and M. Onuki, J. Phys. Soc. Japan, **20**, 1280 (1965).
8. M. Itakura and H. Toyoda, Japan J. Appl. Phys. **4**, 560 (1965).
9. M. Cardona and G. Harbeke, Phys. Rev. **137**, A1467 (1965).

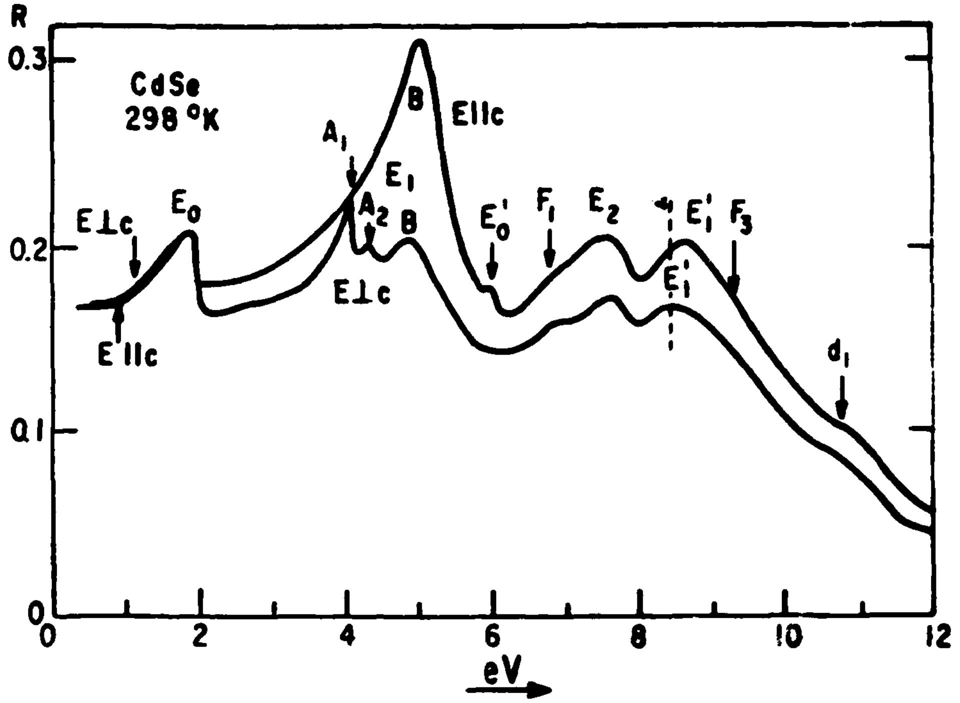

Figure 1. Reflectance of CdSe at room temperature.

CoS_2

Cobalt Disulfide

Cobalt disulfide (CoS_2) is a crystalline material possessing the pyrite structure (that is, like FeS_2) and is known to be a ferromagnet with a metallic conduction. The Curie temperature is at 120°K. Single crystals of CoS_2 can be grown by the chemical vapor transport technique using chlorine as a transporting agent.[1] Crystals several millimeters on a side can be readily grown.

CoS_2 is not known to be a phase transition material. No evidence of abrupt changes in the resistivity or optical properties with temperatures are known. Concerning the latter, only limited data exists from 2.48µm to 0.248µm (near UV). It has been reported that in the vicinity of 0.8ev (=.992µm) a slight variation in the reflectivity does occur.[2] No quantitative measurements of this variation is given, however.

For completeness, we shall present known experimental measurements of the optical properties of CoS_2.[2] These published data are of very recent origin and attest to the relative lack of knowledge of this material. Figure 1 shows the reflectivity from 2.48µm (0.5eV) to 0.248µm (5eV), or from the near IR, through the visible, to the near UV. The variations seen may be described in terms of phonon modes within the lattice. From this single curve, theoretical analysis can extract unique curves for the index of refraction (n), the coefficient of extinction (k), and the real and imaginary parts of the dielectric constant (ε' and ε''). The significance of ε' and ε'' will be discussed shortly.

Figure 2 shows n and k in the same wavelength range. To obtain n and k from R (measured for normal incidence), the Kramers-Kronig method is used. Data for R was necessarily extrapolated into the IR via a linear fit and into the far UV and VUV from known (unpublished) data. From n and k, we can derive ε' and ε'' using the relations

$$\varepsilon' = n^2 - k^2,$$

$$\varepsilon'' = 2nk.$$

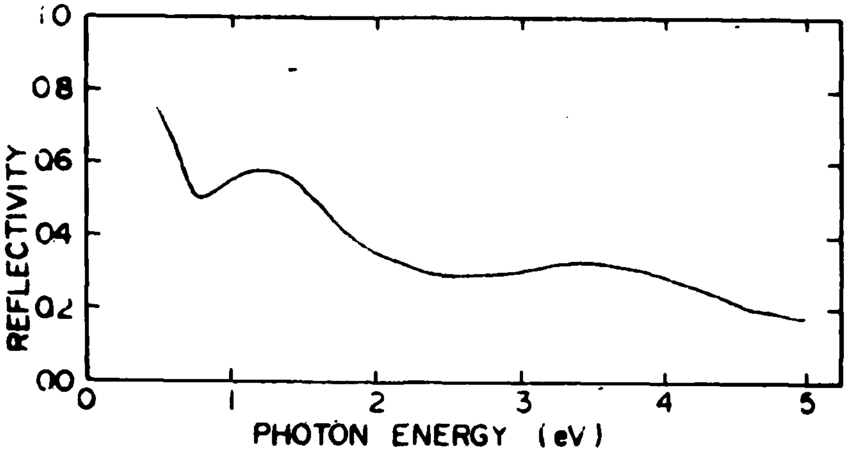

Figure 1. Reflectivity spectrum of a CoS_2 single crystal at room temperature.

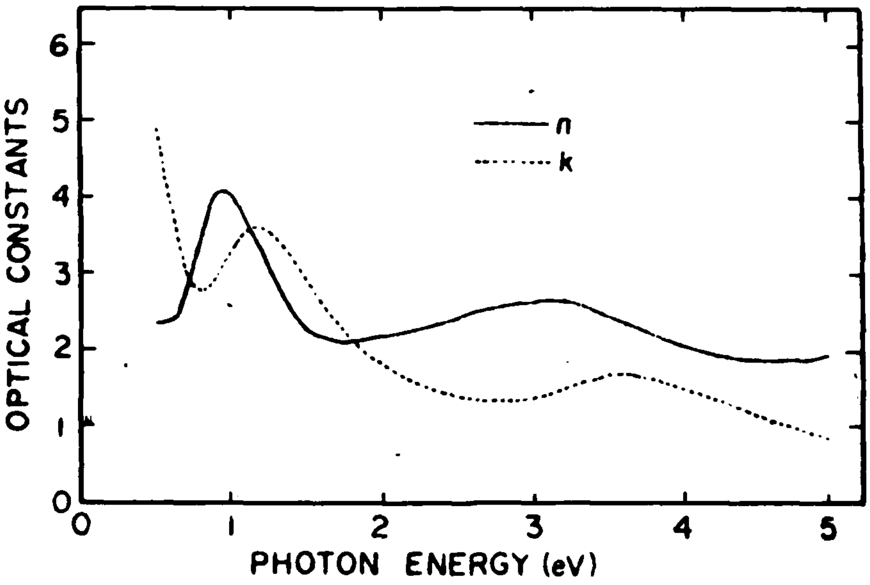

Figure 2. Spectra of optical constants n and k of CoS_2 deduced from the reflectivity spectrum. Solid curve: — n. Dotted curve: ···· k.

These are shown in Figure 3. The significance of ε' is that the first zero (around 0.8eV) can be associated with a free-electron plasma frequency of the material. That is, the plasma frequency, the concentration of free electrons (n_f), and effective dielectric constant ($\varepsilon_{eff}(0)$) are all related by the equation

$$\omega_p^2 = \frac{4\pi\, n_f e^2}{m\, \varepsilon_{eff}(0)} .$$

Here $\varepsilon_{eff}(0)$ can be evaluated using the sum rule

$$\varepsilon_{eff}(0) = 1 + \frac{2}{\pi} \int_0^\infty \frac{\varepsilon''(\omega')}{\omega'}\, d\omega'$$

and $\varepsilon_{eff}(0) = 25.50$. Therefore, computing ω_p from the zero crossing in ε' yields $n_f = 1.17 \times 10^{22}\ \text{cm}^{-3}$.

Knowing n_f is important in order to model the IR properties of CoS_2 with a Drude model. Drude model predictions and actual measurements of IR reflectivity can be useful to not only characterize a material, but to infer its possible phase transition properties.

Finally, the absorption spectra of CoS_2 is shown in Figure 4.[2]

CoS_2 is not known to undergo changes in R, n, or k with temperature. CoS_2 appears to be a possible candidate for further research since it has been neglected until fairly recently -- its optical properties are still not understood.

REFERENCES (CoS_2)

1. R.J. Bouchard, J. Cryst. Growth, 2, 40 (1968).
2. K. Sato and T. Teranishia, J. Phys. Soc. Japan, 50 2069 (1981).

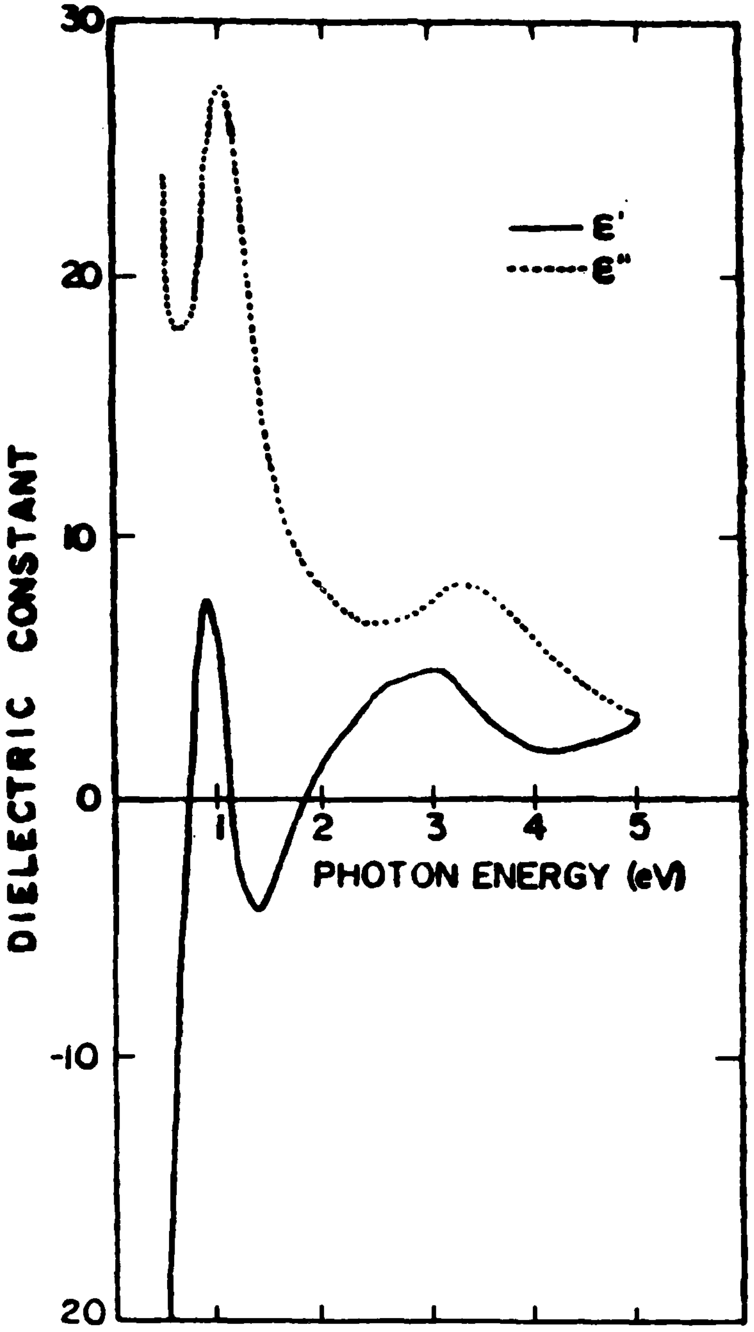

Figure 3. Spectra of the dielectric constant of CoS_2. Solid curve: —— real part (ε′). Dotted curve: ····· imaginary part (ε").

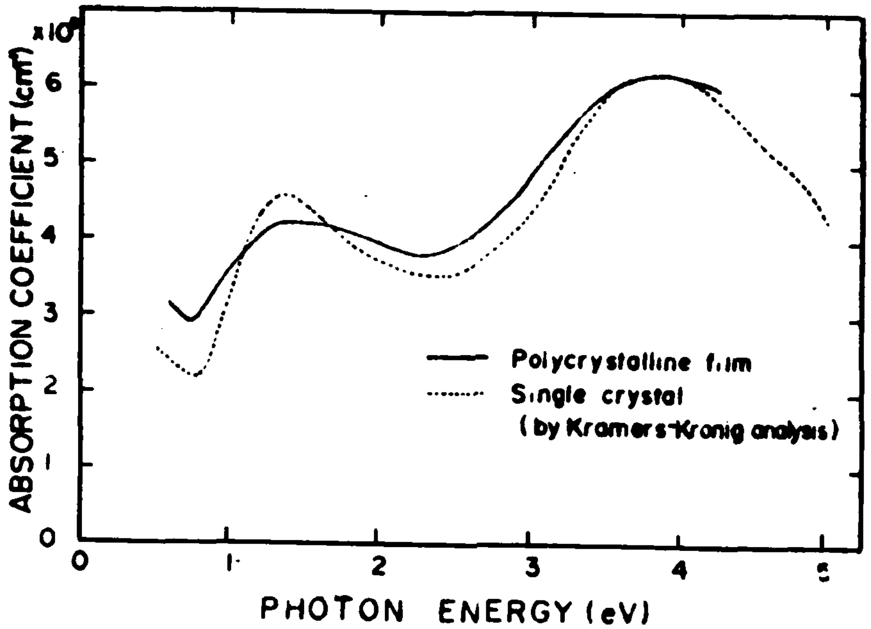

Figure 4. Absorption spectra of CoS_2; Solid curve: —— that of a thin polycrystalline film measured directly (Thickness = 450 Å). Dotted curve: ····· that calculated from the reflectivity spectrum of a single crystal.

CrS

Chromium Monosulfide

CrS and $Cr_{1-x}S$ ($0 < x < 0.12$) have been studied fairly extensively; these compounds possess NiAs superstructures. CrS itself can be prepared as a monoclinic crystal using the flux method.[1] It should be pointed out that the exact stoichiometric CrS is extremely difficult to prepare, and there is a question concerning whether or not it has been achieved.[2]

The electrical properties of CrS_x with $1.00 < x < 1.20$ have been studied.[3] The conductivity, σ (in $ohm^{-1}\ cm^{-1}$), has been measured from 300°C to 500°C for x = 1.0, 1.08, 1.14 and 1.17. Figure 1 illustrates the temperature dependence of electrical conduction. The material behaves as a p-type semiconductor for $x < 1.12$ and as a metallic conductor for $x > 1.13$. That is, at high temperature above about 500°C, CrS_x for all x in the above range behaves as a good metallic conductor whereas for lower temperatures CrS_x behaves differently as x varies across x = 1.12. The change in conductivity from 300°C to 500°C can be attributed to a structural transition from the monoclinic to the NiAs type structure. We should point out that if pressure is applied it may be possible to switch the stoichiometry across the transition at x = 1.12. A phase transition is known to occur for $CrS_{1.42}$.[4]

Before continuing with the phase transition properties for stoichiometric CrS, we shall briefly discuss its crystal structure.[5] In Figure 2 we see the NiAs crystal lattice and its relation to the CrS lattice. The small circles represent metal atoms, the larger circles are anions. In each diagram the environments of one metal atom and of one anion are given. Figure 2a is the ideal NiAs structure. Here the metals are octahedrally surrounded by six anions (in this case As), the anions by six metals in a trigonal prism. The broken lines indicate the conventional unit cell. For CrS, the Cr is surrounded by four S atoms in a rectangle while two more S atoms at larger distances (broken lines) complete an elongated octahedron. Similarly, the S environment may be regarded either as a slanting trigonal prism or as a distorted tetrahedron. CrS possesses the following lattice constants:[5]

$a = 3.826\text{Å}$

$b = 5.913\text{Å}$

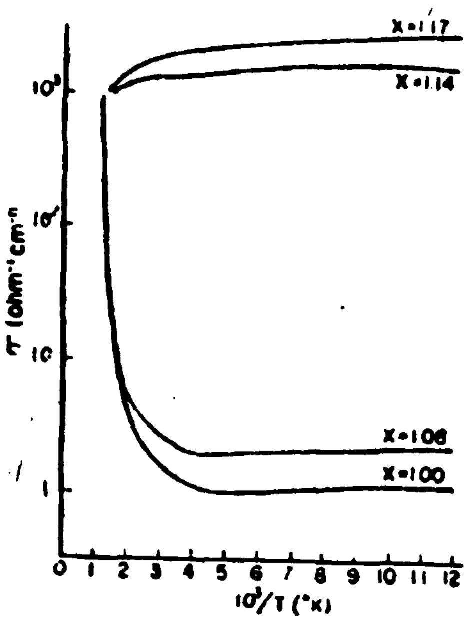

Figure 1. Electrical conductivity of CrS_x as a function of temperature.

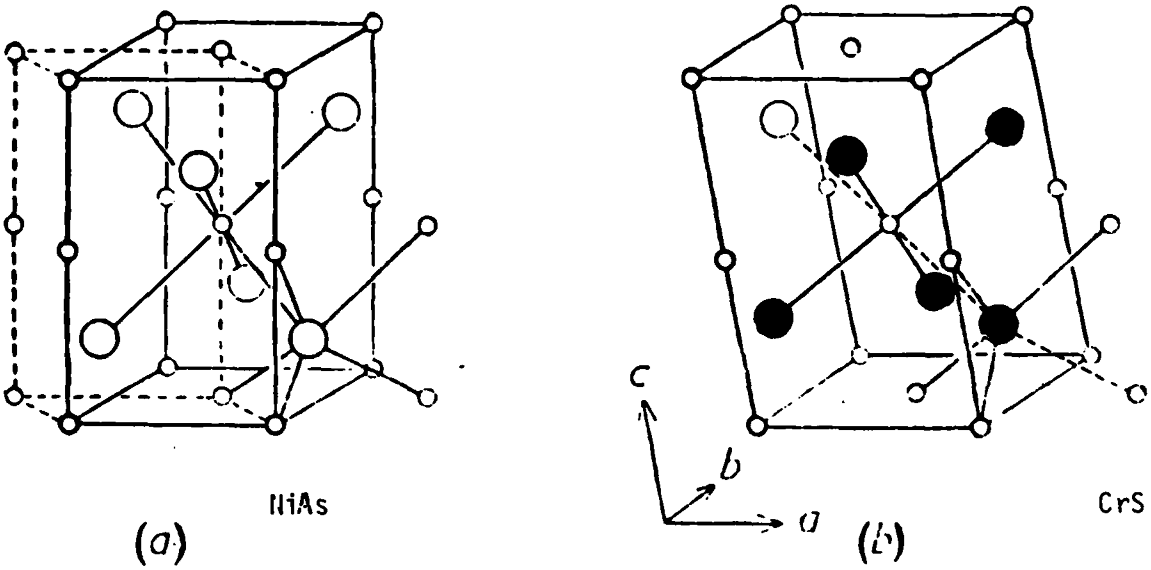

Figure 2. Crystal lattice structure.

$c = 6.089 Å$

$\beta = 101° 36'$

ρ = density = 4.08 g cm^{-3} (ref. 6)

We should add that whereby some investigators believe that stoichiometric CrS is difficult to fabricate, pure CrS has been made (as reported in Ref. 5) in 1899 by Mourlot.[6] More recent studies showed that he actually prepared $CrS_{0.97}$ and that pure CrS should have a density of 4.091 g cm^{-3}.

Concerning the specific heat, shown in Figure 3, for $CrS_{1.17}$ there are glitches near -130°C and 20°C, which may be indicative of a structural phase transition.[7]

CrS does possess a pressure induced phase transition from a semiconducting to a metallic state.[8] CrSe also has the same property. The resistivities for CrS and CrSe were observed through the pressure transition using the four-probe method. Measurements have been made up to 70 kbar, and it was shown that this phase transition is correlated with a monoclinic-to-hexagonal (NiAs) structural transition. In Figure 4 the experimental assembly is shown.

In Figure 5 we see the conductivity measurements for CrS. Note the similarity in behavior to Figure 1. In Figure 6 is given a resistance versus pressure plot. The change in material state is not abrupt as with some sulfides such as SmS, but is quite gradual. The transition pressure is in the vicinity of 24 kbars at ambient temperature. It is reported that there is a phase change at 620°K at atmospheric pressures. According to Reference 8, the mechanism for the semiconductor-to-metal transition in CrS is understood to be due to a change in the electronic structure of the $3d^4$ electron configuration from a nondegenerate to a doubly degenerate state as the structure changed from monoclinic to hexagonal symmetry. A similar transition in CrSe is not well understood.

We were unable to locate any articles on the optical properties of CrS, and it is likely that no measurements have been made to date. Further, we do not see the existence of a hysteresis effect in the resistivity measurements - a normal occurence for materials that switch in optical properties; though the

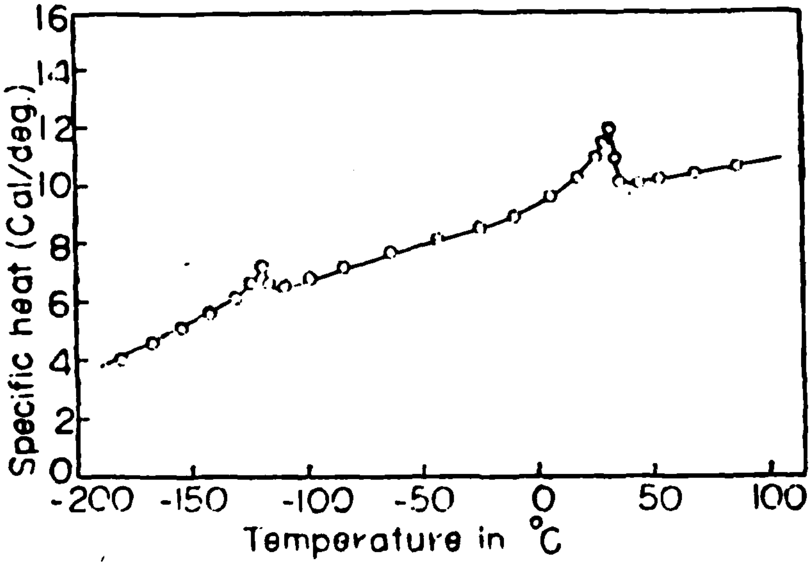

Figure 3. The curve of the specific heat versus temperature of $CrS_{1.17}$.

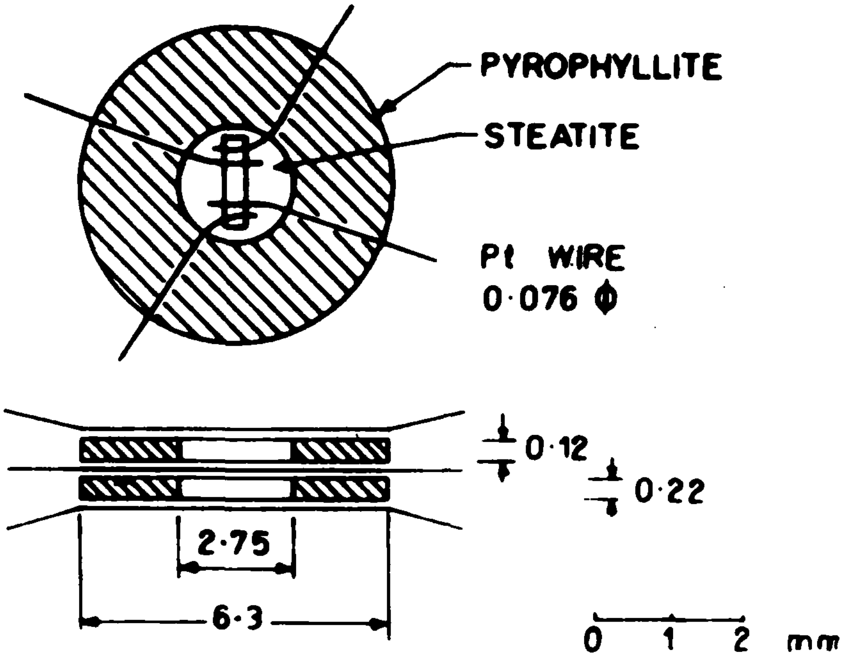

Figure 4. 4-Probe Resistance Cell.

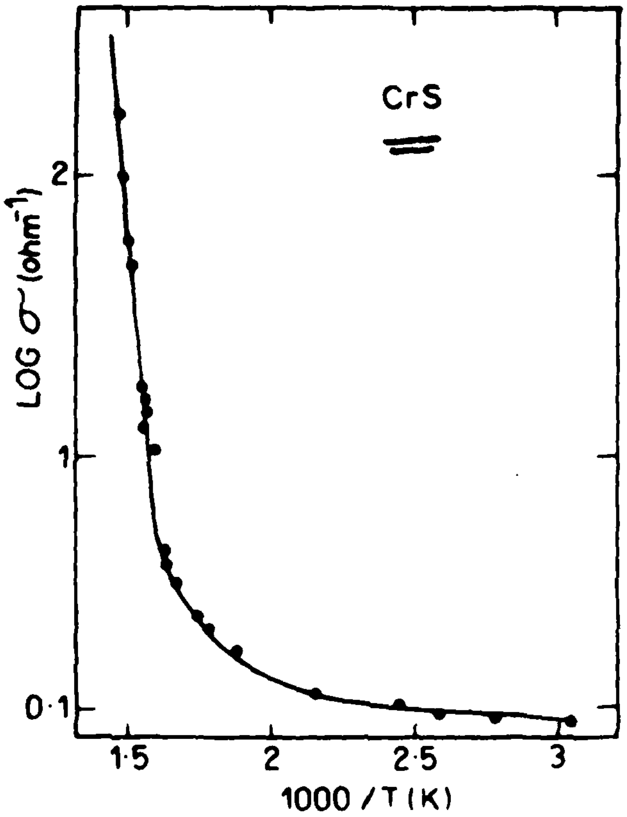

Figure 5. Electrical conductivity of CrS as a function of temperature.

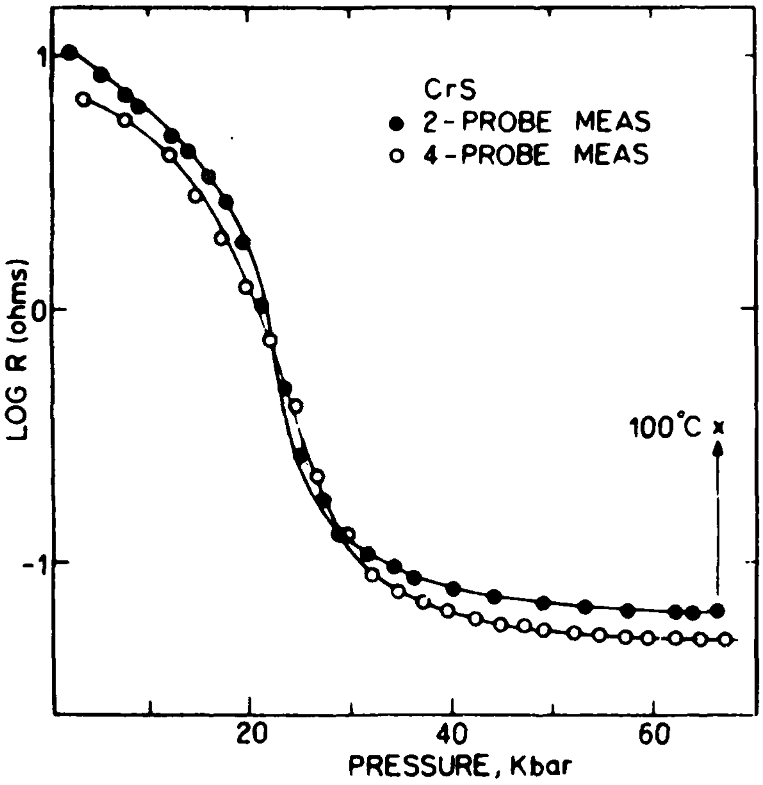

Figure 6. Resistance vs. pressure for CrS.

existence of a hysteric resistivity curve does not necessarily imply a change in optical constants.

REFERENCES (CrS)

1. T.J.A. Popus and C.F. van Bruggen, J. Inorg. Nucl. Chem. 31, 73 (1969).
2. C.N.R. Rao and K.P.R. Pisharody, Prog. in Solid State Chem., 10, 207 (1975).
3. T. Kamigaichi and K. Masumoto, J. Phys. Soc. Japan, 15, 1960 (1960).
4. K. Igaki, et.al., J. Phys. Soc. Japan, 31, 1424 (1971).
5. F. Jellinek, Acta Cryst. 10, 620 (1957).
6. A. Mourlet, Ann. Chem. Phys. (7) 17, 543 (1899).
7. M. Yuzuri, et.al., J. Phys. Soc. Japan, 12 385 (1957).
8. D.K. Joshi, et.al., Mat. Res. Bull. 12, 1111 (1977).

Cu_2S

Copper Sulfide

Copper sulfide occurs naturally in four distinct room temperature phases.[1]

- Cu_2S (chalcocite)
- $Cu_{1.9}S$ (djurelite)
- $Cu_{1.8}S$ (digenite)
- CuS (covellite)

An argument has been presented that non stoichiometric phases $Cu_{2-\delta}S$ are mixtures of Cu_2S and CuS in varying ratio.[2]

At about 100°C copper sulfide undergoes a crystallographic phase transition. The crystal structure in the low temperature phase is orthorhombic and the high temperature phase is a mixture of hexagonal and cubic crystal structures.[3] From the temperature dependence of conductivity, it is observed that $Cu_{1.8}S$ and $Cu_{1.96}S$ undergo phase transition at 90°C and 93°C respectively.[4] Transition temperature for Cu_2S rises from 98°C to 108°C as the composition approaches the exact stoichiometry. Phase transition of high conductivity Cu_2S is sluggish, while that of the low conductivity Cu_2S is very fast.

The electrical properties of Cu_2S and several other nonstoichiometric copper sulfides have been intensively studied by several investigators. Copper sulfide shows a mixed conductor behavior as its conductivity is partly ionic and partly electronic. In the copper deficient copper sulfides, the electronic contribution to conductivity arises from hole carriers introduced by missing copper atoms. For any stoichiometry in the range $(2-\delta) = 1.8$ to 2, the conductivity is not strongly dependent on temperature, except at the phase transition temperature (≈ 100°C) at which a discontinuous drop in conductivity occurs of typically less than an order of magnitude. Beyond the phase transition temperature, the conductivity though does vary over about six orders of magnitude from $Cu_{1.8}S$ to Cu_2S. Figure 1 shows the variation in the conductivity as a function temperature and stoichiometry; S increases from

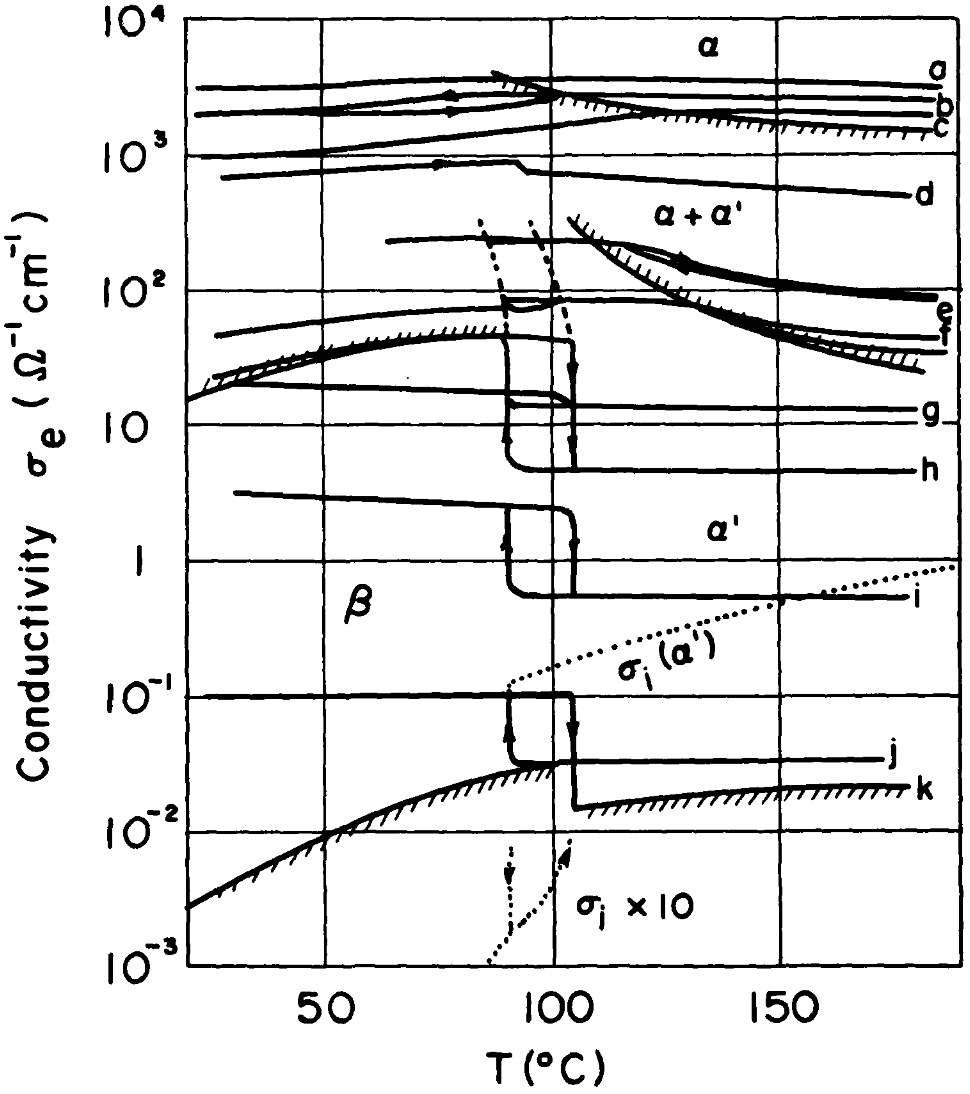

Fig. 1 σ_e vs. T FOR $Cu_{2-\delta}S$ CORRESPONDING TO FIGURE 2.

bottom to the top of the figure. Table 1 gives a summary of a few important properties and their variation with stoichiometry for different copper sulfides. An effective mass of $m^* = 2.1$ has been assumed for all phases.

TABLE 1

Properties of Cu_2S as a Function of Stoichiometry

Phase β	Stoichiometry	Conductivity $\Omega^{-1}Cm^{-1}$	Mobility $Cm^2/v\text{-}s$	Carrier Concentration Cm^{-3}	Plasma Edge λ_p m	Band Gap eV
Digenite	$Cu_{1.8}S$	2300	0.51	2.8×10^{21}	0.71	2.3
Djurelite	$Cu_{1.96}S$	350	$\approx 10^{-2}$	$\approx 10^{22}$	0.38	
Chalcocite	Cu_2S	150	3.6	2.6×10^{18}	7.4	1.0

Based on the data summarized in Table 1, the carrier concentration increases by nearly 3 orders of magnitude for a relatively small change in Cu_2S to $Cu_{1.96}S$ theoretically causing the plasma edge to shift from 6.55μm to 0.334μm. Since the mobility is low, it is expected that the plasma edge is not sharp and an abrupt change in reflectivity is not expected at λ_p. The largest changes in optical properties are expected for relatively small changes in stoichiometry from Cu_2S.

Transmission data for different stoichiometry and different thicknesses of copper sulfide films are shown in Figure 2. Data for the absorption coefficient in the spectral region (0.5 to 1.24 microns) for these same films are shown in Figure 3. The high absorption indicated is most likely due to direct band transitions. Assuming band to band absorption, the band gap variation over the above range of stoichiometry is 1.85 eV (for $2-\delta = 1.89$) to 2.16 eV (for $2-\delta = 1.94$). The variation in band gap over the larger range of stoichiometry i.e., $(1.8 < 2-\delta < 2)$ has been reported to be between 1 and 2.6 eV. This large variation in band gap as a function of stoichiometry suggests a high degree of modulation achievable by absorption/transmission in the visible to very near IR region (0.5μm - 1.24μm). Figure 4 shows transmission and reflectivity curves for a different $Cu_{1.8}S$ film.

Layer	C_1	C_2	C_3	C_4	C_5
Thickness d (μm)	0.13	0.25	0.33	0.45	0.6
Resistivity p300k (Ωcm)	9×10^{-3}	2.5×10^{-2}	5×10^{-2}	3	2×10^{2}
Composition x	1.94	1.95	1.92	1.89	1.89
Optical gap E_g (eV)	2.16	2	2.08	1.93	1.85

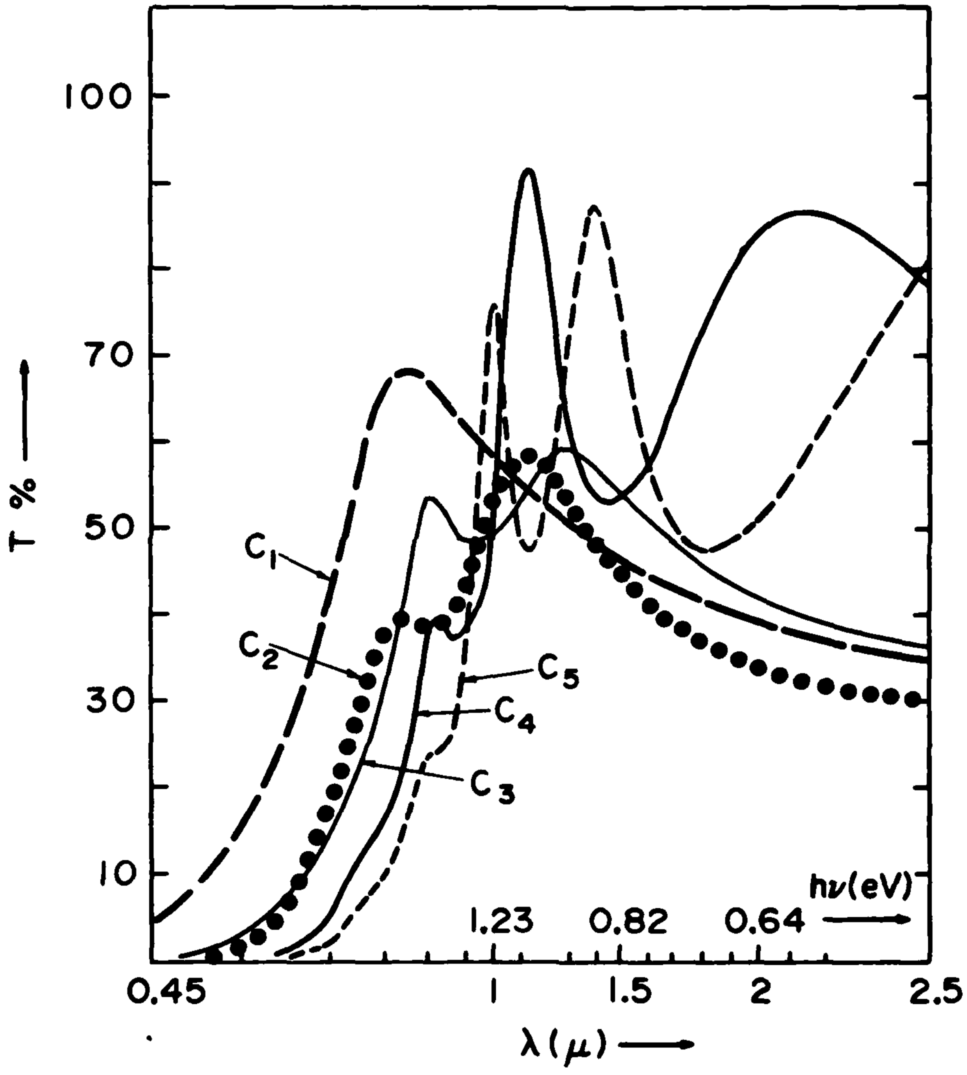

Fig. 2 TRANSMISSION VARIATION VS. WAVELENGTH FOR EVAPORATED Cu_xS LAYER OF DIFFERENT THICKNESSES AS TABULATED ABOVE

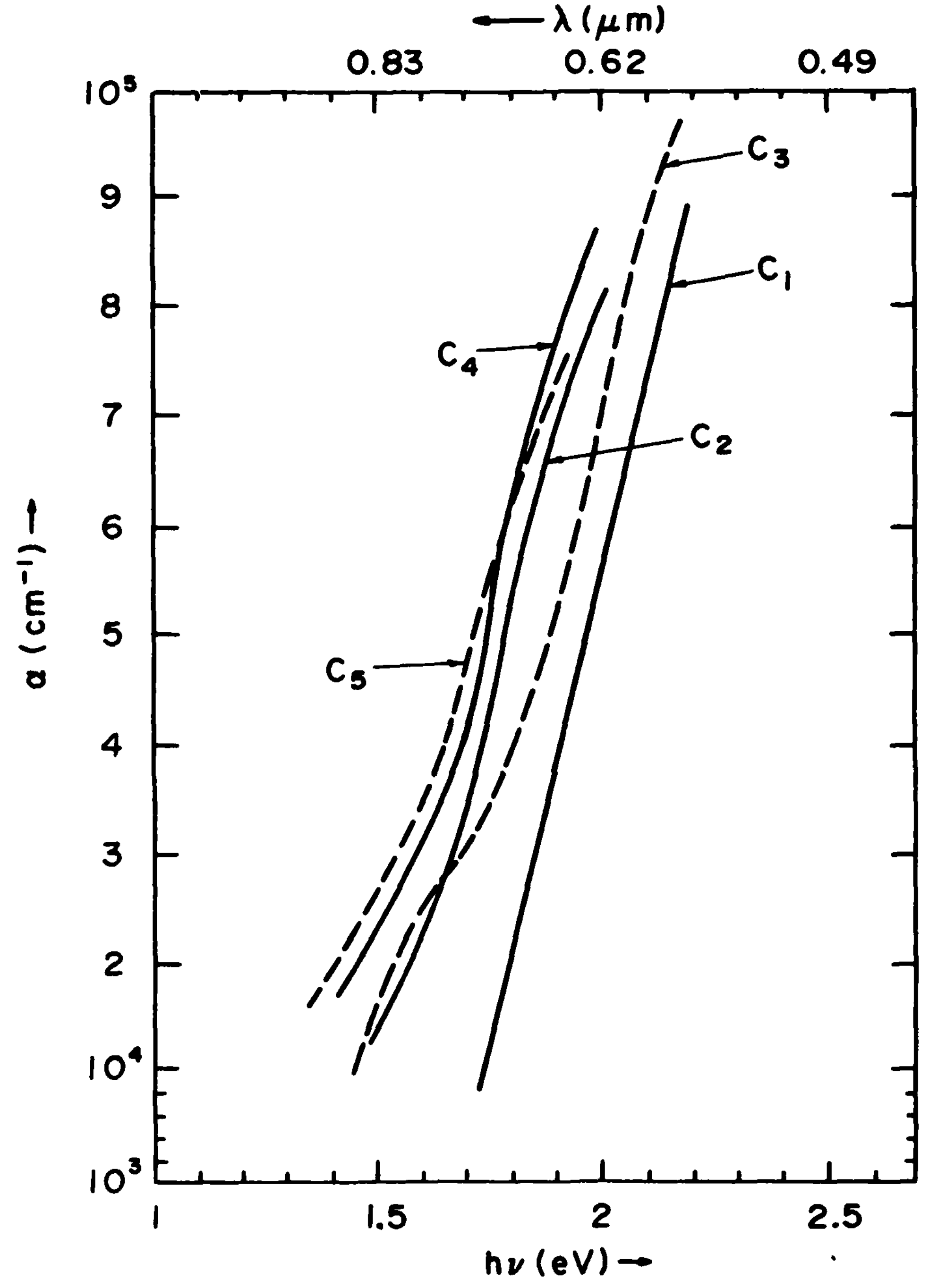

Fig. 3 ABSORPTION COEFFICIENT VS. PHOTON ENERGY

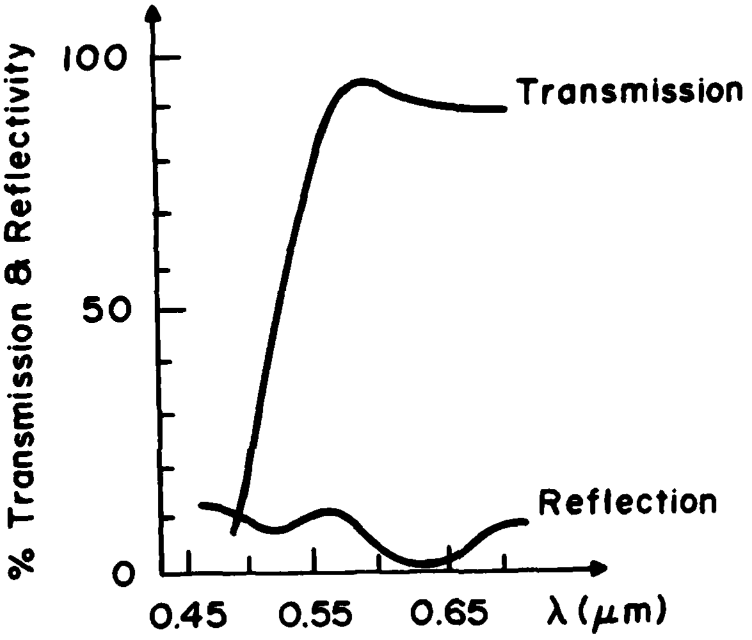

Fig. 4 TRANSMISSION AND REFLECTION FROM A $Cu_{1.8}S$ FILM

At longer wavelengths (1.25µm - 14.28µm) it has been observed that the absorption decreases with increasing wavelength and the reflectivity increases steadily from about 28% at 2.5 microns to 32% at 20 microns for Cu_2S.

The initial work carried out at IITRI consists of four phases: (1) thin film preparation, (2) characterization and determination of the stoichiometry, (3) investigations on the optical and electrical properties of the films as a function of temperature and applied electric field in the spectral regions of interest and (4) develop concepts for some useful devices in the light of the conclusions drawn from the above mentioned studies. Thin films were deposited on sapphire glass, or sodium chloride substrates heated to a temperature of 200-250°C. Three different techniques using $Cu_{1.8}S$ as the starting material have been employed for evaporation; namely, flash evaporation, thermal evaporation using a flat heater above the boat and finally the electron beam method. The first two techniques were most often used. The thickness of the sample was monitored using a quartz crystal oscillator. The substrates were placed at different heights with respect to the evaporation source. By so doing, the stoichiometry could be changed from sample to sample. The films deposited on hot substrates were annealed at the substrate temperature (250°C) for 4 to 6 hours and then cooled to room temperature. The film thicknesses varied from a few tenths of a micron to about 1.5µm. The films were deposited at a background pressure of 1×10^{-5} torr. The particle size of the copper sulfide powder used for evaporation is 100 mesh.

Transmission and reflectivity measurements were carried out initially in the spectral region 1-15µm. Since the plasma edge is lower than 2.5µm, we have concentrated our investigations mostly in the spectral region $0.5 < \lambda < 2.5\mu$. The measurements were taken in two steps: (1) the transmission and the reflectivity were measured at room temperature as a function of wavelength. The sample was then heated to 100°C and the transmission and the reflectivity measured again. (2) Starting from room temperature and selecting a fixed wavelength λ, the sample was heated gradually. There was a continuous change in reflectivity and transmission as the temperature changed from room temperature to about 100°C. Figures 5 and 6 show this interesting feature of the copper sulfide film and it is reasonable to expect that this effect will be useful for achieving a high degree of modulation by reflection/transmission from the copper sulfide films in the visible to very near IR region (0.5µm - 2.5µm).

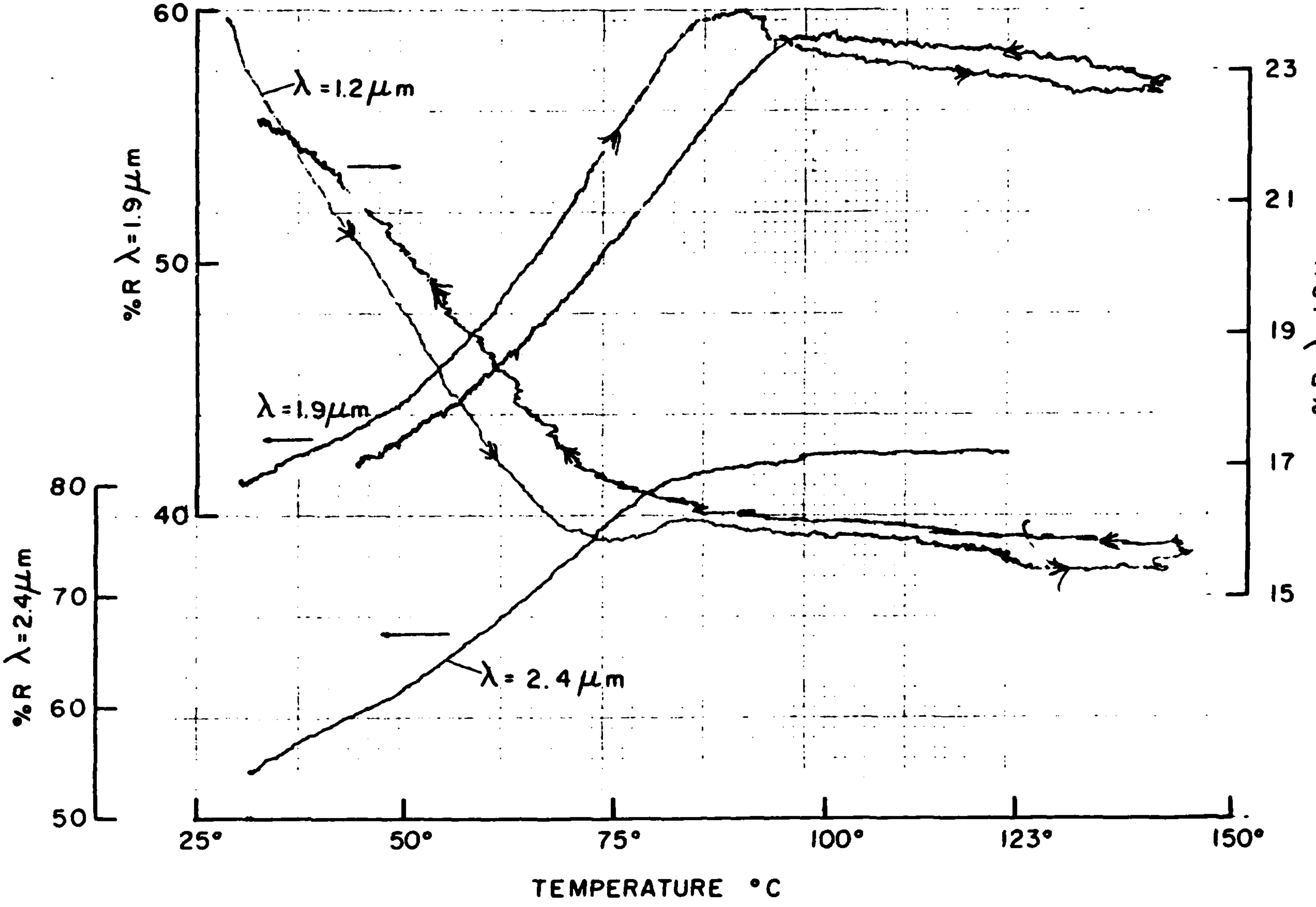

Fig. 5 TEMPERATURE DEPENDENCE OF REFLECTANCE OF A COPPER SULPHIDE FILM AT THREE DIFFERENT WAVELENGTHS

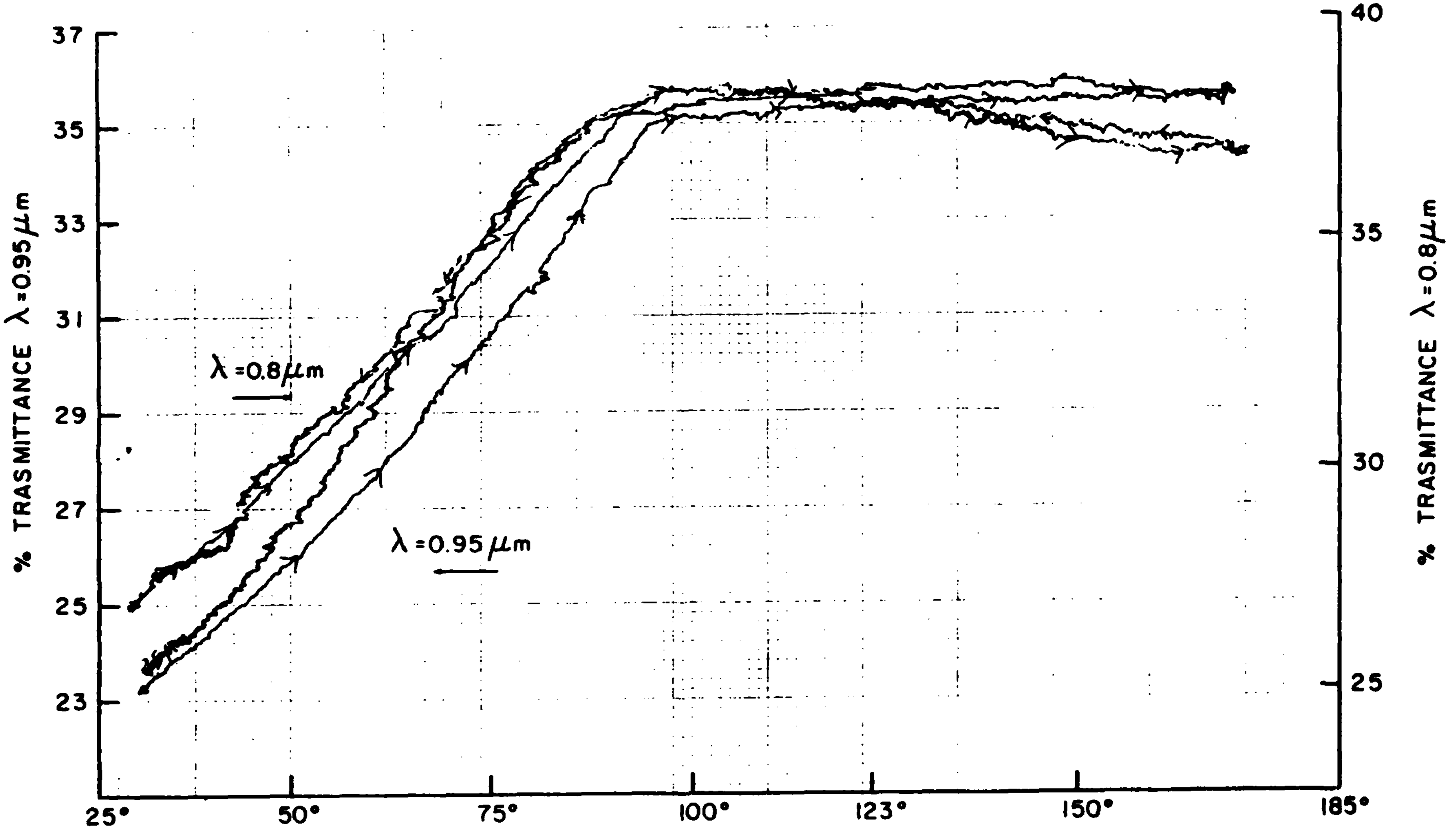

Fig. 6 TEMPERATURE DEPENDENCE OF TRANSMITTANCE OF A COPPER SULPHIDE FILM AT TWO DIFFERENT WAVELENGTHS

Experiments with the films have indicated that (1) copper ions can be electrically transported in and out of copper sulfide thin films, (2) the transmission and reflectivity of copper sulfide films changes substantially as a function of stoichiometry and (3) the refractive index in the very near IR changes as the material undergoes a thermal phase transition at about 100°C.

To validate that the stoichiometry of copper sulfide can be electrically varied, electrochemical titration measurements were made on two cells. The first cell consisted of pressed pellets of CuBr and Cu_2S sandwiched between a copper and platinum electrode. The second cell consisted of a copper sulfide film on a glass substrate mechanically held in contact on one end with a platinum electrode and at the other end a CuBr pellet. The cells were heated in a tube furnace to about 350°C and the cell EMF monitored after passing a fixed current through the cell for varying amounts of time. A dc power supply was connected across the cell and a thermocouple placed in contact with the cell. The current through the cell as a function of temperature, Figure 7, was obtained by applying the voltage across a series resistor and the thermocouple output to inputs of an x-y recorder. Measurements of cell EMF were made at a fixed temperature ($\approx$ 320°C) after passing fixed current through the cell for a measured amount of time. Measurements were made with the power supply circuit open. The cell EMF was found to be variable from zero millivolts to 0.02 millivolts and to be repetitively reversible by reversing the polarity of the power supply. The stoichiometry of the copper sulfide in the cell for a given EMF was determined by assuming zero millivolts for $x = 2.0$ and calculating ΔX from Faraday's law and measured values of current and time. The experimental configuration and general characteristics obtained are shown in Figure 7 and 8.

REFERENCES (Cu_2S)

1. Ramsdell, L.S. Amer. Mineral., 28, 404 (1943).
2. Ichimescu, A-, and G. Teo Dvescu. Bull, Inst. Polgtechnic Bucurestic XXIX, 4, 55 (1967).
3. Frueh, A.J., 2, Kristallogr., 110, 2 (1958).
4. P. Rahlfs, 2 Phys. Chem. B31, 157 (1935).

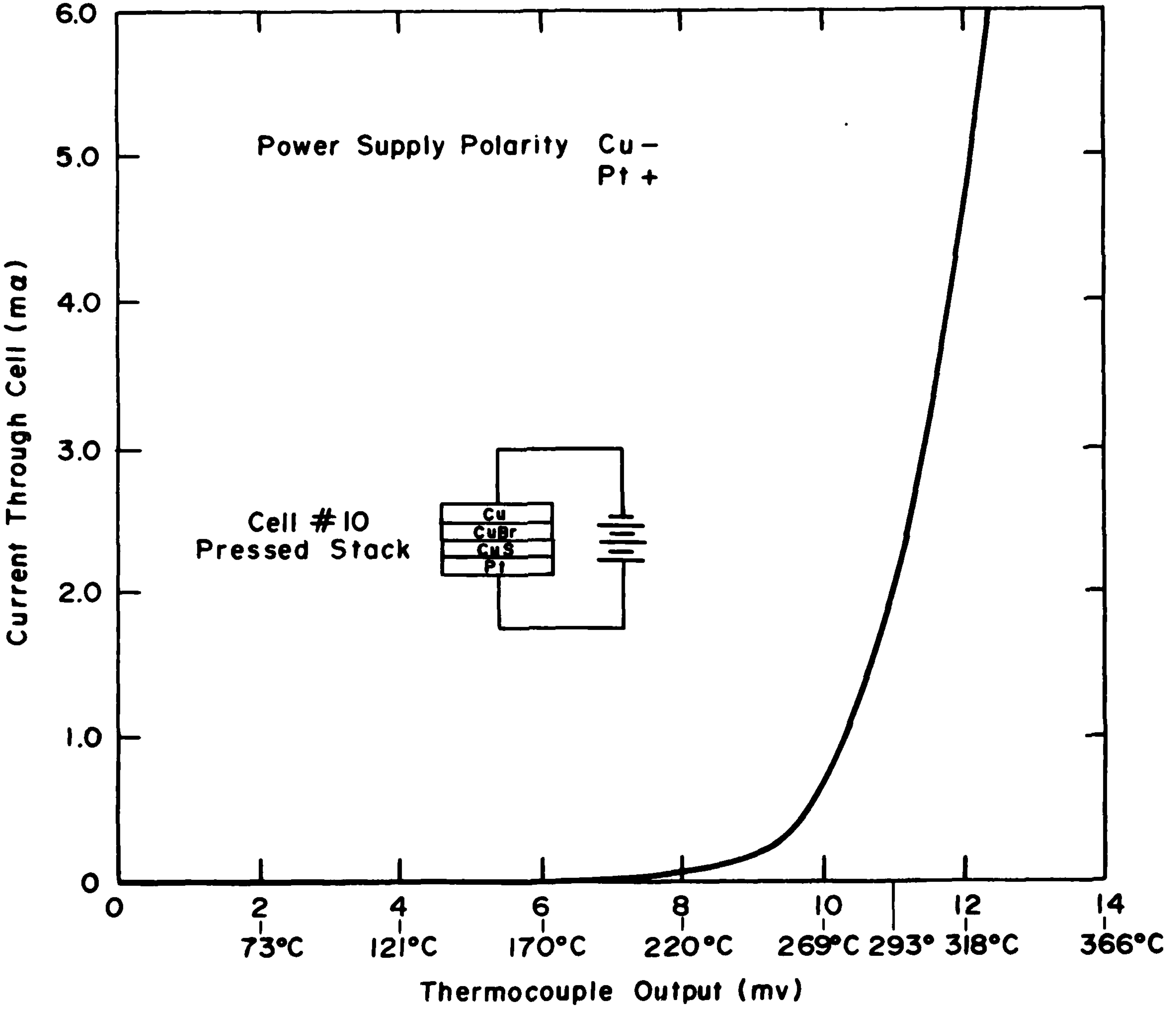

Fig. 7 CURRENT THRU CELL AS FUNCTION OF CELL TEMPERATURE

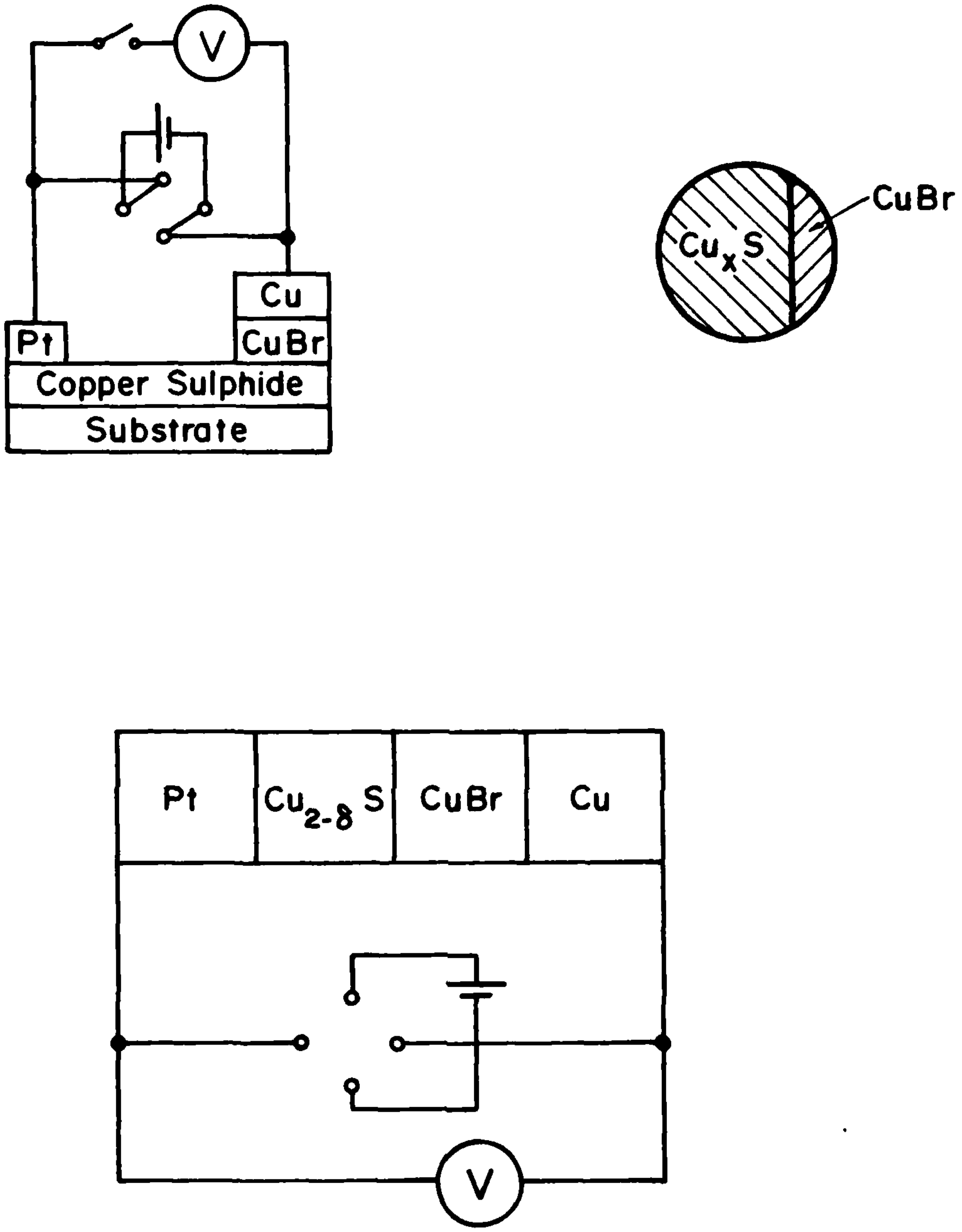

Fig. 8 GALVANIC CELL

Cu_2Se
Copper Selenide

Above 110°, Cu_2Se has a fcc lattice with a = 5.84Å; the low temperature modification has not been interpreted.[1] The low temperature form of $Cu_{1.96}Se$ is tetragonal with a = 11.57Å and c = 11.74Å; above 103°C it is converted to an fcc form with a = 5.85Å.[2] The transition temperature decreases with the copper content and in the case of $Cu_{1.80}Se$,[1,2,3] a fcc lattice is observed with a = 5.75-5.65Å, depending on the copper content,[6] and with a roughly assessed region of homogeneity $Cu_{1.82-1.75}Se$.[4] Figure 1 shows lattice constants of $Cu_{2-x}Se$ as a function of composition.

The high temperature phase of copper selenide is characterized by stability in a very wide range of nonstoichiometry, δ, and large ionic conduction together with hole conduction coming from copper deficiencies. These characteristics are attributed to a special crystallographic "average structure" where copper ions are distributed statistically over a number of available sites.[5] This average structure is similar to that found for copper sulfide and similar electrical and optical properties are, therefore, anticipated.

The electronic conductivity of copper selenide as a function of temperature is shown in Figures 2 and 3 for several compositions. The roman letters a,b,...l in Figure 3 correspond to compositions described by the phase diagram shown in Figure 4. A phase transition occurs for temperatures on the order of 100° to 120°C, the magnitude of the conductivity change depending on the composition. When the temperature is dropped below the phase transition, a mixture of α and β phases generally results. In order to achieve a single phase of β, it is necessary to add copper.

REFERENCES (Cu_2Se)

1. P. Rahlfs, Z. Phys. Chem. B31, 184 (1936).
2. W. Borchert, Z. Kristallogr., 106, 5 (1945).
3. G.A. Efendiev and M.M. Kogines, Izv. AN SSSR, Ser. Fiz. Mt. i Tekhn. Nauk, No. 5, 91, (1960).

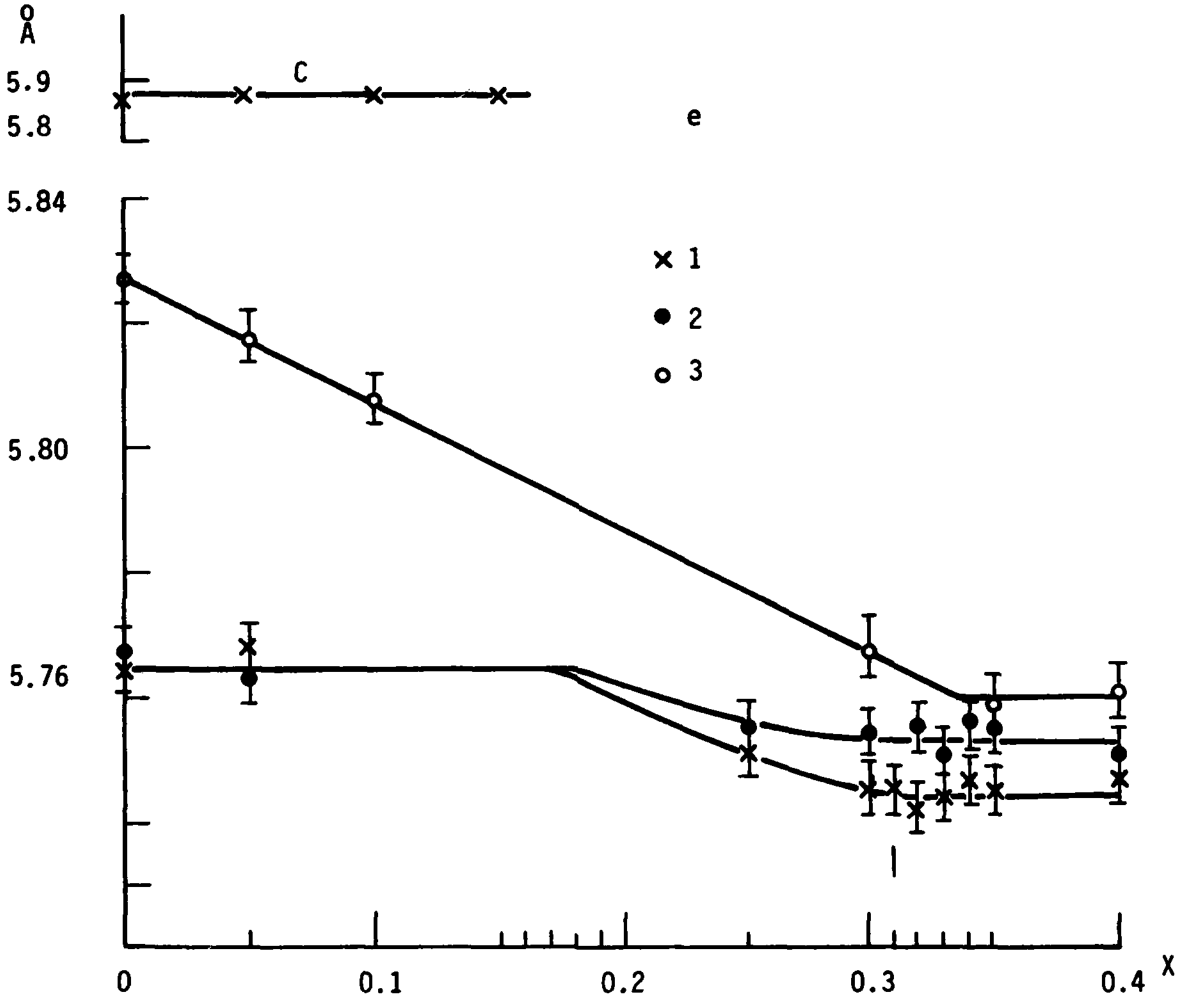

Figure 1. Lattice constants vs composition of compounds: a) $Cu_{2-x}S$; b) $Cu_{2-x}S_{0.75}Se_{0.25}$; c) $Cu_{2-x}S_{0.50}Se_{0.50}$; d) $Cu_{2-x}S_{0.25}Se_{0.75}$; e) $Cu_{2-x}Se$. 1) Room temperatures: phases homogenized at 300°C; 2) room temperatures: phases homogenized at 600°C; 3) t = 150°C; the start of the appearance of lines of the other phase is denoted at the arrow.

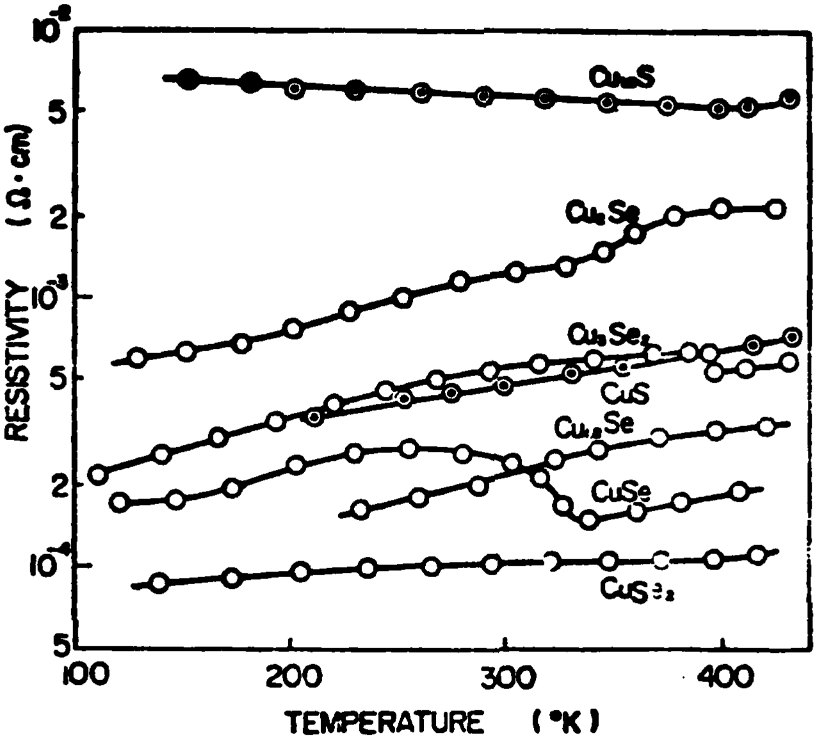

Figure 2. The temperature dependence of resistivities of Cu-Se and Cu-S compounds.

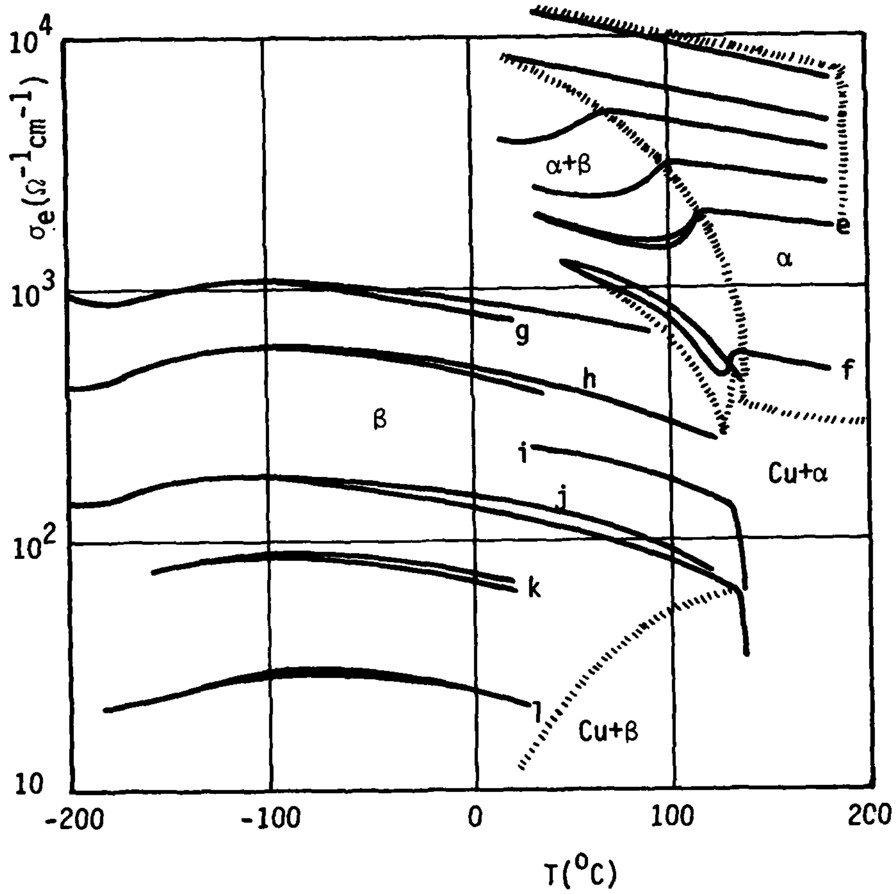

Figure 3. Electronic conductivity σ_e vs T for $Cu_{2-\delta}Se$ with various δ-values. The roman letters a,b,...,l correspond to the same ones in Figs. 2 and 4.

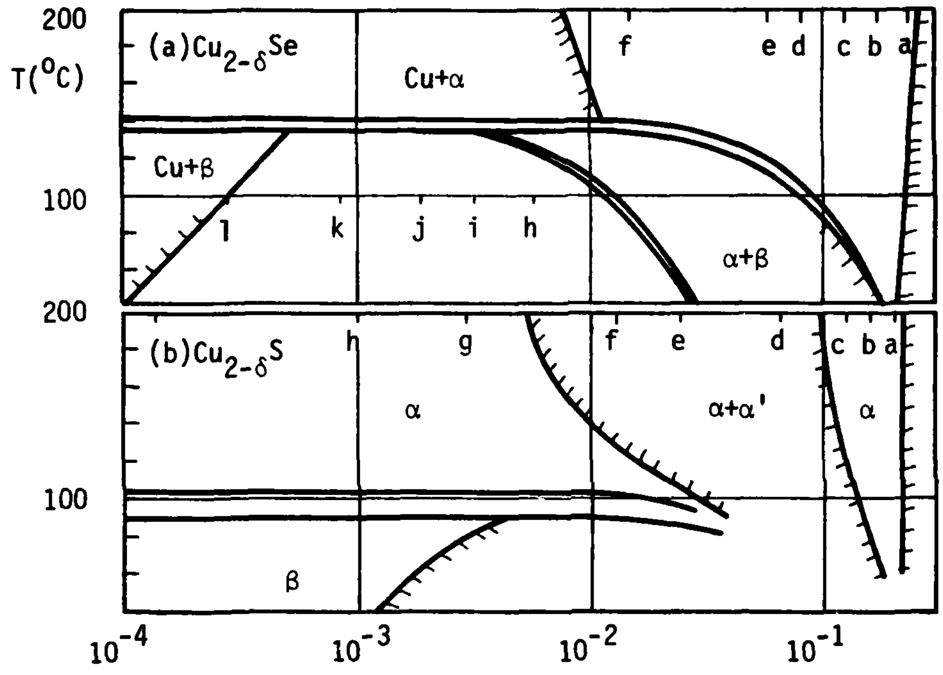

Figure 4. Phase diagrams constructed from E vs T plots; (a) for $Cu_{2-\delta}Se$ and (b) for $Cu_{2-\delta}S$.

REFERENCES Cu_2Se (CONT.)

4. R.D. Heyding, Canad. J. Chem., 44, 1233 (1966).

5. P. Kubaschewski and J. Nolting: Ber. Bunsengs. Physik Chem. 77, (1973) 70.

Cu_2Te

Copper Telluride

Thin films of Cu_2Te have been grown on single crystals of KCl maintained at room temperature by evaporating its constituents from the same boat.[1] Homogenezation was achieved by annealing the films at 300°C. Electron diffraction patterns of the film revealed polycrystalline growth with hexagonal structure having lattice parameters $a = 12.54\text{Å}$; $c/a = 1.731$. Films deposited on heated substrates revealed polycrystalline growth indicating that to obtain oriented growth higher temperatures are necessary.

At 410°C a phase transformation occurs to a face centered cubic structure with $a = 6.11\text{Å}$.[2] On cooling the films, it was found that the original structure was not regained with 340°C indicating significant hysteresis.

Very little information was found on the optical properties of the compounds of copper with sulfur, selenium and tellurium. A translation of a Russian paper describes an analysis of the absorption spectra of Cu_2S, Cu_2Se and Cu_2Te. The shapes of the fundamental absorption edges are shown in Figure 1.[3] Some nontranslated information is referred in References 4 through 10.

REFERENCES (Cu_2Te)

1. S.K. Sharma, J. Mater. Sci. 4, 189 (1969).
2. S.K. Sharma, Ph.D. Thesis Agra University, India (1966).
3. G.P. Sarokin, Inorg. Mater., 15, 9 (Sept. 1979), 1321.
4. G.B. Abdulaev, Sh. Mavlonov, M.G. Shakhtakhtinskii, and A.A. Kuliev, Izv. Akd. Nauk TedzhSSR, 2, 11 (1963).
5. Sh. Mavlonov, A. Radzhavob, A. Saidov, and A. Kuliev, in: Diffusion in Semiconductors (in Russian), Gorkii (1967), p. 272.
6. V.I. Spitsyn and V.S. Arakelyan, Dokl. Akad. Nauk SSSR, 214, 1055 (1974).
7. I.M. Rarenko, I.V. Omachukovskaya, V.G. Nikulitsa, O.E. Panchuk, an E.S. Drutman, Izv. Akad. Nauk SSSR, Neorg. Mater., 12, 108 (1976).
8. V.E. Kosenko, Izv. Akad. Nauk SSSR, Ser. Fiz., 20, 1526 (1956).
9. D.P. Belotskii and M.K. Makhova, Izv. Akd. Nauk SSR, Neogr. Mater., 5 2092 (1969).
10. L.I. Zarubin, I.Yu. Nemish', and I.M. Rarenko, Czech. J. Phys. 18, 117 (1968).

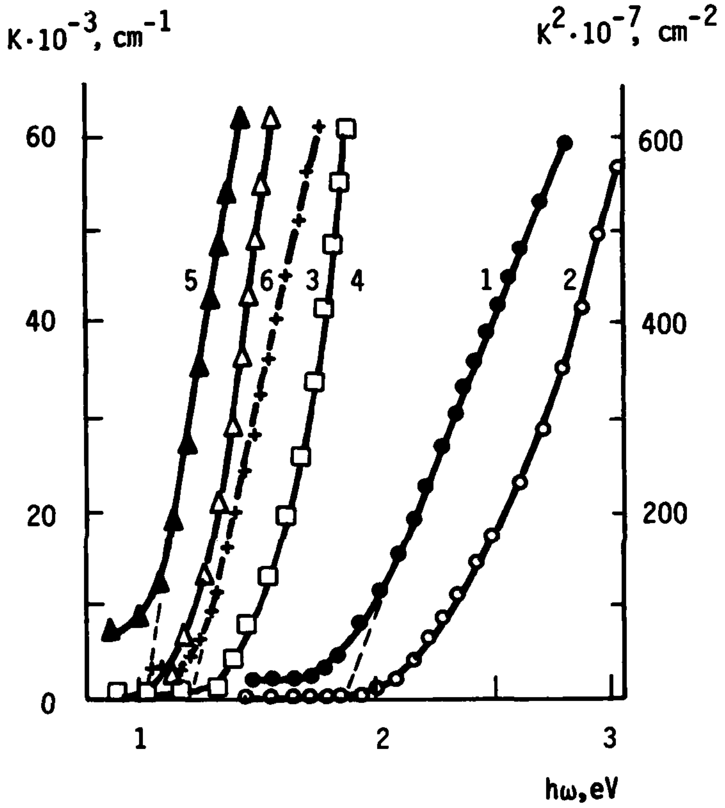

Figure 1. Absorption coefficient (1, 3, 5) and its square (2, 4, 6) vs incident light frequency for Cu_2S (1, 2), Cu_2Se (3, 4) and Cu_2Te (5, 6).

FeS

Iron Monosulfide

FeS amd $Fe_{1-x}S$ and their associated physical properties are still not thoroughly understood. The degree of sulfur content has a profound effect on the nature of physical phase transformations, and possibly even the electrical and optical properties.

For FeS, there is a phase transition around 140°C. This is a ferroelectric to a paraelectric transition and the structure changes from 1C to 2C superstructure.[1,2,3] The conductivity (and hence resistivity) is highly anisotropic.[4] The electrical conductivity changes sharply at the α-transformation along the c-axis, but not perpendicular to it. Further, the α-transformation is sensitive to pressure which lowers the transition temperature by 2.2K/kbar.[5] For $Fe_{1-x}S$ there is evidence that there is a second phase transition for increasing x called the k-transition. Magnetic susceptibility measurements appear to confirm this hypothesis.[1]

There exists a β-transition at 325°C common to all stoichiometries. For $\vec{E} \parallel \vec{c}$, FeS undergoes a semiconductor to metal transition at 411°K. For $\vec{E} \perp \vec{c}$, no phase change is exhibited. For a concise review of the phase transformations in $Fe_{1-x}S$ and FeS along with a phase diagram, reference 6 is suggested.

The resistivity of FeS ($\rho = 1/\sigma$) can be inferred from Figures 1 and 2.[4,7] The sudden variation in σ indicates a phase transition - usually optical changes accompany these changes in electrical properties.

In Figure 3 we see how the resistance R varies for nearly stoichiometric $Fe_{1-x}S$ as a function of temperature. Note the presence of hysteresis near the transition temperature.

Finally, in Figures 4 and 5 we see the change in magnetic susceptibility for $\vec{H} \perp \vec{c}$ and $\vec{H} \parallel \vec{c}$ for H = 3.6kOe. Note the difference in curves.[8]

No optical properties on FeS or Fe_{1-x} have been located in our literature search. The possible changes in reflectivity either are not known or are not striking across the phase transition temperature to warrent much attention. It is suggested that some relatively easy reflectivity measurements in the

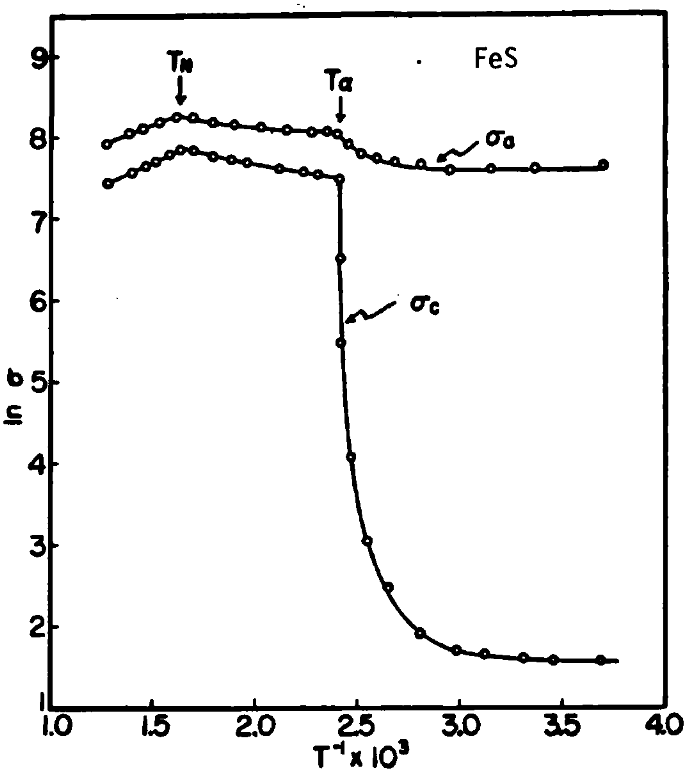

Figure 1. Conductivity versus temperature curves.

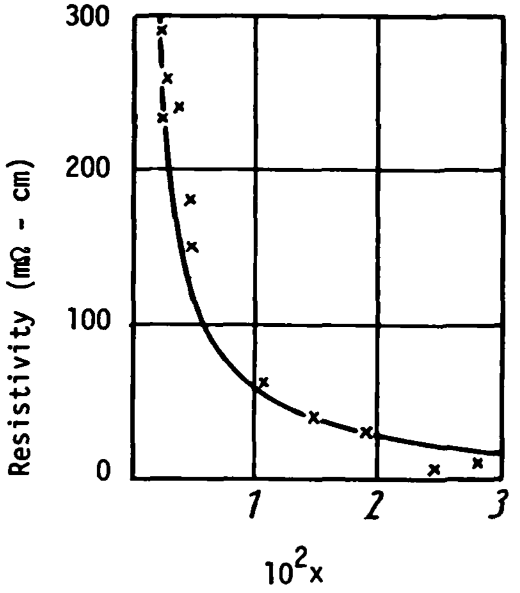

Figure 2. Electrical resistivity at 30°C in dependence on x.

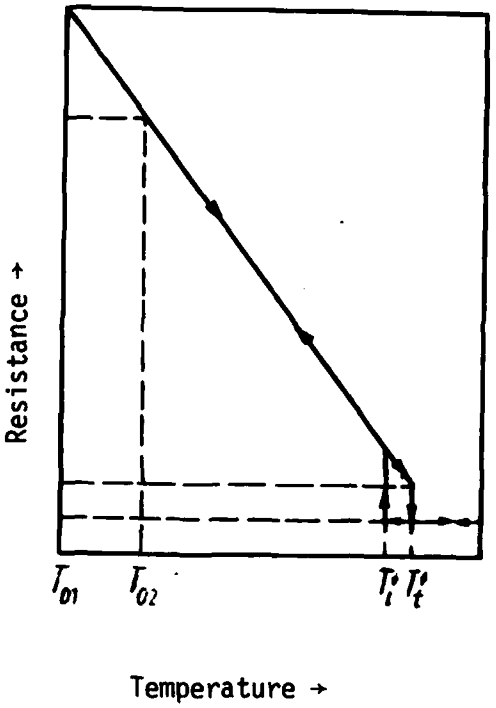

Figure 3. Resistance of nearly stoichiometric $Fe_{1-x}S$ dependence on Temperature ($20^oC < T < 180^oC$).

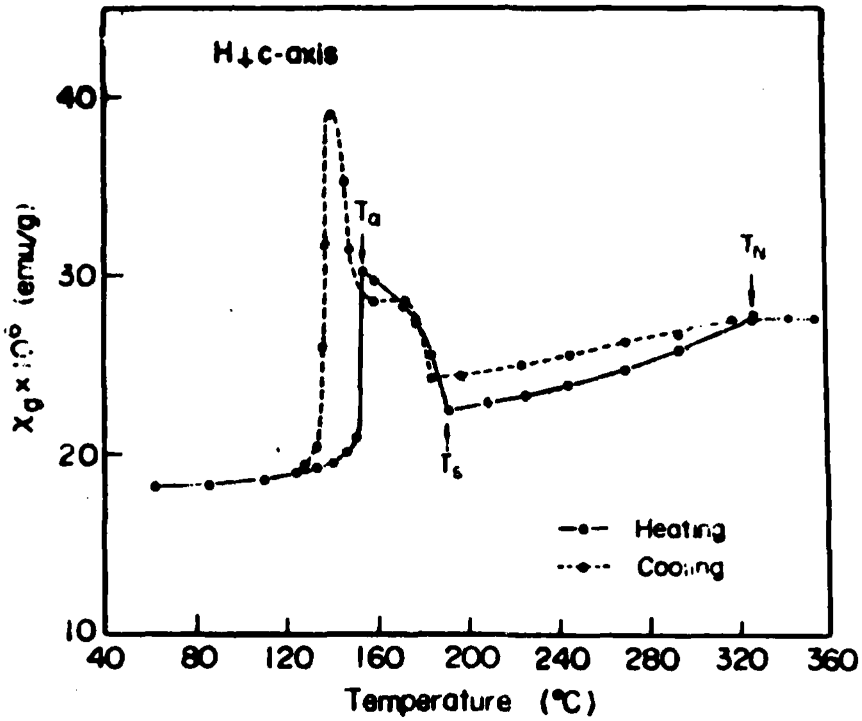

Figure 4. Magnetic susceptibility vs. temperature curves for FeS in the basal plane ($\vec{H} \perp \vec{c}$-axis). H = 3.6 kOe.

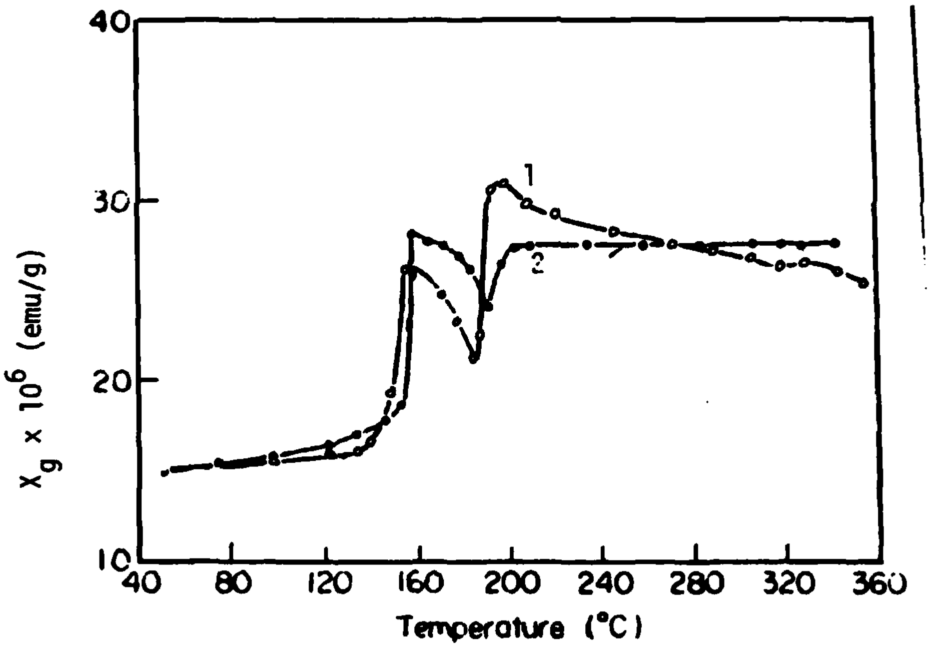

Figure 5. Magnetic susceptibility vs. temperature curves for FeS on heating; Curve 1: $\vec{H}$ || c-axis, Curve 2: angle $\vec{H}$ to c-axis = 50°. H = 3.6 kOe.

2-20 μm region be made across the phase transition temperature to determine if FeS should be subjected to more exhaustive electrical and optical investigations.

REFERENCES (FeS)

1. T. Hirahara, J. Sci. Hiroshima Univ., A22, 215, (1958); A24, 31 (1960).
2. C.B. Van den Berg, and J.B. Van Del Den, and J. Bouman, Phys. Stat. Solidi, 36 K89 (1969); 40, K65 (1970).
3. C.B. Van den Berg, Ferroelectrics, 4, 117 (1972).
4. M. Murakami, J. Phys. Soc, Japan, 16, 187 (1961).
5. K. Ozawa and S. Anzai, Phys, Stat. Solidi, 17, 697 (1966).
6. C.N.R. Rao and K.P.R. Pisharody, Prog. Solid State Chem., 10, 207 (1975).
7. W. Moldenhauer and W. Brückner, Phys. Stat. Sol. (9), 34, 565 (1976).
8. T. Takahaski, Solid State Comm. 13, 1335 (1973).

FeS_2

Iron Disulfide, Pyrite or Marcasite

FeS_2 or pyrite is a transition-metal dichalcogenide which is a Van Vleck paramagnet and a semiconductor.[1,2] The room temperature resistivity is about 0.1 Ω-cm, which classifies it as a poor conductor. There are two forms that FeS_2 exists in, pyrite and marcasite.[3] The former is cubic with the rock salt structure with the Fe^{+2} and S^{-2} ions at the lattice points. Each Fe^{+2} is in an octahedron surrounded by sulfur atoms and each sulfur is surrounded by three Fe^{+2} ions and one sulfur. For the marcasite structure, which is a deformed rectile or CaCl structure, the sulfur atoms are packed hexagonally and half of the octahedral holes are filled with Fe atoms. The crystal structures of each state have been investigated at different temperatures and pressures.[4,5]

Depending upon the chemistry of the material, both p-type and n-type semiconductivity have been reported. Further, it has been reported that marcasite is more conducting than pyrite.[6] FeS_2 has an optical energy band gap of about 0.9eV. The activation energy from electrical measurements is about 0.2eV around room temperature and around 0.5ev at higher temperatures.[7] Figure 1 shows the crystal structure for pyrite.

In Figure 2 we see the resistivity - temperature plot for FeS_2 and NiS_2 from 100°K to about 600°K.[8] We see that ρ (Ω-cm) varies from about 2×10^{-1} to 100 over a span of about 100°K. In Figure 3 we see the resistivity of pyrite as a function of reciprocal temperature.[2] We see that the n-type and p-type resistivities are markedly different -- each sample was obtained from different natural single crystals of FeS_2. The samples in this study were claimed to be of extremely high purity.

There exists a reasonable amount of data on the optical properties of FeS_2, mostly on the pyrite structure. In Figure 4 we have the infrared reflectivity from 0.03eV to 0.15eV, which corresponds to 41 μm and 8.3 μm, respectively.[9] This range of measurement is, we believe, very significant for the understanding of how FeS_2 can be used in a hardened optics system. The very important 10.6 μm line is included. This particular set of data was taken at 300°K, however. The structure indicates lattice or phonon dynamics near

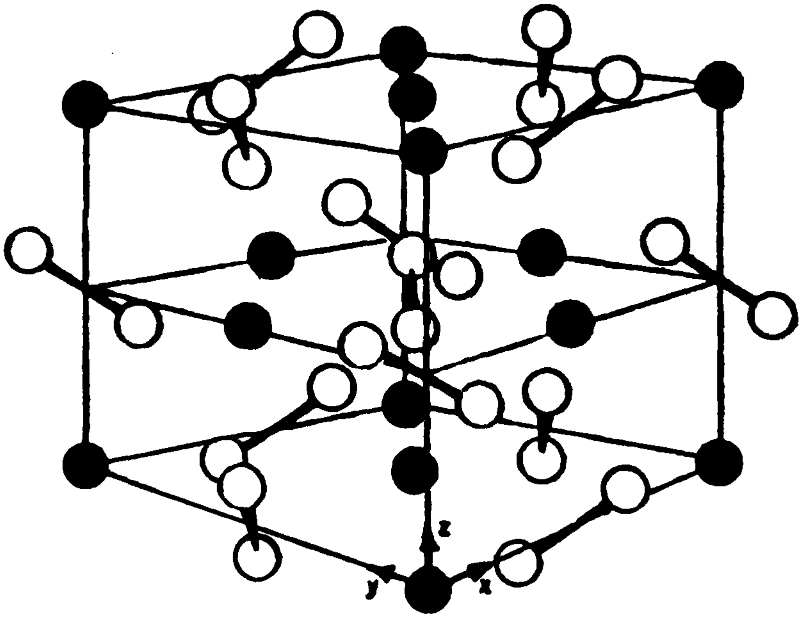

Figure 1. Crystal structure and primitive unit cell of pyrite. The black spheres represent iron atoms, while the white spheres represent sulfur atoms.

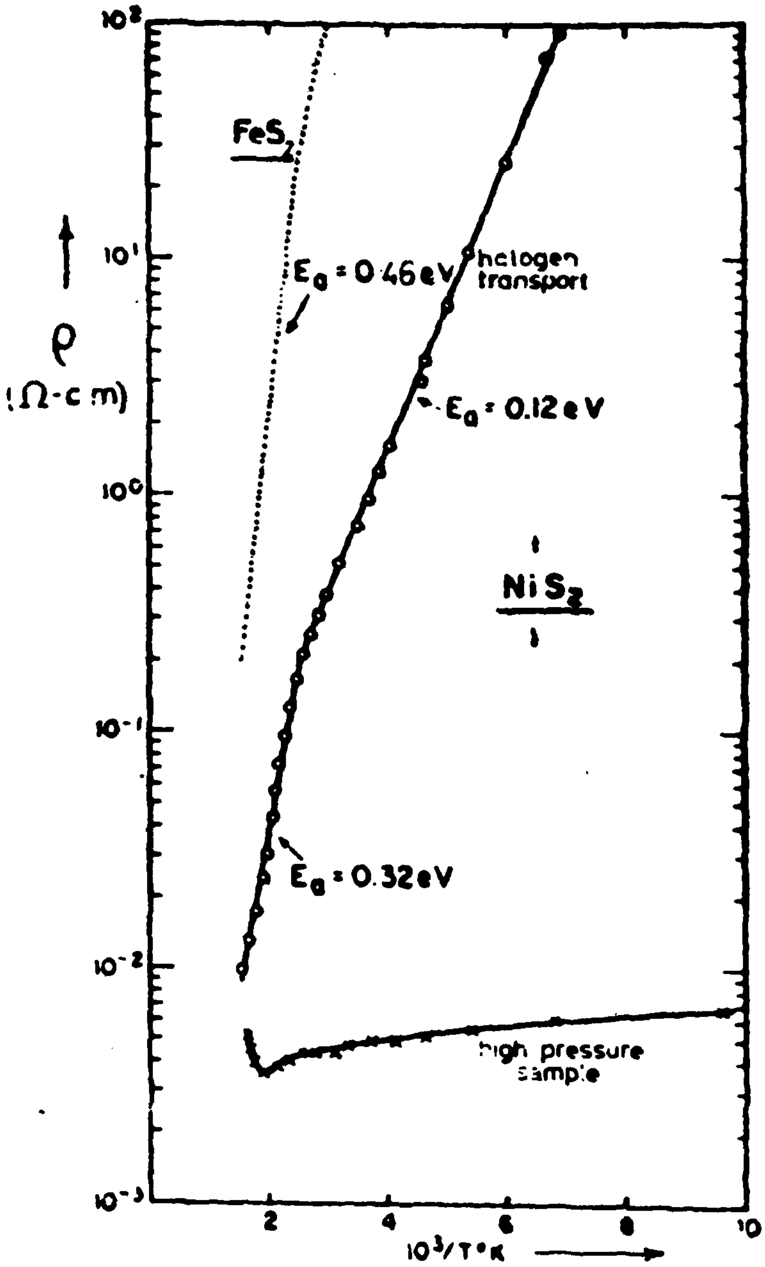

Figure 2. Resistivity vs. Temperature plot for the pyrite semiconductors FeS_2 and NiS_2 .

AD-A146 658 HANDBOOK OF PHASE TRANSITION SULFIDES SELENIDES AND TELLURIDES(U) TACTICAL WEAPONS GUIDANCE AND CONTROL INFORMATION ANALYSIS CE.. W J WILD ET AL. JUL 84 2/3

UNCLASSIFIED GACIAC-HB-84-02 DLA900-80-C-2853 F/G 7/4 NL

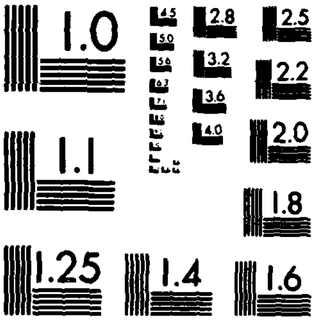

OPY RESOLUTION TEST CHART

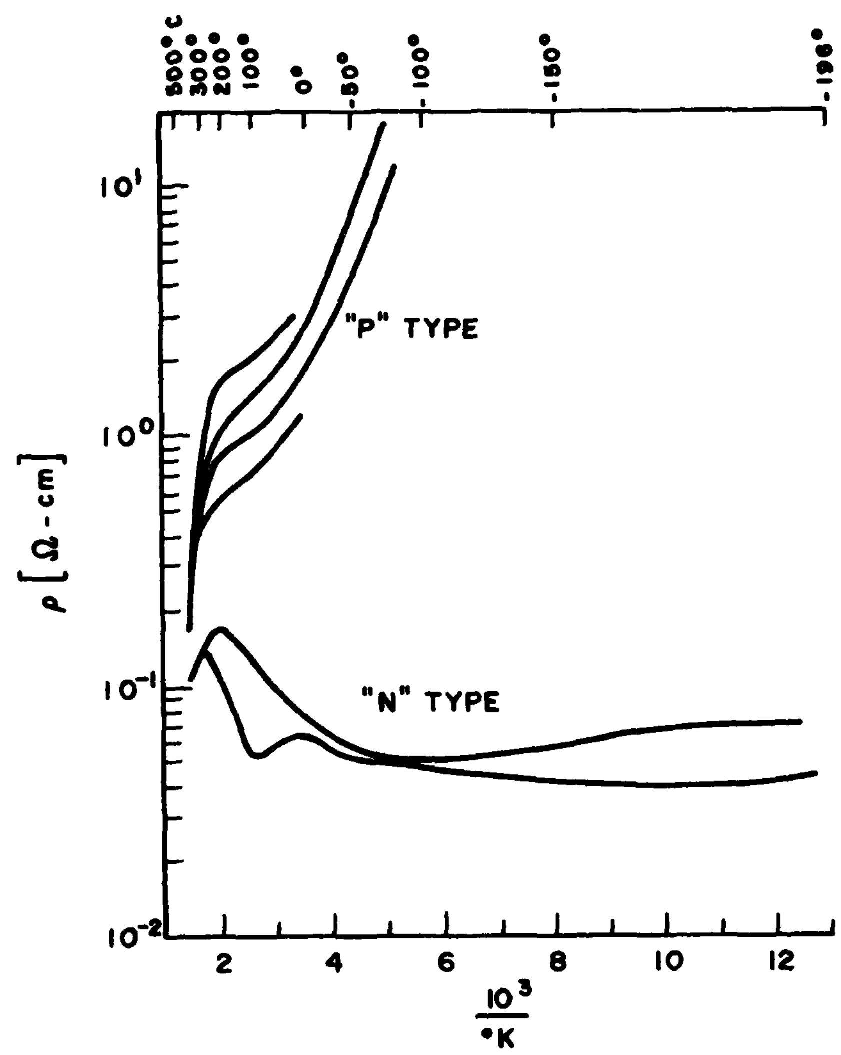

Figure 3. Resistivity as a function of reciprocal temperature for mineral iron pyrite.

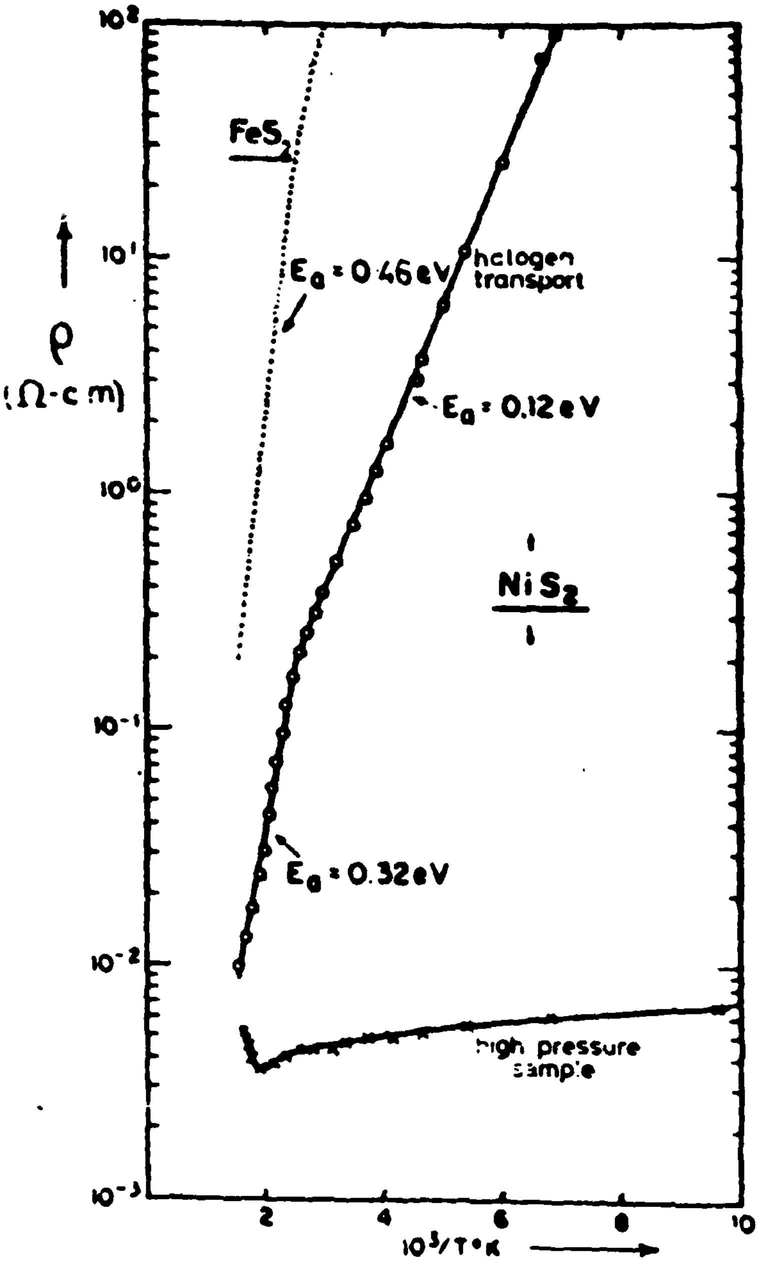

Figure 2. Resistivity vs. Temperature plot for the pyrite semiconductors FeS_2 and NiS_2 .

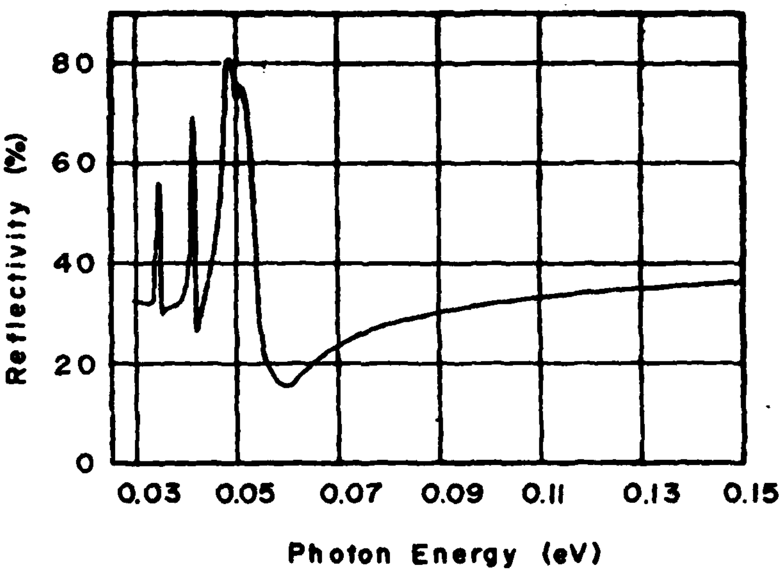

Figure 4. Spectral reflectivity of FeS_2 at 300^0K in the infrared region.

the long wavelength end, and a flat profile for energies greater than 0.07 ev. We must add that this same identical behavior occurs for β-Ag_2S; the flat profile corresponds to a constant index of refraction and negligible extinction. For α-Ag_2S, there is a significant change as the material becomes a Drude metal. If FeS_2 undergoes a phase change at some temperature above 300°C, and assuming that it may be at least approximately a Drude metal, then there is good reason to believe that the optical properties will significantly change. We should point out that for pyrite, a phase transition is not yet known with certainty, wheras marcasite appears to undergo a crystallographic transition near 400°C to pyrite structure. The below flow diagram illustrates the state of knowledge:

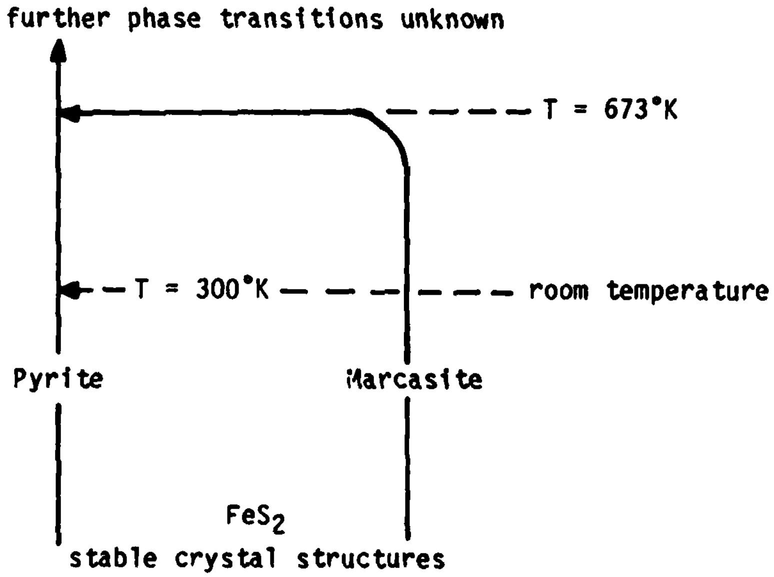

The UV data for FeS_2 (pyrite) is given in Figure 5.[9]

The dielectric constant $\varepsilon(\omega)$ for FeS_2 in the pyrite form has been computed from the near-normal incidence reflectivity data in the 200 cm^{-1} to 700 cm^{-1} range. To compute ε' and ε'' from R, either the Kramers-Kronig or classical oscillator fit can be used though the former requires data extrapolated between 0 cm^{-1} and ∞ cm^{-1} (infinite frequency dielectric constant). Then for $\varepsilon = \varepsilon' + i\,\varepsilon''$, where

$$R(\omega) = \left| \frac{\varepsilon(\omega) - 1}{\varepsilon(\omega) + 1} \right|^2$$

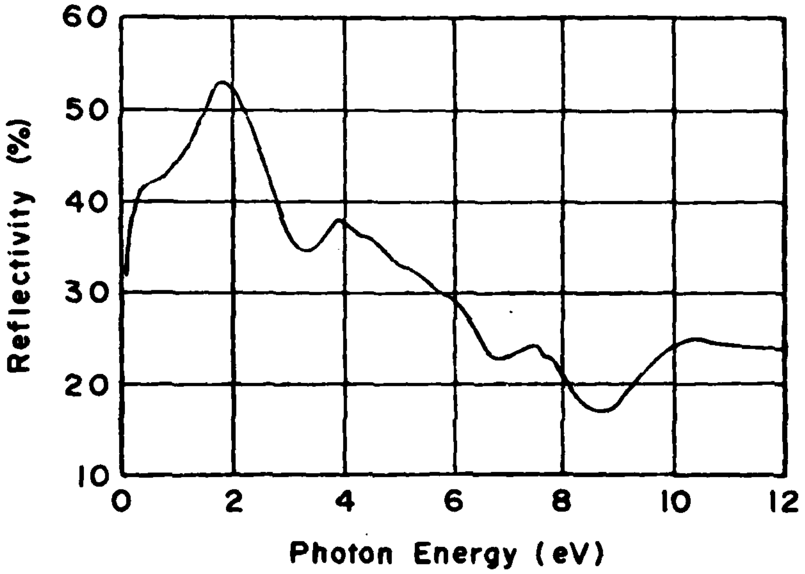

Figure 5. Spectral reflectivity of FeS_2 at 300°K *in the ultraviolet region.*

the classical oscillator model has

$$\varepsilon' = \varepsilon_\infty + \sum_j \frac{4\pi\rho_j\omega_j(\omega_j^2 - \omega^2)}{(\omega_j^2 - \omega^2)^2 + (\gamma_j\omega_j\omega)^2},$$

$$\varepsilon'' = \sum_j 4\pi\rho_j\omega_j^2 \frac{\gamma\omega_j\omega}{(\omega_j^2 - \omega^2)^2 + (\gamma_j\omega_j\omega)^2},$$

for oscillator dispersion frequency ω_j, damping constant γ_j, and oscillator strength for the jth mode ρ_j. From ε' and ε'' we can derive n and k via the formulae:

$\varepsilon' = n^2 - k^2$,

$\varepsilon'' = 2nk$.

In Figure 6 we have the reflectivity spectra for FeS_2 as modelled using the above formulae. In Figure 7 we see the quantity $|\varepsilon| = \sqrt{\varepsilon\varepsilon^*} = (\varepsilon'^2 + \varepsilon''^2)^{1/2}$. Figure 8 gives ε' and Figure 9 gives ε''. Figure 10 gives ε' and ε'' for higher energies. In Figures 11, 12, and 13 we have the refractive index and extinction coefficient for FeS_2 (pyrite structure).

The optical energy gap of FeS_2 is indirect and at 300°K we have E_g = 0.92eV.[10] The energy gap is temperature dependent and obeys the Varshni formula:

$$E_g(T) = E_g(0) - \frac{\alpha T^2}{T + \beta},$$

where $E_g(0)$ is at 0°K and α and β are constants that are determined by experiment. Here

$E_g(0) = 0.835\text{eV}$

$\alpha = -6.5 \times 10^{-4}\text{eV°K}^{-1}$

$\beta = -1395°\text{K}$

The energy level scheme of FeS_2 (pyrite) is given in Figure 14.[9]

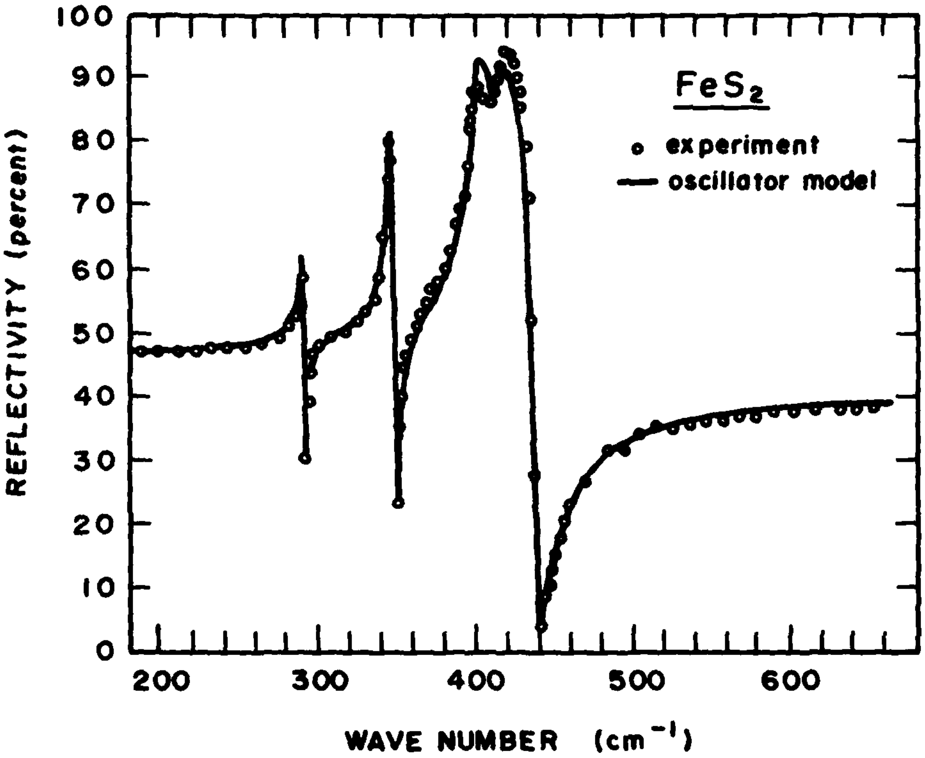

Figure 6. Reflectivity of FeS_2 as a function of wave number.

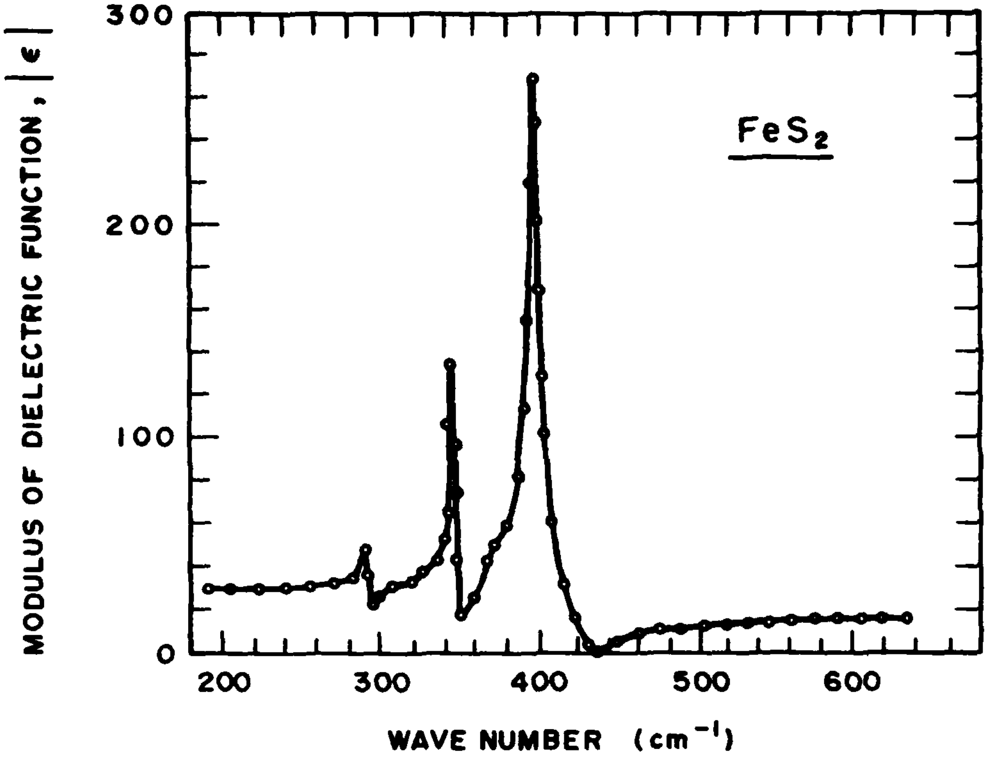

Figure 7. Modulus of the complex dielectric function vs. wave number.

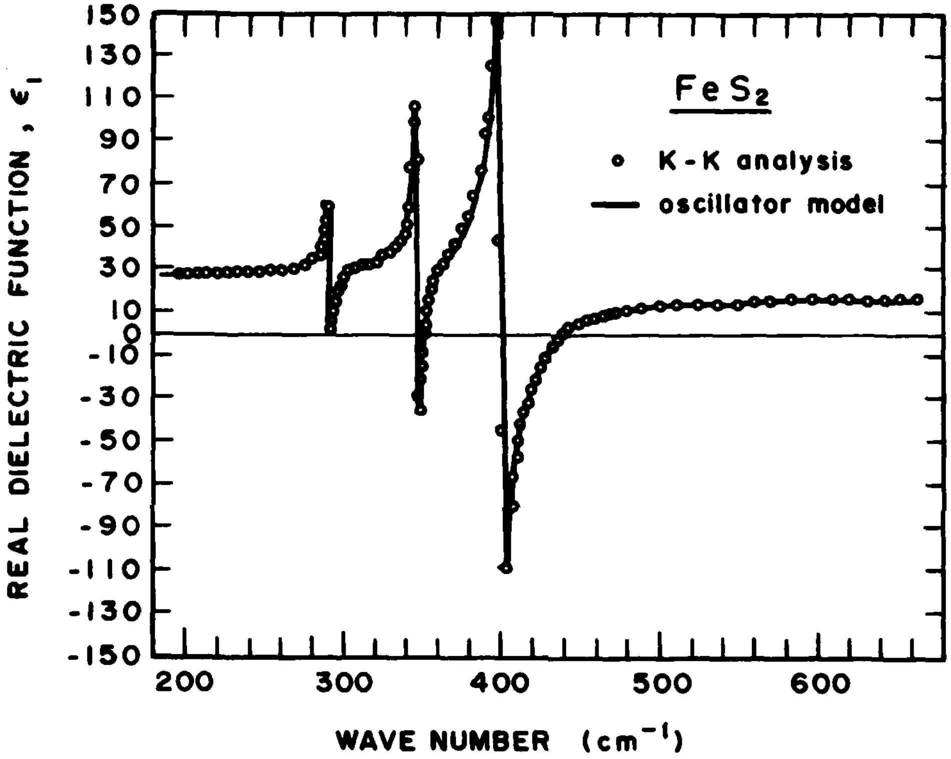

Figure 8. Real part of the complex dielectric function vs. wave number.

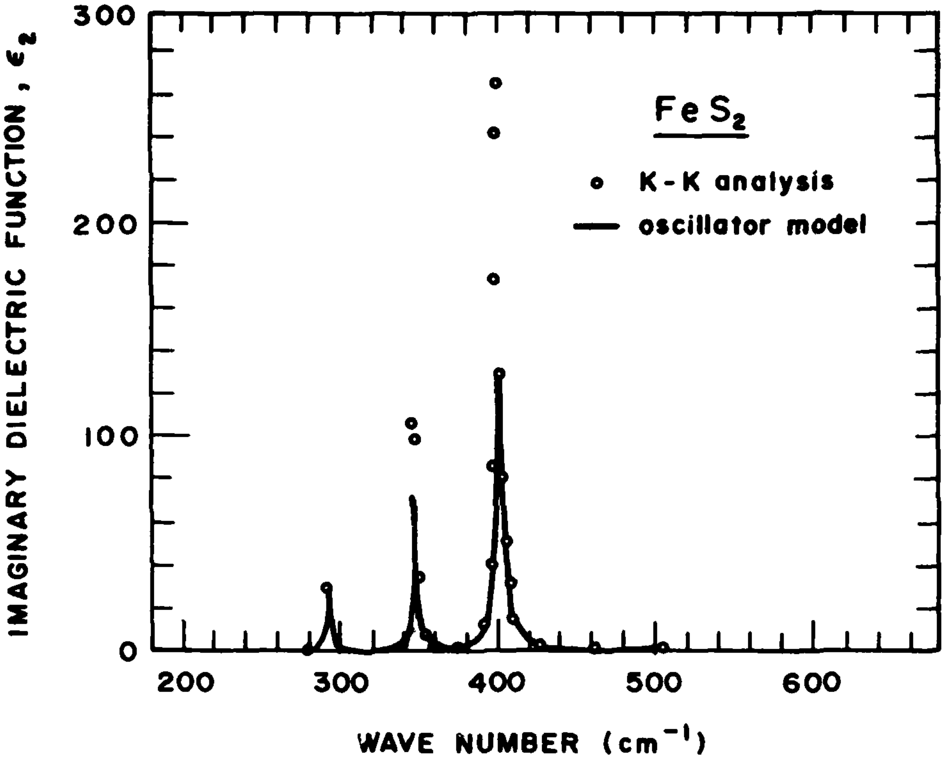

Figure 9. Imaginary part of the complex dielectric function vs. wave number.

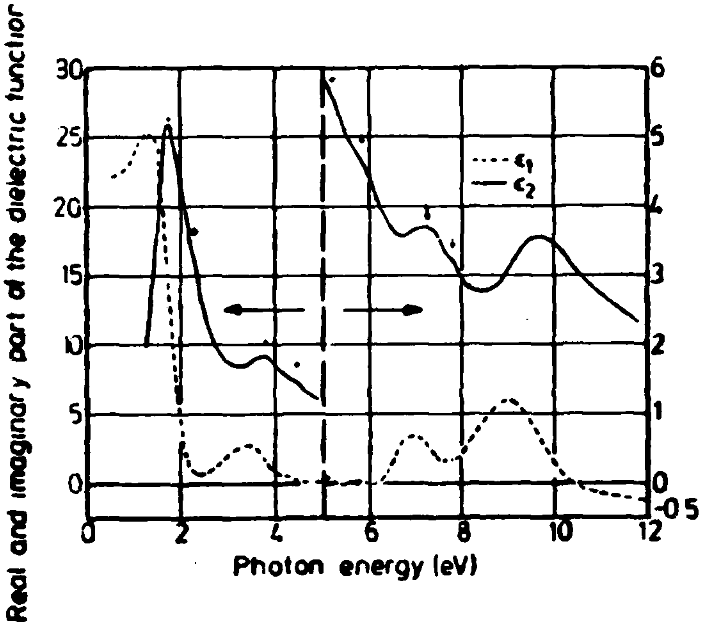

Figure 10. Dielectric function of FeS_2 at 300^0K.

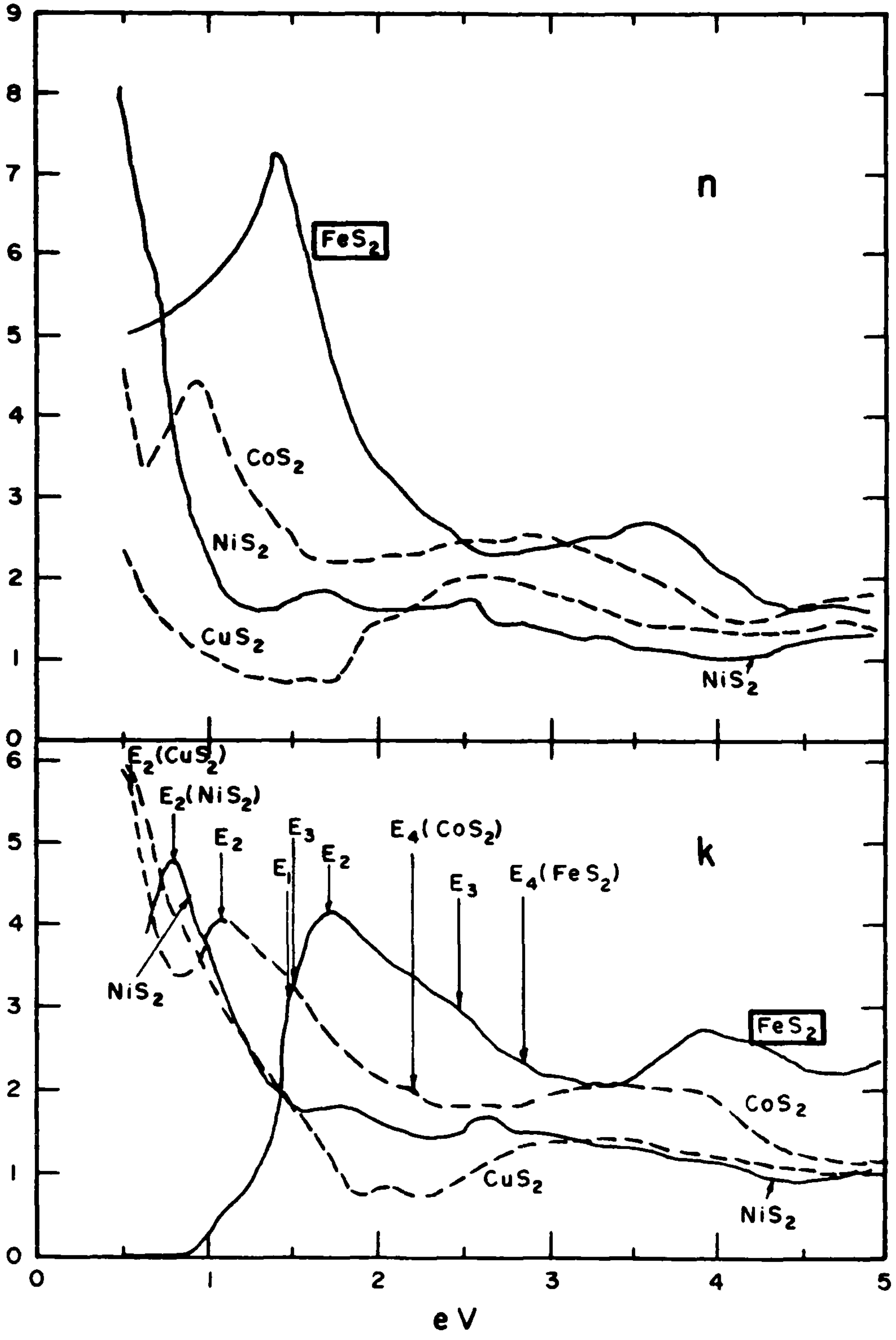

Figure 11. Real and imaginary parts of the complex refractive index for FeS_2, CoS_2, NiS_2 and CuS_2.

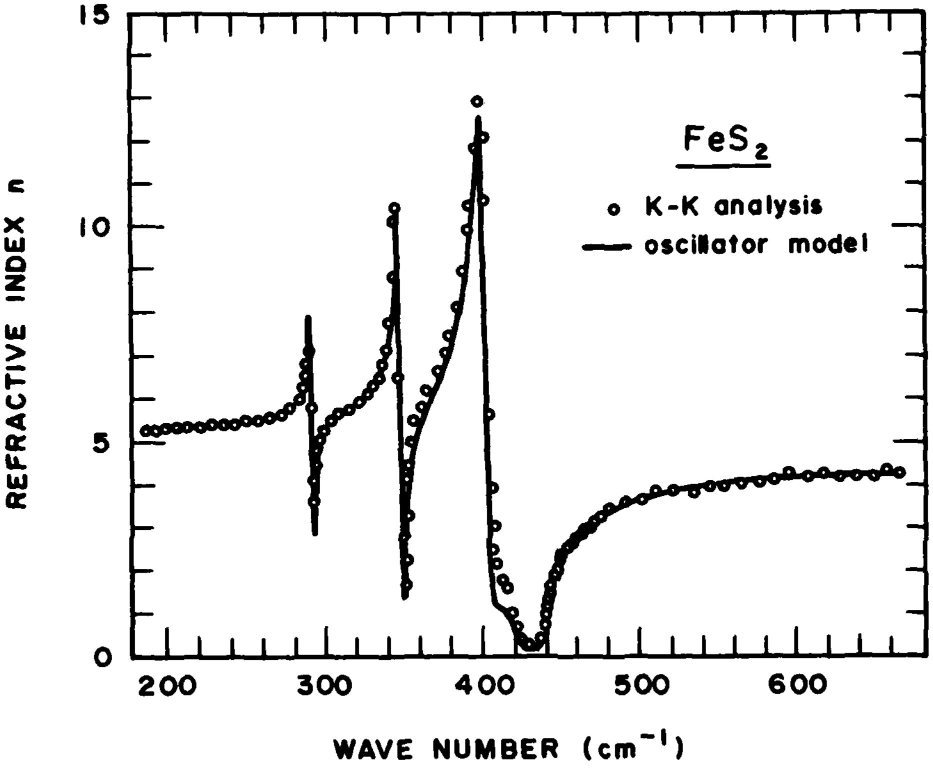

Figure 12. Refractive index as a function of wave number.

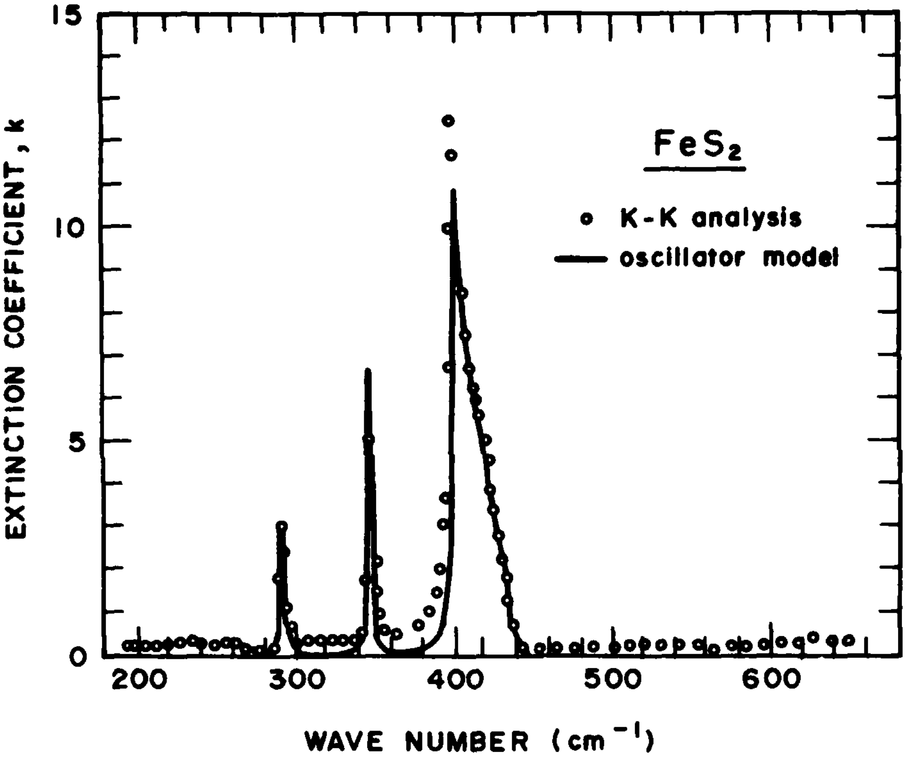

Figure 13. Extinction coefficient as a function of wave number.

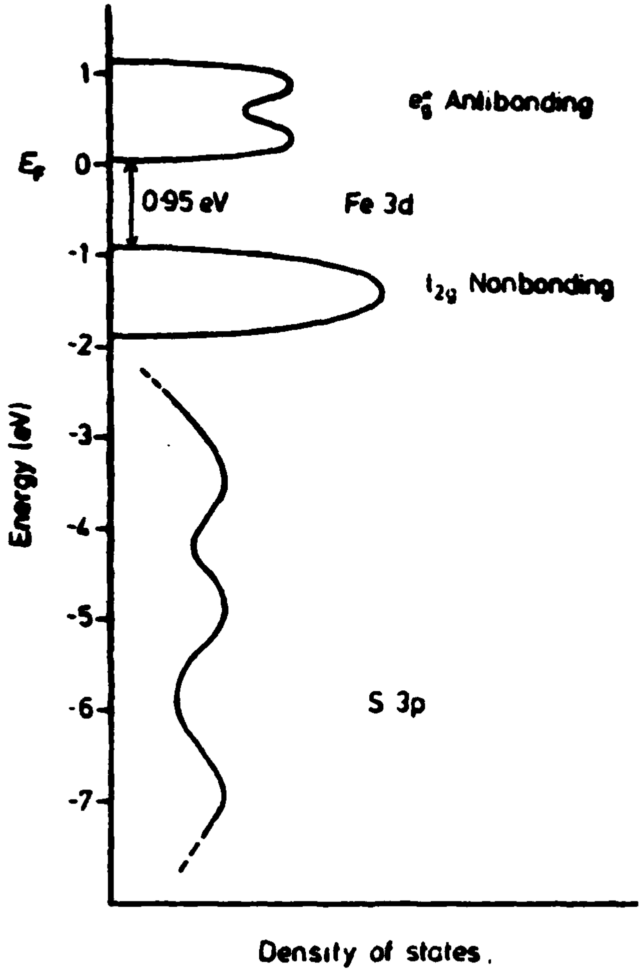

Figure 14. Energy level scheme of FeS_2.

There does not appear to be any difficulty in growing single crystals of FeS_2 unless one desires to carefully distinguish pyrite from marcasite (in any case, the crystals can be grown at an elevated temperature to get pyrite). The FeS_2 crystals are grown similarly to CoS_2 and NiS_2 crystals. We have not found any literature on the thin film deposition techniques for FeS_2.

REFERENCES (FeS_2)

1. P. Burgardt and M.S. Seehra, Solid State Commun. 22, 153 (1977).
2. J.C. Marinace, Phys. Rev. 96, 593 (1954).
3. N. Elliot, J. Chem. Phys. 33, 903 (1960).
4. M.E. Straumaris, et.al., Am. Mineral. 49, 206 (1964).
5. R.L. Clandenen and H.G. Drickamer, J. Chem. PHys. 44, 4223 (1966).
6. P. Pascal, Noureautraite de Chemie Mineral, Massan, Paris (1956-1963).
7. C.N.R. Rao and K.P.R. Pisharody, Prog. in Solid State Chem. 10, 207 (1975).
8. J.A. Bither, et.al., Inorg. Chem. 7, 2208 (1968).
9. A. Schlegal and P. Wachter, J. Phys. C. 9, 3363 (1976).
10. N.M. Ravindra and V.K. Srivastava, Phys. Stat. Sol. (a) 65, 737 (1981).

HfS_2
Hafnium Disulfide

Hafnium disulfide is a group IV transition - metal dichalcogenide which has attracted interest primarily due to its anisotropic behavior in the far-infrared. HfS_2 can be prepared via direct reaction at around 900°C to get single crystals; they are of dark red color. The crystals possess the CdI_2 type hexagonal structure (Figures 1,2) with a = 3.635 Å and c = 5.837Å. HfS_2 is basically an insulator with diamagnetic behavior with a measured optical gap of 1.96eV.[1] From reference 2, the measured lattice parameters are given as a = 3.63Å and c = 5.854Å and the coordination (at the metal atom) is octahedral.[3]

A typical plane of the HfS_2 crystal consists of metal atoms sandwiched between two planes of the chalcogenides. Within a layer, each metal atom is octahedrally surrounded by six sulfur atoms as seen in Figures 1,2. We should now point out that while reference 1 indicates HfS_2 to be an insulator, from the crystal structure properties, reference 3 suggests HfS_2 to be a semiconductor.

A fair amount of experimental data exists on the optical properties of HfS_2. This includes absorption measurements, transmission and reflection measurements. All measurements that we have been able to locate were taken at room temperature. Further, there is a dependence on the crystal orientation because of the anisotropy inherent in the material.

Figure 3 shows the measured behavior in the far infrared for both HfS_2 and $HfSe_2$. Here the electric field vector, $\vec{E}$, is perpendicular to the c-axis. A classical oscillator fit is given for comparison. Figures 4,5, and 6 show the reflectivity of HfS_2 for higher energies; note that these measurements are in good agreement.[4] In Figure 6, the experiment and theoretical spectra show disagreement though the salient features are similar. Figures 7 and 8 show the measured absorption coefficient (α, in cm^{-1}) and transmittance (for a 70μ thick specimen of HfS_2).[3]

Detailed information concerning the band structure of HfS_2 is available,[3] though we have been unable to locate much data on the electrical characteristics, eg., resistivity (conductivity) as a function of temperature, carrier concentration, etc.

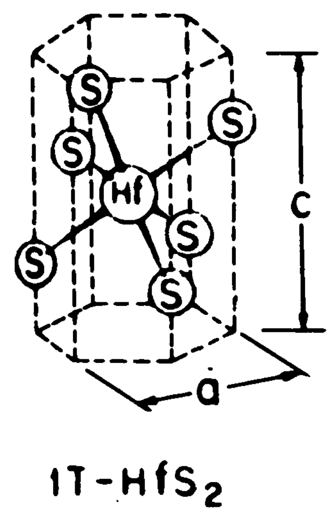

Figure 1. Symmetric unit cells for the C6 (1T-HfS_2), C27 (2H-TaS_2), and C7 (2H-MoS_2) crystal structures.

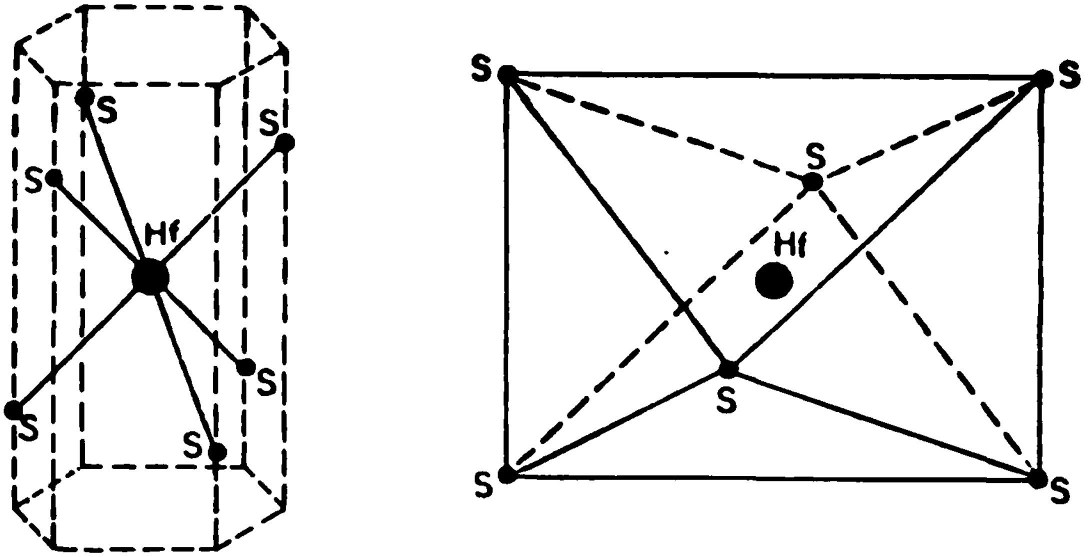

Figure 2. (a) Hexagonal unit cell of HfS_2. (b) Octahedral coordination within one layer.

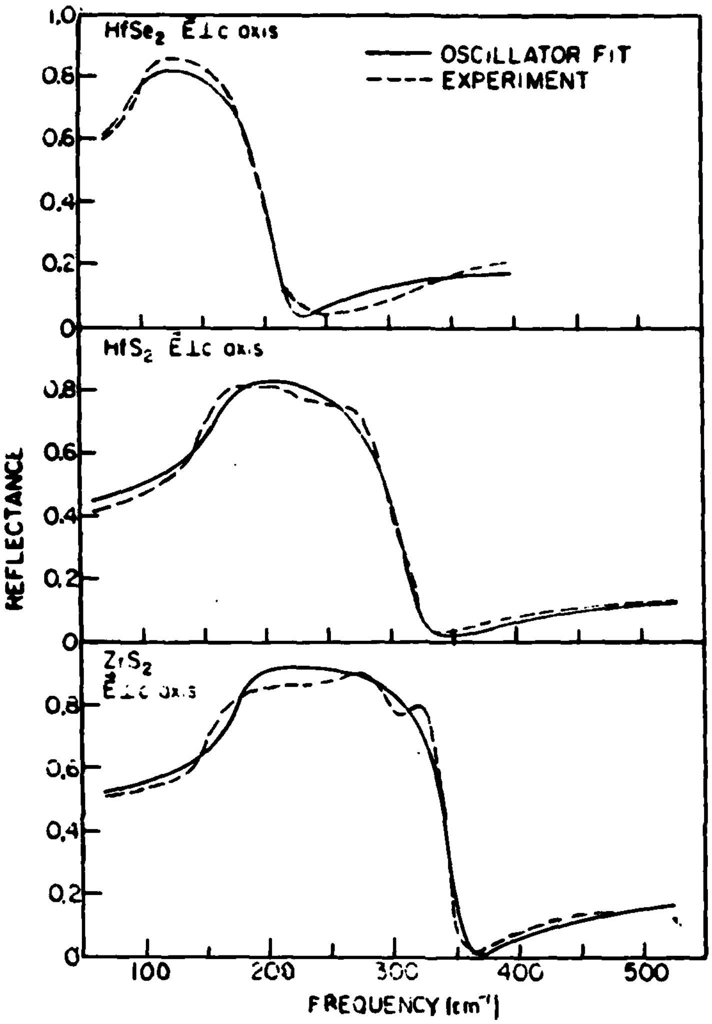

Figure 3. Room Temperature reflectance spectra for ZrS, HfS$_2$, and HfSe$_2$ for $\vec{E} \perp \vec{c}$ axis.

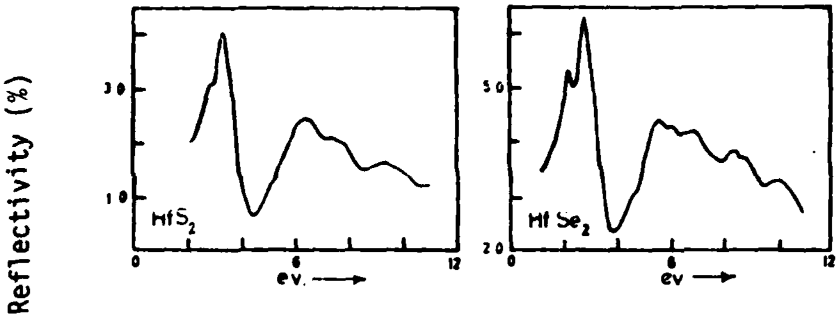

Figure 4. Reflectivity for HfS$_2$ and HfSe$_2$.

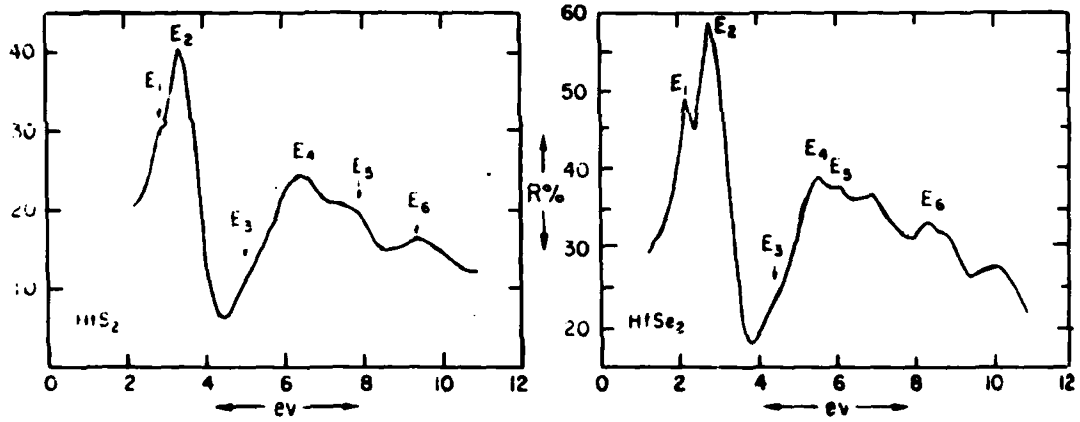

Figure 5. Room temperature fundamental reflectivity of HfS$_2$ and HfSe$_2$.

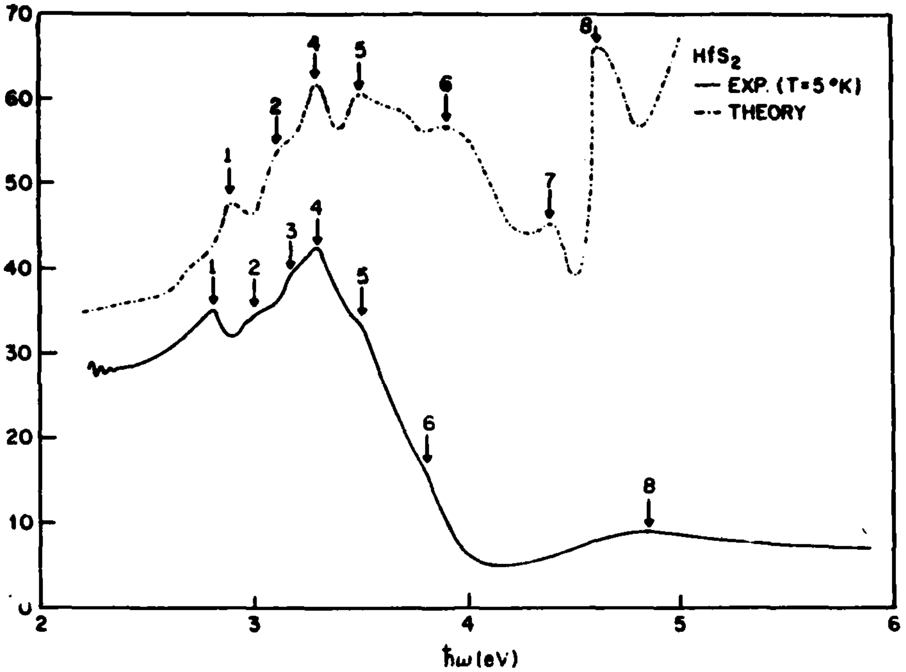

Figure 6. Experimental and theoretical spectra of HfS_2.

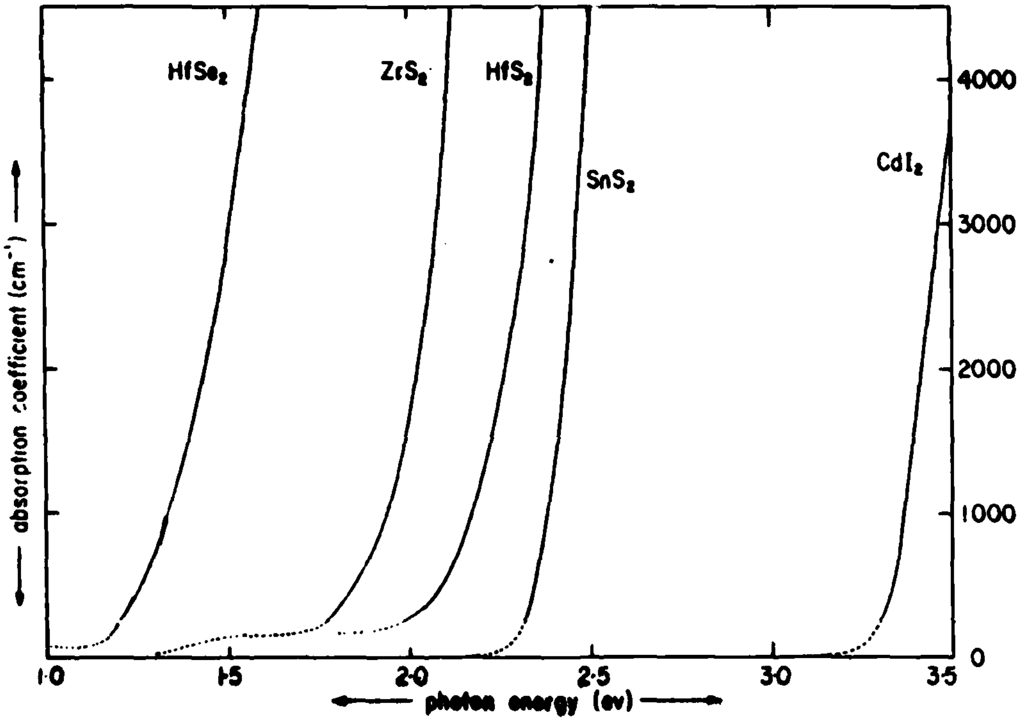

Figure 7. Room temperature optical absorption edge data for ZrS_2, HfS_2, $HfSe_2$, SnS_2 and CdI_2.

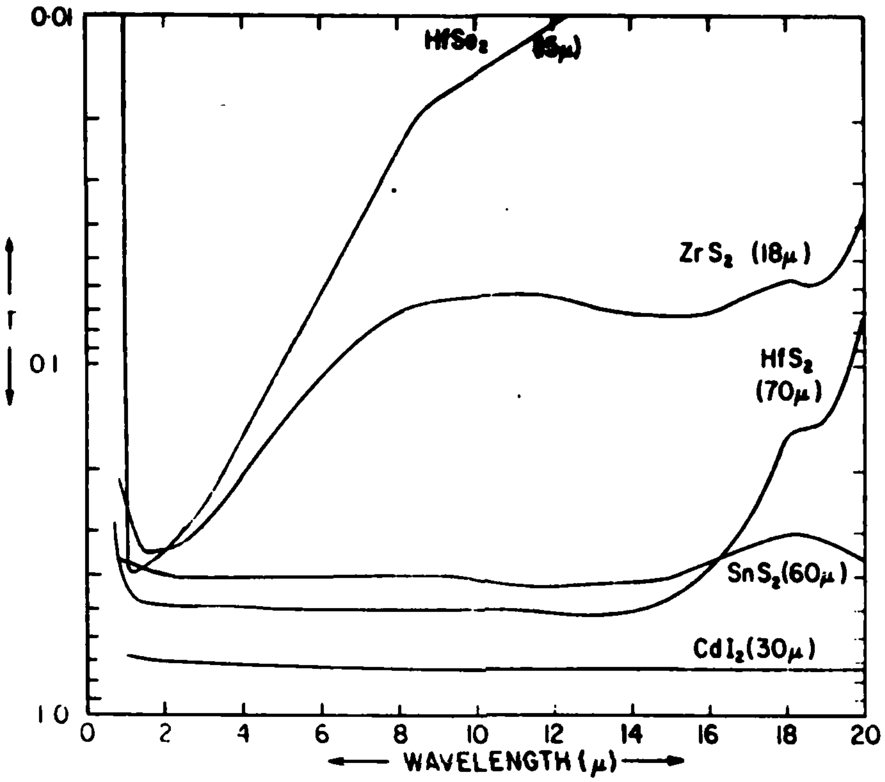

Figure 8. Room temperature infrared transmission of ZrS_2, HfS_2, $HfSe_2$, SnS_2 and CdI_2 (sample thickness given in parentheses).

It remains to be seen if HfS_2 undergoes a phase transformation and how such a transition will affect the optical behavior.

REFERENCES (HFS_2)

1. C.N.R. Rao and K.P.R. Pisharody, Prog. Solid. State Chem., 10, 207 (1975).
2. C. Lucousky, et.al., Phys. Rev. B7, 3859 (1973).
3. C.Y. Fong, et.al., Phys. Rev. B13, 5442 (1976).
4. J.A. Wilson and A.D. Yoffe, Adv. Phys. 18, 193 (1969).

HfS_3
Hafnium Trisulfide

Hafnium trisulfide or HfS_3 is a transition-metal trichalcogenide which crystallizes monoclinically.[1,2] The metal ions are in the center of distorted trigonal prisms which share trigonal faces forming isolated chains. The chains run parallel to the b crystallographic axis and are displaced from neighboring column by one-half the unit cell along the b axis. The monoclinic unit cell contains eight atoms as seen in Figure 1.[3] Its dimensions are a = 5.09Å, b = 3.59Å, c = 8.97Å, β = 97.38Å, and the crystal's space group is C^2_{2h}. (Here C_{2h} consists of a twofold rotation about an axis, a reflection through the plane perpendicular to this axis and the inversion through the origin. Further information details on the meaning and nature of space groups can be found in reference 4.) There are 24 normal modes at the center Γ of the Brillouin zone which can be represented by the irreducible representation of the C_{2h} point group. Of these normal modes, 12 are Raman active and 9 are infrared active. These two types of activity are mutually exclusive because an inversion center is present. HfS_3 crystals can be grown using the chemical vapor transport technique using iodine in concentrations of 2-4 mg cm^{-3} tube volume.[5] The best crystals are synthesized with the temperature at the end of the ampoule at 800 and 900°C.

HfS_3 shows several Reststrahlen bands in the far infrared. Figure 2 shows the reflectance for both polarizations and a comparison with the classical oscillator fit model. Figure 3 shows the calculated frequency dependence of the imaginary part of the dielectric constant ($\varepsilon(\nu) = \varepsilon_1(\nu) + i\varepsilon_2(\nu)$) for both polarizations. The optical parameters can be calculated using the Kramers - Kronig or classical oscillator methods. Figure 4 shows the transmission spectra for HfS_3 at room temperature.[3]

Concerning the classical oscillator technique: A first approximation for the oscillator parameter was obtained from the complex dielectric permittivity $\varepsilon^* = \varepsilon_1 + i\varepsilon_2$, and the energy-loss function, $-\text{Im}(1/\varepsilon^*)$. The position of the peaks in ε_2 and in $-\text{Im}(1/\varepsilon^*)$ located the TO and LO phonon frequencies, respectively. The reflectivity spectra were analyzed by finding the parameters of the damped oscillator factorized form,

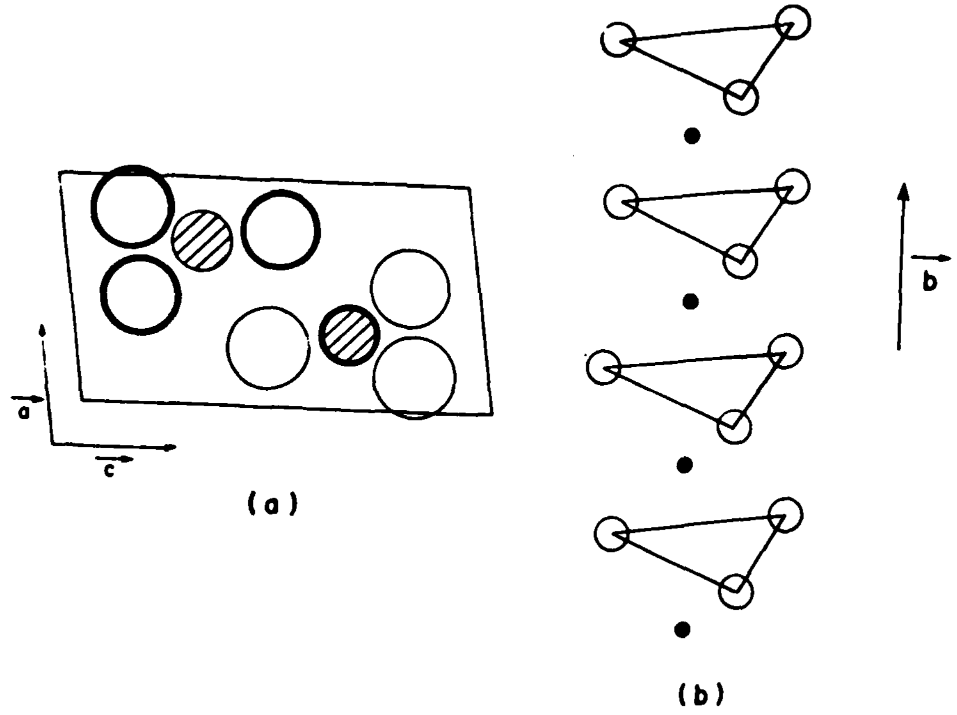

Figure 1. (a) The structure of HfS_3 projected along b axis. Hafnium atoms are indicated by hatched circles and sulfur by open circles. Atoms with heavy contours are at $y = 1/4$ and those with light contours at $y = 3/4$. (b) A chain of HfS_3 along b axis.

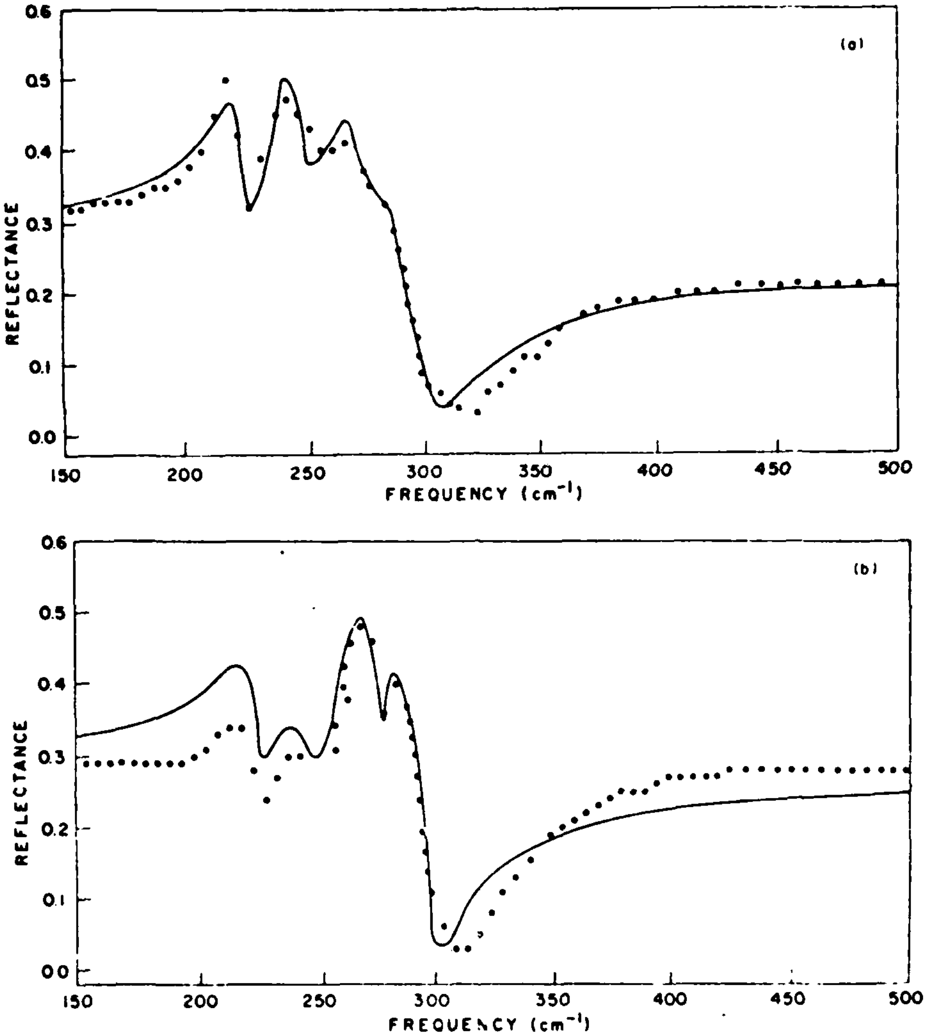

Figure 2. HfS_3 typical room-temperature reflectance spectra (data points) and oscillator fits (solid lines) for polarization (a) parallel, (b) perpendicular to the chains.

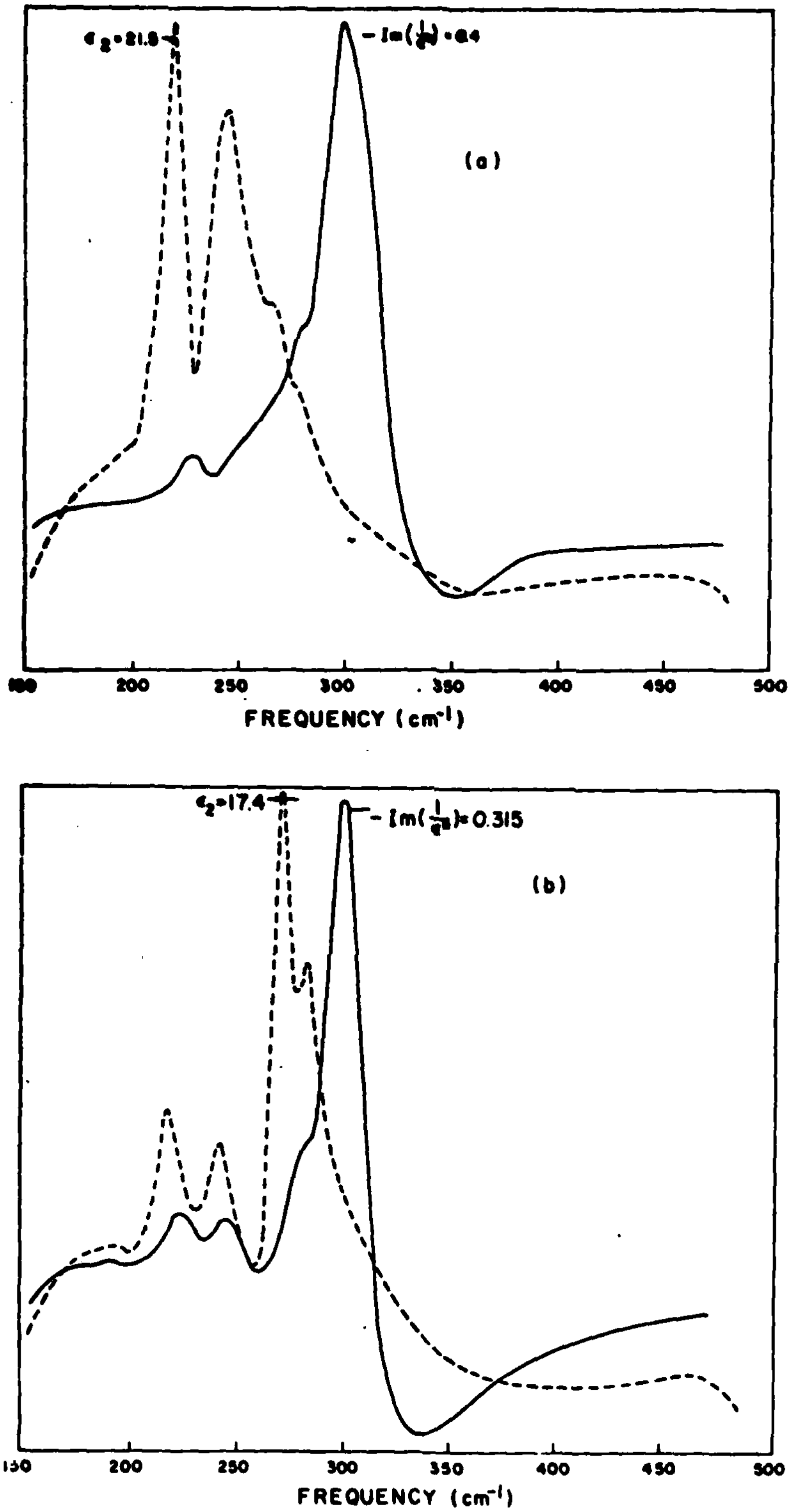

Figure 3. Calculated frequency dependence of ϵ_2 (dashed lines) and $-Im(1/\epsilon^*)$ (solid lines) of HfS_3 from the reflectivity spectra. (a) parallel, (b) perpendicular to the chains.

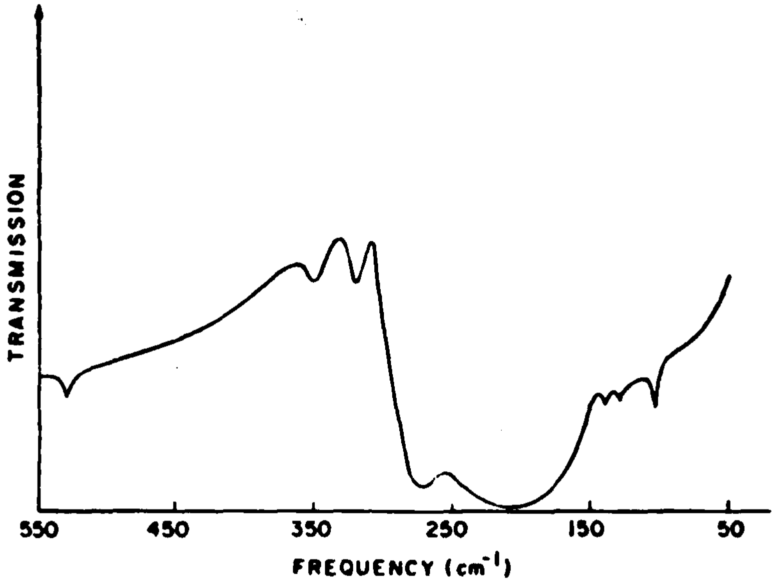

Figure 4. HfS_3 transmission spectra at room temperature for polarization parallel and perpendicular to the chains.

$$\varepsilon(\omega) = \varepsilon_0 \prod_{j=1}^{M} \frac{\omega_{jLO}^2 - \omega^2 - i\gamma_{jLO}\omega}{\omega_{jTO}^2 - \omega^2 - i\gamma_{jTO}\omega}$$

here ε_∞ is the high frequency dielectric constant, ω_{jTO}, γ_{jTO}, and ω_{jLO}, γ_{jLO} are the frequency and damping of the jth oscillator for the transverse and longitudinal phonon, respectively. It has been observed that the magnitude of the reflectance is very crystal dependent, affecting thus the calculated values for ε_∞, γ_{jLO}, and γ_{jTO}. Here ω_{jLO} and ω_{jTO} are insensitive to the effect. For ε_∞, the measured value depends on symmetry type, values being either 8.7 or 10.0. In reference 3, the various classical oscillator parameters are tabulated. HfS_3 is very similar in optical properties to ZrS_3.

For wavelengths shorter than 350 cm^{-1} the reflectivity becomes flat and fairly constant - this is characteristic of many of the transition - metal chalcogenides and dichalcogenides. We have not found any literature pertaining to a possible phase transition and accompanying change in optical characteristics.

REFERENCES (HfS_3)

1. S. Furuseth, L. Brattas, and A. Kjekshus, Acta. Chem. Scand. A29, 623 (1975).
2. W. Kornet and K. Plieth, Z. Anorg. Allg. Chem., 336, 207 (1965).
3. S. Jandl and J. Deslandes, Phys. Rev. B24, 1040 (1981).
4. G.F. Koster, Space Groups and Their Representations, Academic Press, New York, 1957.
5. D. Reidel in Preparation and Crystal Growth of Materials with Layered Structures, edited by R.M.A. Leith (Reidel, Dordrecht, 1977).

HgS

Mercury Monosulfide or Cinnabar

Cinnabar or HgS exists in two polymorphic forms.[1] The form α-HgS is stable at room temperature and possesses the cinnabar structure. The high temperature form β-HgS, or metacinnabar, possesses the cubic zinc-blende structure. The unit cell of α-HgS contains 3 HgS molecules. β-HgS is black and is obtained by precipitation from mercuric salt solutions; it is converted to α-HgS on heating. The phase transformation between trigonal (α-HgS) and cubic (β-HgS) forms of HgS takes place between 280 and 340°C.[2,3] At high pressures, HgS transforms to a distorted NaCl-type structure.[4] A new hexagonal form of HgS has also been reported.[5]

β-HgS is an n-type degenerate semimetal. The Fermi level is 0.1eV above the bottom of the conduction band. α-HgS is an insulator with electron mobility of the order of 30 cm/V-sec. α-HgS is photoconductive with a peak photoconductivity at about 6000Å.

The optical properties of black β-HgS show that its band structure is similar to that of α-Sn. Also, HgSe and HgTe are zero gap semimetals with similar properties.

For α-HgS, Figure 1 shows the infrared reflectivity from 20μm to 50μm. The structure gives information concerning the lattice structure of the material.[6] In Table 1 is presented the refractive (birefringent) indices for α-HgS between 0.62μm and 11.0μm. Using the formula

$$R = \frac{(n-1)^2}{(n+1)^2},$$

we can compute R assuming no extinction.[7] In Figure 2 we have the transmission spectra for α-HgS at two temperatures: 77°K and 295°K. From 150cm^{-1} to 250cm^{-1} there is a significant change in the transmittance -- that the reflectivity may alter is a possibility since there is a change in the extinction coefficient.

For β-HgS, the static dielectric constant is 18.2 at room temperature as calculated from the transverse and longitudinal phonon structure using the Lyddane-Sachs-Teller relationship.[7,8] The high frequency (infinite)

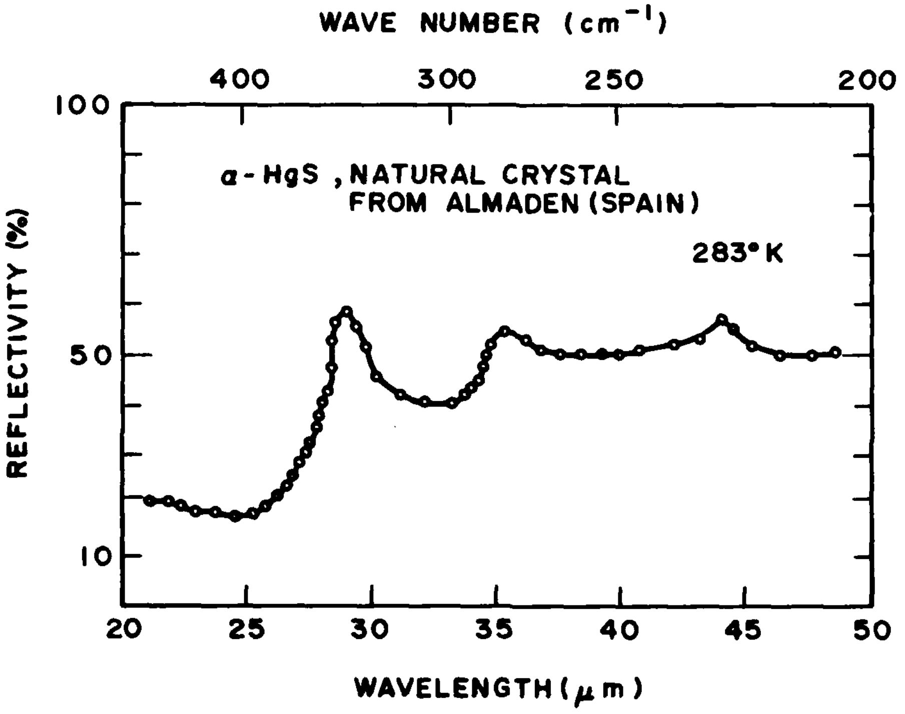

Figure 1. Room temperature reflectivity spectrum for α-HgS.

TABLE I

TEMPERATURE 25°C

$\lambda(\mu)$	$(\nu = 1/\lambda)\text{x}\ 10^{-4}$ cm^{-1}	n^e	n^o
0.62	1.6129	3.2560	2.9028
0.65	1.5385	3.2064	2.8655
0.68	1.4706	3.1703	2.8384
0.70	1.4286	3.1489	2.8224
0.80	1.2500	3.0743	2.7704
0.90	1.1111	3.0340	2.7383
1.00	1.0000	3.0050	2.7120
1.20	0.8333	2.9680	2.6884
1.40	0.7143	2.9475	2.6730
1.60	0.6250	2.9344	2.6633
1.80	0.5556	2.9258	2.6567
2.00	0.5000	2.9194	2.6518
2.20	0.4545	2.9146	2.6483
2.40	0.4167	2.9108	2.6455
2.60	0.3846	2.9079	2.6433
2.80	0.3571	2.9052	2.6414
3.00	0.3333	2.9036	2.6401
3.20	0.3125	2.9017	2.6387
3.40	0.2940	2.9001	2.6375
3.60	0.2778	2.8987	2.6358
3.80	0.2632	2.8971	2.6353
4.00	0.2500	2.8963	2.6348
5.00	0.2000	2.8863	2.6267
6.00	0.1667	2.8799	2.6233
7.00	0.1429	2.8741	2.6156
8.00	0.1250	2.8674	2.6112
9.00	0.1111	2.8608	2.6066
10.00	0.1000	2.8522	2.6018
11.00	0.0909	2.8434	2.5914

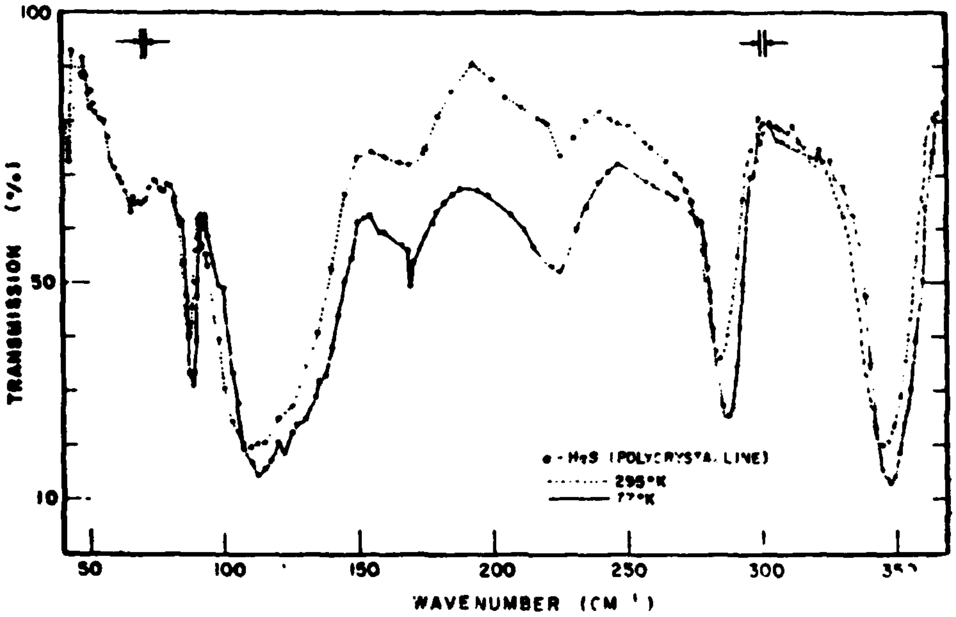

Figure 2. Transmission spectrum of polycrystalline trigonal mercury sulfide.

dielectric constant is calculated to be 11.36 using this same relationship. β-HgS has a high carrier concentration causing difficulties in deriving values for the static dielectric constant from the opticalreflectivity data in the far infrared beyond the reststrahlen band. The high reflectivity values at wavelengths above 100 μm indicate that the absorption of light in the material cannot be neglected.

We have, however, been unable to locate much literature concerning the phase transition itself between α - and β-HgS. The temperature is not exact, but depends on pressure. Also, we have been unable to locate published reflectivity curves for β-HgS which would allow us to make a direct comparison for each state at a given wavelength. We believe that HgS can be put in the category of "possible candidate material," but a deeper search into the literature is necessary. Further, it appears that due to the presence of the phase transition, it is difficult to grow pure crystals of α-HgS. We do not know if thin films of HgS can be produced.

REFERENCES (HgS)

1. K.L. Aurivillius, Acta. Chem. Scand. 4, 1413 (1950).
2. E.H. Carlson, J. Cryst. Growth, 1, 271 (1967).
3. O.L. Curtis, J. Appl. Phys. 33, 2461 (1962).
4. A.N. Mariana and E.P. Warekois, Science 142, 672 (1973).
5. A.G. Mikolaichuk and Ya. I. Dutchak, Chem. Abstr. 65, 9847a (1966).
6. H.D. Riccuis and K.J. Siemen, J. Chem. Phys. 52, 4090 (1970).
7. W.L. Bond, et.al., J. Appl. Phys. 38, 4090 (1967).
8. R.H. Lyddane, et.al., Phys. Rev. 59, 673 (1941)

In_2S_3

Indium Sulfide or Di-Indium Trisulfide

In_2S_3 exists as cubic α-In_2S_3 and tetragonal β-In_2S_3. Until recently, no detailed studies on the structure and the vibrational properties of In_2S_3 have been reported.

β-In_2S_3 is the stable room temperature phase. At 420°C there is a transition to α-In_2S_3. The β-phase is tetragonal and undergoes a disordering into the cubic defect lattice having the cation sites and the vacancies in a random arrangement.[1,2] Above 750°C, there is a third phase, γ-In_2S_3, which possesses a trigonal structure.[3] There is a fairly extensive literature concerning the crystal structure of these phases of In_2S_3, a summary of which is given in Reference 4.

β-In_2S_3 is a birefringent material. We have located data on its far infared reflectivity for when the electric field vector ($\vec{E}$) is both parallel and perpendicular to the crystal $\vec{c}$ axis. The reflectivity spectra is dependent on whether the sample is quenched or annealed. The results are shown in Figure 1. Note that the quenched sample shows a much higher reflectivity in the low-frequency range than the annealed sample. There are eight vibrational bands.

In Figure 2 we have the analogous measurements for α-In_2S_3. Again, there is a noticable difference for each sample.

The literature indicates that In_2S_3 is a switchable phase transition material; but as Figures 1 and 2 illustrate, the far infrared spectra does not change appreciably with phase, but rather more so with sample preparation. We have been unable to locate any literature on the electrical or near IR properties of In_2S_3.

REFERENCES (In_2S_3)

1. G. King, Acta Cryst. 15, 512 (1962).
2. H. Hahn and W. Klinger, Z. Anorg. Allg. Chem. 260, 97 (1949).
3. H. Diehl and R. Nitsche, J. Cryst. Growth, 28, 306 (1975).
4. K. Kambas et.al., Phys. Stat. Sol (6), 105, 291 (1981).

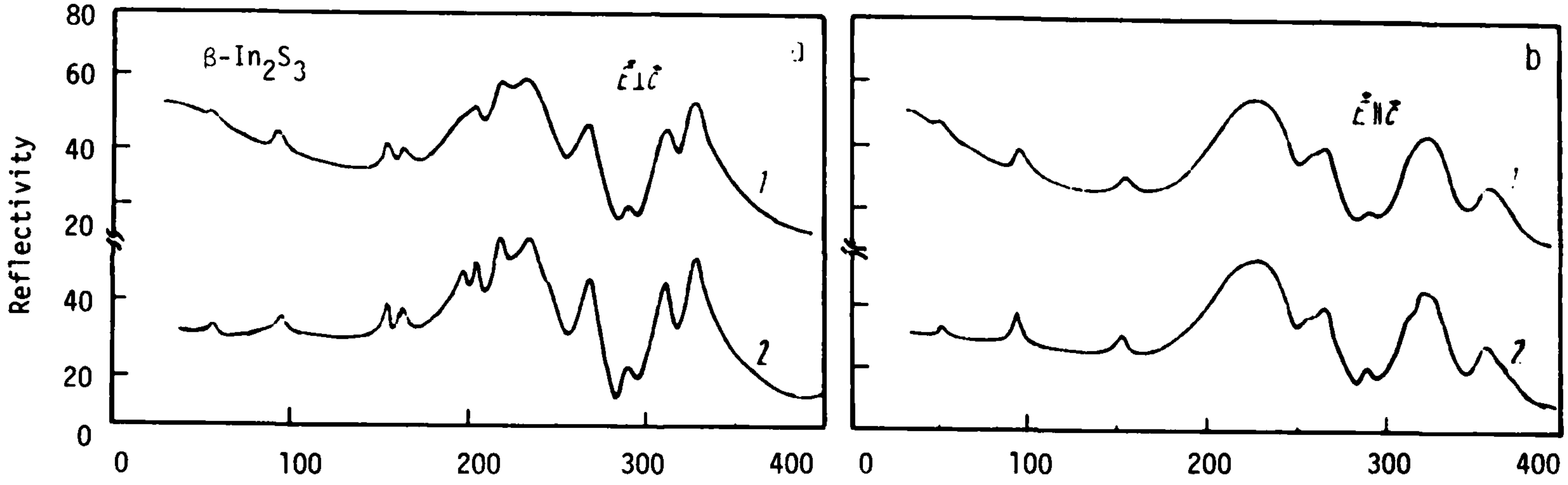

Figure 1. Far Infrared reflectivity spectra of β-In$_2$S$_3$; (a) $\vec{E} \perp \vec{c}$, (b) $\vec{E} \parallel \vec{c}$. (1) Quenched sample; (2) annealed sample.

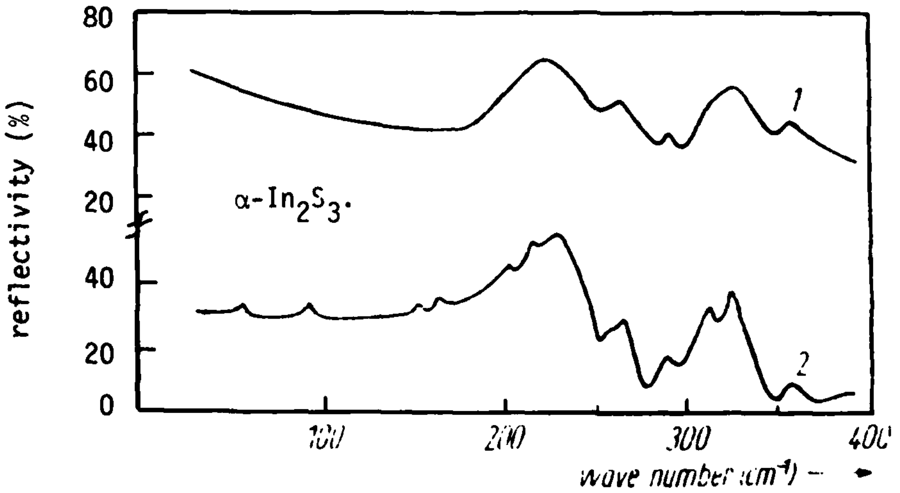

Figure 2. Far infrared reflectivity spectra of α-In_2S_3. (1) Quenched sample; (2) annealed sample.

MnS

Manganese Monosulfide

MnS or manganese monosulfide occurs in three forms. They are the "green form" or α-MnS and the "pink form" or β-MnS.* α-MnS possesses the same crystalline structure as NaCl whereas the β-MnS form has the zinc blende or wurtzite structure.[1] For all three forms, each Mn^{+2} ion has twelve nearest neighbors, however the number of adjacent S^{-2} atoms varies. For the α-MnS form with the NaCl structure there are six S^{-2} neighbors to each Mn^{+2}; for the zinc blende or wurzite structural form there are four S^{-2} neighbors. For α-MnS, each Mn^{+2} ion is bonded through a sulfur atom to its twelve nearest neighbors by 180° linkages, i.e., Mn-S-Mn linkages. In the β-species, each Mn^{+2} is bonded tetrahedrally through sulfur atoms to its nearest Mn neighbors. The crystal lattice parameters have been studied as a function of pressure and temperature.[2-4]

β-MnS is meta-stable at room temperature. At about 200°C, it undergoes a transition to α-MnS. Further, β-MnS changes to α-MnS under high pressures.[5] α-MnS also undergoes a small rhombohedral deformation below the Neel temperature. Preparation of α-MnS is usually (for single crystals) done using the vapor transport method.[6] Single crystals of β-MnS have been grown from silica gels under proper conditions of temperature and concentration.[7]

For α-MnS, the specific heat shows a cusp in the vicinity of the Neel temperature, as shown in Figure 1.[8]

In Table 1 and 2 and Figure 2 we present further data on the magnetic structure of the three polymorphic states of MnS.[9] In Figures 3 and 4 we present further information on the sructure of the MnS lattice in all three states. Note that MnS's three polymorphs can exist at room temperature, though as mentioned above, α-MnS can be converted to β-MnS at certain temperatures and pressures. In Figure 5 we see the magnetic ordering scheme for cubic β-MnS.[10]

---

* β-MnS alone possesses two different crystalline states - see Table 1.

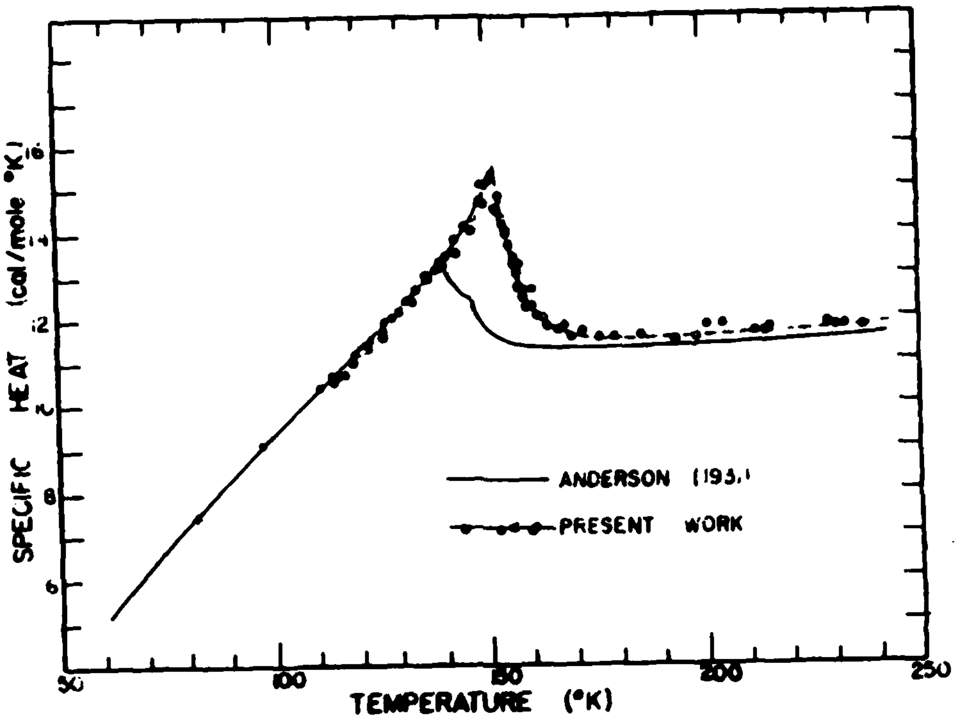

Figure 1. Specific heat of α-MnS in the vicinity of the Neel temperature.

TABLE 1

POLYMORPHIC FORMS OF MnS

Form	Crystal Structure	Magnetic Structure	Electrical Properties
α-MnS	Rock salt structure	See Figures 1,2 Table 2	Figures 6,7
β-MnS	Zinc blende	See Figure 2 Table 2	unknown
β-MnS	Hexagonal-wurtzite	See Figure 2 Table 2	unknown

TABLE 2

MAGNETIC SUSCEPTIBILITY OF MnS AS A FUNCTION OF TEMPERATURE

Form											
α-cubic	T(°K)	61	76	167	195	298	340	365	375	405	
	$\chi_{mol} X 10^6$	6450	6500	6600	6420	5560	5270	5085	5050	4855	
β-cubic[a]	T(°K)	76	91	195	295	396	417	440			
	$\chi_{mol} X 10^6$	3490	3610	3750	3470	3240	3190	3130			
β-hexagonal	T(°K)	59	76	91	195	295	386	419	441	457	471
	$\chi_{mol} X 10^6$	3900	4165	4265	4040	3765	3540	3450	3400	3355	3330

[a] Corrected for the presence of hexagonal phase.

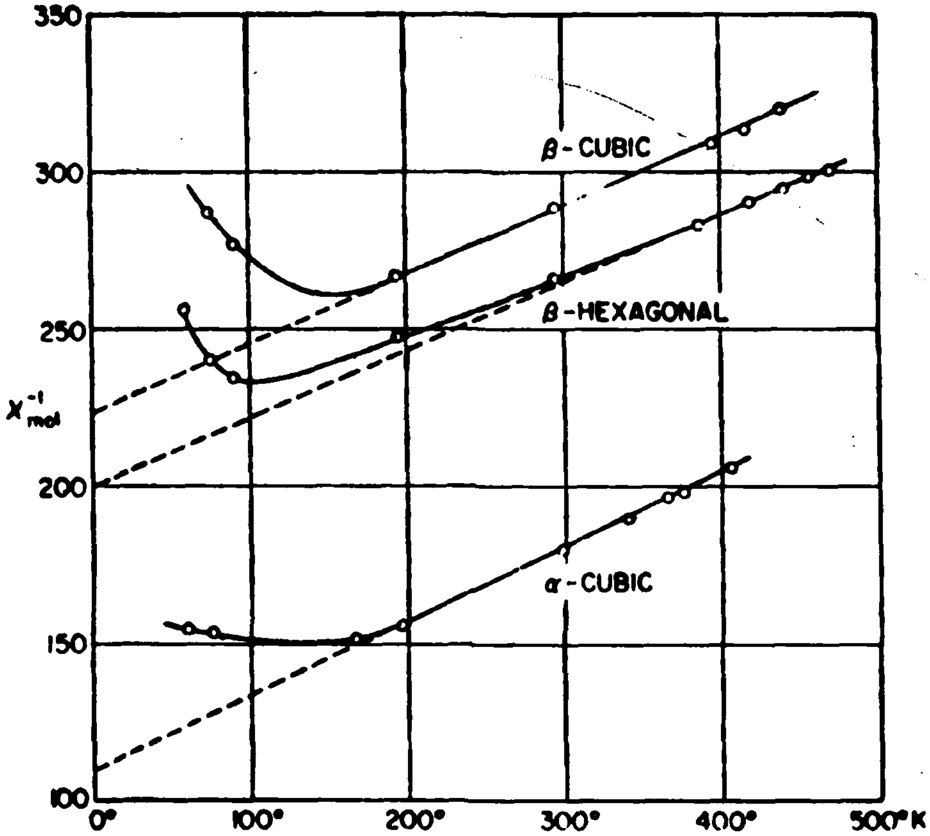

Figure 2. Magnetic susceptibility of MnS as a function of temperature.

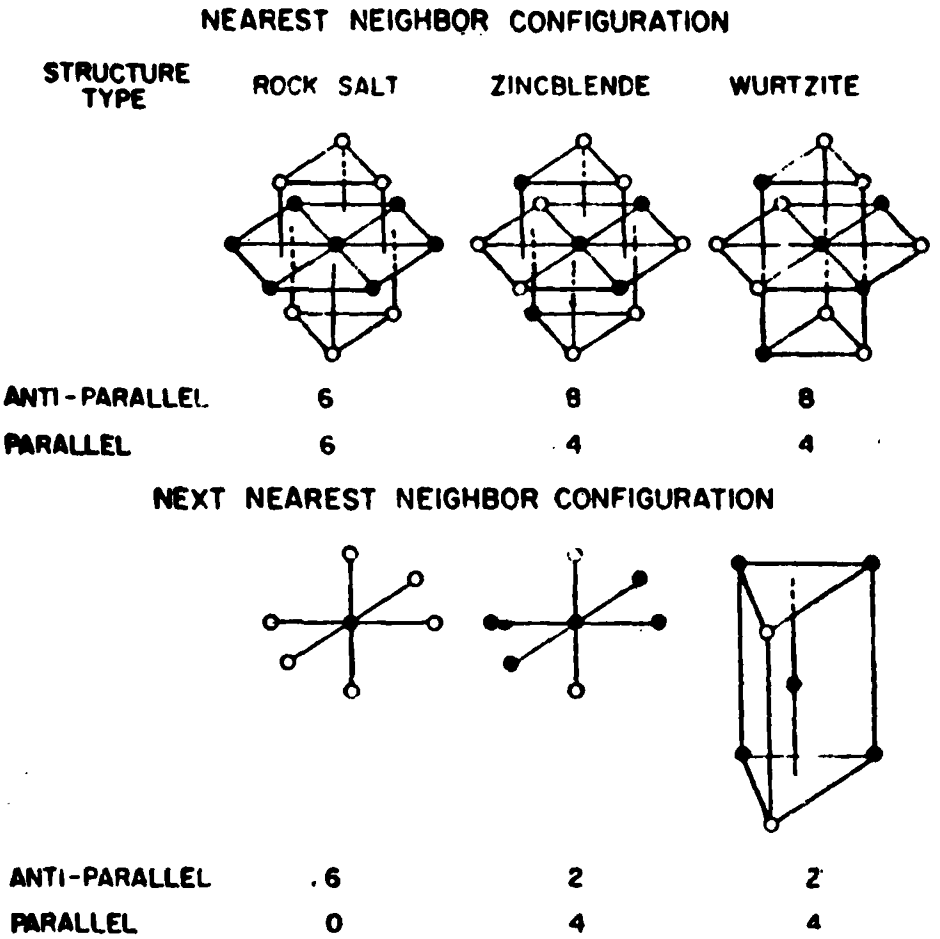
NEAREST NEIGHBOR CONFIGURATION
STRUCTURE TYPE
ROCK SALT
ZINCBLENDE
WURTZITE
NEXT NEAREST NEIGHBOR CONFIGURATION

NEAREST NEIGHBOR CONFIGURATION	ROCK SALT	ZINCBLENDE	WURTZITE
ANTI-PARALLEL	6	8	8
PARALLEL	6	4	4

NEXT NEAREST NEIGHBOR CONFIGURATION	ROCK SALT	ZINCBLENDE	WURTZITE
ANTI-PARALLEL	.6	2	2
PARALLEL	0	4	4

Figure 3. Metal-metal nearest neighbor and next nearest neighbor configurations for the three polymorphic forms of MnS.

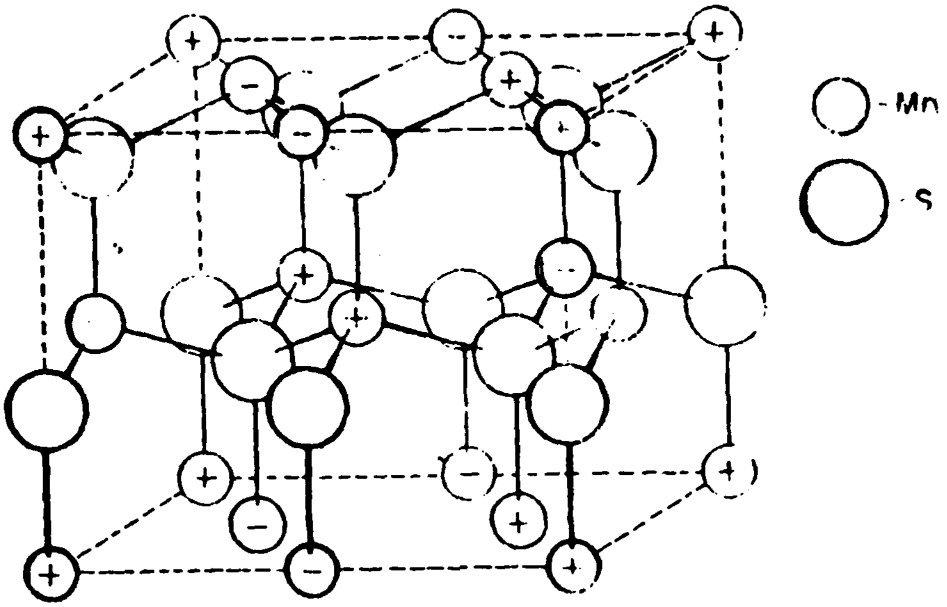

Figure 4. Magnetic structure of β-MnS (wurtzite form). The orthohexogonal unit cell is shown.

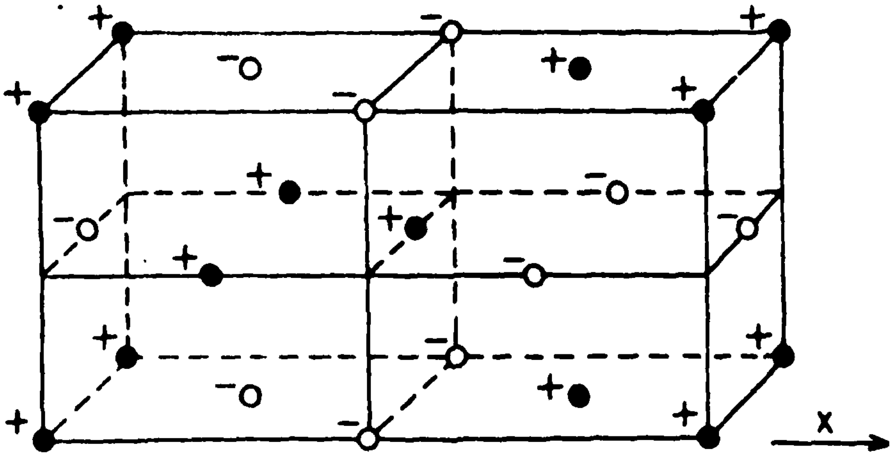

Figure 5. Magnetic ordering scheme deduced from diffraction studies. Spins lie in the yz plane but the direction within this plane is not completely determined.

The cubic form of β-MnS undergoes a first-order magnetic phase transition. Also, this phase transition displays a hysteresis type character.[10] A theoretical study for this transition developed a magnetic ordering Hamiltonian which predicted that this transition may be either first or second order in nature.[10]

There appears to be an adequate understanding of the electrical properties of α-MnS. For α-MnS, the conductivity increases with temperature, as expected for a semiconductor; the exact magnitude also depends on stoichiometry.[11] There is a structure in the conductivity curve (a "knee") near the Neel temperature at 152°K. The conduction mechanism in MnS probably involves hopping. Figure 6 shows the temperature dependence of the resistivity for α-MnS. Figure 7 shows the same parameter after two heating-cooling cycles.[12] In Reference 8 a bond model for α-MnS was developed to aid in explaining the electrical and optical absorption properties.

There are three main absorption peaks for α-MnS, denoted by A, B, and C. They are at 16,420 cm^{-1}, 19,398 cm^{-1}, and 22,016 cm^{-1}, respectively, and are due to transitions with the d-electrons.[8] Further, these peaks show a slight variation in amplitude and position with temperature, as shown in Figure 8. There also seems to be a dependence on the method of sample preparation. Note that the optical absorption is related to the coefficient of extinction k by the relation:

$$\alpha = \frac{4\pi k}{\lambda} .$$

In Figure 9 we see how the absorption coefficient appears if we compute it from k using data obtained from reflectance measurements. Conversely, since α varies with temperature, it is safe to say that reflectance will vary, perhaps only slightly, with temperature.

In Table 3 we give the variation of the index of refraction in α-MnS with wavelength. This was determined by making thin films of α-MnS and using the relationship:

$$m\lambda = 2nd$$

where d is the film thickness and m an integer. Reflectance losses at each surface was taken into account.[8]

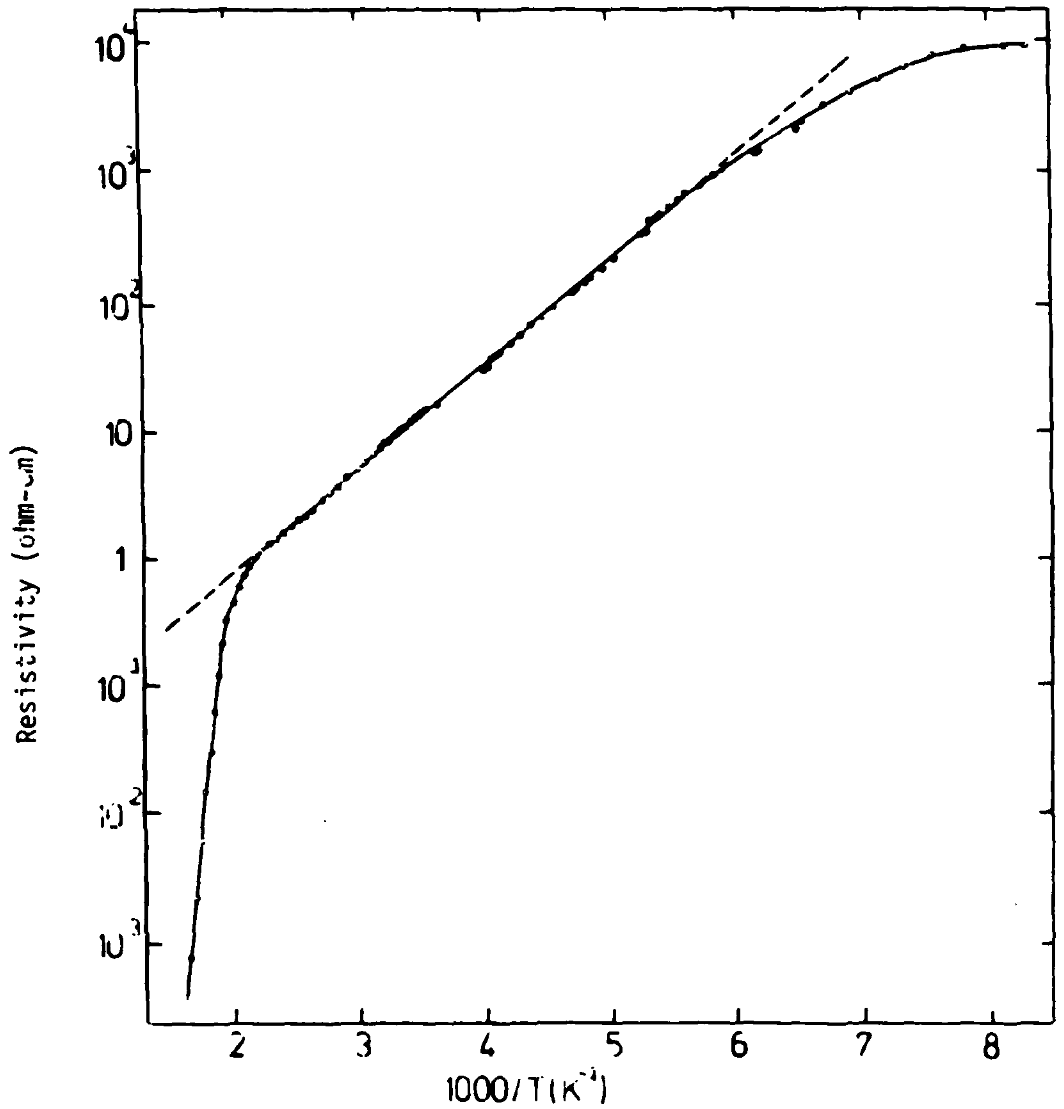

Figure 6. Temperature dependence of the resistivity ρ of a single crystal of α-MnS, grown by iodine-vapor transport and quenched from 600K.

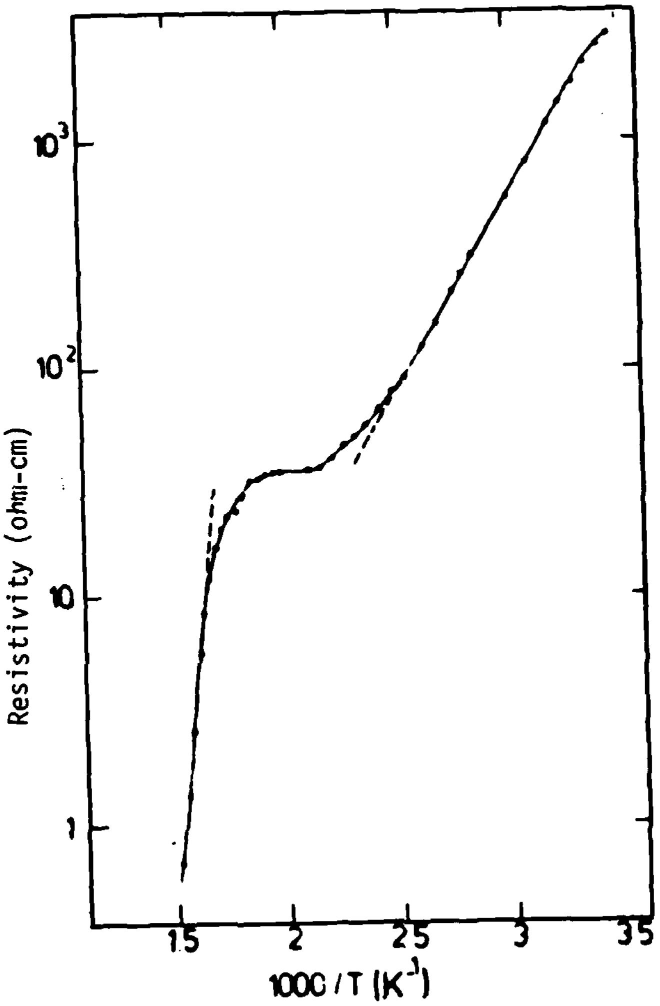

Figure 7. Temperature dependence of the resistivity of the same crystal as used in Figure 6 after two heating-cooling cycles.

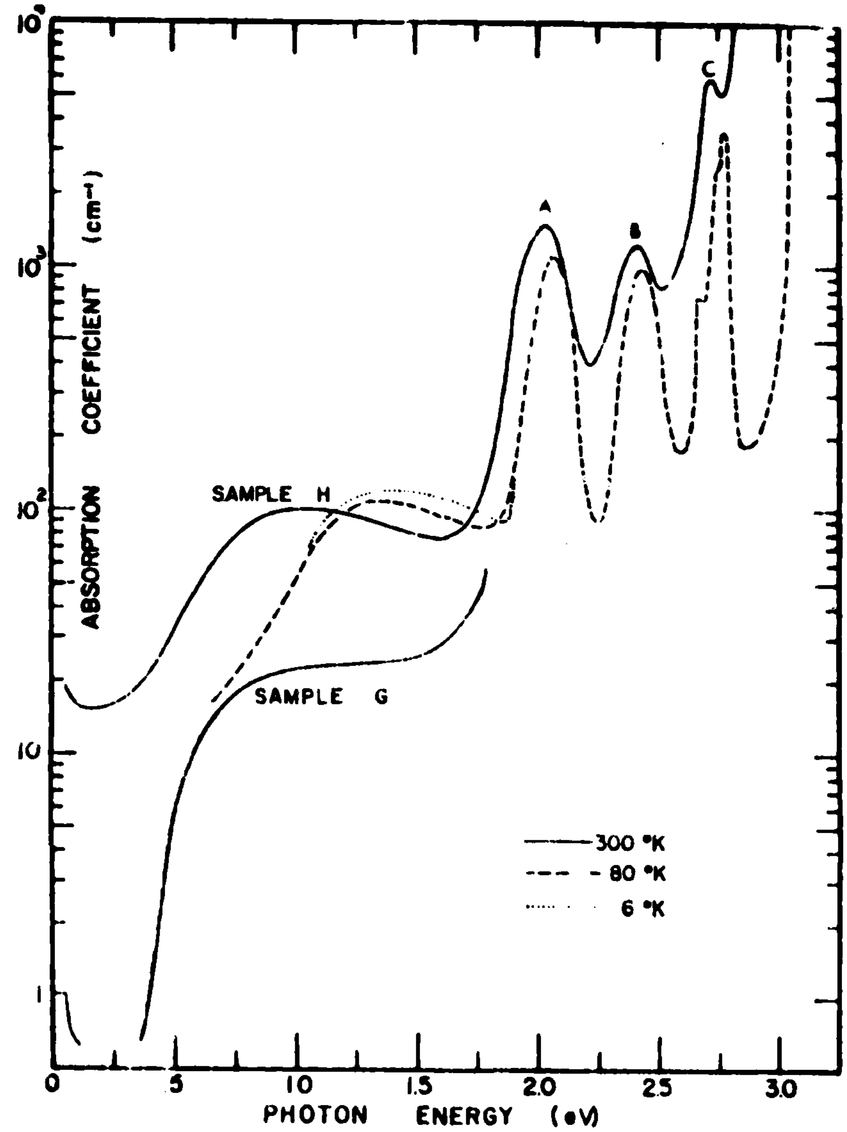

Figure 8. Optical absorption spectra of MnS crystals.

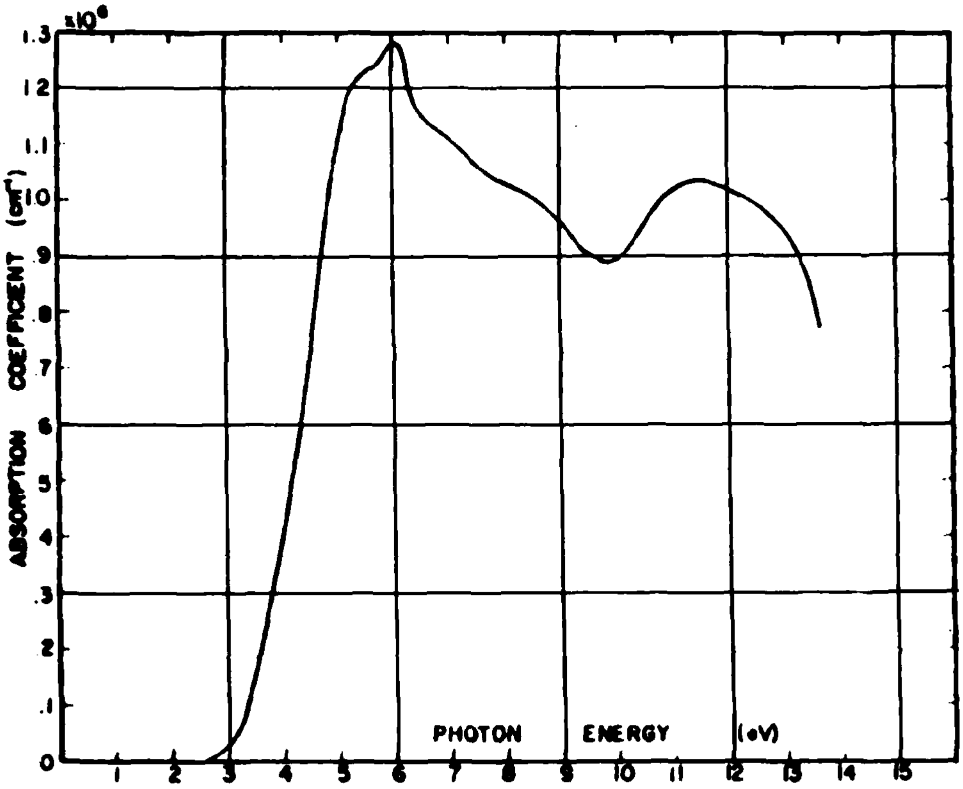

Figure 9. Spectral dependence of the absorption coefficient calculated from reflectance data.

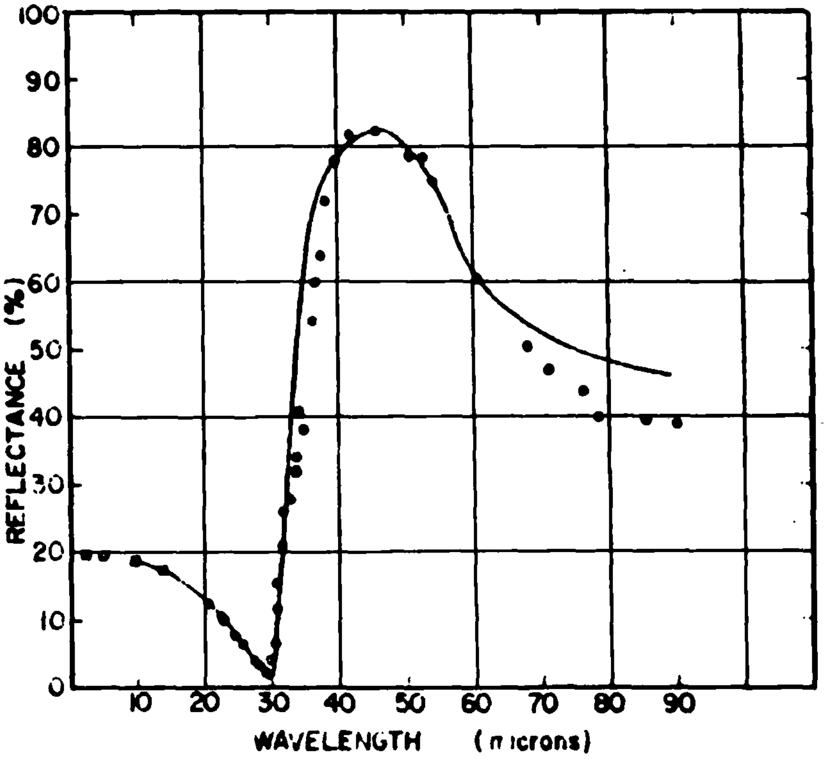

Figure 10. Infrared reflectance of a polished powder sample of MnS compared with the best fit to a one-frequency dispersion calculation. Open circles and squares are data points and the solid curve represents the calculated curve.

TABLE 3
VARIATION OF INDEX OF REFRACTION WITH WAVELENGTH FOR α-MnS

Wavelength (microns)	Index of Refraction (n)
0.6	2.807
0.7	2.753
0.8	2.720
0.9	2.697
1.0	2.682
1.1	2.671
1.2	2.663
1.3	2.657
1.4	2.651
1.5	2.646
1.6	2.642
1.7	2.639
1.8	2.637
1.9	2.634
2.0	2.632
2.5	2.628
3.0	2.625
4.0	2.614
5.0	2.605
6.0	2.595
7.0	2.582
8.0	2.570
9.0	2.554
10.0	2.532
11.0	2.508
12.0	2.478
13.0	2.435

Figures 10, 11 and 12 show the far infrared, infrared, visible and UV reflectance for α-MnS. Note that near 30-40 microns a feature which can be modeled using an oscillator fit appears. From the reflectivity data the dielectric function $\hat{\varepsilon} = \varepsilon_1 + i\varepsilon_2$ can be derived. Also, from this we can derive the index of refraction and extinction coefficient. These are shown in Figures 13 and 14. n and k can be obtained from R using the Kramers - Kronig method, whereas ε_1 and ε_2 can be obtained from n and k via the equations:

$$\varepsilon_1 = n^2 - k^2 ,$$
$$\varepsilon_2 = 2nk .$$

From $\hat{\varepsilon}$, we can compute other parameters for the material, such as the plasma frequency and plasma edge in the UV, if it exists (usually in metals). The band gap for α-MnS is 3.2eV, which leads us to conclude that it is an insulator. We have not been able to determine the corresponding optical properties for the two states in β-MnS.

We suspect that if β-MnS possesses a metallic character, that the absorption will markedly change throughout the infrared. There is no known literature that addresses the nature of the phase transition or if it is reversible, except that dealing with magnetic structure. Exactly how the optical properties change is also unknown.

REFERENCES (MnS)

1. G. Brauer, Handbook of Preparative Inorg. Chem., Vol. 1, p. 2 (1963).
2. S. Furuseth and A. Kjekshus, Acta. Chem. Scand., 19, 1405 (1965).
3. R.L. Clandenon and H.G. Drickamer, J. Chem. Phys. 44, 4223 (1966).
4. I. Wakabayashi, et.al., J. Phys. Soc. Japan, 25, 227 (1968).
5. C.J.M. Rooymans, J. Inorg. Nucl. Chem. 25, 253 (1963).
6. R. Nitsche, J. Phys. Chem. Solids, 17, 163 (1960).
7. A. Schwarz, et.al., Mat. Res. Bull 2, 375 (1967).
8. D.R. Huffman and R.L. Wild, Phys. Rev. 148, 526 (1966).
9. L. Corliss, N. Elliot, and J. Hastings, Phys. Rev. 104, 924 (1956).
10. J.M. Hastings, et.al., Phys. Rev. B24, 1388 (1981).
11. C.F. Squire, Phys. Rev. 56, 960 (1939).
12. H.H. Heikens, et.al., J. Phys. Chem. Solids, 39, 833 (1978).

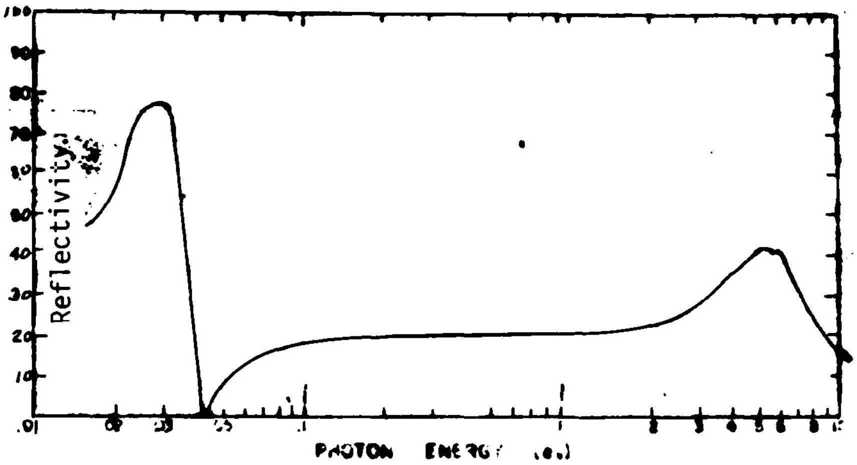

Figure 11. Reflectance spectrum of MnS

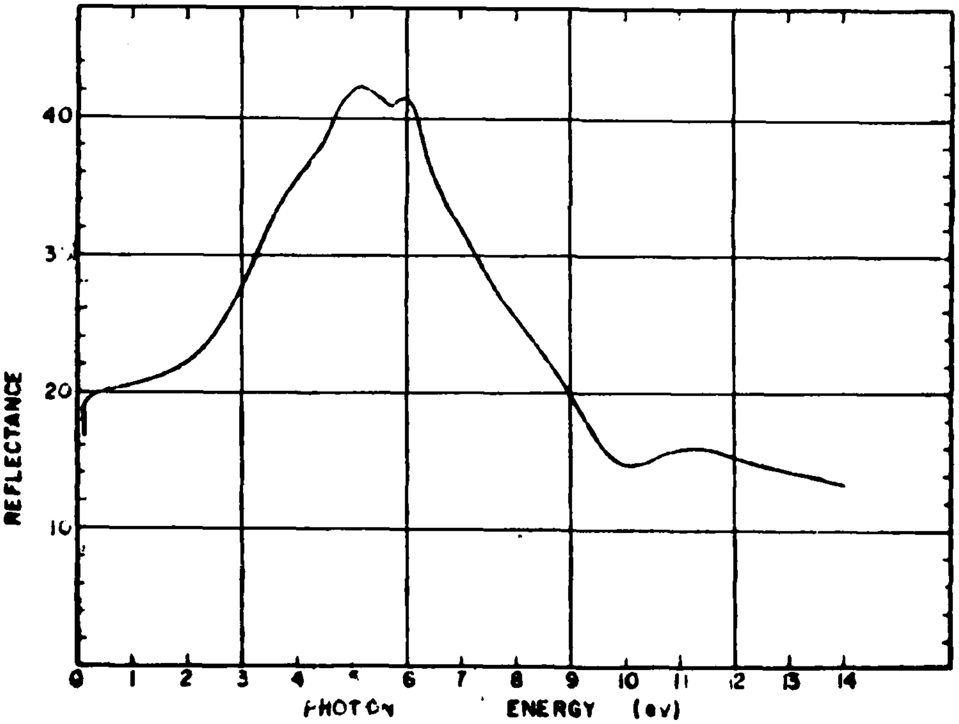

Figure 12. High energy reflectance spectrum of single-crystal MnS.

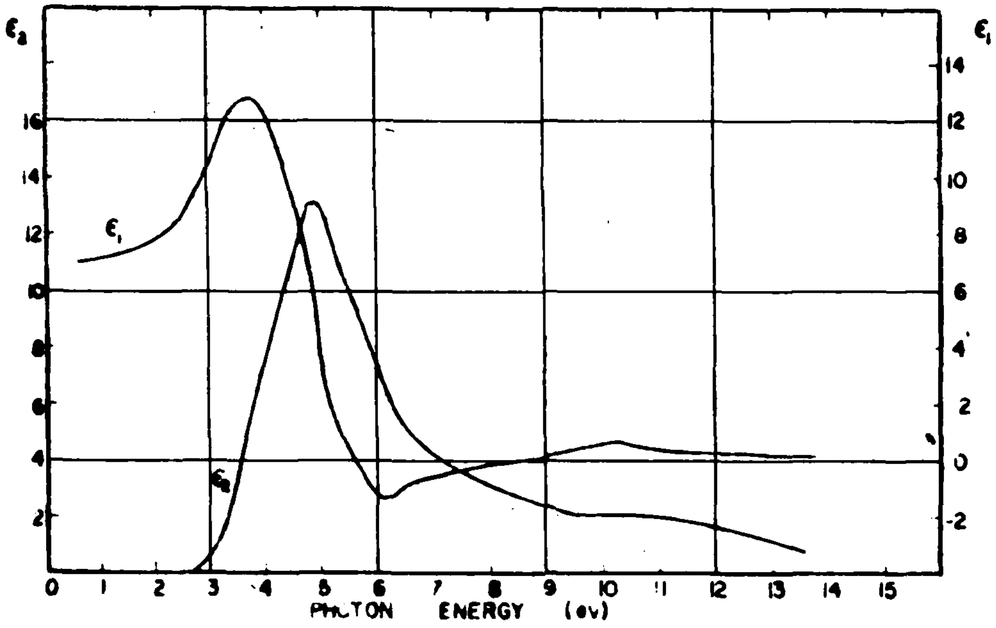

Figure 13. Spectral dependence of the real and imaginary parts of the dielectric constant calculated from reflectance data.

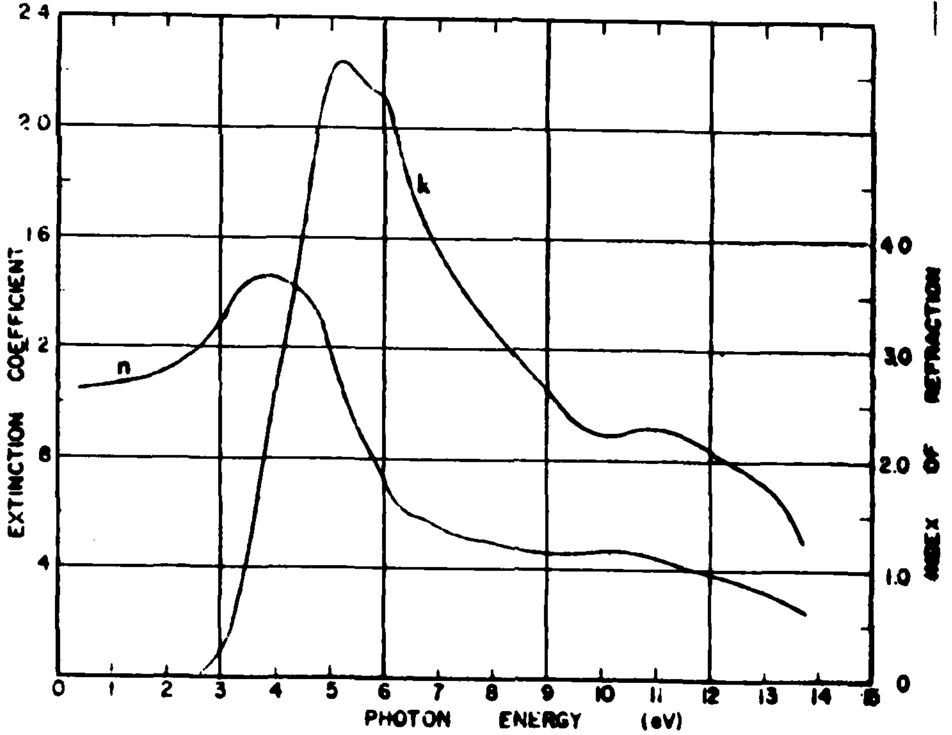

Figure 14. Spectral dependence of the real and imaginary parts of the refractive index calculated from reflectance data.

MnS_2

Manganese Disulfide

MnS_2 is a transition-metal dichalcogenide with the pyrite type crystal structure. MnS_2 is a semiconductor with a band gap in the near infrared; it is paramagnetic and becomes antiferromagnetic at about 49°K. The bonding of the sulfur atoms is in the form "pseudo-tetrahedran" with a sulfur atom at the center, one arm formed by a sulfur-sulfur bond and the other three arms formed by sulfur-metal bonds. The metal atoms are sixfold coordinated to their nearest neighbor sulfur atoms. The arrangement of the bonding to the sulfur atoms is that of a distorted octahedran.[1,2]

The agnetic susceptibility of MnS_2 has been measured at various temperatures and the magnetic unit cell is twice the chemical unit cell.[3] According to Reference 4, the antiferromagnetic - paramagnetic phase transition is at 49.20°K, as determined by susceptibility measurements. Also, heat capacity studies give a transition temperature of 47.93°K.[5,6] The electrical properties of MnS_2 have been explained qualitatively by a semiempirical molecular orbital scheme.[7] MnS_2 appears to be the only pyrite that exhibits localized electron behavior;[8] in the other pyrites, covalent mixing with the two σ bonding orbitals of e symmetry (charge symmetry) is strong enough to create a narrow σ^*-bond of itinerant electron states as well as a low-spin state of the cation.[9]

Figure 1 illustrates the pyrite structure. Here "X" denotes a sulfur atom, but it can also be a selenium or tellerium atom.[3] In Figure 2 the magnetic susceptibility measurements for MnS_2, $MnSe_2$ and $MnTe_2$ are presented, all as a function of temperature. For these measurements the Gouy method was used in the range 76° - 500°K. [Let us recall what the magnetic susceptibility is. Let $\vec{M}$ be the magnetic polarization of a material which is derivable in terms of the magnetic dipole moment per unit volume. The magnetic polarization of the material produces a magnetic flux density which is sectionally additive to the magnetic flux density present in free space to constitute the net magnetic flux density $\vec{B}$. That is:

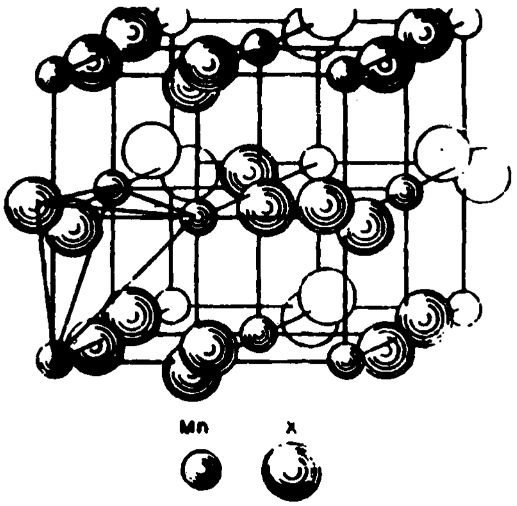

Figure 1. The pyrite structure.

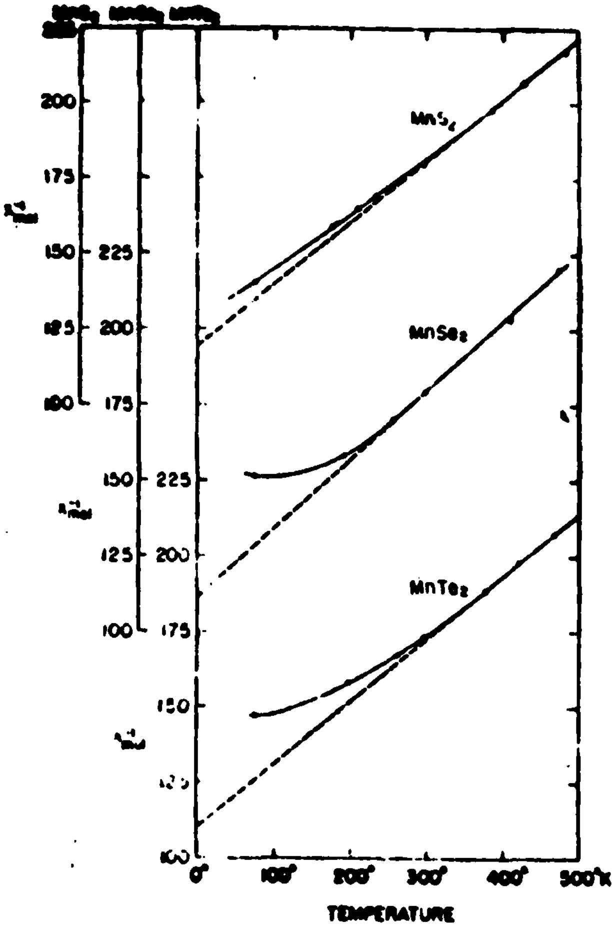

Figure 2. Inverse susceptibilities of MnS_2, $MnSe_2$, and $MnTe_2$ as a function of temperature.

$$\vec{B} = \mu_0 \vec{H} + \vec{M}$$

Often $\vec{M}$ is proportional to $\vec{H}$, the constant of proportionality being the magnetic susceptibility, χ_m. Hence $\vec{M} = \chi_m \vec{H}$, and for $\vec{B} = \mu\vec{H}$ we have $\mu = \mu_0 + \chi_m$ for μ_0 the magnetic permeability of free space and μ the permeability.]

Concerning the optical properties of MnS_2, we have only been able to locate one paper which presents reflectivity curves in the far infrared in the 140 - 450cm^{-1} region. This region is primarily of interest for studying the phonon structure of the material and to determine the necessary parameters for a classical oscillator fit. Figure 3 and 4 show the reflectivity and a 3- and 4-fit classical oscillator curve for comparison. We see that the 4-fit model more accurately fits the experimental data, as expected.[1]

An important observation is the nature of the curve for frequencies above 280cm^{-1}. This has resemblance to the curve for FeS_2. This type of phenomena also occurs for β-Ag_2S. From the little we see, we can extrapolate to conclude that MnS_2 is transparent in the IR through the 10.6µm and 3.8µm lines. If there is a phase transition at some temperature above 300°K (which is unknown), then it is likely that this curve may undergo a significant change. That is, MnS_2, like Ag_2S, may go from a semiconducting state to a metallic (Drude metal) with a large alteration in optical constants, e.g., n and k, the index of refraction and extinction coefficient. To date, such a change has not been observed.

REFERENCES (MnS_2)

1. J.L. Verble and F.M. Humphrey, Solid State Commun., 15, 1693 (1974).
2. S. Furuseth and A. Kjekshus, Acta Chem. Scand., 19, 1405 (1965).
3. J.M. Hastings, et.al., Phys. Rev. 115 13 (1959).
4. M.S. Lin and H. Hacker, Solid State Commun., 6, 687 (1968).
5. M.E. Fischer, Phil. Mag. 7, 1731 (1962).
6. E.E. Westrum and F. Grønvold. J. Chem. Phys. 52, 3820 (1970).
7. T.A. Bither, et.al., Inorg. Chem. 7, 2208 (1968).

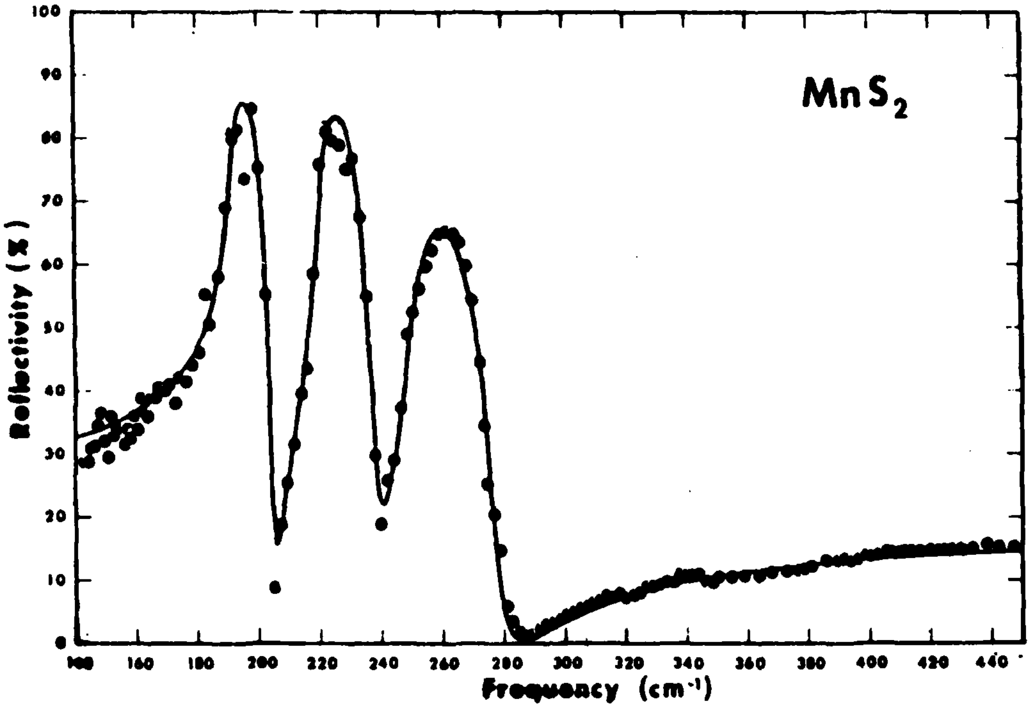

Figure 3. Three oscillator fit to the infrared reflectivity of MnS$_2$. The points are the experimental data and the curve is the theoretical fit.

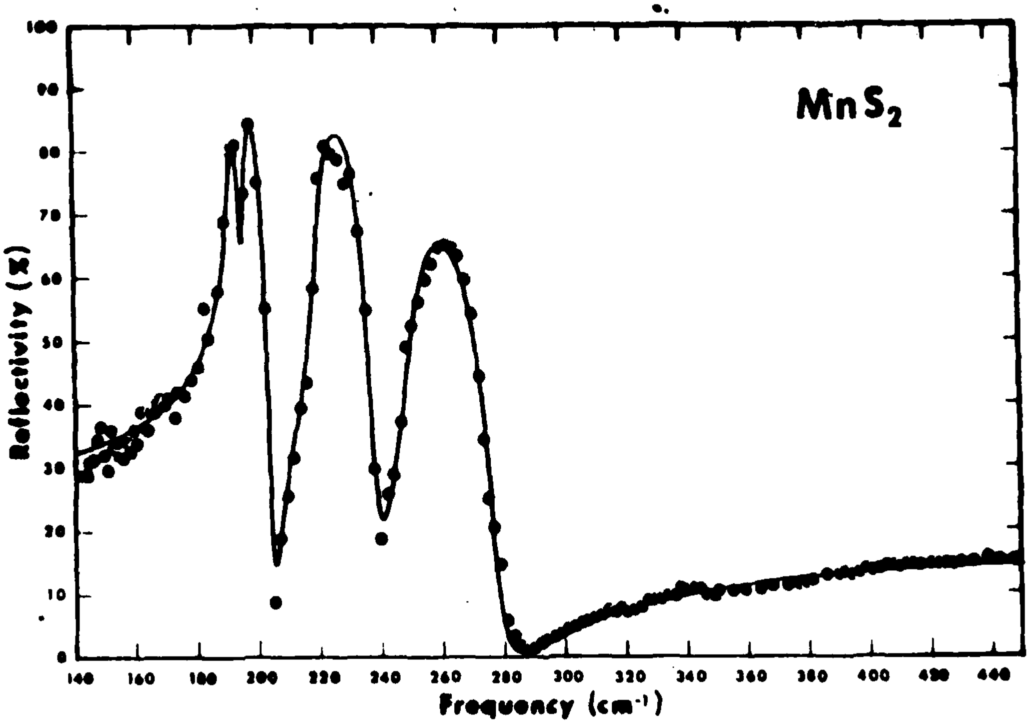

Figure 4. Four oscillator fit to the infrared reflectivity of MnS$_2$. The points are the experimental data and the curve is the theoretical fit.

REFERENCES MnS_2 (CONT.)

8. J.B. Goodenough in Solid State Chemistry, edited by C.N.R. Rao, Marcel Dekker, New York, 1974.

9. C.N.R. Rao and K.P.R. Pisharody, Prog, in Solid State Chem., 10, 207 (1975).

MoS_2

Molybdenum Disulfide or Molybdenite

Molybdenum disulfide (or molybdenite) is a hexagonal layer compound and occupies a central position in the large class of layered compounds formed by transition metals and sulfur, selenium, or tellurium. Molybdenite exists in two polytypes, 2H-MoS_2 and 3R-MoS_2, depending on the arrangement of the S-Mo-S layer.[1] In both forms the Mo atom is surrounded by S-atoms forming a trigonal prism. The 2H-MoS_2 structure can be transformed to 3R-MoS_2 under high pressure.[2]

MoS_2 is a diamagnetic semiconductor, which, due to the layered structure, exhibits both electrical and optical anisotropy. MoS_2 also exhibits photoconducting properties.[3] A fairly good, but brief, review of the properties of MoS_2 including a band structure diagram for 2H-MoS_2 is given in Reference 4.

Before presenting curves on the optical properties of the two polytypes of MoS_2, we shall technically define what they are. Each polytype have trigonal prismatic coordinates. The 2H polytype refers to 2 layers per unit cell stacked in hexagonal symmetry (space group $D^4{}_{6h}$). The 3R polytype refers to 3 layers in rhombohedral symmetry and belongs to the space group $C^5{}_3$. The layers are bonded together by the weak van der Waals force, similar to graphite - as a result MoS_2 is an excellent lubricant. Figure 1 shows the primitive unit cell arrangement for 2H-MoS_2.[5]

Optical reflection studies have been performed for MoS_2 in the far infrared, visible, and UV regions of the spectrum. These measurements were made with the polarization electric field vector either parallel or perpendicular to the c-axis of the crystal. That is, for $\vec{E} \parallel \vec{c}$ or $\vec{E} \perp \vec{c}$. MoS_2 shows reflectivity curves that can be modeled by the classical oscillator theory. In Figure 2 we see an example of the FIR spectra in the 300 cm^{-1} to the 550 cm^{-1} range.[5] All published measurements of R in the FIR for MoS_2 indicate this type of structure which yields information concerning the phonon structure of the lattice. These studies have been performed almost exclusively at room temperature - no temperature dependence has been reported.

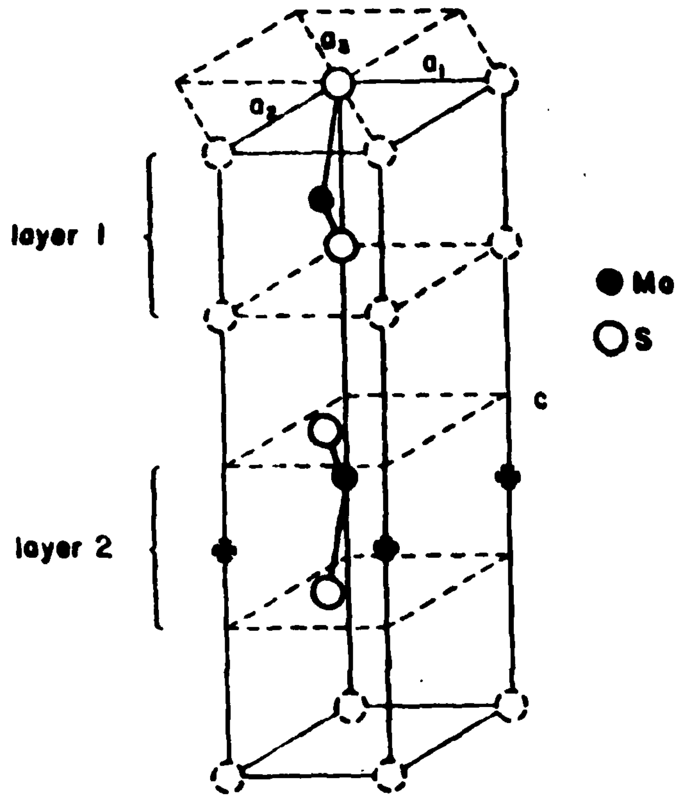

Figure 1. Primitive unit cell of MoS_2(2H)

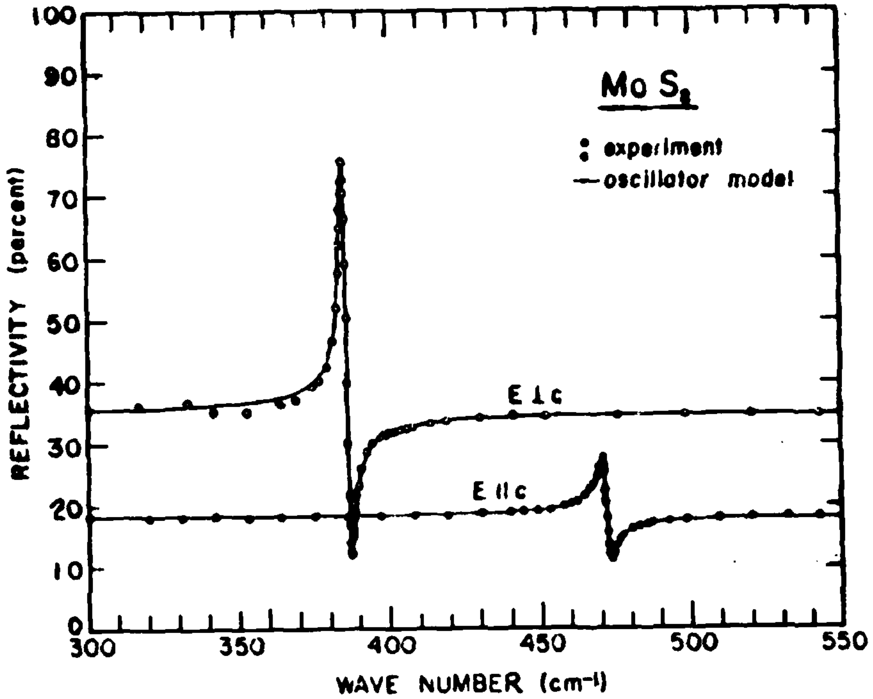

Figure 2. Reflectivity of MoS_2 (2H) at room temperature. $\vec{E} \perp \vec{c}$ and $\vec{E} \parallel \vec{c}$

Reflectivity measurements in the visible have, however, been done at T = 100°K as shown in Figure 3.[6] Curves (2) and (3) in Figure 3 are different because curve (3) is obtained from the cleaved crystals. These are all normal incidence measurements.

Transmission measurements appear to be primarily in the near UV.[7] There appears to be only one curve illustrating how the optical properties of MoS_2 change with temperature.[7] This curve is shown in Figure 4. These twin peaks are in the near UV, however.

Most studies concerning MoS_2 are not about any possible phase transition. It is not clear if one exists, and if so, what the accompanying changes in optical and electrical properties are and to what extent.

REFERENCES (MoS_2)

1. F. Jelliner, Arkiv. Kemi, 20, 447 (1963).
2. S.S. Meyer, Inorg. Chem. 6, 1063 (1967).
3. B.L. Evans and K.T. Thompson, Brit. J. Appl. Phys. 1, 1619 (1968).
4. C.N.R. Rao and K.P.R. Pisharody, Prog. Solid State Chem. 10, 207 (1975).
5. T.J. Wieting and J.L. Verble, Phys. Rev. B3, 286 (1971)
6. W.Y. Liang, Physics Letters, 24A, 573 (1967).
7. A.R. Beal, J.C. Knights, and W.Y. Liang, J. Phys. C, Solid State Phys., 5, 3540 (1972).

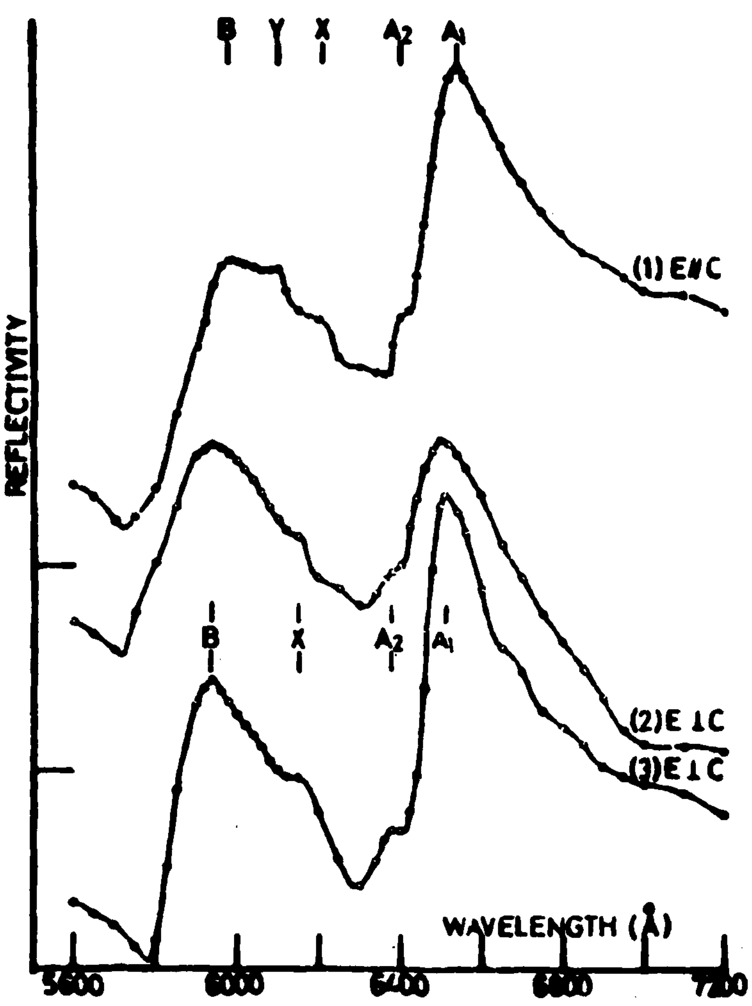

Figure 3. Reflectivity curves for MoS_2 in the visible region.

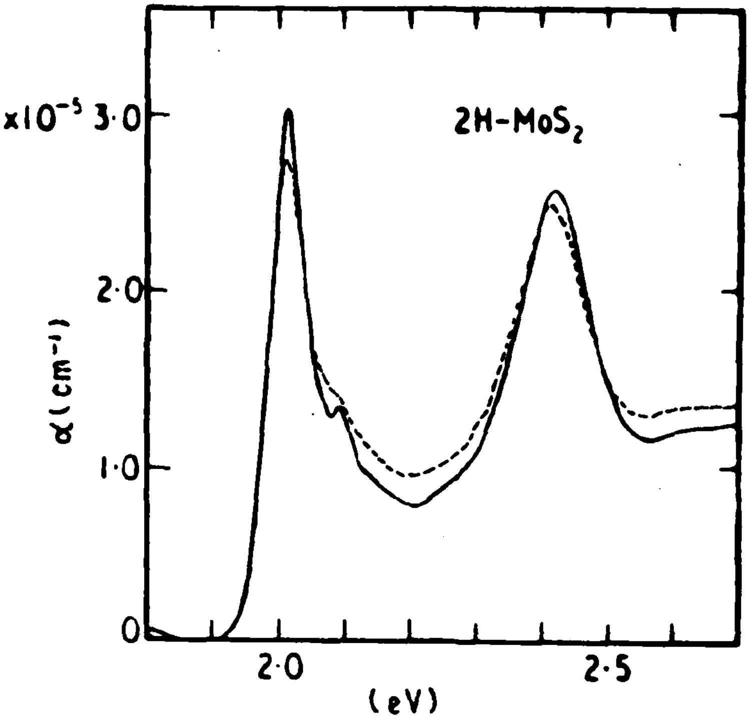

Figure 4. Temperature dependence of A,B peaks in $2H\text{-}MoS_2$, solid curve $5^{0}K$; dotted curve $77^{0}K$.

Mo_2S_3

Dimolybdenum Trisulfide

Mo_2S_3 has recently been shown to undergo three distinct phase transitions below room temperature.[1] The phase transitions were observed via resistivity and magnetic susceptibility measurements for single crystal samples.

The crystal structure of Mo_2S_3 has been determined to be monoclinic, the space group of which being C^2_{2h}.[2,3] There are two formula units per unit cell. The sulfur atoms form a distorted close-packed lattice with the Mo atoms inserted in two-thirds of the octahedral holes of this lattice. The Mo atoms are shifted from the centers of the S octahedra whereby zig-zag Mo-Mo chains are formed along the crystalline b-axis. These Mo-Mo distances in these chains are comparable to those in pure molybdenum metal, whereas the metal-metal distances perpendicular to the b-axis are considerably larger. Therefore, Mo_2S_3 is expected to exhibit quasi-one-dimensional behavior.

Single crystals of Mo_2S_3 are prepared by the vapor-phase transport technique with iodine as the transporting agent. The crystals are grown at very high temperatures and chemical analyses can be used to accurately determine the stoichiometry.[1]

The resistivity of the samples are measured using the standard four-probe technique. The magnetic susceptibility of Mo_2S_3 is measured by the Faraday method (magnetic field strength of 10.4 kOe) using a Cahn electrobalance.[4] Sample temperatures are determined by resistance thermometers and by Stokes-antistokes measurements.

Figure 1 and 2 show the resistivity of Mo_2S_3 as a function of temperature for two different cooling rates.[1] For Figure 1, it is 1°K/min and for Figure 2 it is 5°K/min. There are hysteresis curves corresponding to first-order phase transitions at 182°K and 145°K on the cooling cycle and at 198°K and 180°K on the warming cycle. There is also a large and broad peak in the resistivity at 80°K, and some hysteresis is evident. In Figure 2, these phase transitions are still visible but less abrupt. For cooling rates in excess of 10°K/min, the peak at 80°K disappears entirely.

Figure 3 shows the results of susceptibility measurements.[1] The temperature range is 60 - 300°K. Mo_2S_3 is a diamagnetic substance and note

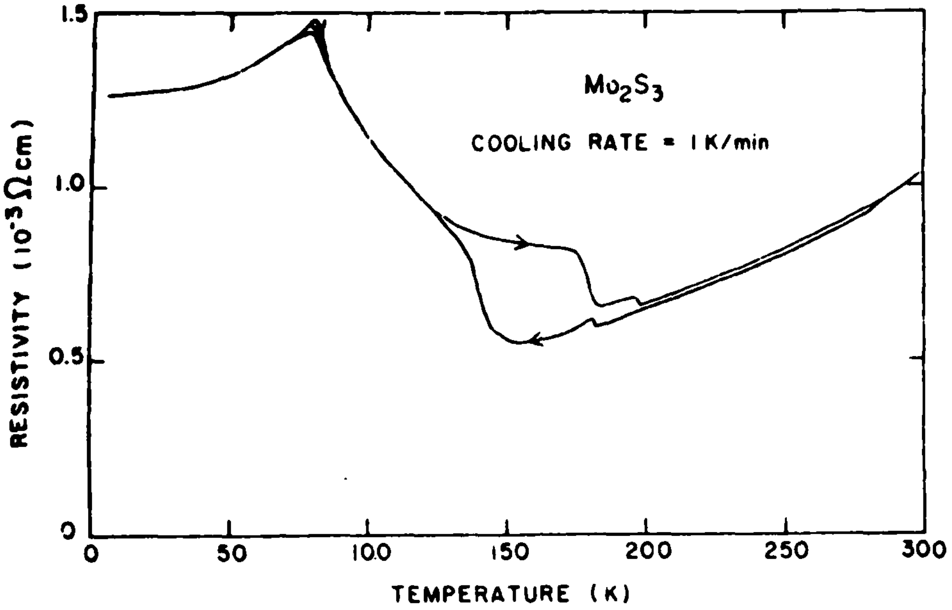

Figure 1. Resistivity of Mo_2S_3 as a function of temperature. The cooling rate was approximately 1°K/min.

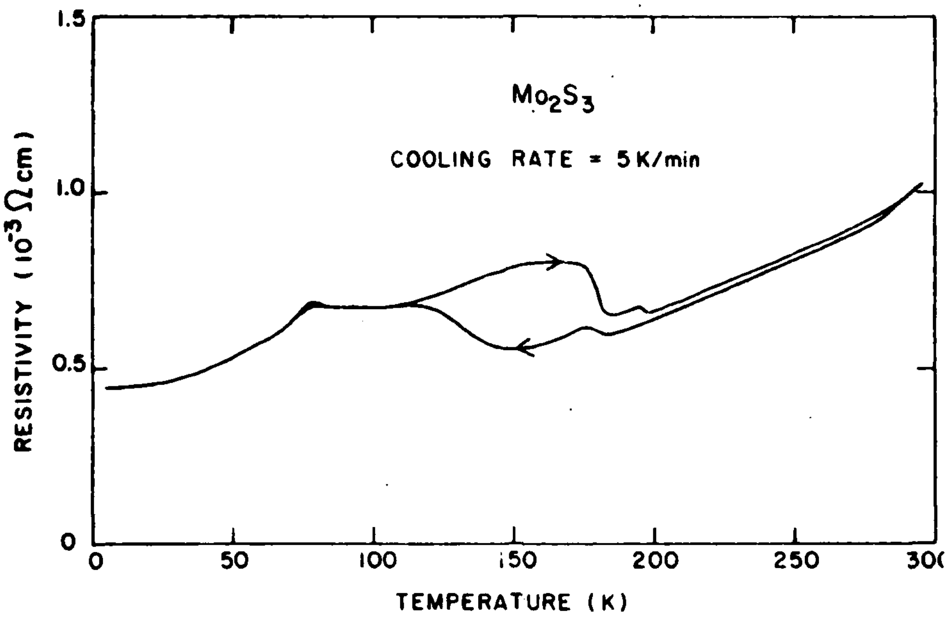

Figure 2. Resistivity of Mo_2S_3 as a function of temperature. The cooling rate was approximately 5^0K/min.

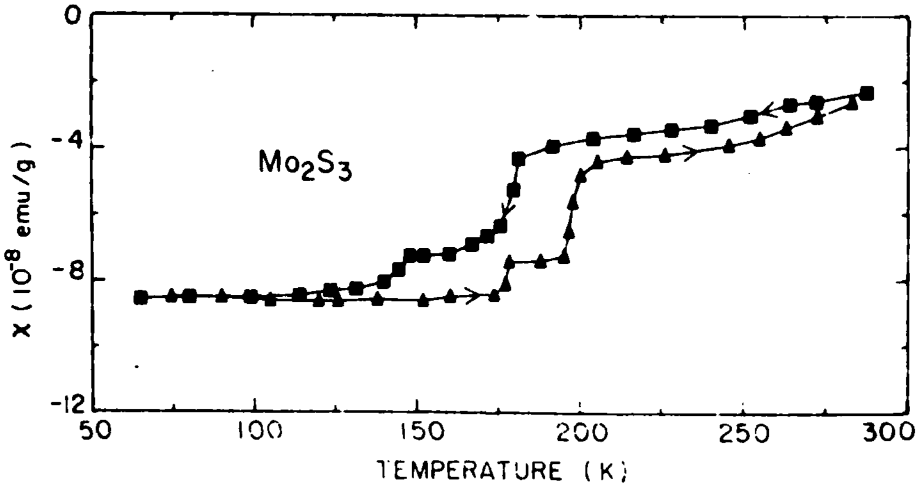

Figure 3. Magnetic susceptibility of Mo_2S_3 as a function of temperature. The solid lines are guides to the eye.

that χ is small for all temperatures (where x is the susceptibility). Note that the changes in χ occur at the same temperatures that the resistivity changes, and that a hysteresis effect also occurs. This type of behavior is due to a loss in Fermi surface at each transition, since fewer carriers would reduce the conduction-electron paramagnetic contribution to the susceptibility. Also, no susceptibility anomaly occurs at 80°K, even though the cooling rate is below 1° K/min. Raman spectroscopy indicates there is a structural alteration at 80°K, but the evidence for such at the two higher phase transitions appears uncertain.

The mechanism for the phase transitions has been attributed to charge-density-wave transitions (as occur in TaS_3 and $NbSe_3$). This is supported by the apparent decrease in size of the Fermi surface at the two higher temperature transitions. No non-ohmic behavior has been found in Mo_2S_3 using dc electric fields between 0.1 mV/cm and 200 mV/cm (though pulsed measurements could give different results).

No literature on the optical properties of Mo_2S_3 has been found. Further, little data on thin film fabrication has been found, though standard sputtering or CVD methods should work. Since the magnitude of the change in resistivity and susceptibility at each phase transition is less than an order-of-magnitude, it may be expected that optical properties will not change drastically. Such changes may be expected if the carrier concentration (free carriers) will change or if a significant structural change occurs. From the evidence given here, these changes are relatively minor. Significant changes may take place in the far infrared.

REFERENCES (Mo_2S_3)

1. M.H. Rashid, et.al., Solid State Commun. 43, 675 (1982).
2. F. Jellinek, Nature, London 192, 1065 (1961).
3. F. Kadijh, R. Huisman, and F. Jellinek, Acta. Cryst. B24, 1102 (1968).
4. F.R. Szofron, et.al., Rev. Sci. Inst. 46 1186 (1975).

$MoSe_2$
Molybdenum Diselenide

Molybdenum diselenide or $MoSe_2$ is a layered transition-metal dichalcogenide; a member of the group of compounds which resembles, from the theoretical point of view, a two-dimensional solid. Single crystals of $MoSe_2$ are difficult to make. $MoSe_2$ is a hexagonal layer compound with packing sequence Se-Mo-Se; the molybdenum and selenium atoms are arranged in sheets parallel to the base of the hexagonal unit cell. One layer in the structure is composed of sheets of selenium atoms on both sides of a molybdenum sheet. Each layer is related to its neighboring layers by a screw displacement. Within each Se-Mo-Se layer each Mo atom forms s,p,d hybrid bonds to the six nearest neighbor Se atoms in the trigonal prism coordination. The single crystals may be cleared with ease along the basal plane.[1]

We have located information on the optical properties of $MoSe_2$ in the 5-40μm range.[1,2] These measurements were made using single $MoSe_2$ crystals grown by the vapor phase transport method without the use of any transport agent. Since the crystals were in the form of thin sheets, all the results given are for $\vec{E} \perp \vec{C}$. Lattice absorption bands in the infrared arise from the direct interaction of infrared photons and phonons in the crystal lattice. For $MoSe_2$, the strongest such interaction is between a photon and a single long wavelength optical phonon which is responsible for the evident Reststrahlen bands in the material.

Figure 1 shows the absorption coefficient, α (cm^{-1}), in the far infrared at 77°K. Note the good agreement between the measured values and the classical oscillator fit. Only one absorption band at 482 cm^{-1} is seen in the 5-40μm region. No change in the absorption coefficient with temperature is observed.[1] Further, no multiphonon assignment could be given to this band (Figure 1) on the basis of known lattice frequencies; this may be due to the presence of impurities in the sample.

From transmission measurements using the relation $p\lambda = 2nd$, where interference fringes are evident, the index of refraction can be computed. This is given in Figure 2. We see a rather abrupt change near 280 cm^{-1}. No

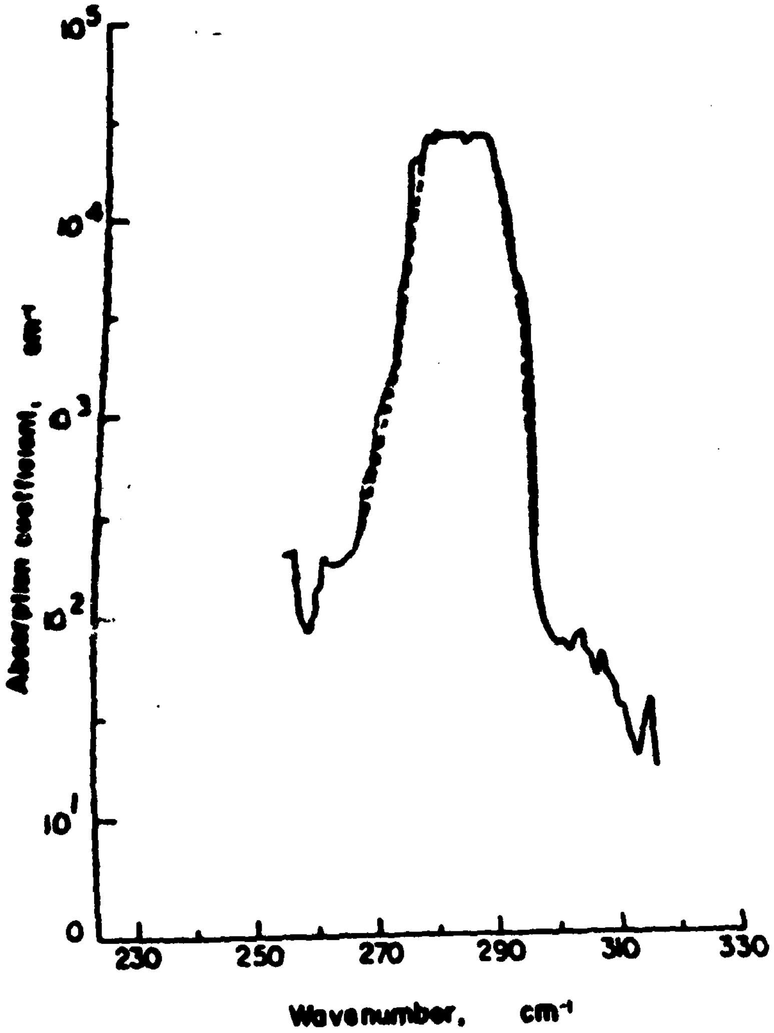

Figure 1. Absorption coefficient vs. wavenumber curve in $MoSe_2$ at 77°K in the fundamental infrared lattice vibration region. The dotted curve is calculated theoretically.

dependence on the temperature has been reported. Figure 3 shows the transmission as a function of λ from about 20 to 21 µm.

Figure 4-7 show the variation in the refractive index at 77°K and 290°K and the variation of ε_1 and ε_2 (where $\varepsilon(\nu) = \varepsilon_1(\nu) + i\ \varepsilon_2(\nu)$) with frequency.[3] Although there is a slight change between the two temperatures, it is small. These graphs are from about 2 µm up into the ultraviolet. (Please note that the scales are displaced vertically for each temperature so that the two curves are really about identical.) These curves were deduced from reflectivity data via the Kramers-Kronig method.

Though it appears that more than one polytypic form of $MoSe_2$ exists (a high and a low temperature polymorph, one of which must be formed at high temperature), there is no evidence of an irreversible phase transition between them. Very little data on the electrical and optical (as well as thermal) properties is available.

REFERENCES ($MoSe_2$)

1. A.K. Garg, H. Sehgal, O. Aguihotri, Solid State Commun., 12, 1261 (1973).
2. A. Aredda and E. Fortin, J. Phys. Chem. Solids, 41, 865 (1980).
3. B.L. Evans and R.A. Hazelwood, Phys. Stat. Sol. (a), 4, 181 (1971).

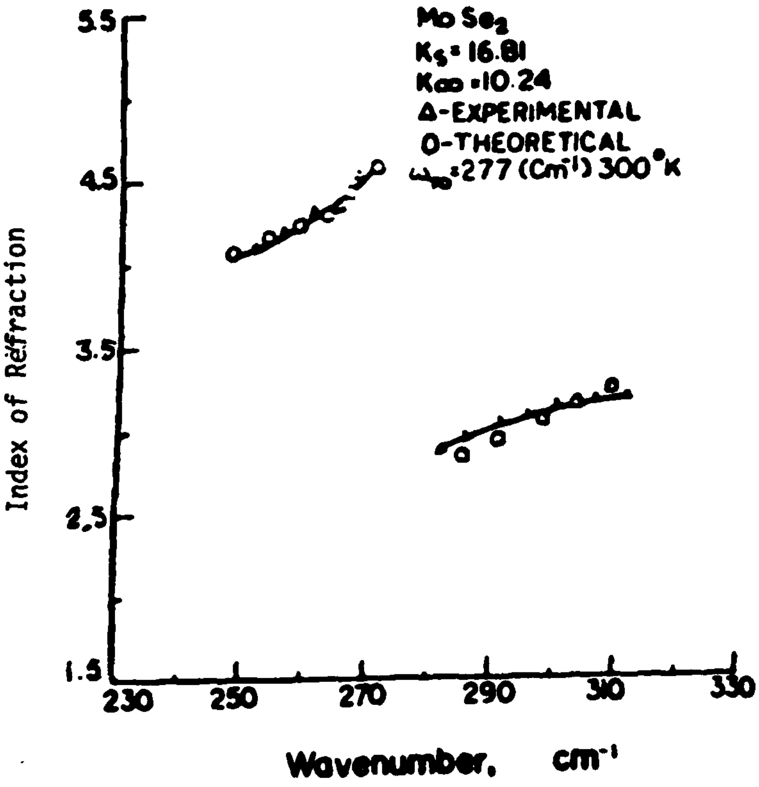

Figure 2 - Index of refraction vs. frequency near the fundamental infrared lattice vibration region.

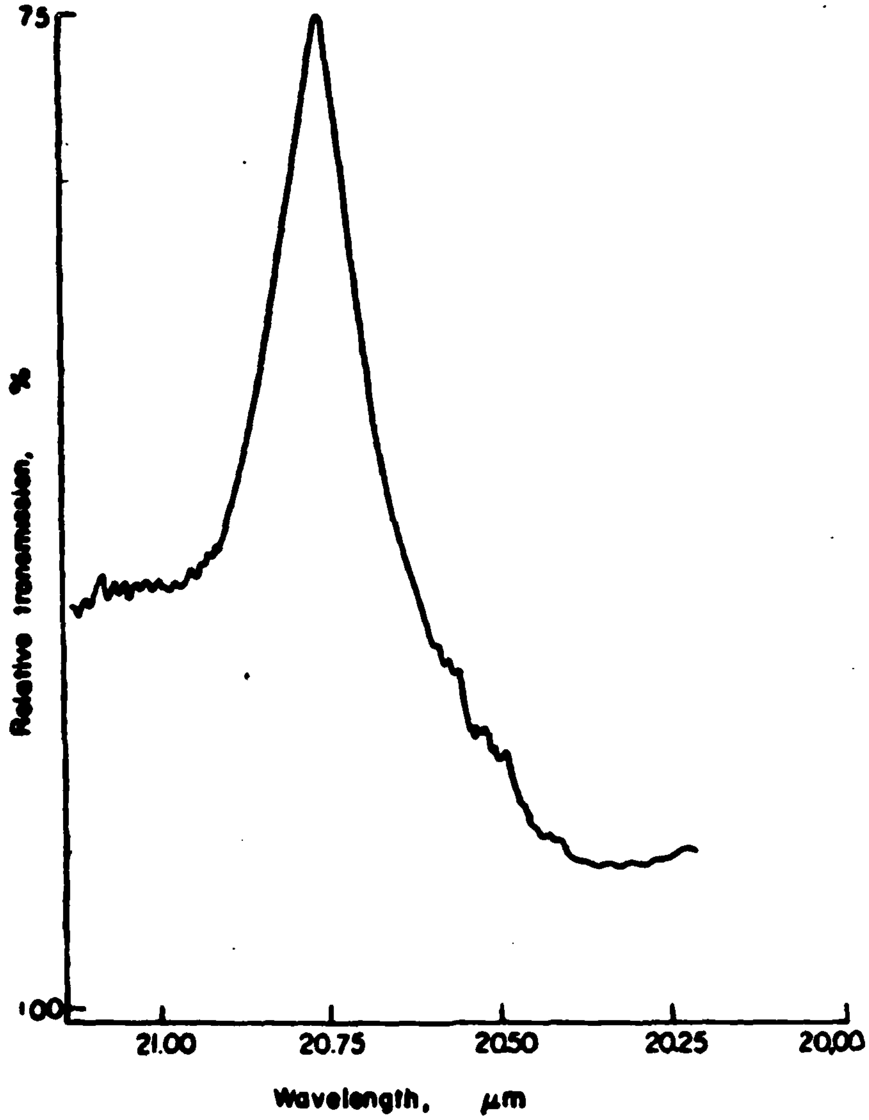

Figure 3. Percentage transmission in a $MoSe_2$ crystal in the region of 20-21μm. The band at 482 cm^{-1} has been attributed to the oxygen impurity in the crystal.

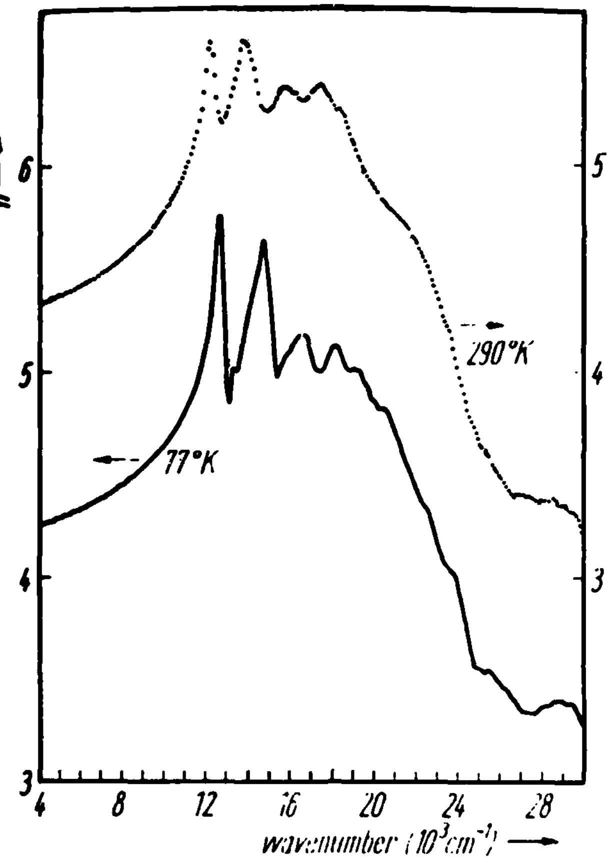

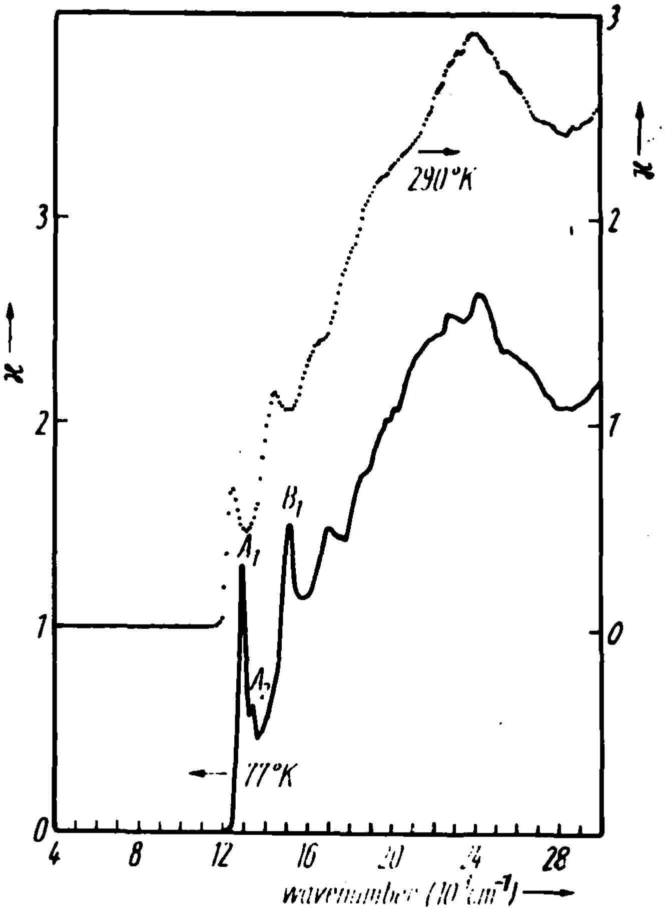

Figure 4. Spectral variation or ordinary refractive index n for α-MoSe$_2$ at 290^0 (dotted) and 77^{0}K (full line).

Figure 5. Spectral variation of n ($\vec{E} \perp \vec{c}$) for α-MoSe$_2$ at 290^0 (dotted) and 77^{0}K (full line).

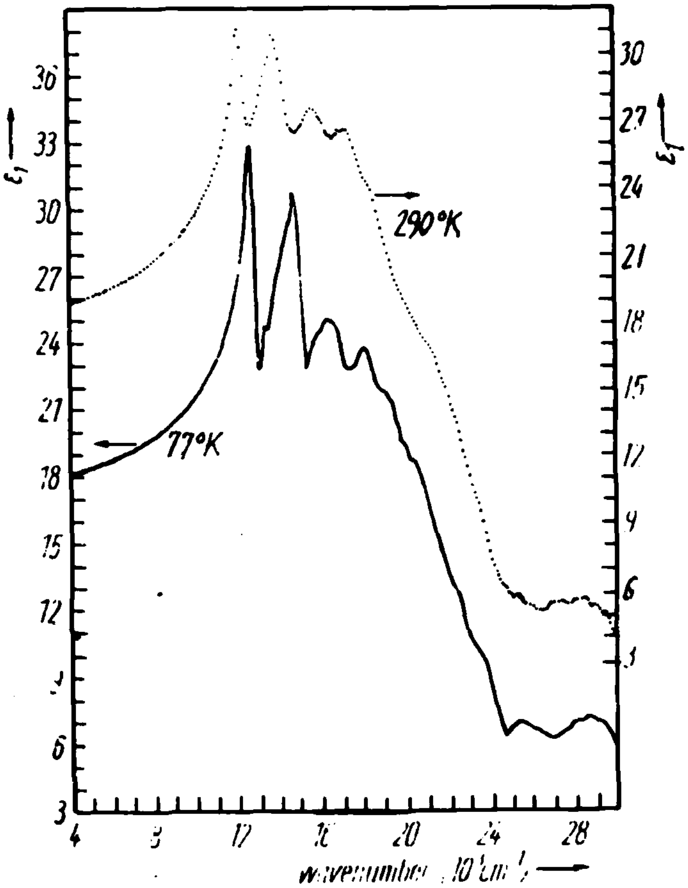

Figure 6. Spectral variation of ϵ_1 (= n^2-k^2) for α-MoSe$_2$ at 290^0 (dotted) and 77^{0}K (full line).

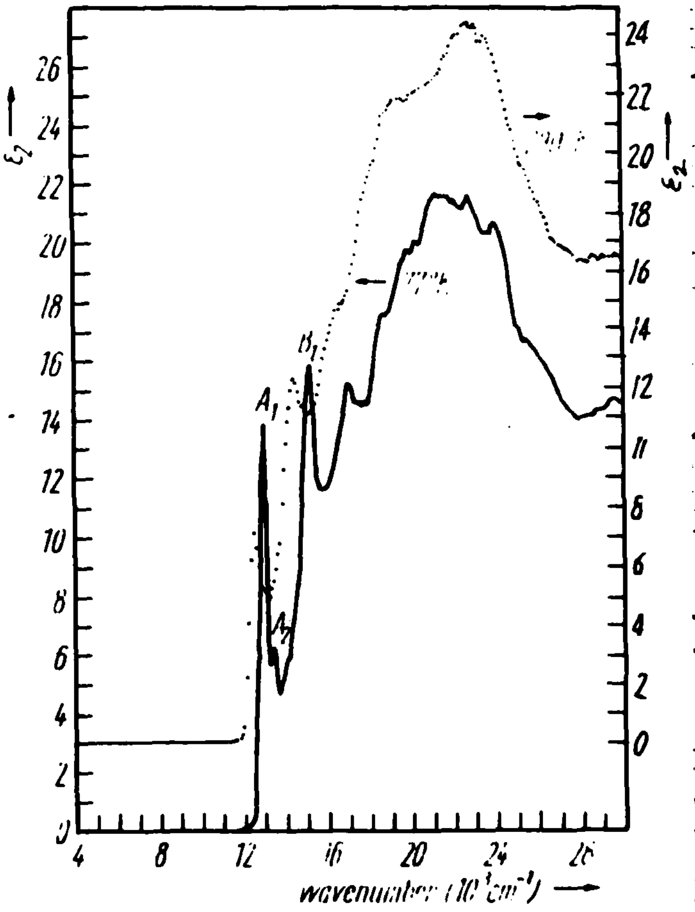

Figure 7. Spectral variation of ϵ_2 (= 2nk) for α-MoSe$_2$ at 290^0 (dotted) and 77^{0}K (full line).

$MoTe_2$
Molybdenum Ditelluride

$MoTe_2$ or molybdenum ditelluride is unusual among the group VIA transition metal dichalcogenides in that it possesses two basic structural polytypes. α-$MoTe_2$ is stable and isostructural with MoS_2 with the Mo atom surrounded by a trigonal prism of Te atoms, while β-$MoTe_2$ is metastable at room temperature and has a more complex structure similar to that of WTe_2. For β-$MoTe_2$ the metal atoms lie in octahedra of Te atoms but shifted away from the center towards an octahedron face so that metal zig-zag chains result.[1] The metal-metal bonding buckles the Te sheets, distorting the Te octahedra. For temperature above 1200°K β-$MoTe_2$ is in a stable form. Because there are Mo-Mo chains within the layers, this material exhibits both one and two-dimensional characteristics (see Figure 1).[2] The α-phase will undergo a phase transition to the β-phase at temperatures at or in excess of 1175°K.[3] (We should mention that β-$MoTe_2$, and hence also WTe_2 possesses the structure of a distorted CdI_2 lattice.) Being a layered compound, $MoTe_2$ is characterized by a strong anisotropy with respect to the crystal c-axis.[4] Structural parameters can be obtained via a powder spectrum using a diffractometer and filtered Cu-Kα X-radiation.[5] This analysis says that $MoTe_2$ possesses a hexagonal C7 type structure with a density of 7.78 ± 0.2 gm/cm^3 so that there are 1.974 $MoTe_2$ per unit cell.[6,7] Crystals of $MoTe_2$ can be grown directly from the vapor phase to yield single crystals in the α-phase.[8]

The low temperature α-phase is diamagnetic and semiconducting; the high-temperature β-phase is paramagnetic and metallic.[3] If we raise the temperature on a sample of β-MoTe, it transforms to α-$MoTe_2$ at 750°K with a corresponding change in the resistivity (a large increase), then ρ will decrease when β-$MoTe_2$ is formed again at 1175°K.[2] Figure 2 shows an anomaly in the resistivity of β-$MoTe_2$ from 10°K to 300°K with a hysteresis effect.[2] This anomaly occurs for both in plane components of the resistivity. This is believed to be due to a first-order structural phase transition, there are no superlattice reflections occuring at the temperature of the anomaly. One explanation may be in a shortening of the Mo-Mo bond length within the Mo chains. The resistivity is measured using the standard Van der Pauw method.[9]

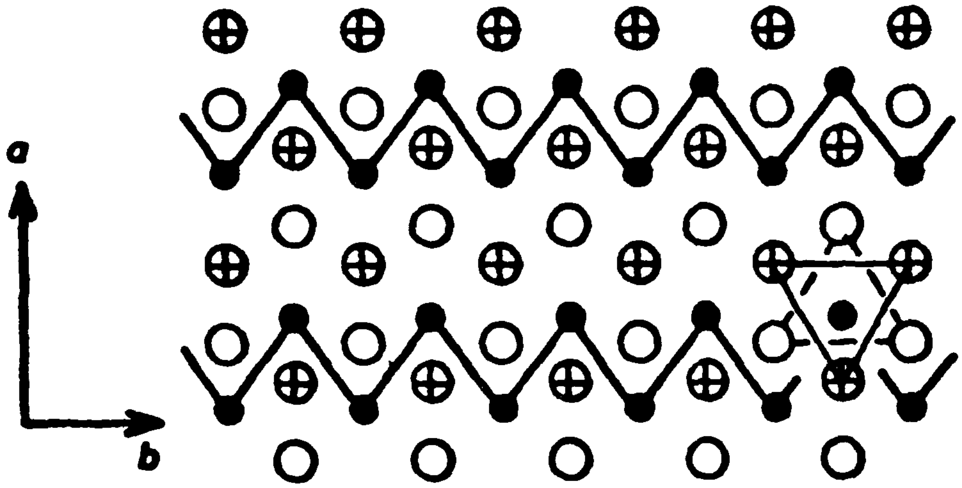

Figure 1. Plan of the structure of a single layer of β-$MoTe_2$, illustrating the formation of zig-zag chains of Mo atoms (after Brown 1966). ⊕ represents the top sheet of Te atoms and ○ the lower sheet, while ● represents the middle sheet of Mo atoms.

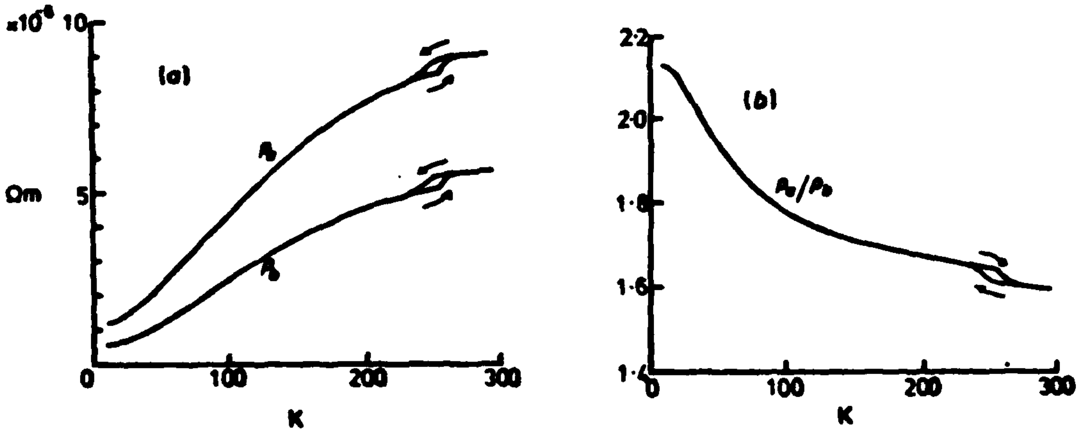

Figure 2. (a) Temperature dependence of the two in-plane components, ρ_a and ρ_b, of electrical resistivity of β-$MoTe_2$.
(b) In-plane electrical anisotropy ρ_a/ρ_b.

Optical properties of $MoTe_2$ have been determined from 0.77eV to 6.2eV,[7] and from 0.5 to 3.8eV.[10] From reflectivity measurements a Kramers-Kronig analysis will give either the complex dielectric constant or the index of refraction and extinction coefficient. For $MoTe_2$, the optical reflectivity is anisotropic in that there is a strong dependence on the polarization. Figure 3 shows a typical arrangement for the measurement of reflectivity for a polished sample.[7] Note that the actual angle of measurement is very close to normal, though not exactly so. The largest error attributable to this is about 3%.

Figure 4 shows the room temperature reflectivity of $MoTe_2$ from 0.77eV to 6.2eV (from the UV to about 2μm). Treating the measured reflectivity as a known, represented by R(E), where E is the energy (of the photon), then n and k are related to R(E) and the phase θ by the relation:

$$\frac{n - 1 - ik}{n + 1 - ik} = \sqrt{R} \exp(i\theta)$$

This is the basis of the Kramers - Kronig method.[11]

The complex dielectric constant, $\hat{\varepsilon} = \varepsilon_1 + i\varepsilon_2$, is related to n and k via the expressions:

$$\varepsilon_1 = n^2 - k^2$$

$$\varepsilon_2 = 2nk$$

Figure 5 and 6 show the behavior of these quantities. It is also possible to define two "energy loss functions," as $-\mathrm{Im}(1/\varepsilon)$ and $-\mathrm{Im}(1/(\varepsilon+1))$. These are proportional to the characteristic energy loss of fast electrons traversing the bulk and surface of the material, respectively. They show the excitation spectra of the bound electrons, screening effects, etc.[7] In reference 10, curves are given for the anisotropic reflectivity at 77°K and 300°K. We have been unable to locate specific data on the high temperature phase.

$MoTe_2$ exists in two forms: α and β. It does not, however, appear to be a switchable phase transition material in that each phase can coexist over a wide temperature range. Accompanying the resistivity of the β-phase is an

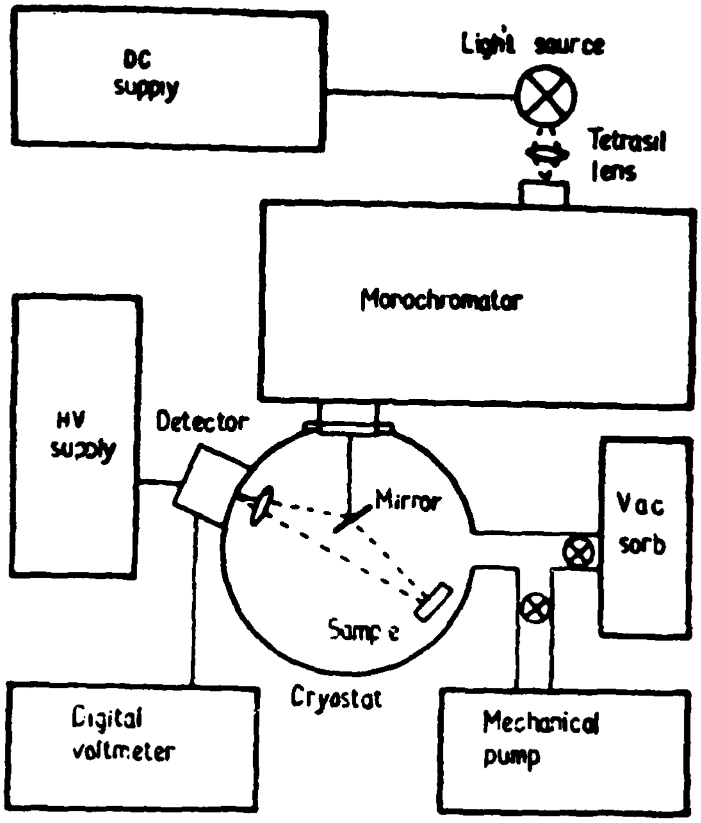

Figure 3. Outline of the experimental arrangement.

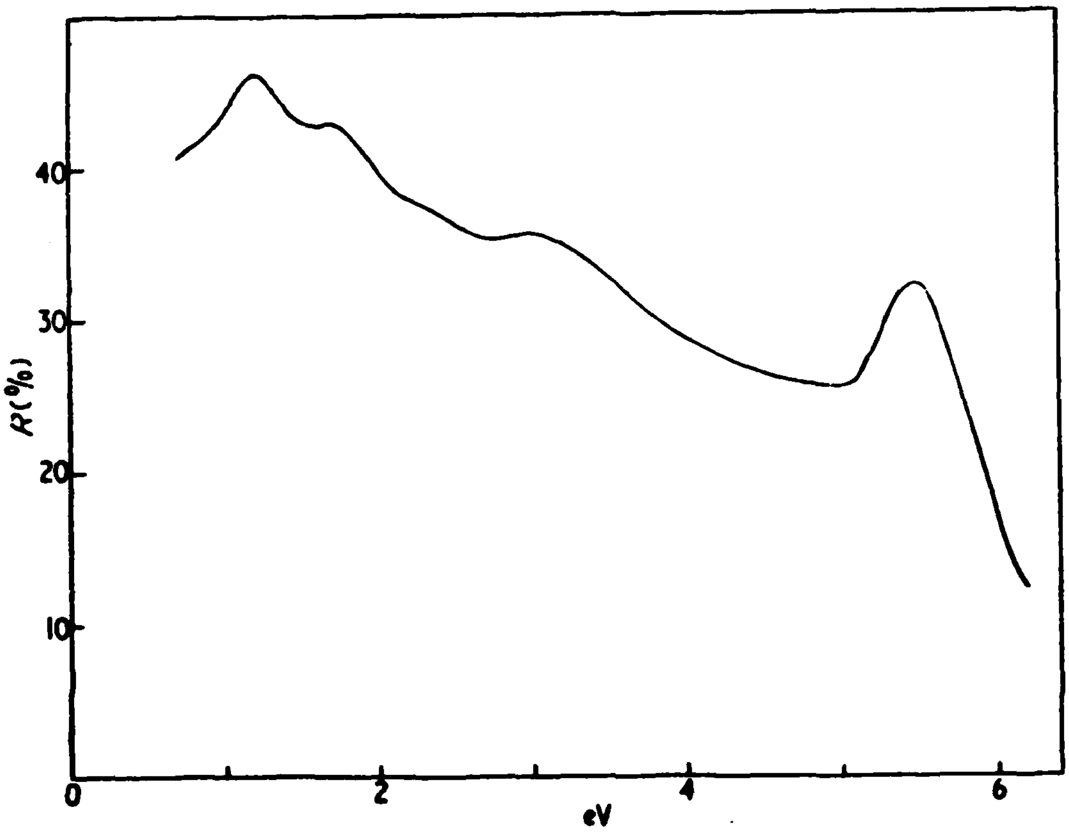

Figure 4. Room temperature reflectivity of $MoTe_2$.

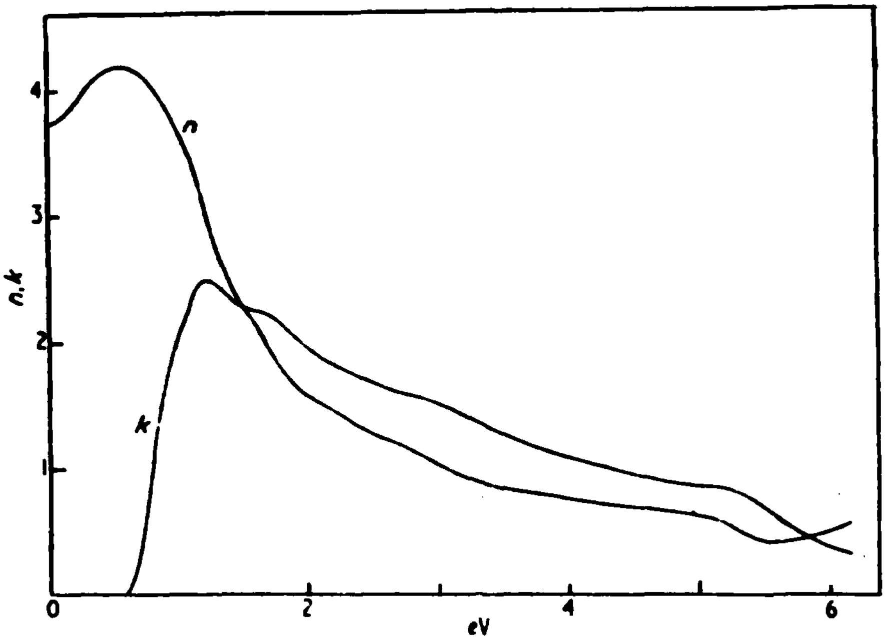

Figure 5. Real and imaginary parts of the refractive index n and k of $MoTe_2$ from Kramers-Kronig analysis.

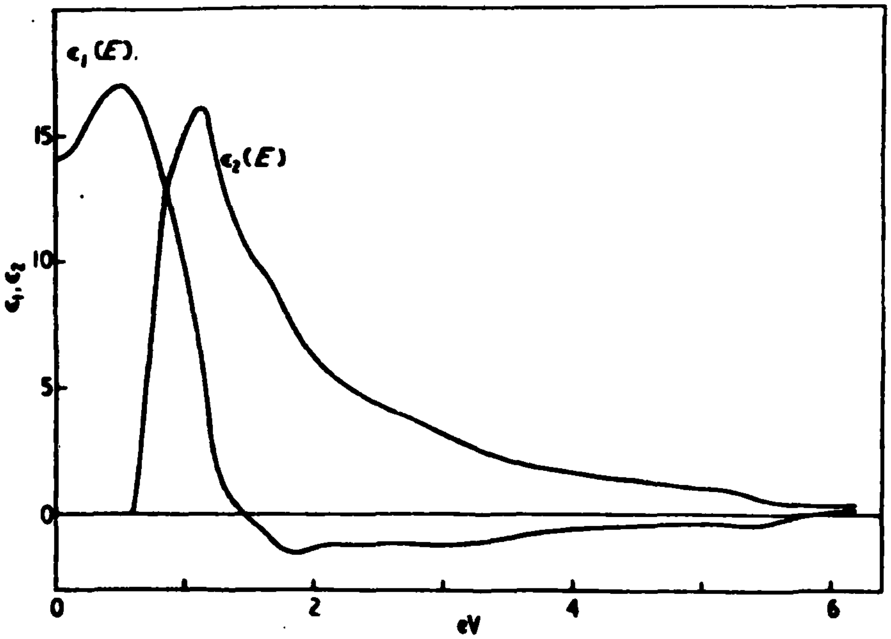

Figure 6. Real and imaginary parts of the dielectric constant ε_1 and ε_2 of $MoTe_2$ from Kramers-Kronig analysis.

unusual hysteresis effect of somewhat controversial origin. But no completely reliable optical data exists which indicates a change in the optical parameters n and k.

REFERENCES ($MoTe_2$)

1. B.E. Brown, Acta. Crystallogr., 20, 268 (1966).
2. H.P. Hughes and R.H. Friend, J. Phys. C: Solid State Phys., 11, L103 (1978).
3. R. Clarke, E. Marseglia and H.P. Hughes, Phil. Mag. B, 38, 121 (1978).
4. J.A. Wilson and A.D. Yoffe, Adv. Phys., 18, 193 (1969).
5. D. Puotinen and R.E. Newnham, Acta. Crystallogr., 14, 698 (1961).
6. O. Knop and R.D. MacDonald, Can. J. Chem. 39, 897 (1961).
7. V. Grasso, G. Mondio, and G. Saitta, J. Phys. C: Solid State Phys., 5, 1101 (1972).
8. B.L Evans and R.A. Hazelwood, Phys. Stat. Sol. (a), 4, 181 (1971).
9. L. Van der Pauw, Philips, Res. Rep. 13, 1, (1958); ibid., 16, 187 (1961).
10. B. Davey and B.L. Evans, Phys. Stat. Sol. (a), 13, 483 (1972).
11. I. Simon, J. Opt. Soc. Am., 41, 336 (1951).

$NbSe_3$
Niobium Triselenide

$NbSe_3$ or niobium triselenide is a trichalcogenide which has only recently been successfully fabricated.[1] $NbSe_3$ crystallizes in the form of fibrous strands which are easily separated. The structure has been determined by single-crystal x-ray diffraction.[2,3] Six Se atoms form the vertices of a right triangular prism with a Nb atom at the center of the prism. Six prisms form the unit cell, which measures (10.006 ± 0.005) x (3.478 ± 0.002) x (15.626 ± 0.008) $Å^3$.[4] The distance between Nb atoms is 3.478 ± 0.002Å along the b-axis and varies from 4.45 to 4.25Å in the a-c plane. The compound is formed by the direct reaction (without carrier) of Se and Nb in stoichiometric proportions. The structure of $NbSe_3$ is shown in Figure 1; it helps one to understand why $NbSe_3$ possesses a fibrous structure. There appears to be little thermal effect on the lattice itself between 4.2°K and 300°K as only a 0.2% contraction is measured in this temperature range.[1]

The electrical resistivity can be measured using the standard four probe technique. At room temperature the resistivity is on the order of 600 μohm-cm, depending on the crystal size (this is for a strand with dimensions 7 x 0.05 x 0.01 mm^3). The electrical resistivity varies with temperature as seen in Figure 2. Above 145°K $NbSe_3$ shows a metallic behavior since the resistivity decreases with decreasing temperature. Between 10°K and 150°K two maxima occur. The existence of these two resistance anamolies has been believed to be due to phase transitions. They occur at 125°K and 49°K. The amplitude of these peaks are 10% of the room temperature resistivity for the high temperature peak and 30% for the low temperature peak. No hysteresis effect has been detected.

The resistivity peaks respond to the external pressure. The lower peak disappears at a pressure of 6 kbar; the upper peak is reduced by 30% at 4 kbar. This is similar to the effects observed in $NbSe_2$, where it has been shown that charge density waves are responsible for resistivity anomalies.[5]

There has been a renewal of interest in $NbSe_3$ recently, as seen in the literature. Much of the recent research pertains to nonlinear effects; to date we have been unable to locate any data on the optical characteristics.

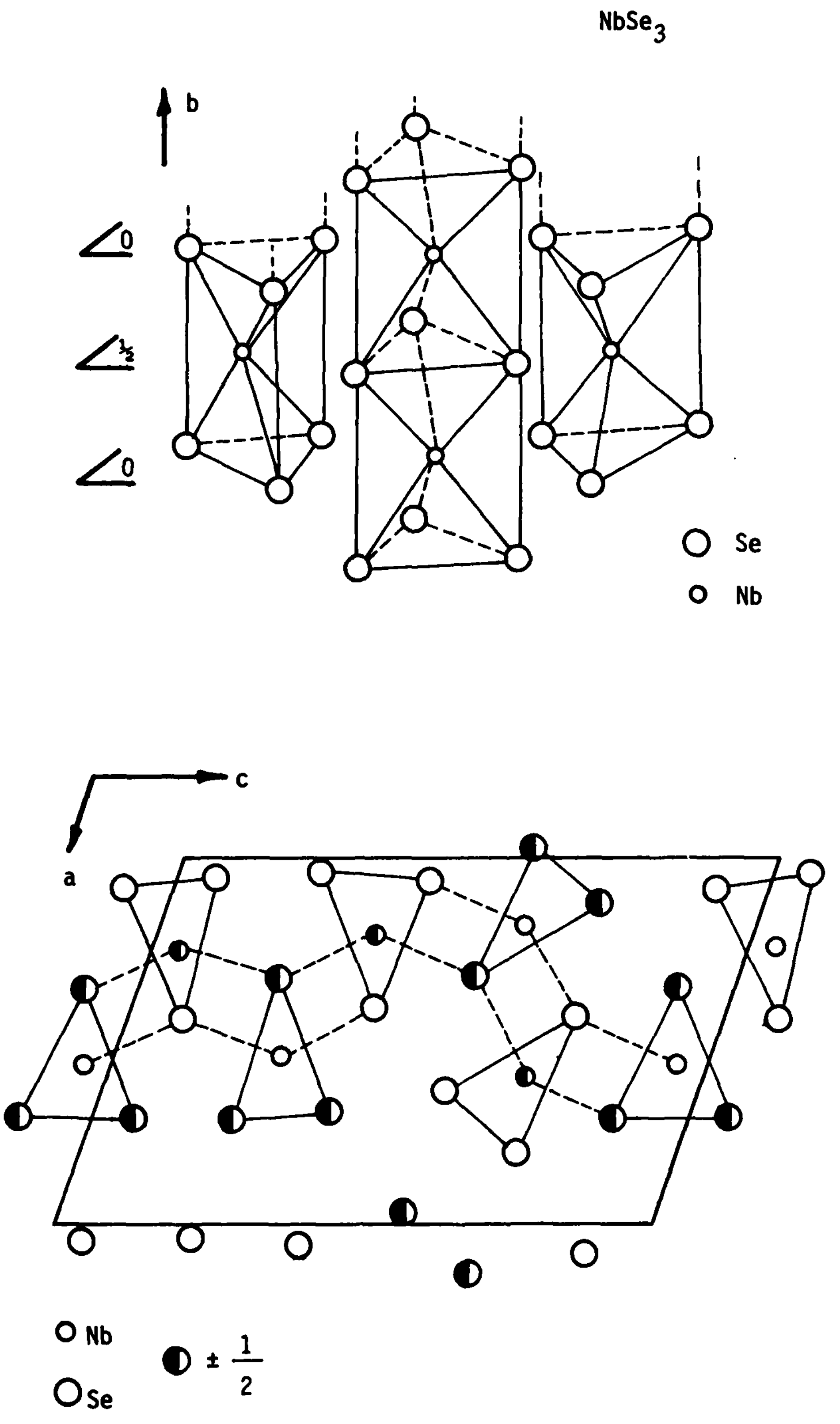

Figure 1. Structure of $NbSe_3$. Upper part: stacking along the b-axis of trigonal prisms $NbSe_6$. Lower part: projection of the structure on the ac plane.

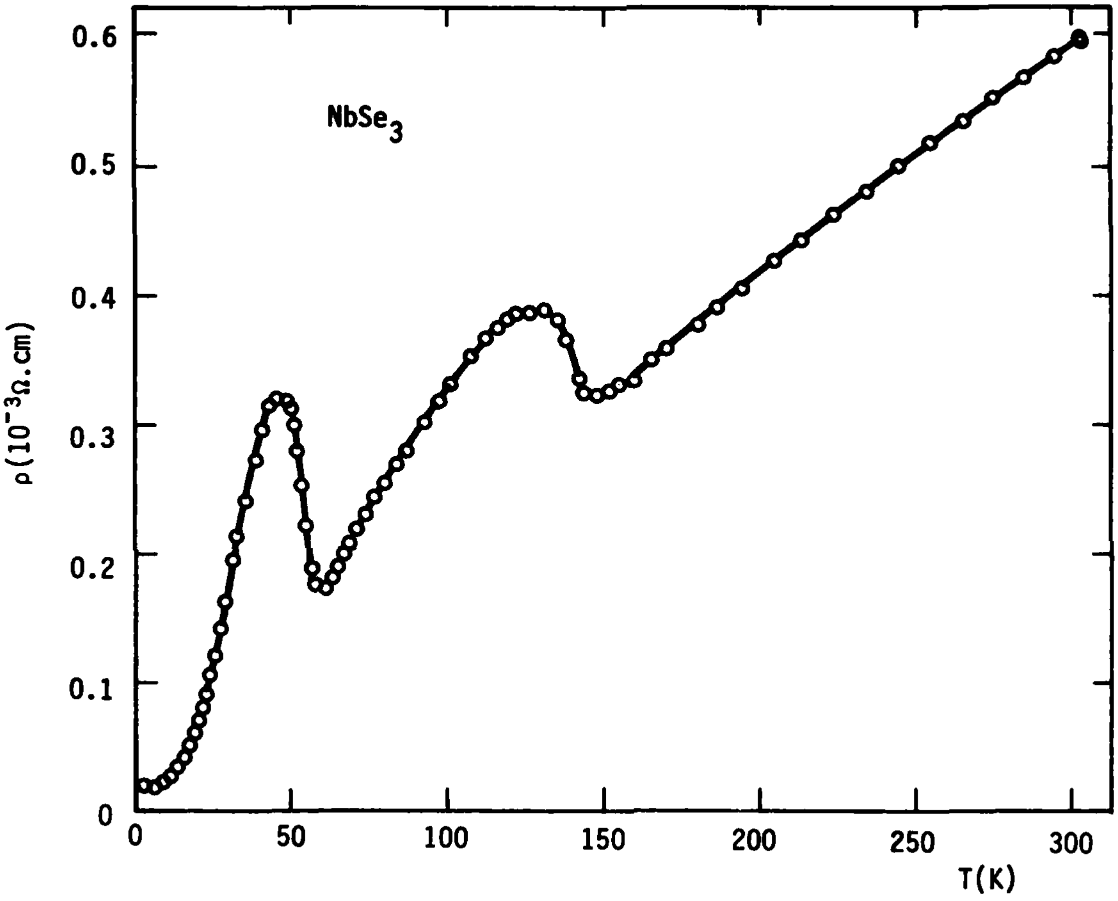

Figure 2. Electrical resistivity as a function of temperature along the b-axis of NbSe$_3$ showing the two phase transition at T_{e1} = 145K and T_{e2} = 59K. The resistivity maxima are for 125 and 49K.

REFERENCES ($NbSe_3$)

1. J. Chaussy, et.al., Solid State Commun., 20 759 (1976).
2. A Meerschant and J. Rouxel, J. Less - Common Metals, 39, 197 (1975).
3. K. Selte, et.al., J. Less - Common Metals, 11, 14 (1966).
4. P. Monçeau, et.al., Phys. Rev. Lett., 37, 602 (1976).
5. R. Delaplace, et.al., J. Phys. (Paris), Lett., 37, L13 (1976).
   Also see C. Berthin, et.al., Solid State Commun. 18, 1393 (1976).

NiS

Nickel Monosulfide

NiS or nickel monosulfide has two polymorphs with uniquely different properties: α-NiS and β-NiS.[1] Below 620°K, NiS has rhombohedral symmetry and above 620°K, it has NiAs structure.[2]

The low temperature state is semimetallic. The other high temperature phase is stable if quenched from above 620°K, and possesses a hexagonal structure. This polytype exhibits a phase transition at 264°K for stoichiometric NiS and goes from a semiconducting to a metallic phase. The transition is accompanied by a contraction of the lattice - a net decrease in c/a ratio. Further, the transition possesses a negative pressure dependence. The transition mechanism is not well understood, and may not be entirely due to a change in lattice constant.[3]

Figure 1 illustrates the position of Ni atoms and their spin orientation.[2] Other lattice parameters and band structure constants are given in Table 1.[3]

TABLE 1
TEMPERATURE EFFECTS AT Γ POINT

	Γ_1^+		Γ_3^+		Γ_2^-	Γ_5^+			Γ_6^+		Γ_6^-
a	-2.31	+4.90	-7.04	-0.03	-1.70	-1.69	-4.45	+1.45	-1.56	-0.90	-2.49
b	-2.12	+4.79	-7.07	-0.16	-1.46	-1.73	-3.59	+1.35	-1.52	-0.92	-1.97
c	-2.20	+4.37	-6.56	-0.07	-1.74	-1.67	-4.30	+1.43	-1.54	-0.92	-2.43

a = high temperature lattice parameters (c = 5.13155Å, a = 3.4431Å)

b = high temperature lattice parameters with Debye - Waller

c = low temperature lattice parameters (c = 5.3822Å, a = 3.45353Å)

Figures 2 and 3 show how the transition temperature and pressure vary for NiS.[4,5] The nature of the transition for hexagonal NiS is quite interesting, as there are striking changes in the specific heat, C_p (Joules per mole per °K).[6] There are significant changes in the electrical resistivity at the transition temperature. Curves for single crystal stoichiometric NiS are available as well as for $NiS_{1.01}$, $NiS_{1.015}$ -- in the latter case the

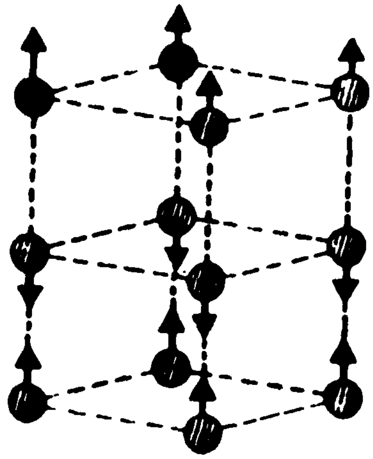

Figure 1. Spin structure in hexagonal NiS. The sulfur atoms are not shown.

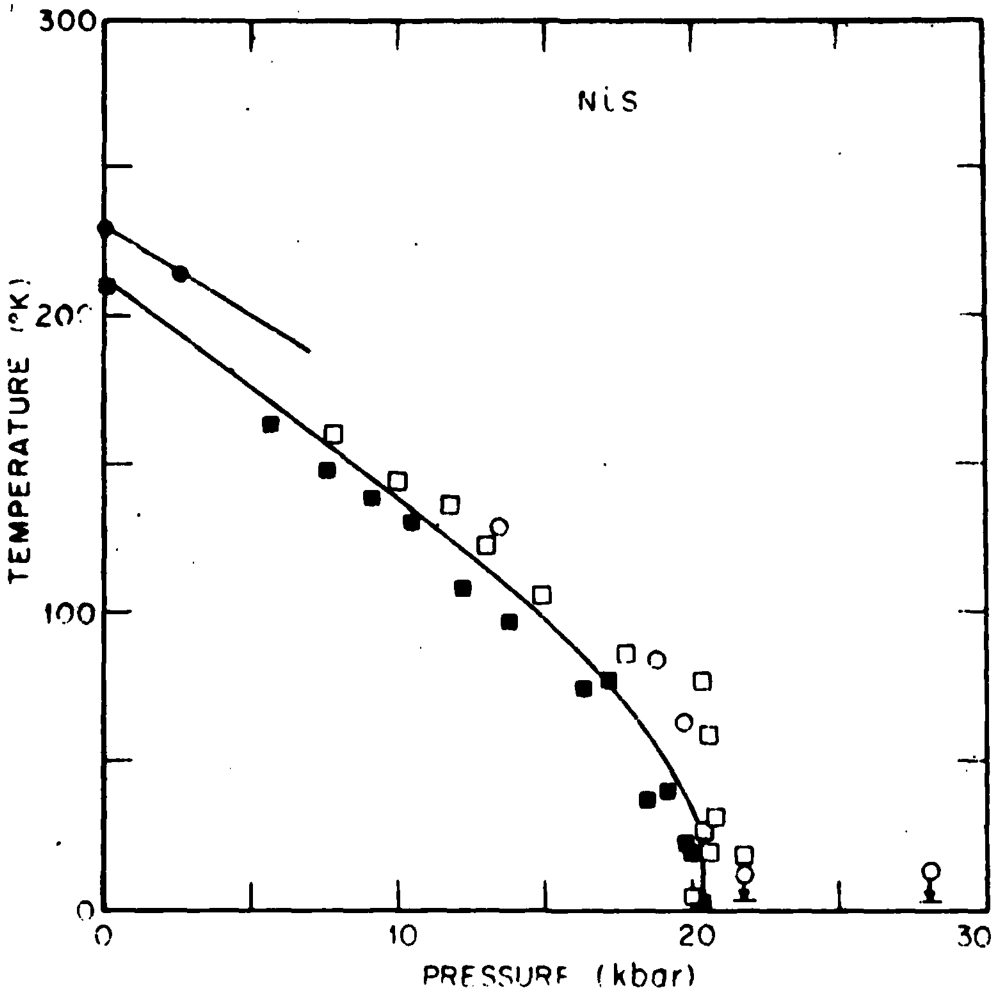

Figure 2. Pressure-temperature phase diagram for NiS. Open and closed symbols are for increasing and decreasing temperature of pressure. Circles are sample with T_N = 230°K at 1 atm and squares for sample with T_N = 210°K.

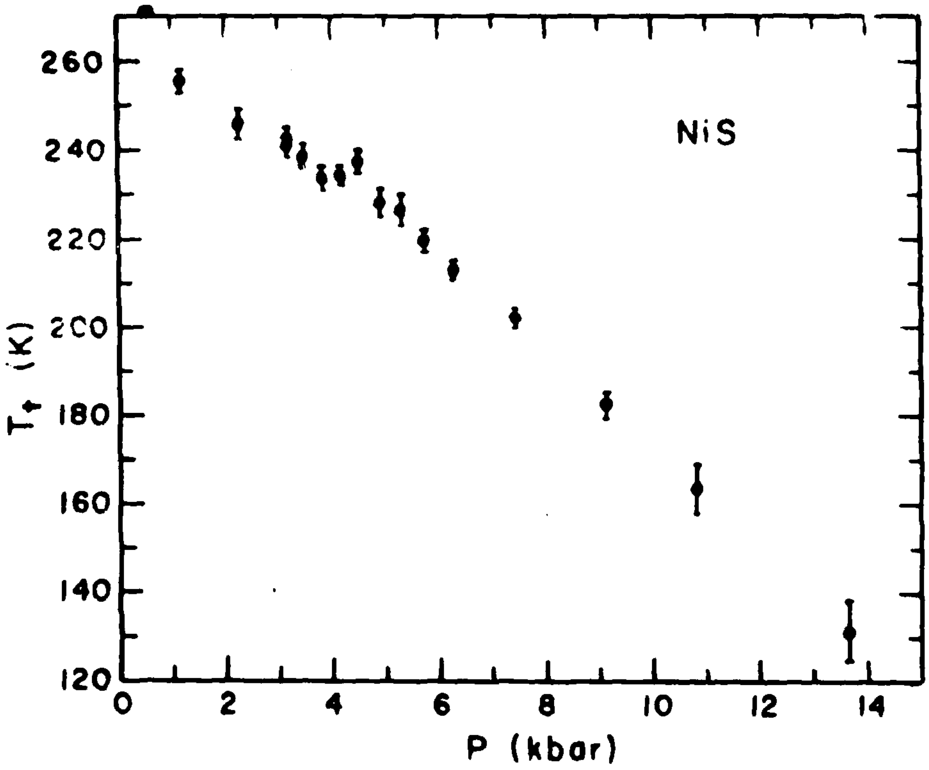

Figure 3. Pressure dependence of the metal - nonmetal transition temperature in hexagonal NiS. There is a local increase in T_t near 4.5 kbar and a 30 percent difference in the magnitude of dT_t/dP measured above and below this region.

resistivity is anisotopic (different for $\vec{E} \parallel \vec{c}$ and $\vec{E} \perp \vec{c}$). For a single crystal of NiS, we get the curve shown in Figure 4.[2] We should, for completeness, mention that the resistivity has been measured using the four-point contact method.[7] Phosphor bronze pressure contacts were used giving excellent ohmic characteristics over the entire temperature range of measurements. Overall, the electrical characteristics of NiS seem to be well understood for the hexagonal (α) phase.

Optical properties, however, are considered to carry the greatest weight for our recommendations. In Figure 5 we see[8] the reflectivity from about 100 cm^{-1} (far infrared) to about 10^5 cm^{-1} (near UV) for $\vec{E} \perp \vec{c}$. We see that there is a dip near 0.14 eV (8.86 microns) where reflectivity goes from about 92% at 300°K to 68% at 80°K. In Figure 6 we see the imaginary part of ϵ, the dielectric constant (where $\epsilon = \epsilon' + i\epsilon''$). In Figure 7 the far infrared reflectivity is given.

REFERENCES (NiS)

1. F. Hulliger, J. Phys. Chem. Solids, 26 639 (1965).
2. T. Sparks and T. Komoto, Rev. Mod. Phys., 40, 752 (1968); Phys. Lett A25, 398 (1967).
3. R.V. Kasowski, Solid State Comm. 14, 103 (1974).
4. D.B. McWhan, et.al., Phys. Rev. B5, 2552 (1972).
5. W.J. Keeler and R.E. Jones, Solid State Comm. 17, 83 (1975).
6. J. Traham and R.G. Goodrich. Phys. Rev. B6, 199 (1972).
7. L.J. Van der Pauw, Phillips Res. Rep. 13, 1 (1958).
8. A.S. Barker and J.P. Remeika, Phys. Rev. B10, 987 (1974).

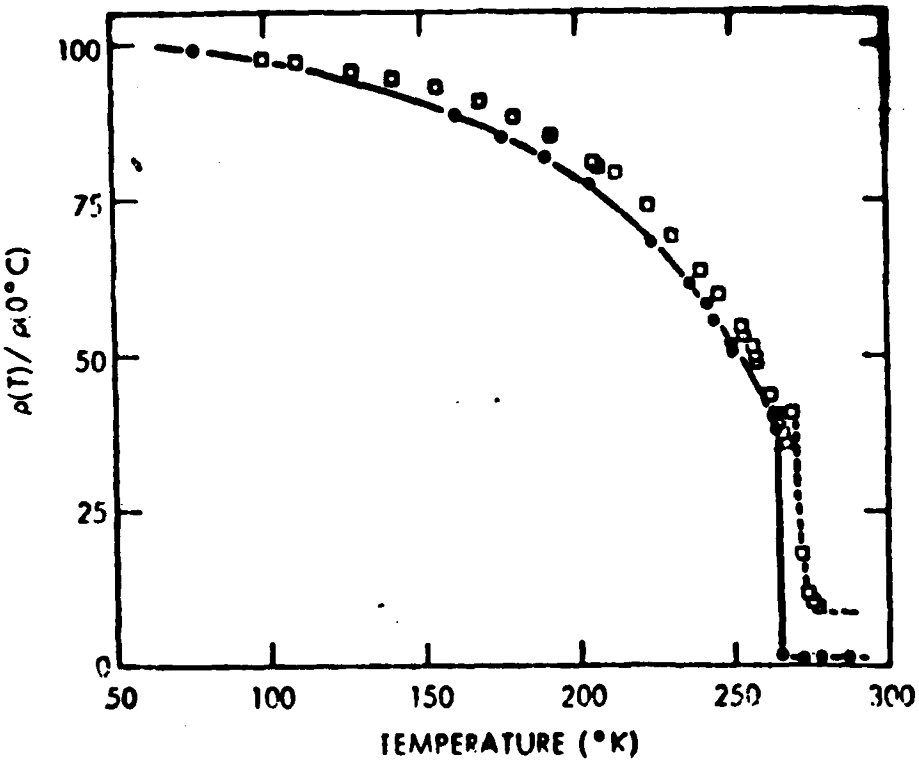

Figure 4. Relative resistivity versus temperature for a single crystal of NiS.

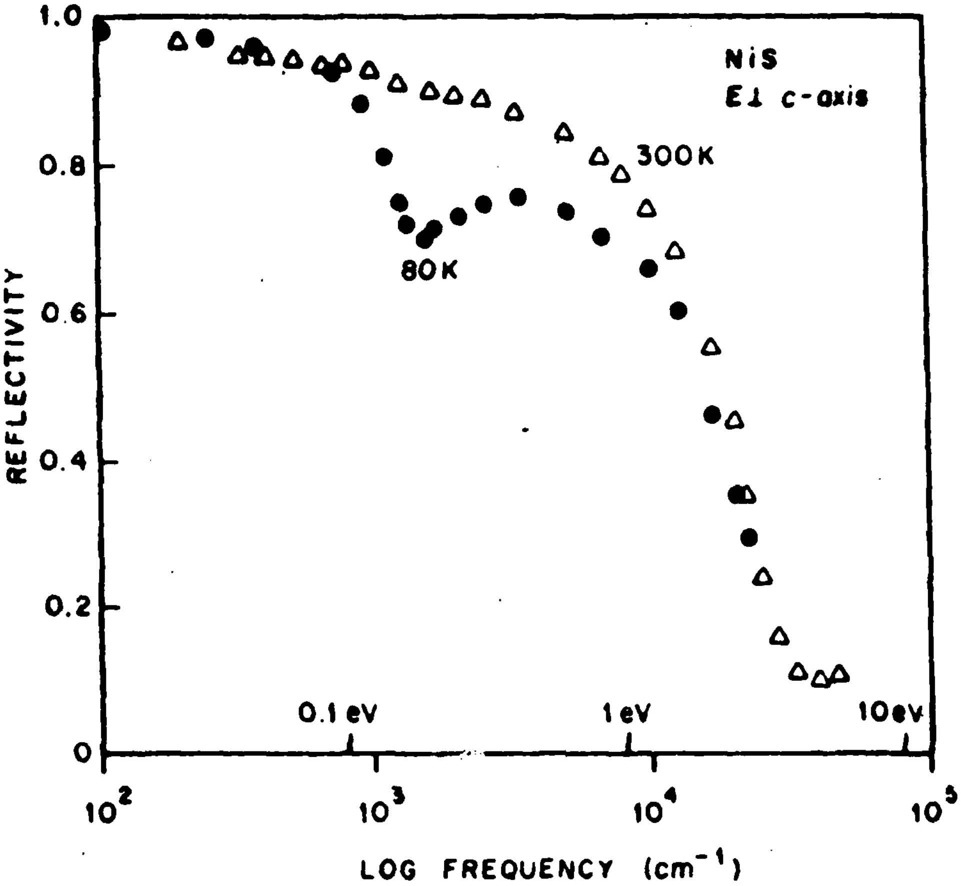

Figure 5 - Polarized reflectivity spectra for a sample of NiS taken above and below the transition temperature of 230^0K.

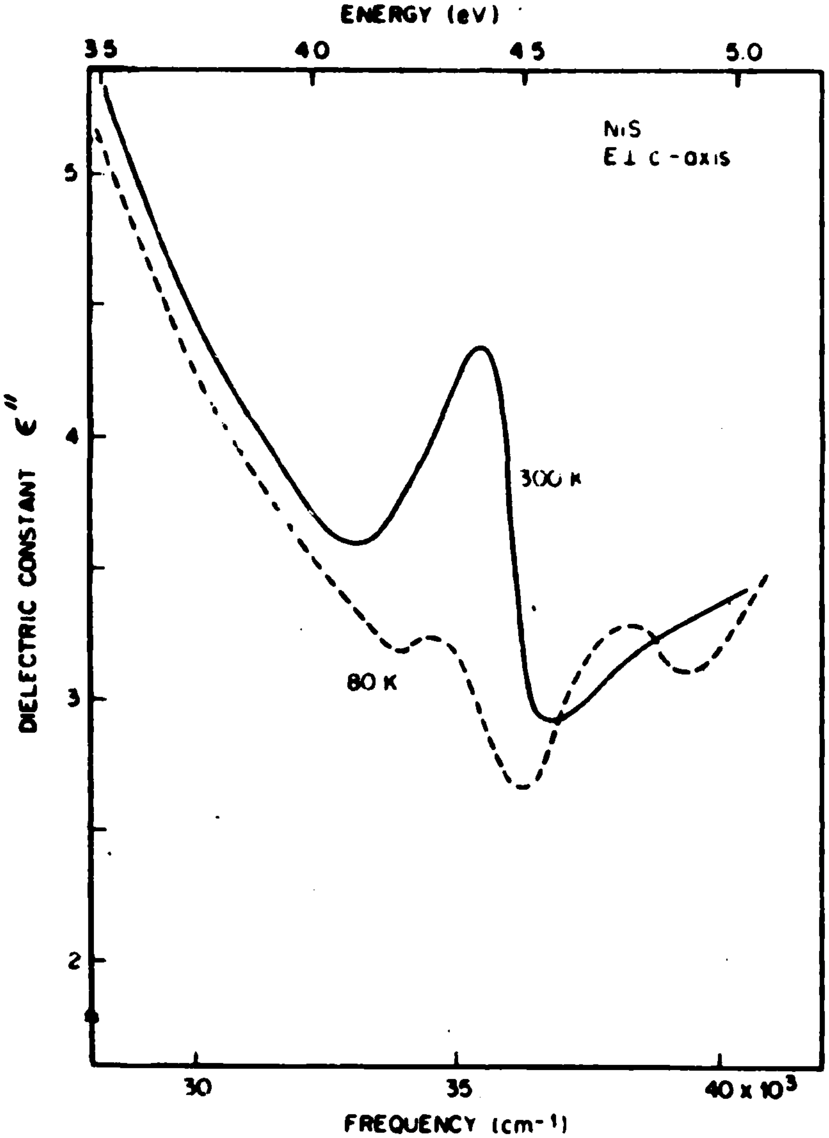

Figure 6 - Imaginary part of the dielectric constant ε'' obtained by Kramers-Kronig analysis of the reflectivity data in the visible and ultraviolet regions.

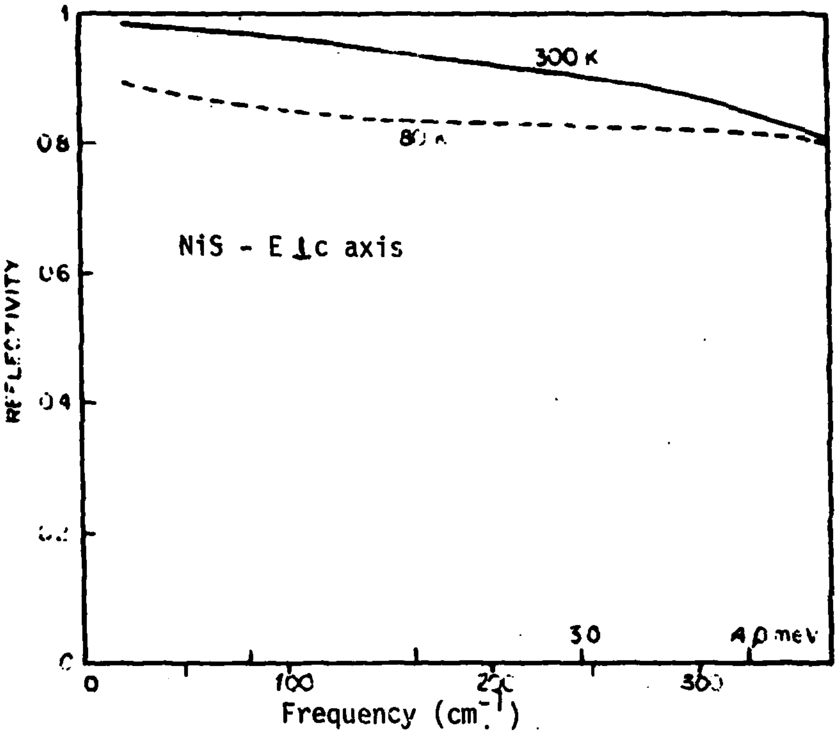

Figure 7. Far-infrared reflectivity of NiS. The 80-K data have a rather large uncertainty in their normalization; they have been chosen to equal the 300-K reflectivity near the 350 cm^{-1}.

NiS_2

Nickel Disulfide

Nickel disulfide is a metal-insulation phase transition material which exhibits two magnetic transitions:

1. Paramagnetic → antiferromagnetic at T = 40°K to 65°K
2. Antiferromagnetic → weak ferromagnetic at T = 31°K

The mechanism has been interpreted by a Mott-Hubbard model in which electron correlation effects play an essential role.[1] The diagram shown below indicates the pressure dependence of the two phase transition temperatures.[2]

It should be mentioned that the first transition temperature will increase by substitution of Se for S and by doping with Co and Cu, which decrease and increase the respective electron concentration in NiS_2. For the second transition, the temperature of transition will decrease with the introduction of impurity atoms. A volume change on the order of about 0.4% occurs with no change in the crystal symmetry.

NiS_2 is itself a cubic crystal with structure of the pyrite type. Figure 2 illustrates this structure.[3] NiS_2 occurs in nature as the mineral valcite with a density of 4.44 gm/cm^3.

In order to determine if NiS_2 would be useful for laser hardening applications, two physical measurements give useful insights: resistivity (or conductivity), and reflectivity changes, both as a function of temperature, pressure and perhaps stoichiometry. (It should be pointed out that there is a spike in the specific heat curve near 30°K for $NiS_{1.93}$.) However, both conductivity and resistivity measurements indicate no change near the transition temperature.[4] Published optical properties of NiS_2 are extremely limited in scope. The index of refractive index and extinction coefficient (n and k) are both known from 0.5eV to 5eV (about 2 microns, in the near IR, to the near UV).[5] These curves are shown in Figure 3. The reflectivity at normal incidence is determined by the formula:

$$R = \frac{(n-1)^2 + k^2}{(n+1)^2 + k^2} .$$

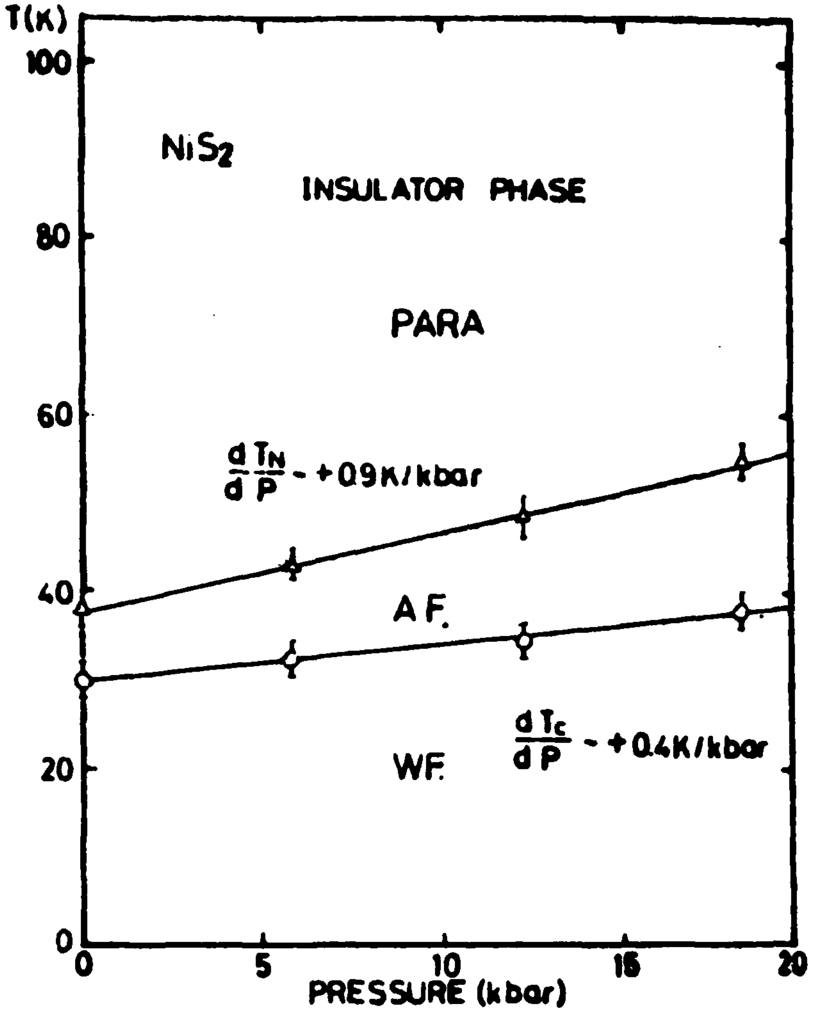

Figure 1. Pressure effect on the temperature of transition.

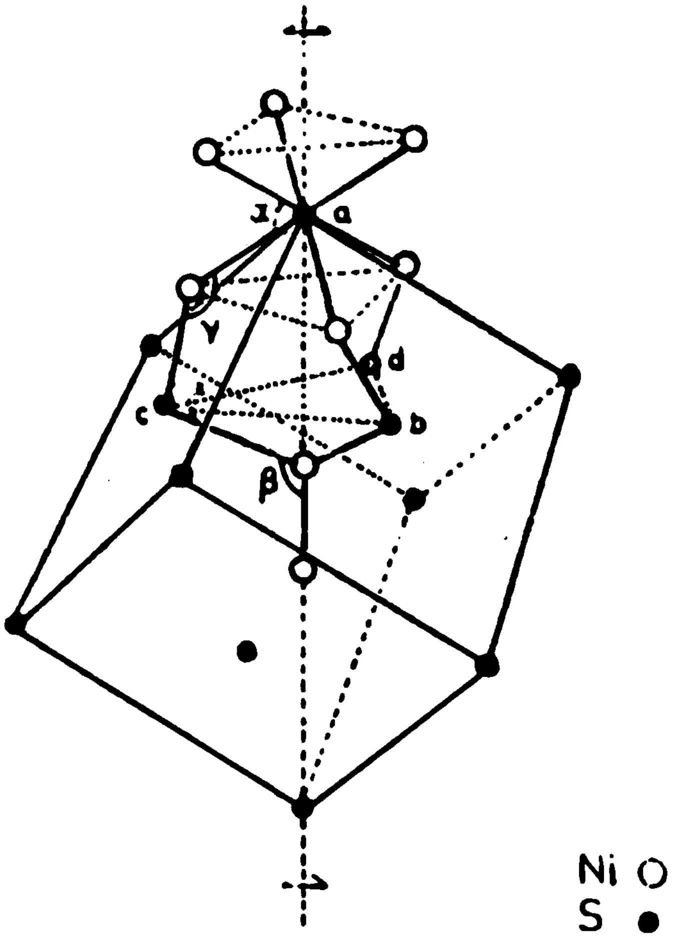

Figure 2. Crystal structure of NiS_2.

AD-A146 658 HANDBOOK OF PHASE TRANSITION SULFIDES SELENIDES AND 3/3
TELLURIDES(U) TACTICAL WEAPONS GUIDANCE AND CONTROL
INFORMATION ANALYSIS CE.. W J WILD ET AL. JUL 84
UNCLASSIFIED GACIAC-HB-84-02 DLA900-80-C-2853 F/G 7/4 NL

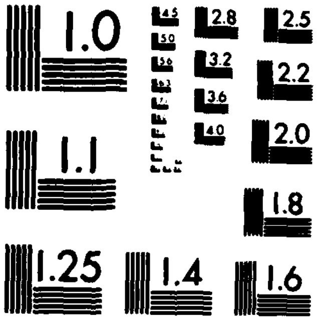

OPY RESOLUTION TEST CHART

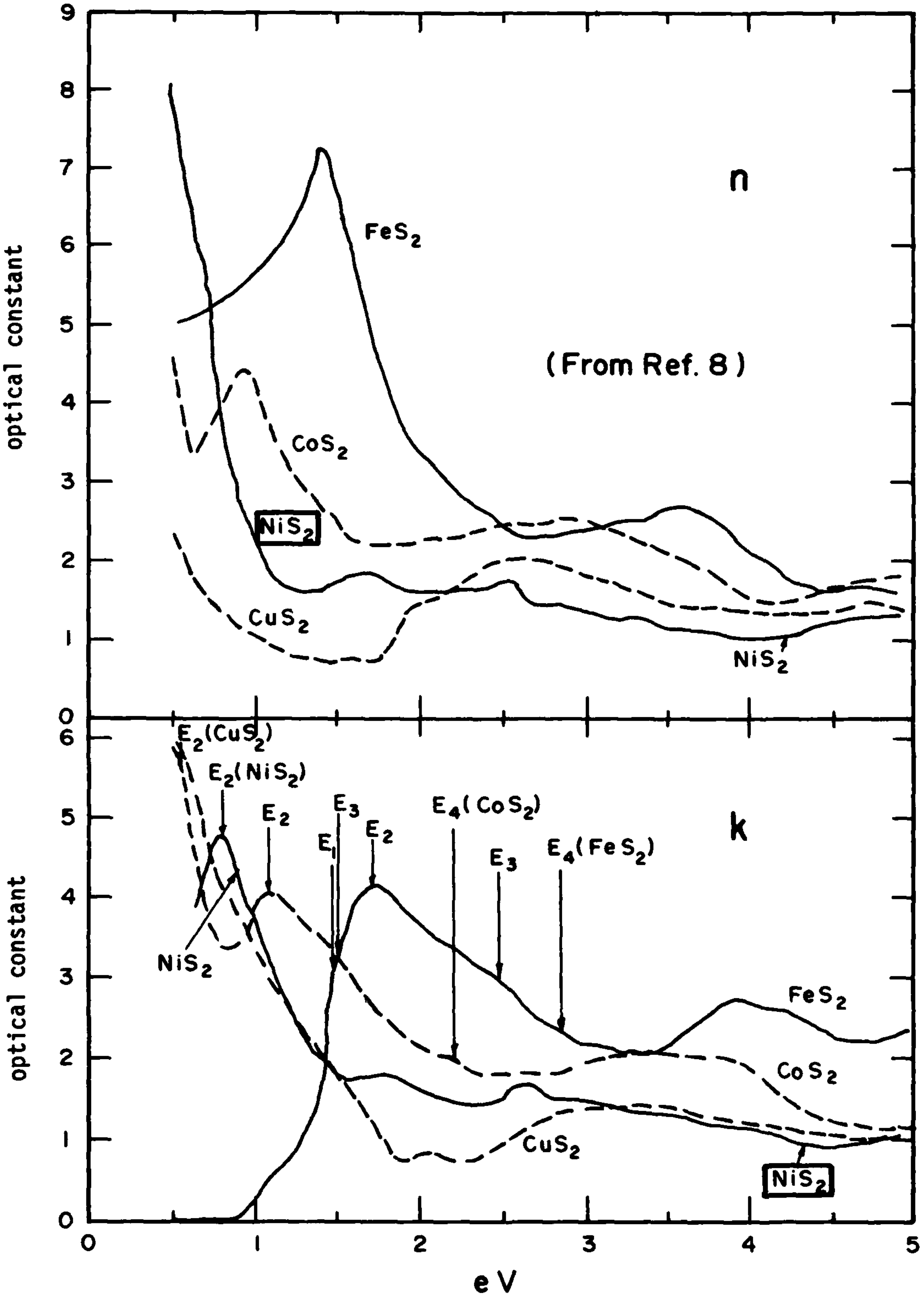

Figure 3. Real and imaginary parts of the complex refractive index for FeS$_2$, CoS, NiS and CuS$_2$.

These measurements were in fact determined from measurement of R using the Kramers - Kronig method. The data were taken at room temperature.

REFERENCES (NiS_2)

1. N.F. Mott, Metal-Insulator Transitions, Taylor and Francis, London (1974).
2. N. Mori and T. Watanabe, "Pressure Effects and Magnetic Transition Temperatures of NiS_2", Solid State Comm. 27, 567 (1978).
3. J.A. Wilson and G.D. Pitt, "Metal-Insulator Transition in NiS_2", Phil. Mag., 23 1297 (1971).
4. R.L. Kautz, M.S. Dresselhaus, D. Adler, and A. Linz, "Electrical and Optical Properties of NiS_2", Phys. Rev. B6, 2078 (1972).
5. J.A. Bither, et.al., "Transition Metal Pyrite Dichalcogenides: High Pressure Synthesis and Correlation of Properties", Inorg. Chem 7 2208 (1968).

$NiS_{2-x}Se_x$
Nickel-Sulfur-Selenium Solid Solution

$NiS_{2-x}Se_x$ is a solid solution; when the stoichiometry parameter $x = 0$, we have nickel disulfide (NiS_2 - reviewed separately). NiS_2 is a Mott insulator due to electron-electron correlations in the e_g band.[1,2,3] (The e_g band is in the 3d group and contains four states per cation.) For $x = 2$, $NiSe_2$, the material is metallic in agreement with arguments based on the filling of the 3d e_g band so that increased selenium concentration must eventually yield a semiconductor-metal transition.[4] In the $NiS_{2-x}Se_x$ system the alloying simply increases the bandwidth without changing the carrier concentration.

Single crystals of $NiS_{2-x}Se_x$ are grown by chemical vapor deposition (CVD) where bromine is used as a transport agent.[5] Stoichiometric mixtures of pure nickel, sulfur, and selenium were used to prepare a polycrystalline starting material, from which single crystals are grown. Lattice constant measurements are used to monitor the growth of the crystals.[6] Generally it is possible to grow crystals to a stoichiometric accuracy of about 5%.

For the study of the electrical conductivity of $NiS_{2-x}Se_x$ samples in the range $4 < T < 600°$, a 4-probe van der Pauw technique is considered standard.[7] Thermoelectric studies are best performed using the heat pulse technique.[8] Figure 1 shows the electrical conductivity in the range $0.1 < x < 1.5$.[4] The data here indicates a thermally activated behavior for $x < 0.55$ and tend to a common maximum of about $10^3\ \Omega^{-1}\ cm^{-1}$ at high temperatures. For $x < 0.55$ the results are qualitatively similar to those for NiS_2. Three distinct activation energies are apparent, as further elaborated upon in Figure 2. These all decrease with increasing x and approach zero as x approaches 0.6. At this value of x the selenium concentration increases to the point where a metal insulator phase transition occurs. For higher values of x the samples are metallic over the entire temperature range ($4 < T < 600°K$). For $x < 0.3$, the solid solution have at all temperatures a conductivity behavior similar to pure NiS_2. In the range $0.4 < x < 0.55$, a phase transition is exhibited at low temperatures ($T < 100°K$) to a metallic state. Figure 3 shows how the activation energies vary with selenium concentrations. Figure 4 shows the behavior of the resistivity with temperatures for various values of x. Note the behavior for $0.4 < x < 0.55$ in

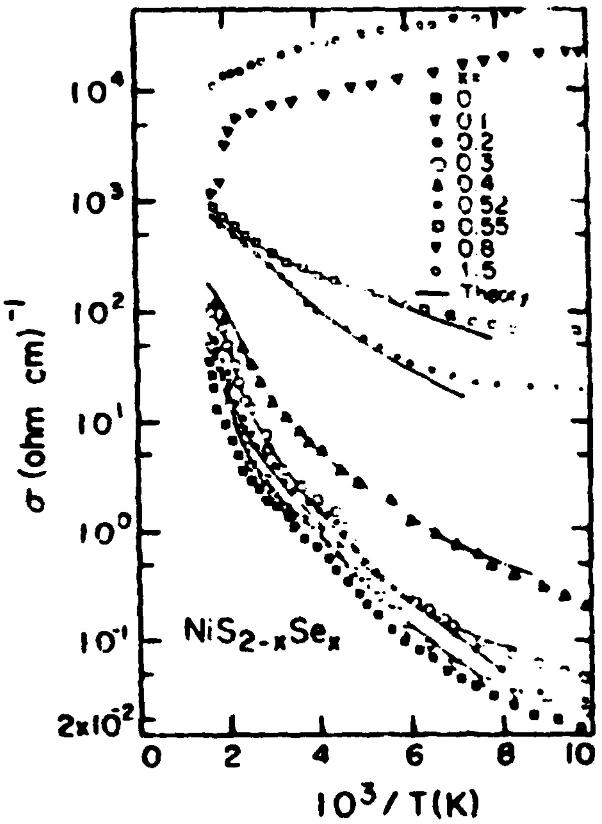

Figure 1. Conductivity versus inverse temperature.

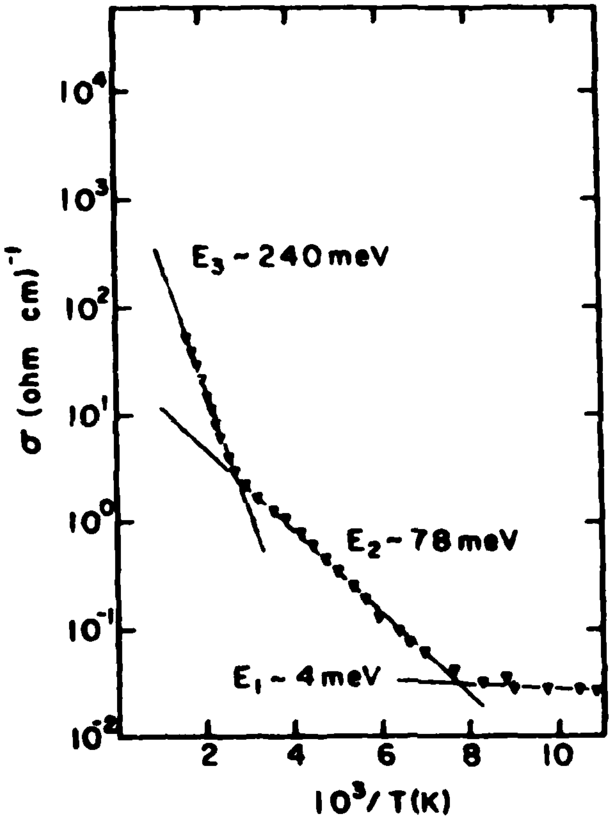

Figure 2. Conductivity versus inverse temperature for $NiS_{1.9}Se_{0.1}$. The three activation energies E_1, E_2, and E_3 are obtained from the slopes of the lines shown in the figure.

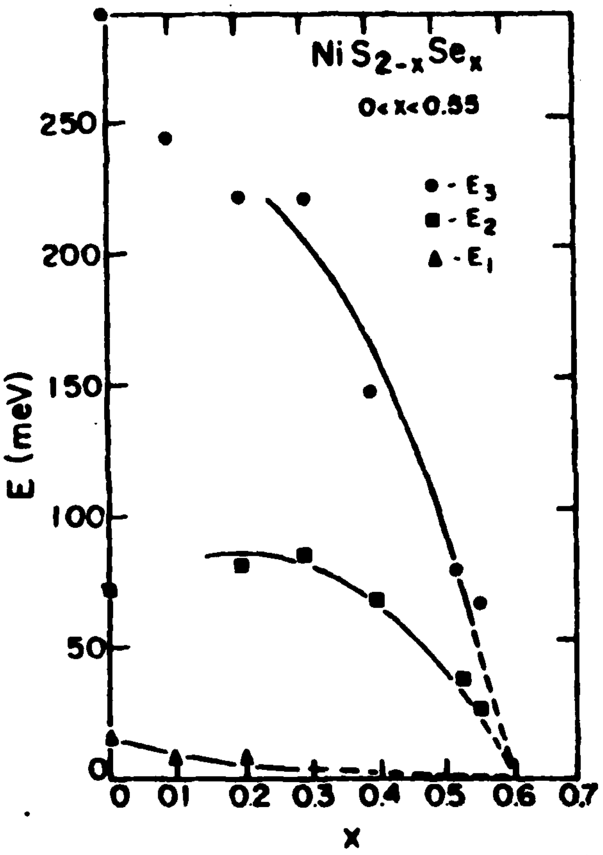

Figure 3. Activation energies E_1, E_2, and E_3 vs. selenium concentration x. E_1 corresponds to low temperature, E_2 to intermediate temperature, and E_3 to high temperature (see Figure 2). All the activation energies E_1 approach (broken curves) zero for x ~ 0.6 at the metal-insulator transition.

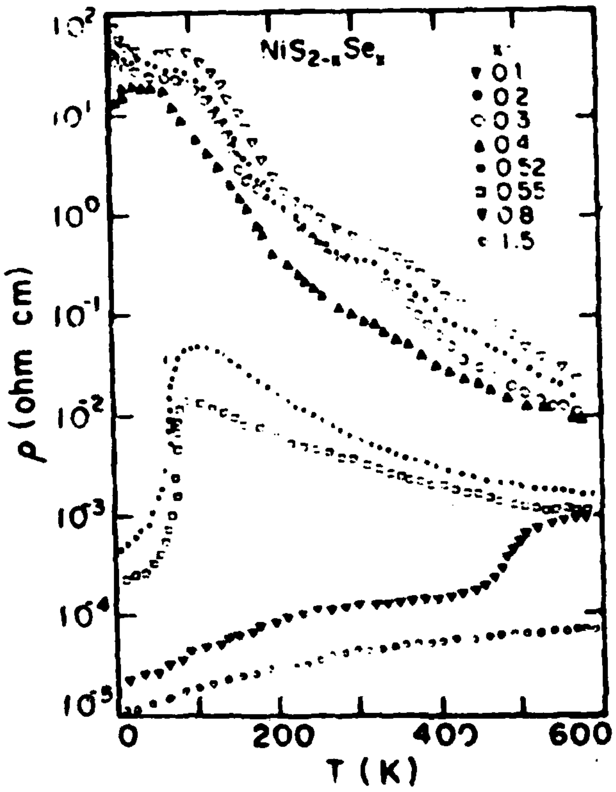

Figure 4. Resistivity versus temperature for the same data as in Figure 1 but giving emphasis to the low-temperature behavior.

Figure 4 - this rapid charge change in electrical resistivity is characteristic across many phase transition boundaries for many substances.[4,5]

In the regime of $0.4 < x < 0.55$ a transition from semiconductor-to-metal occurs at low temperature. This is somewhat surprising considering that the system remains semiconducting at high temperatures even after the correlation splitting of the bands vanishes.[9] That this is possible can be explained using small-polaron band models.[10] Figure 5 shows a plot of conductivity as a function of temperature.[4] The transition temperature increases from about 70°K for $x = 0.47$ to about 120°K for $x = 0.55$.

We have been unable to locate any significant data concerning the optical properties of the $NiS_{2-x}Se_x$ system. It would be very interesting to possess a detailed knowledge of how the various parameters balance with varying x, but perhaps one clue can be had from the observation that for all x the carrier concentration remains constant (be they electrons, holes, polarons, etc.).[4] This suggests that (if we accept a Drude approximation) the optical properties will not significantly change across the transition boundary. Further studies are obviously necessary.

REFERENCES ($NiS_{2-x}Se_x$)

1. T.A. Bither, et.al., Inorg, Chem. 1, 2208 (1968).
2. A.K. Mabatah, et.al., Phys. Rev. Lett, 39, 494 (1977).
3. J.M. Hastings and L.M. Corliss, IBM J. Res. Dev., 14, 227 (1970).
4. P. Kwizera, M.S. Dresselhaus, and D. Adler, Phys. Rev. B21, 2328 (1980).
5. R.J. Bouchard, J.L. Gillsar, and H.S. Jarrett, Mat. Res. Bull., 8, 489 (1973).
6. D.D. Klemms, Neues Jahrb. Mineral. Monalski, 1962, 32 (1962).
7. L.J. van der Pauw, Philips Res. Rep. 13, 1 (1958).
8. P.C. Kolund and A.K. Mabatah, Rev. Sci. Instrum., 48, 775 (1977).
9. A.K. Mabatah, et.al., Phys. Rev. B21, 1676 (1980).
10. T. Holstein, Ann. Phys. (N.Y.) 8, 325 (1959).

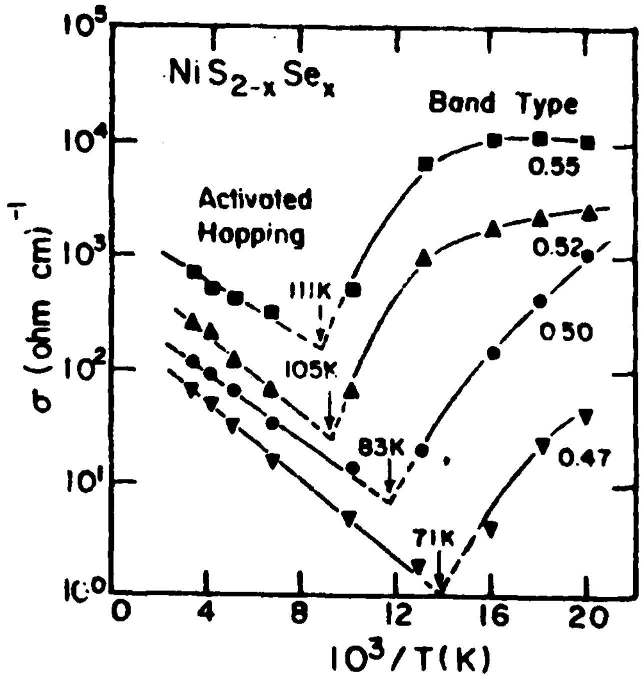

Figure 5. Conductivity versus inverse temperature $10^3/T$ for $NiS_{2-x}Se_x$ showing polaron-band behavior at low temperatures.

SmS

Samarium Monosulfide

Samarium Monosulfide has been subjected to very intensive study since its discovery as a pressure induced phase transition material in 1970.[1-6] The effect is due to a 4f → 5d electron delocalization in the solid. At 293°K, there is an abrupt change in resistivity and lattice constant at 6.5 kbar pressure without any change in the crystal structure. There is a conversion from Sm^{2+} to Sm^{3+}; the material goes from a semiconductor to a metallic state. Also, there is a hysteresis effect as the semiconductor state does not reappear until the pressure goes down below 0.8 kbar. There is a significant amount of published material on SmS in the Soviet open literature; many of their results corroborate measurements made in the West.

Figure 1 shows the wavelength dependence of reflectivity of SmS in the semiconducting to metallic states. Figure 2 shows the change in reflectivity at the semiconductor-to-metal transition and it has the typical hysteresis effect. The resistivity of SmS versus pressure is shown in Figure 3. The change is dramatic - similar changes occur in SmSe and SmTe. Finally, Figures 4 and 5 show the dielectric and absorption properties of SmS.[6] We can see signficant changes in optical properties.

REFERENCES (SmS)

1. A. Jayaraman, V. Narayanamurti, E. Bucher, and R.G. Maine, Phys. Rev. Lett. 25, 1430 (1970).
2. B. Batlogg, E. Kaldis, A. Schlegel, and P. Wachter, Physical Review B14, 5503 (1976).
3. L.N. Glurdzhidze, et.al., Sov. Phys. Solid State 20(9), 1573 (1978).
4. J.L. Kirk, et.al., Physical Review B6, 3023 (1972).
5. D.W. Pohl, et.al., Applied Optics, 13 95 (1974).
6. D.W. Pohl, et.al., Solid State Comm. 17, 705 (1975).

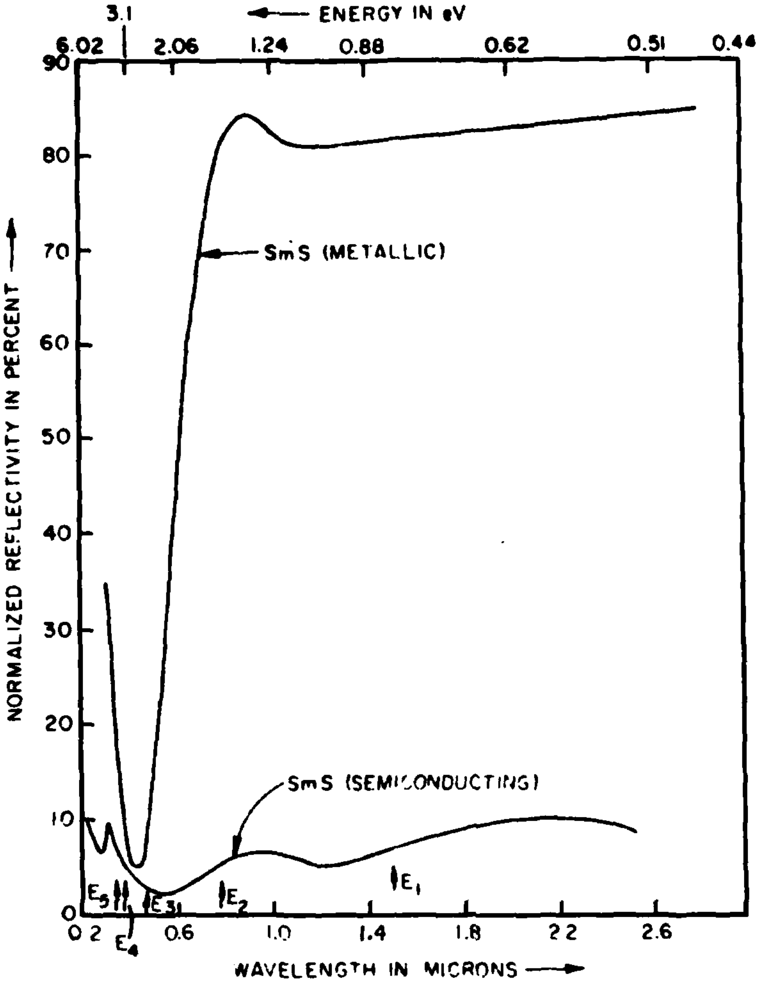

Figure 1. Wavelength dependence of reflectivity of SmS in the semiconducting and metallic states.

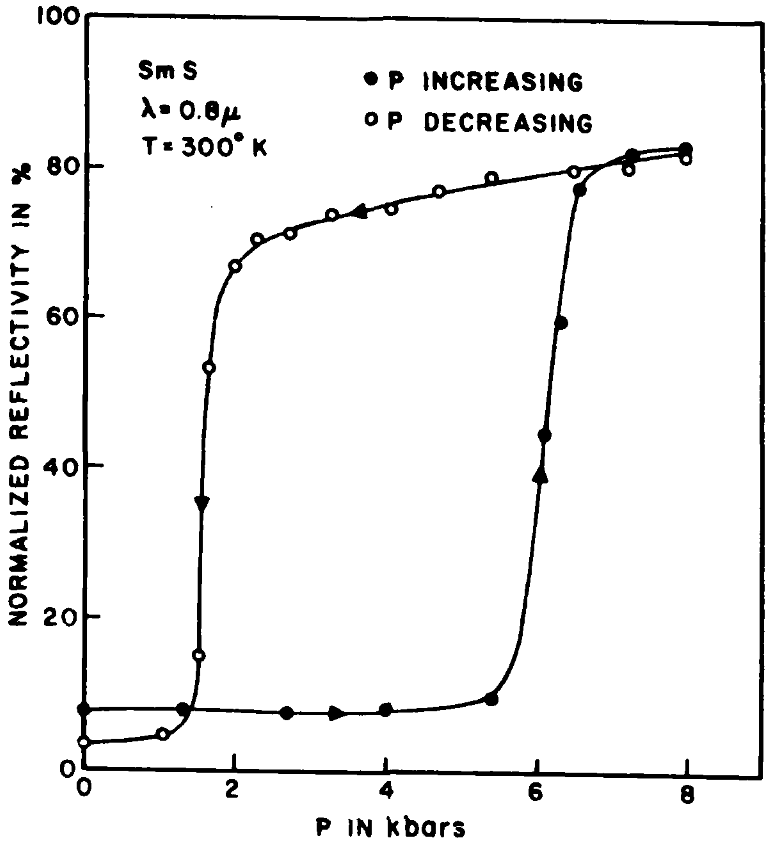

Figure 2. Change in reflectivity at the semiconductor-to-metal transition in SmS at 0.8 μ. Note the hysteretic nature of the transition.

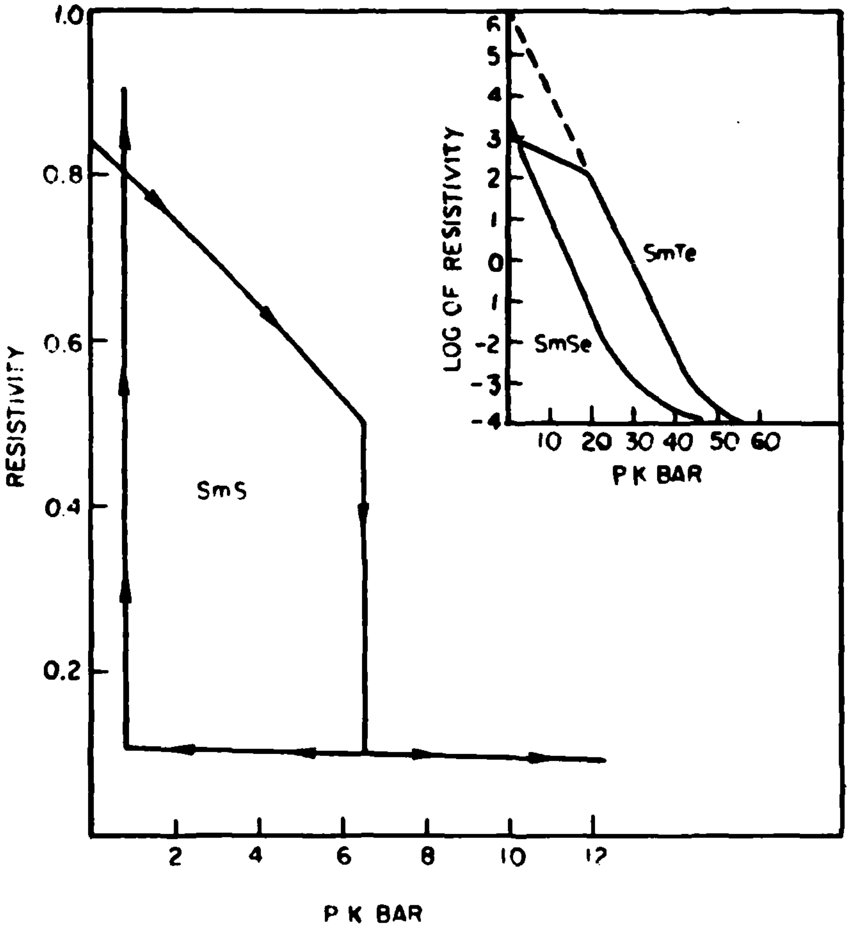

Figure 3. Normalized resistivity versus pressure for single crystal SmS. The actual resistivity at pressures greater than 6.5 kbar is ~ 3-4 x 10^{-4} Ω cm. The data for SmTe and SmSe are shown in the inset.

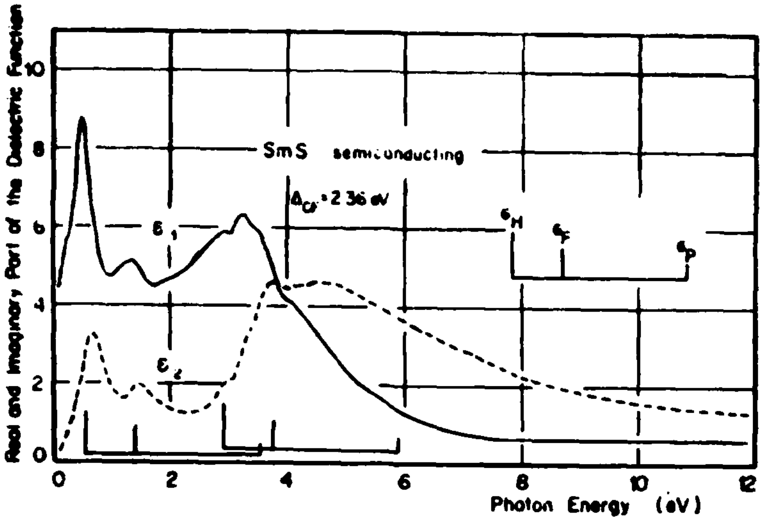

Figure 4. Dielectric function of semiconducting SmS.

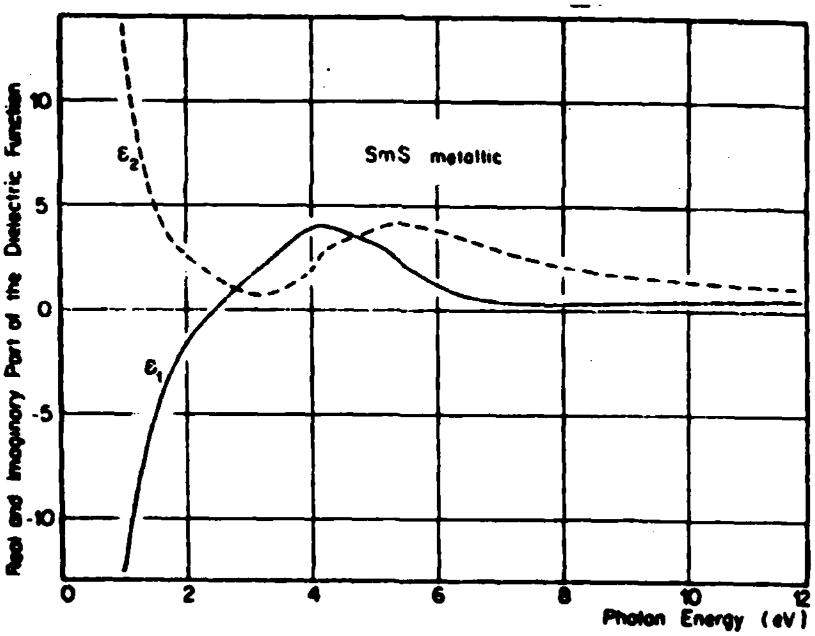

Figure 5. Dielectric function of metallic SmS.

SnS_2

Tin Disulfide

$SnSe_2$

Tin Diselenide

Tin disulfide (SnS_2) and tin diselenide ($SnSe_2$) are layered semiconductors with CdI_2 layer structure. They both can exist in a great number of different polytypes, several common types being 18R, 4H and 2H types.[1] As like other layered compounds, SnS_2 and $SnSe_2$ have attracted much attention due to their essentially bidimensional character. The space group of the CdI_2 structure is D^3_{3d}, which is symmorphic.[2,3] The cations are placed at (000) in the hexagonal unit cell and the two anions at (1/3, 2/3, u) and (2/3, 1/3, -u) defined by the c/a ratio and the parameter $u \approx 0.25$, producing a layer structure with the cation sheet sandwiched between two anion sheets which in turn face each other across the layers. Each cation is strongly bonded to six anion first neighbors which form a perfect octahedran if u takes the special value $u^* = a/\sqrt{6}\ c$, and each anion sits at the top of a pyramid of three cations. Each anion has twelve second neighbor anions and if $c/a = 2 \quad 2/3$ and $u = 0.25$ the anions have perfect hexagonal close packed structure.[2] Detailed knowledge of the crystal structure is useful in understanding electronic band structures.

For $SnSe_2$, the measured lattice parameters are given in Table 1.[4] For comparison the parameters of several other substances are also given. This table includes the Group IV dichalcogenides having the space group C6 structure. SnS_2 crystal parameters are also given. Figure 1 shows how the lattice parameter a_0 changes with the temperature.[4]

For SnS_2 the electrical conductivity is given in Figure 2 for a single cleaved crystal. There are three distinct regions, each obeying an equation of the form $\sigma = \sigma_{no} \exp(-E_n/kT)$. For region 1 we have $\sigma_{10} = 2.86\Omega^{-1}cm^{-1}$ and $E_1 = 0.4eV$; for region 2, $\sigma_{20} = 1.3 \times 10^{-6}\Omega^{-1}cm^{-1}$ and $E_2 = 0.11eV$; and for region 3 we have $\sigma_{30} = 2.85 \times 10^{-8}\Omega^{-1}cm^{-1}$ and $E_3 = 0.05eV$. For the resistivity, there is a thermal switching behavior when $10^3/T \approx 3.6$ (or $T \approx 280°K$); this is shown in Figure 3. After forming and switching has been observed, the SnS_2 crystal shows a high resistance state which is always lower than the initial resistance, normally by a few orders of magnitude. The I-V

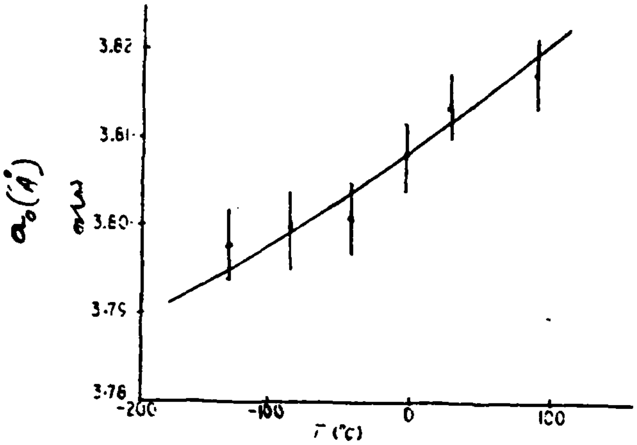

Figure 1. Variation with temperature of lattice parameter a_0 of single $SnSe_2$ crystals.

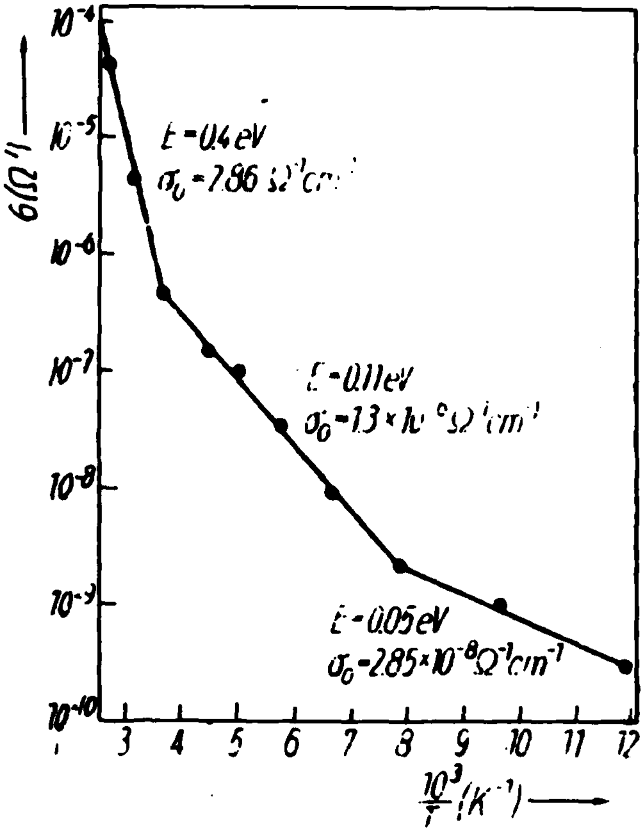

Figure 2. The ohmic dielectrical characteristics of SnS_2 showing three distinct regions for σ.

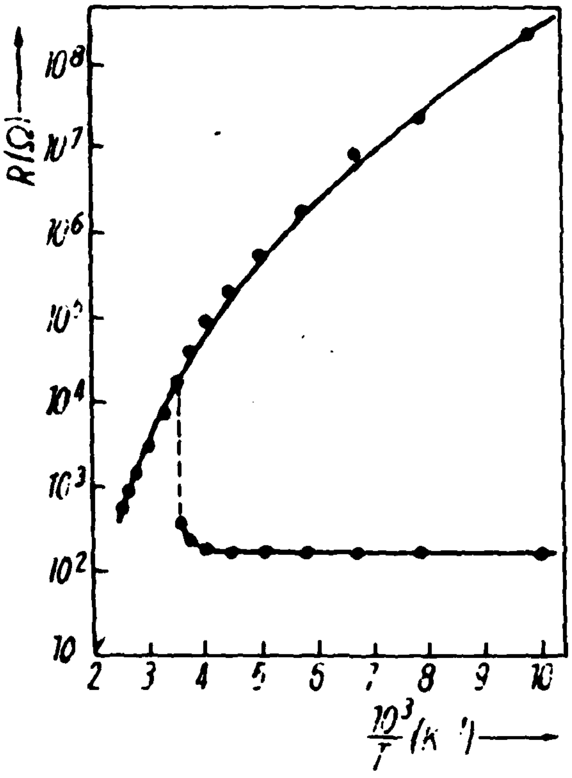

Figure 3. Switching behavior of SnS_2.

TABLE 1

LATTICE PARAMETERS, RESISTIVITY AND ENERGY GAPS OF GROUP IV DICHALCOGENIDES HAVING THE C6 STRUCTURE

	a_0 (Å)	c (A)	c/a (Ref)	p (Ωcm)(Ref)	E' (ev)	Eg (ev)
TiS_2	3.4080 (± 2)	5.7014 (± 3)	1.673	$8x10^{3}$n†		1.95r
	3.405 (± 5)	5.678 (± 5)	1.67	10^{3}		
	3.39	5.70	1.68			
$TiSe_2$	3.537 (± 3)	6.00 (± 3)	1.70	$2x10^{-3}$†		1.55r
	3.535	6.004	1.70	10^{-2}		
$TiTe_2$	3.773 (± 5)	6.516 (± 5)	1.73	10^{-4}†		1.00r
	3.76	6.48	1.72	$0.7x10^{-4}$		
ZrS_2	3.662	5.809	1.586	10n†	1.68	2.75r
	3.662	5.813	1.587	0.3		
	3.660	5.825	1.593			
	3.66 (± 3)	5.85 (± 3)	1.60			
$ZrSe_2$	3.76 (± 1)	6.15 (± 1)	1.63	10^{-1}n†		2.00r
	3.770	6.137	1.63			
$ZrTe_2$	3.952	6.660	1.68	10^{-3}†		
HfS_2	3.635	5.837	1.61	10^{9}†	1.96	2.90r
	3.622 (± 2)	5.88 (± 3)	1.62			
$HfSe_2$	3.748	6.159	1.64	20n†	1.13	2.20r
	3.733 (± 5)	6.146 (± 5)	1.65	0.05		
$SiTe_2$	4.28 (± 1)	6.71 (± 1)	1.57	10^{9}	1.8	2.18
SnS_2	3.639 (± 5)	5.884 (± 5)	1.62	10^{7}n	2.21	2.88
					2.07	3.8 r
$SnSe_2$	3.811 (± 2)	6.137 (± 3)	1.61	0.28n	0.97	1.62
	3.84 (± 2)	6.13 (± 3)	1.60	0.11n	1.0	
					0.98,1.3	1.97

† Compressed powder. E' indirect band gap. Eg lowest direct band gap (r denotes reflection peak). n donotes n-type semiconductors.

curves also show non-ohmic behavior at higher voltages. The value of the switching temperature depends on the current passing through the crystal and as the low resistance state presumably consists of a metallic filament, then the local temperature may indeed be higher than that measured. For zero current it is found that heating in the low resistance state may be continued until the high resistance curve is reached, where the crystal automatically reverts to the high resistance state. PbI_2 also possesses this feature of resistance "memory".[5]

For $SnSe_2$, Figure 4 shows the temperature variation of the resistivity and the conductivity. The standard four-probe method is used to get these measurements. These measurements lead one to believe that $SnSe_2$ is an n-type semiconductor at 290°K, the carrier concentration being $1.57 \times 10^{18} cm^{-3}$. There is presently some disagreement over the exact value of the carrier concentration.[6,7] It is claimed that $SnSe_2$ crystals grown using the Bridgeman technique are p-type with carrier concentration about $10^{18} cm^{-3}$.[8] Figures 5 - 13 show the optical measurements for SnS_2 and $SnSe_2$.[9-11] For these plots we note that the complex index is $\hat{n} = n + ik$ and k is the extinction coefficient (related to the absorption coefficient by $\alpha = \frac{4\pi k}{\lambda}$). Data is given for 77°K and 290°K. Most of the data given here is for the visible and UV; Figures 11 and 12 go into the near IR. Note that whereas there is a variation with temperature, it is nevertheless quite small and there does not appear to be any significant variations in any of the measured regions. There is a degree of anisotropy for both SnS_2 and $SnSe_2$. For the dielectric constant we have $\varepsilon(\nu) = \varepsilon_1(\nu) + i\varepsilon_2(\nu)$. The index and extinction coefficients are computed from the reflectivity via standard Kramers-Kronig analysis.

SnS_2 and $SnSe_2$ both appear to have been extensively studied. There does not appear to be any significant phase transition and alteration of optical properties (at least in the range of 77°K to 300°K).

REFERENCES (SnS_2)

1. R. Mitchell, Y. Fujiki, and Y. Ishijawa, Nature, 247, 537 (1974).
2. J. Robertson, J. Phys. C. 12, 4753 (1979).
3. G.F. Koster, Space Groups and Their Representations, Academic Press,

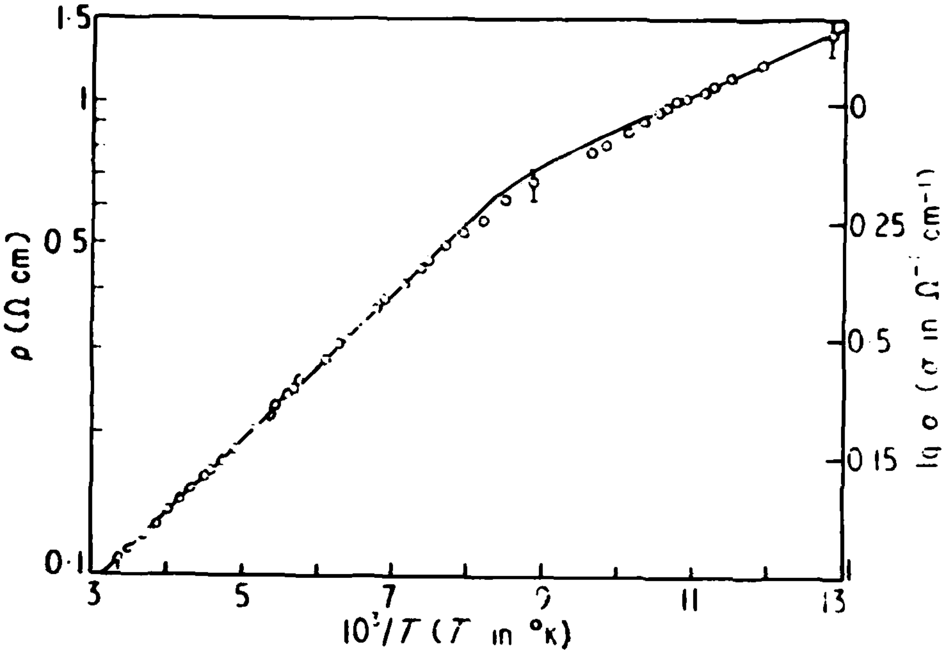

Figure 4. The resistivity ρ and conductivity σ of $SnSe_2$ plotted against $10^3/T$.

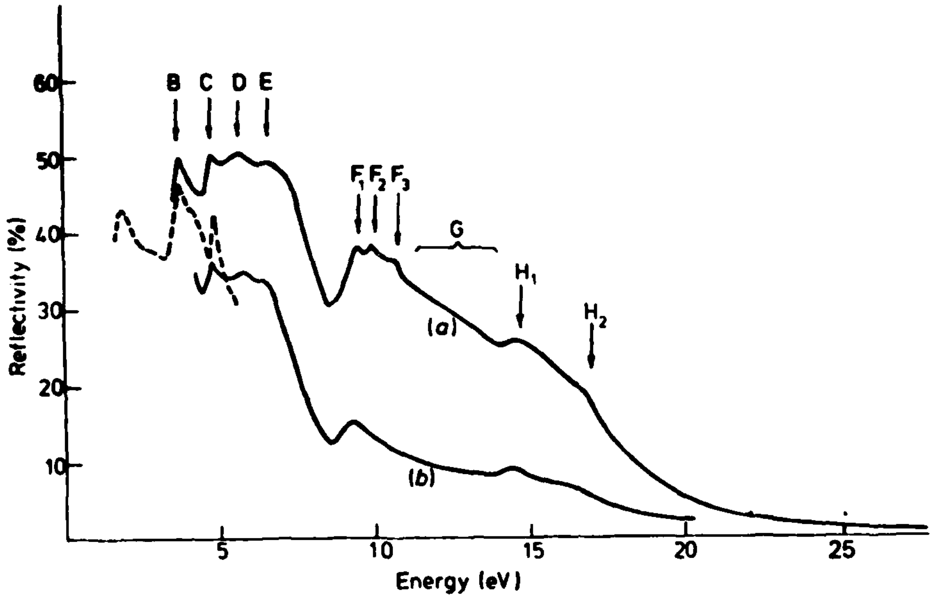

Figure 5. Full line: reflectivity curves of $SnSe_2$ single crystals: (a) freshly cleaved sample; (b) air-exposed sample (more than 100 hours). Broken line: Camassel et al (1976) reflectivity curve of $SnSe_2$.

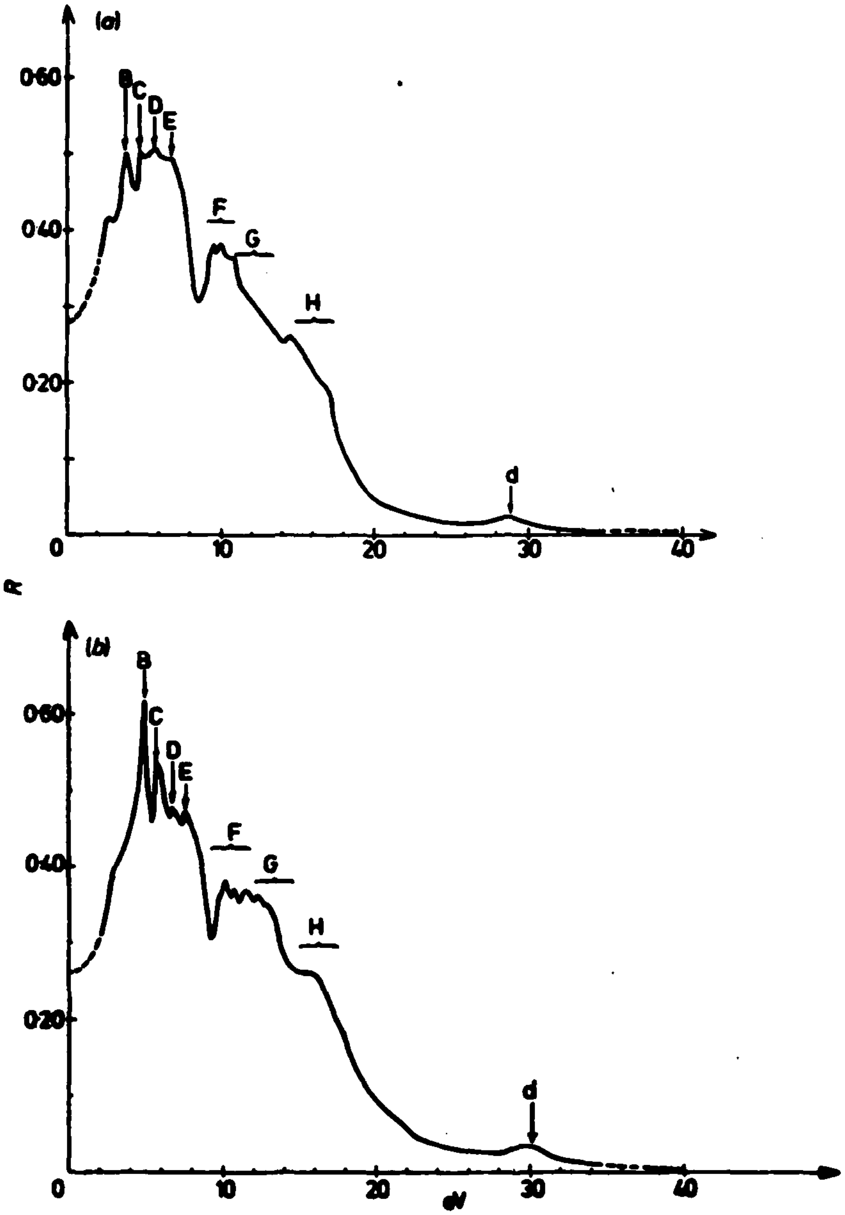

Figure 6. Reflectivity curve of (a) SnSe$_2$ and (b) SnS$_2$ for $\vec{E} \perp \vec{c}$; our experimental curves as full curves, extrapolations as broken curves.

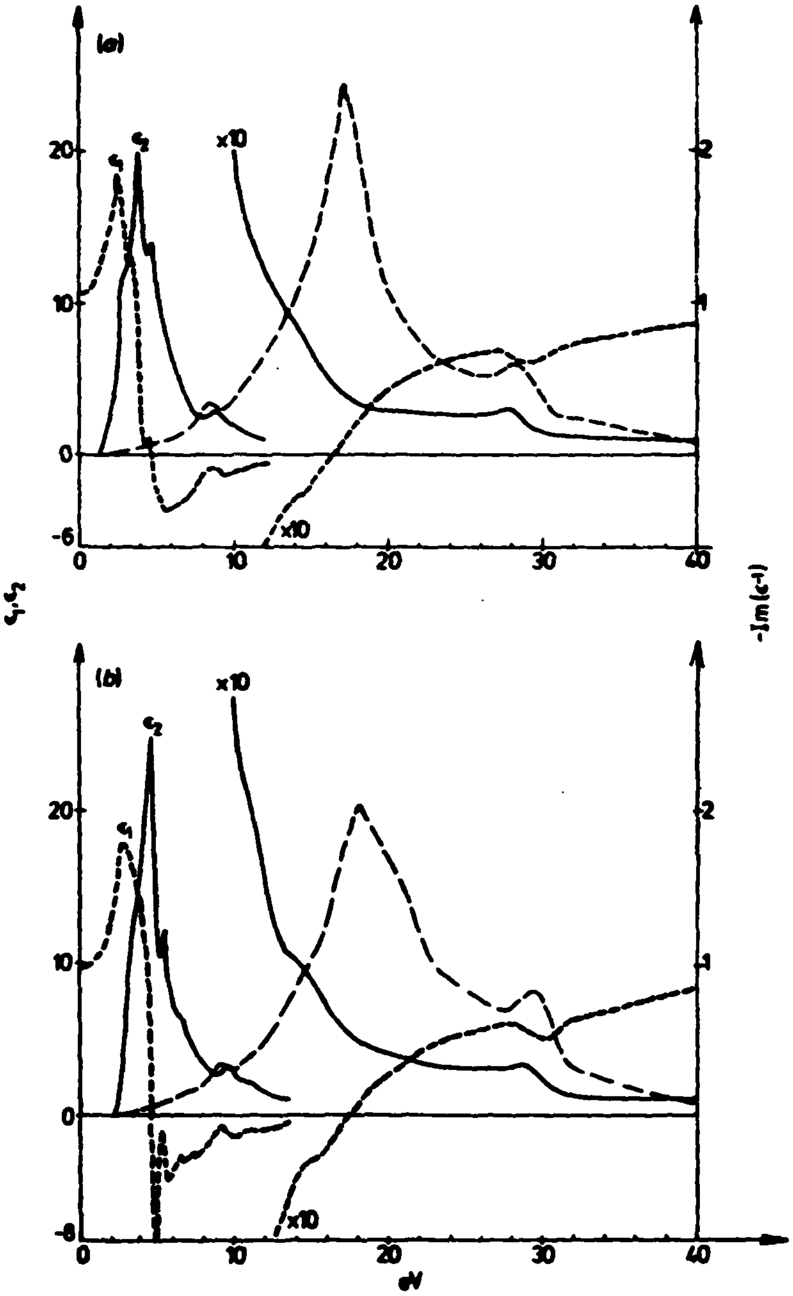

Figure 7. Dielectric constants (ε_1, ε_2) and energy-loss function (unlabelled broken curve) of (a) $SnSe_2$ and (b) SnS_2.

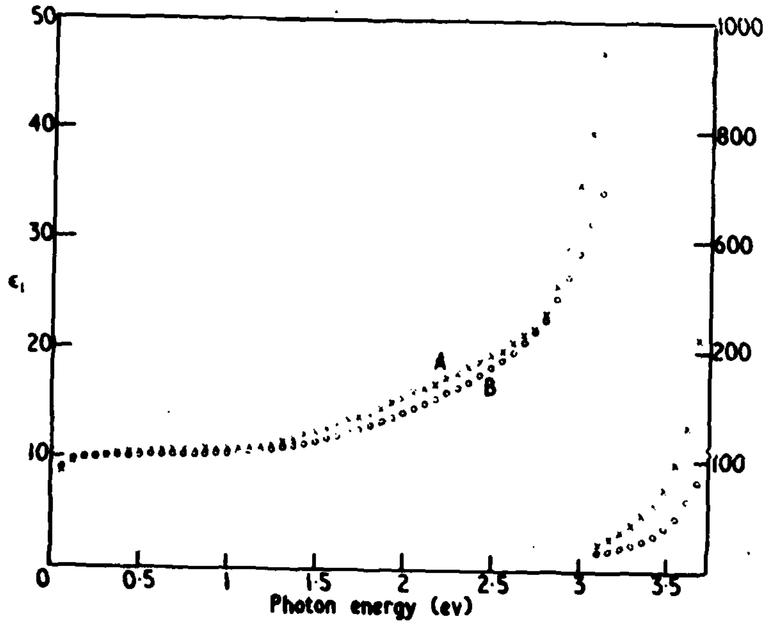

Figure 8. Spectral variation of ε_1 for $SnSe_2$ at A, 290°K, and B, 77°K.

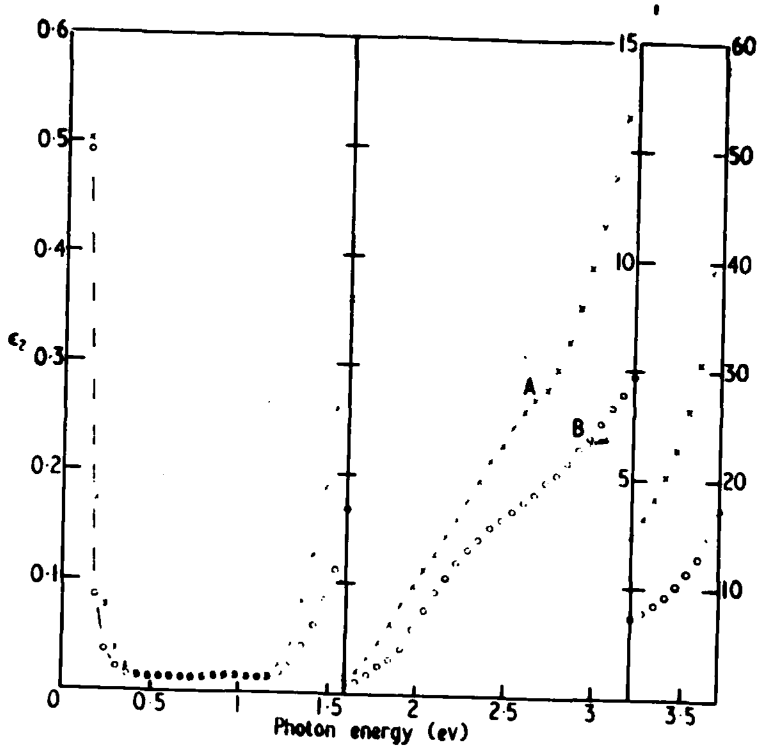

Figure 9. Spectral variation of ϵ_2 for $SnSe_2$ at A, 290^0K, and B, 77^0K.

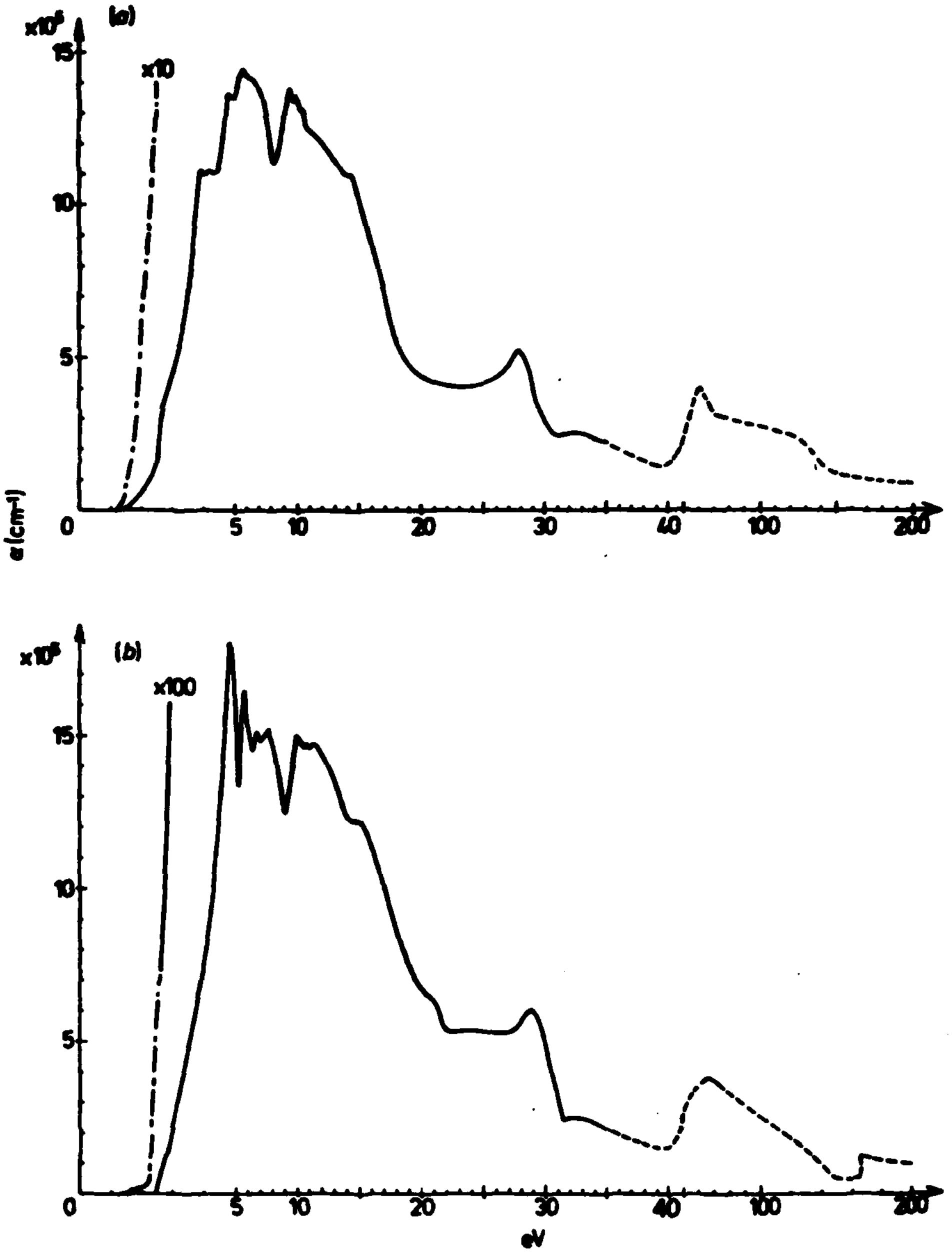

Figure 10. Absorption coefficient of (a) $SnSe_2$ and (b) SnS_2.

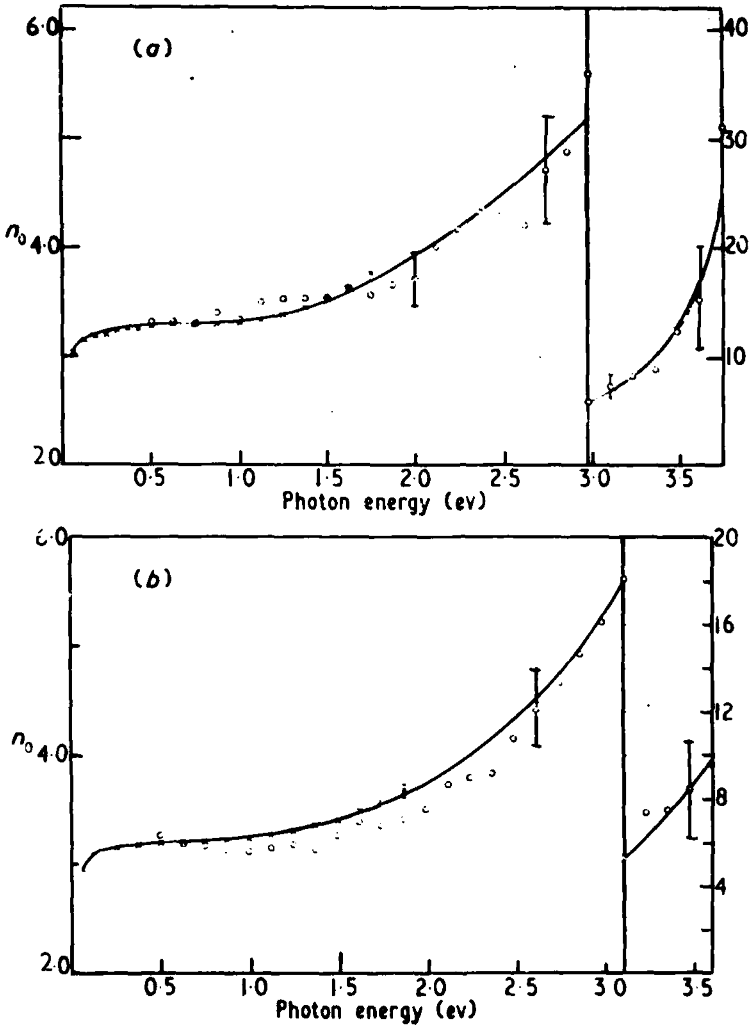

Figure 11. Spectral variation of the ordinary refractive index n_0 of $SnSe_2$ at (a) 290^0K, (b) 77^0K. (x) determined from interference spectra and (o) thick crystal reflectivity R_0.

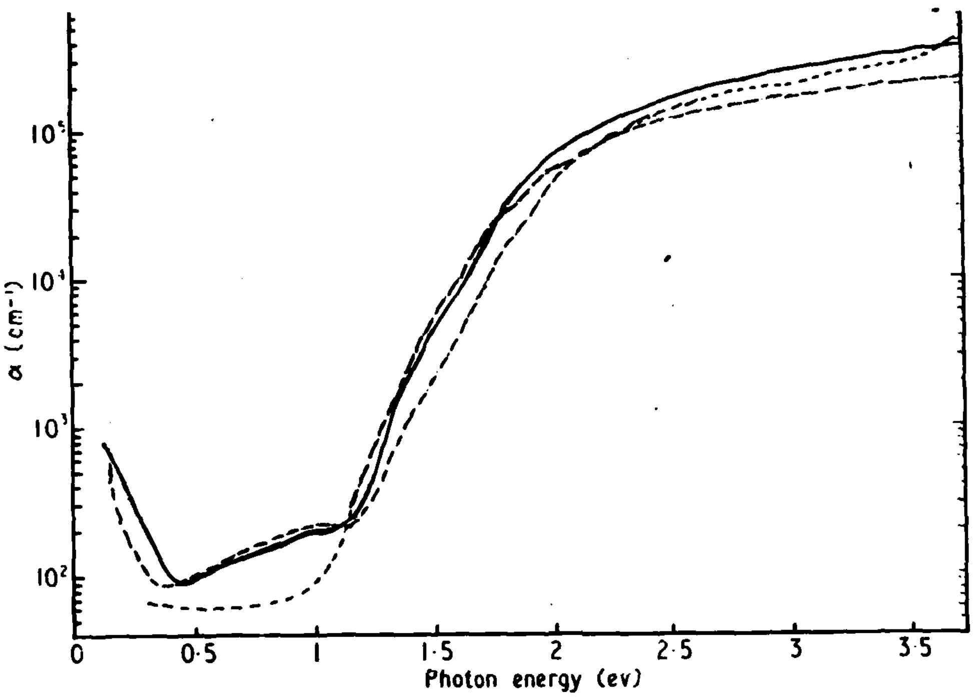

Figure 12. Spectral variation of the ordinary absorption coefficient α of $SnSe_2$ at 290°K (full line) and 77°K (chain line). Also shown are the measurements of Domingo et al. (1966) (broken line) and Lee and Said (1968) (dotted line).

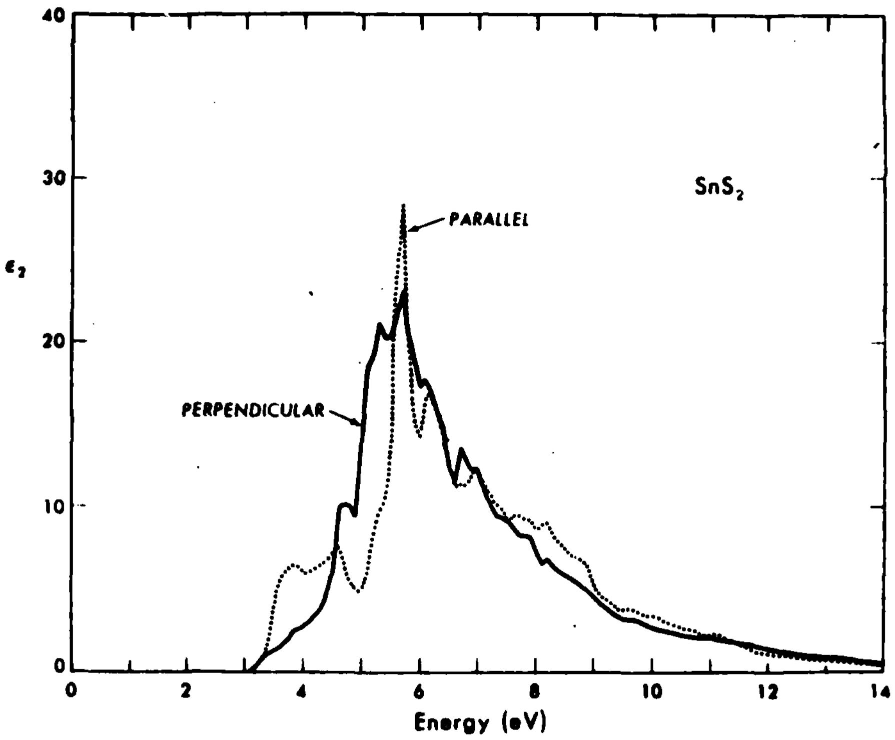

Figure 13. Calculated $\varepsilon_2(\omega)$ for SnS_2.

REFERENCES SnS_2 (CONT.)

4. B.L. Evans and R.A. Hazelwood, Brit. J. Appl. Phys. (J. Phys. D), Ser. 2, 2, 1507 (1969).
5. G. Said and P.A. Lee, Phys. Stat. Sol. (9), 15, 99 (1973).
6. P.A. Lee and G. Said, Brit. J. Appl. Phys. (J. Phys. D), ser. 2, 1, 837 (1968).
7. G. Domingo, et.al., Phys. Rev., 143, 536 (1966).
8. G. Busch, et.al., Helv. Phys. Acta., 34, 359 (1961).
9. Y. Bertrand, et.al., J. Phys. C. 10, 4155 (1977).
10. C. Fang and M. Cohen, Phys. Rev. B5, 3095 (1972).
11. Y. Bertrand, et.al., J. Phys. C., 12, 2907 (1979).

SnS_xSe_{2-x}
Tin-Sulfur-Selenium Solid Solution

SnS_xSe_{2-x} is a solid solution with a layered structure for $0 < x < 2$. This class of compounds consists of sheet molecules which are joined by a weak Van der Waals bond. SnS_xSe_{2-x} crystals are grown using the chemical vapor transport technique with iodine as the transporting agent.[1,2] Single crystals with surface areas up to $5 cm^2$ and uniform thickness up to 100µm can be readily grown.

For the study of the thermal changes in the optical properties of SnS_xSe_{2-x}, a low temperature (liquid nitrogen) cryostat was developed, as shown in Figure 1.[3] The index of refraction is determined using interference fringe maxima. For SnS_2, at 300°K the index of refraction is 2.70 and $\Delta n/\Delta T \times 10^6\ ({}^oK^{-1}) = 40$ (the change of index with temperature). For SnSSe we have $n = 2.91$ and $\Delta n/\Delta T \times 10^6\ ({}^oK^{-1}) = 120$; for $SnSe_2$, $n = 3.16$ and $\Delta n/\Delta T \times 10^6\ ({}^oK^{-1}) = 160$. These cases correspond to $x = 0$, 1 and 2. Figure 2 shows the dispersion curves for each compound. These dispersion curves satisfy the relation:

$$\frac{n_\infty^2 - 1}{n^2 - 1} = 1 - \frac{\lambda_o^2}{\lambda^2} ,$$

where n_∞ is the index at large wavelengths. Figure 3 shows the temperature coefficient of the refractive index as a function of wavelength.

For the absorption coefficient ,α, this can be calculated from the relation (for indirect transitions):

$$\alpha = \frac{(h\nu - E_g \pm E_p)^m}{h\nu} ,$$

where E_g is the energy gap and E_p the phonon energy. Here m is an index which takes on various values depending on whether the transitions are allowed or forbidden. Often $m = 2$. α is plotted for various temperatures versus photon energy in Figure 4. We see that the change in α with temperature is fairly significant.

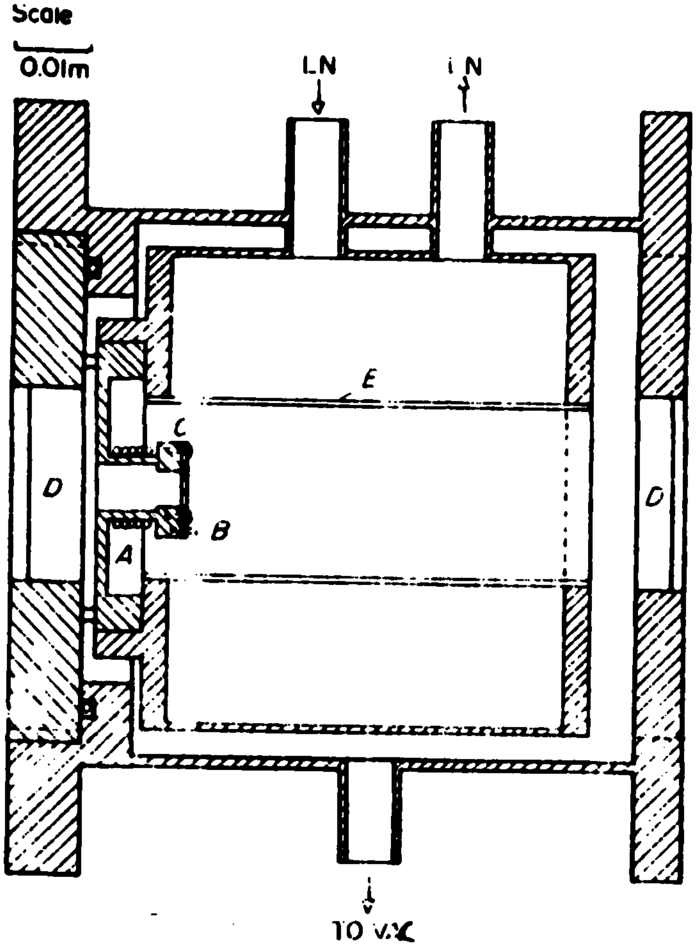

Figure 1 - Cross-section diagram of the optical cryostat.

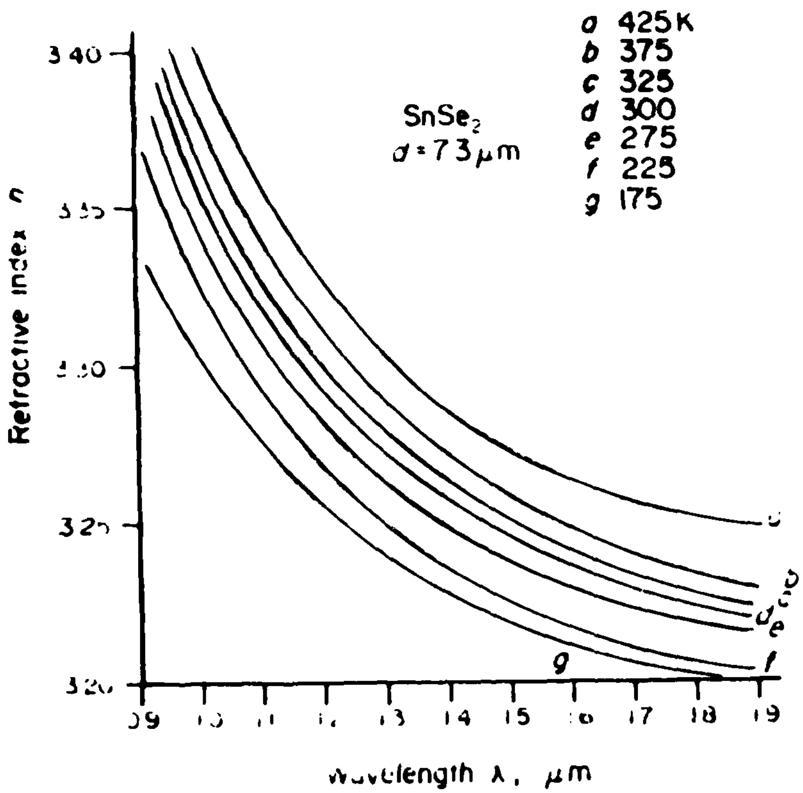

Figure 2(a) Dispersion Curve for the Compound SnSe$_2$.

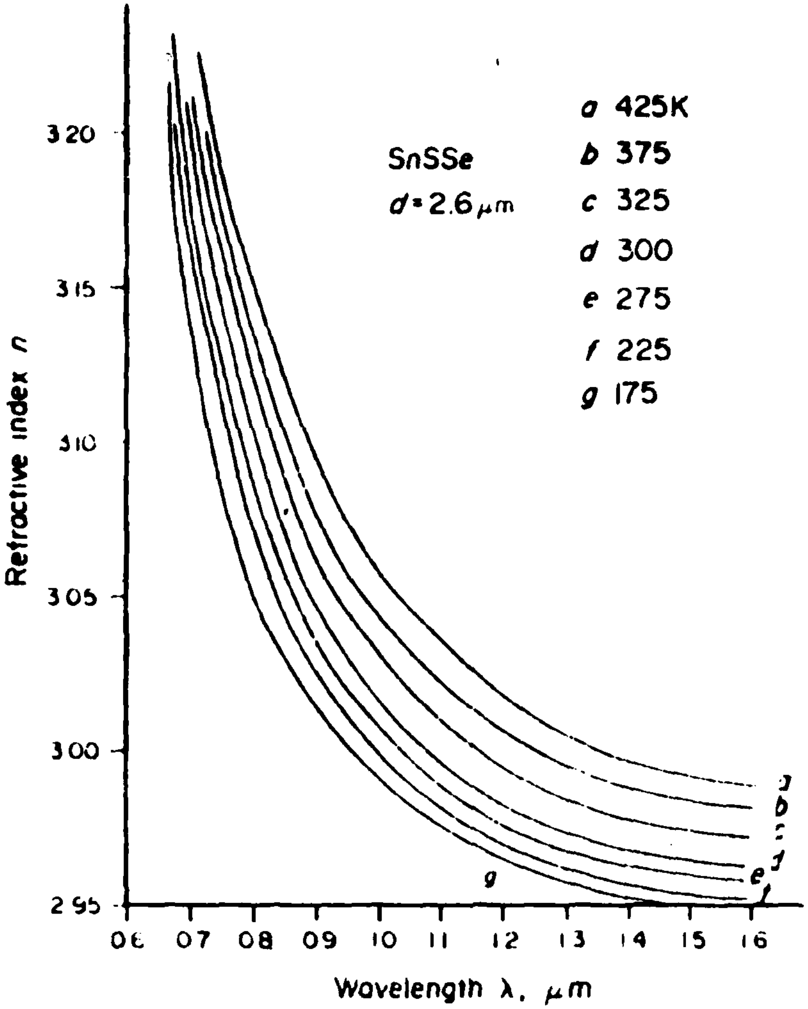

Figure 2(b) - Dispersion Curve for the Compound SnSSe

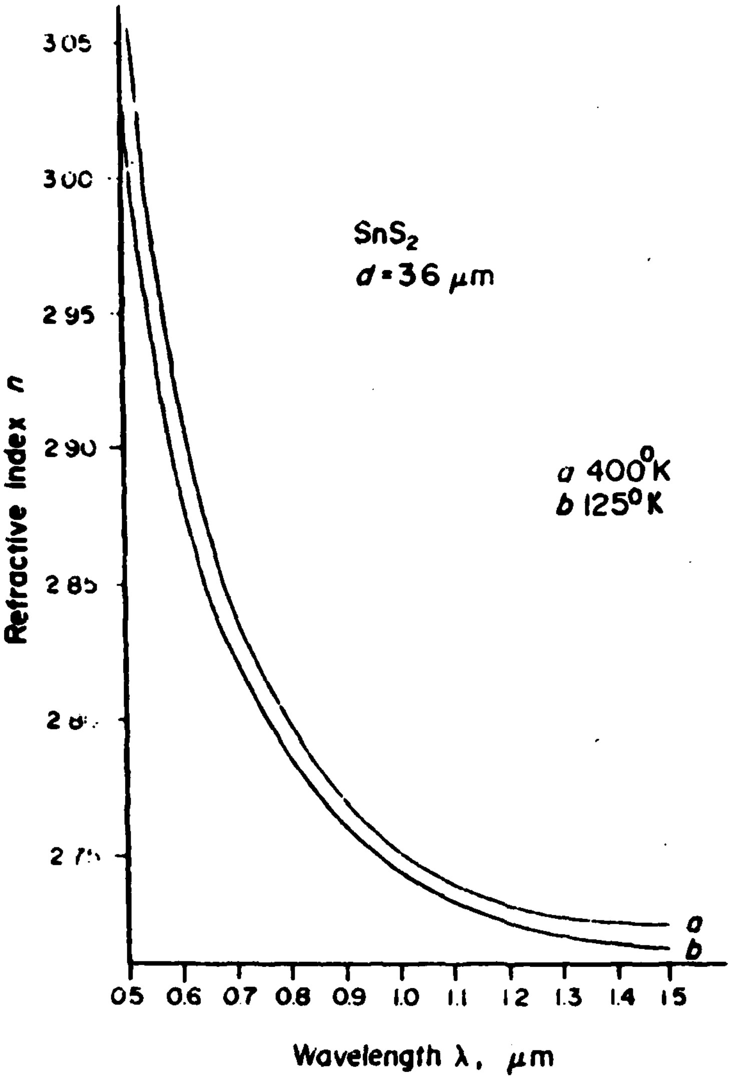

Figure 2(c) - Dispersion Curve for the Compound SnS$_2$.

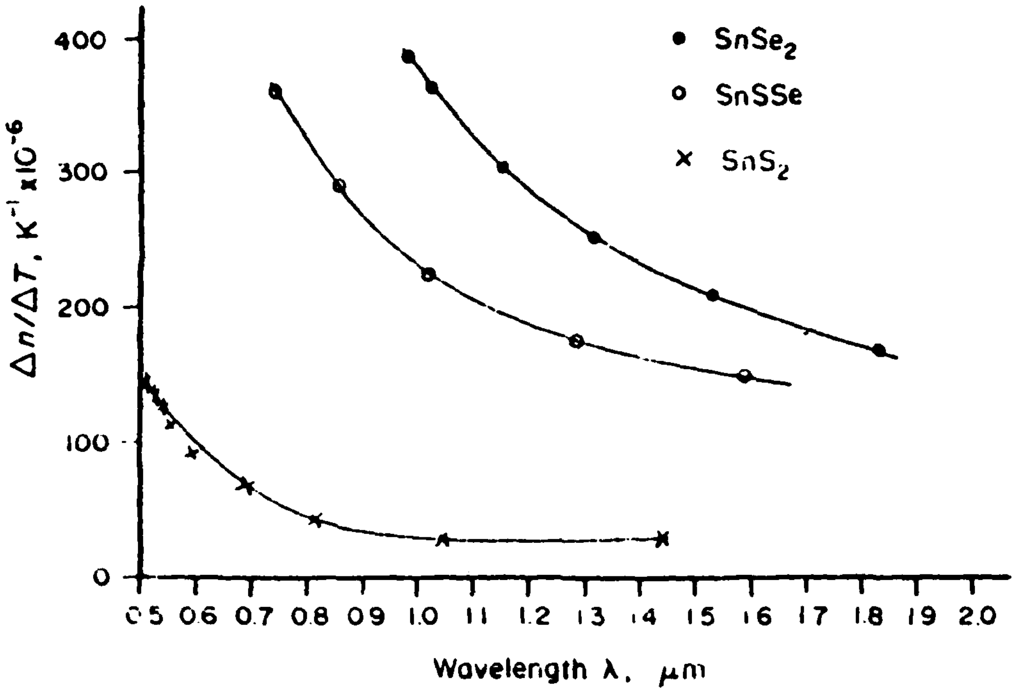

Figure 3 - The temperature coefficient of the refractive index as a function of the wavelength for SnS_xSe_{2-x} (x = 0,1,2).

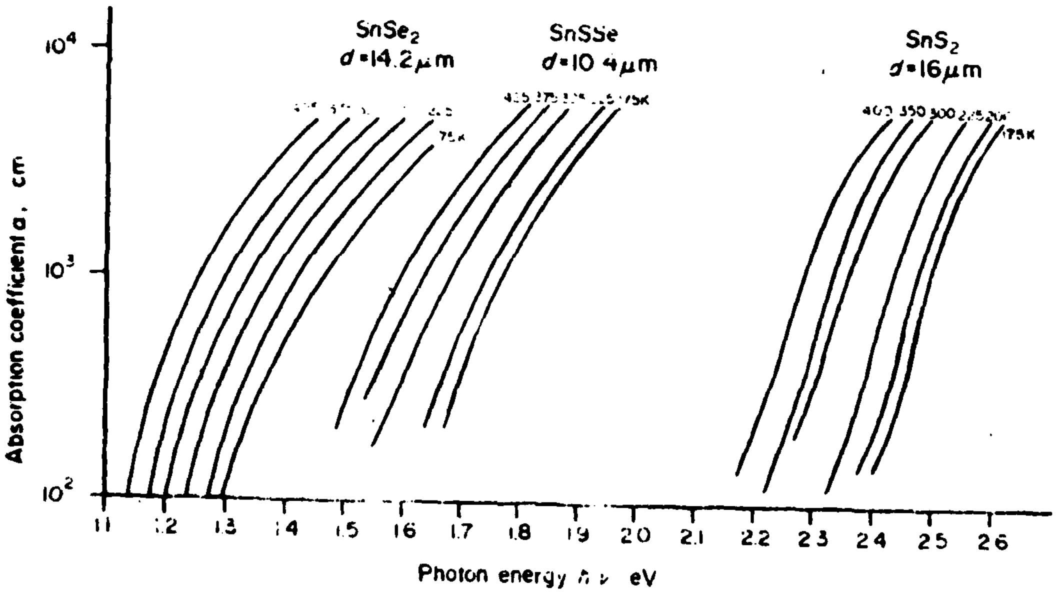

Figure 4 - The absorption coefficient for SnS_xS_{2-x} (x = 0,1,2) as a function of photon energy and temperature.

There is no evidence of a phase transition in SnS_xSe_{2-x}, but it possesses the nice feature that the optical constants can be adjusted by the choice of x, and they do vary with temperature. This may be useful for the design of graded index (inhomogeneous) films. Further study will be required to realize the true potential of this class of compounds.

REFERENCES (SnS_xSe_{2-x})

1. H. Schafer, Chemistry Transport Reactions, Academic Press, New York (1964).
2. P.A. Lee, et.al., J. Phys. Chem. Solids, 30, 2719 (1969).
3. P.A. Lee and G. Said, J. Phys. Chem. Solids, 38, 1317 (1977).

TaS_2
Tantalum Disulfide

Tantalum disulfide comes in four polytypes: 1T-TaS_2, 2H-TaS_2, 3R-TaS_2, and 6R-TaS_2.[1] The polytype 4H-TaS_2 is also known[2], though it behaves as if it is a mixture of 1T-TaS_2 and 2H-TaS_2.[3] 1T-TaS_2 has the same structure as that of TiS_2 where each Ta atom is surrounded by six sulfur atoms in an octahedral coordination.[4,5] The atomic arrangement in 1T-TaS_2 can be described as |AbC|AbC|, where the upper case letters denote the sulfur sites in a hexagonal close packing while the lower-case letters represent the Ta sites. 1T-TaS_2 is prepared by reacting the elements at 1000°C followed by quenching to room temperature. 2H-TaS_2 is a black metallic phase which can be obtained by annealing 1T-TaS_2 at 500°C for several days. It is isostructural with 2H-NbS_2. The ordering of the atoms in 3R-TaS_2 is described as |AbA|BcB|CaC| while in 6R-TaS_2 it is |AbA|BcA|BcB|CaB|CaC|AbC|, using the b nomenclature described above. In 6R-TaS_2, Ta atoms have both octahedral and trigonal prismatic coordinations. These polytypes are stable between 500°C and 800°C and the phase transformations between them have not been studied in detail. Except for 1T-TaS_2, all the polytypes of TaS_2 form non-stoichiometric $Ta_{1+x}S_2$. For 2H-TaS_2 the superconducting transition temperature seems to increase to about 3°K in $Ta_{1.03}S_2$.[6]

1T-TaS_2 is a diamagnetic semiconductor at room temperature. There exists a marked variation in the electrical resistivity with temperature as seen in Figure 1. This plot indicates the presence of two phase transitions (note the hysteresis effects) at 190°K and at 348°K.[4] The high temperature transition is accompanied by a change from semiconducting to metallic behavior while at the low temperature phase transition the resistivity increases by an order of magnitude. 1T-TaS_2 is expected to be metallic because of the presence of the excess d-electrons in the conduction band.[3] It is possible that there is strong metal-metal interactions which causes the t_{2g} band to split into a filled and empty band. Other mechanisms have been put forward in Reference 7. The phase transitions in 1T-TaS_2 are also very sensitive to pressure.[8] The crystal structure for both 1T-TaS_2 and 2H-TaS_2 are shown in Figure 2. Table 1 gives some electrical data for 1T-TaS_2.

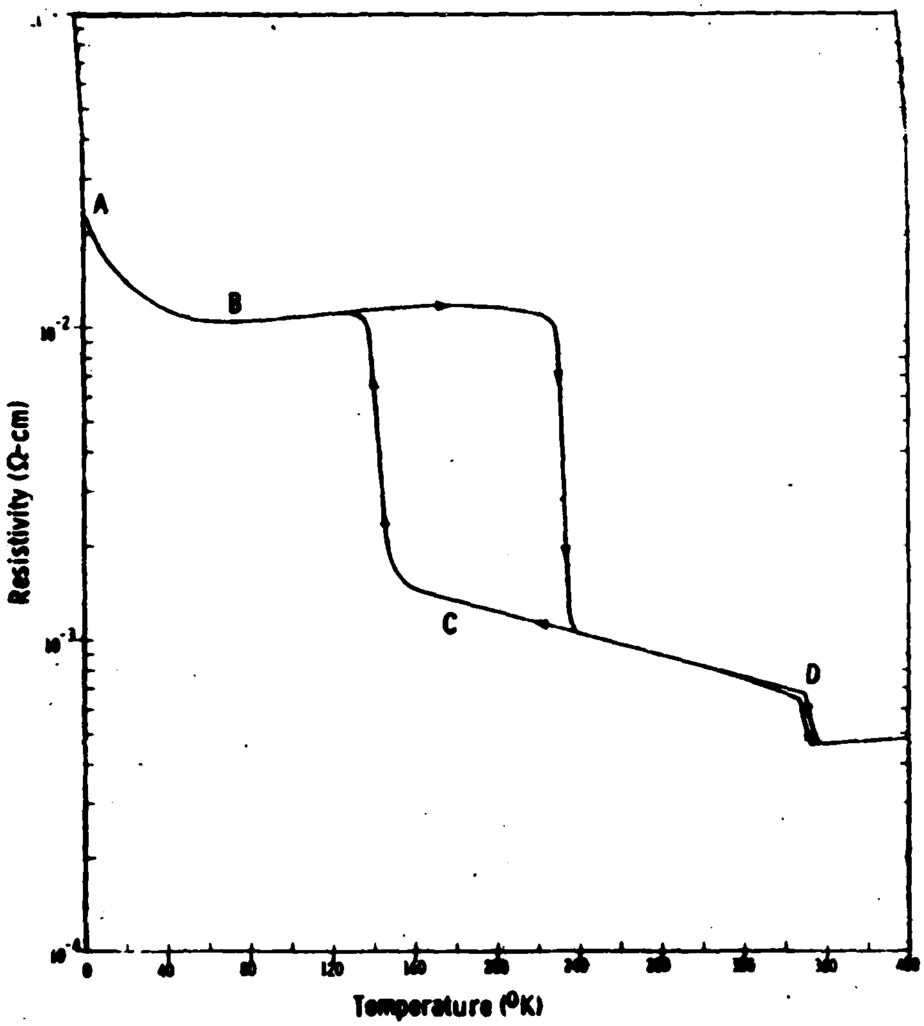

Figure 1. The logarithm of the resistivity of 1T TaS_2 versus the temperature.

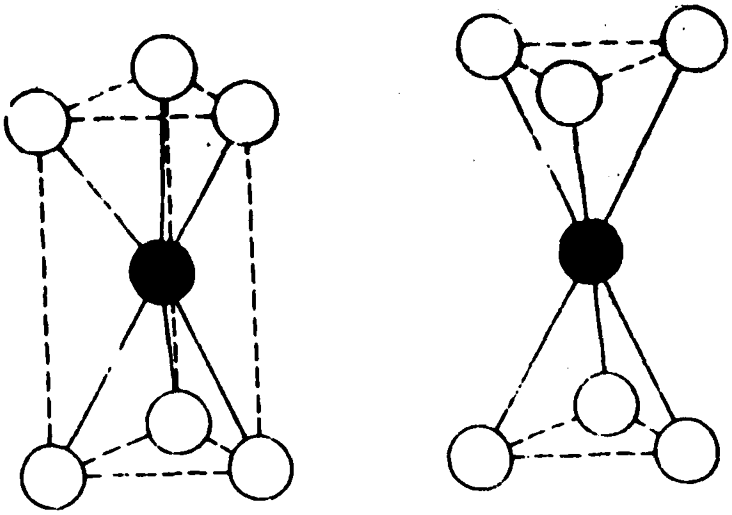

2-H TaS_2

Trigonal Prism

a = 3.315 Å

c = 6.04 Å

$\frac{c}{a}$ = 1.825 (Ideal 1.816)

1-H TaS_2

Octahedron

a = 3.36 Å

c = 5.90 Å

$\frac{c}{a}$ = 1.755 (Ideal 1.633)

Figure 2. A comparison of the crystal structure of the 1T and 2H polytypes of TaS_2.

Electrical and magnetic properties of 2H-TaS_2 show evidence of a phase transition at 70°K due to a small crystallographic distortion.[9] At 70°K the Hall coefficient changes sign from a positive to a negative value accompanied by a change in the slope of the resistivity curve. This may be due to charge density waves and periodic structure distortions.[10]

TABLE 1

Comparison of the Hall and Density Measurements

	293°K	373°K
Resistivity (Ω-cm)	1.5×10^{-3}	6.5×10^{-4}
Hall Electron Density (cm^{-3})	5.8×10^{22}	1.1×10^{23}
Electron Density (1 elec/Ta atom)	1.7×10^{22} (cm^{-3})	

Figure 3 shows how the resistivity varies with temperature for 2H-TaS_2. Figure 4 shows the effect of pressure on the resistivity of 1T-TaS_2 and 2H-TaS_2. Figure 5 shows the behavior of the magnetic susceptibility with temperature for two polytypes.

Not much is known concerning the optical properties for any of the TaS_2 polytypes - little is also known about how changes may occur at the various phase transitions discussed above. Figure 6 shows how 1T-TaS_2 behaves throughout most of the infrared at room temperature. Figure 7 shows the variation in transmittance at two temperatures.[11]

REFERENCES (TaS_2)

1. F. Jellinek, J. Less Common Metals, 4, 9 (1962).
2. R. Huisman and F. Jellinek, J. Less Common Metals, 17, 111 (1969).
3. C.N.R. Rao and K.P.R. Pisharody, Prog. in Solid State Chem., 10, 207 (1975).
4. A. Thompson, et.al., Solid State Commun. 9, 981 (1971).
5. L. Conroy and K. Pisharody, J. Solid State Chem. 4, 345 (1972).
6. K. Pisharody, Unpublished results, discussed in Reference 3.

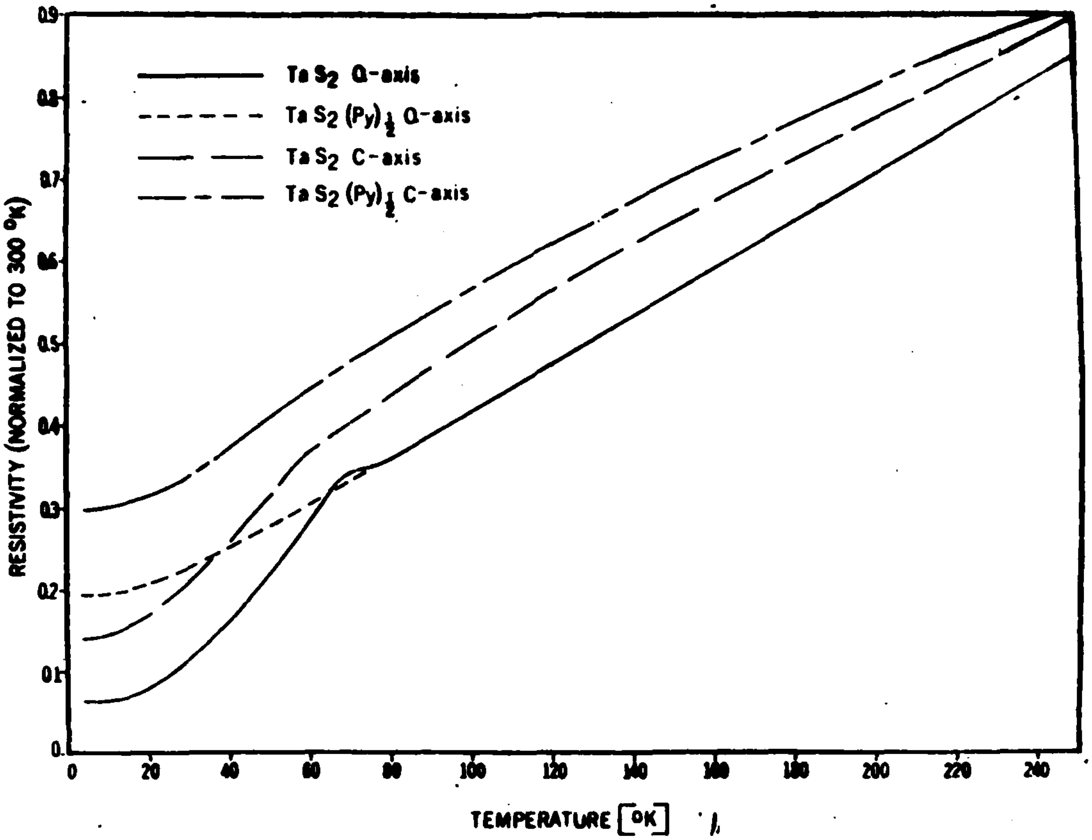

Figure 3. Resistivity vs. temperature for 2H-TaS_2 and $TaS_2(py)_{\frac{1}{2}}$. The curves are normalized to the room temperature values of the resistivity.

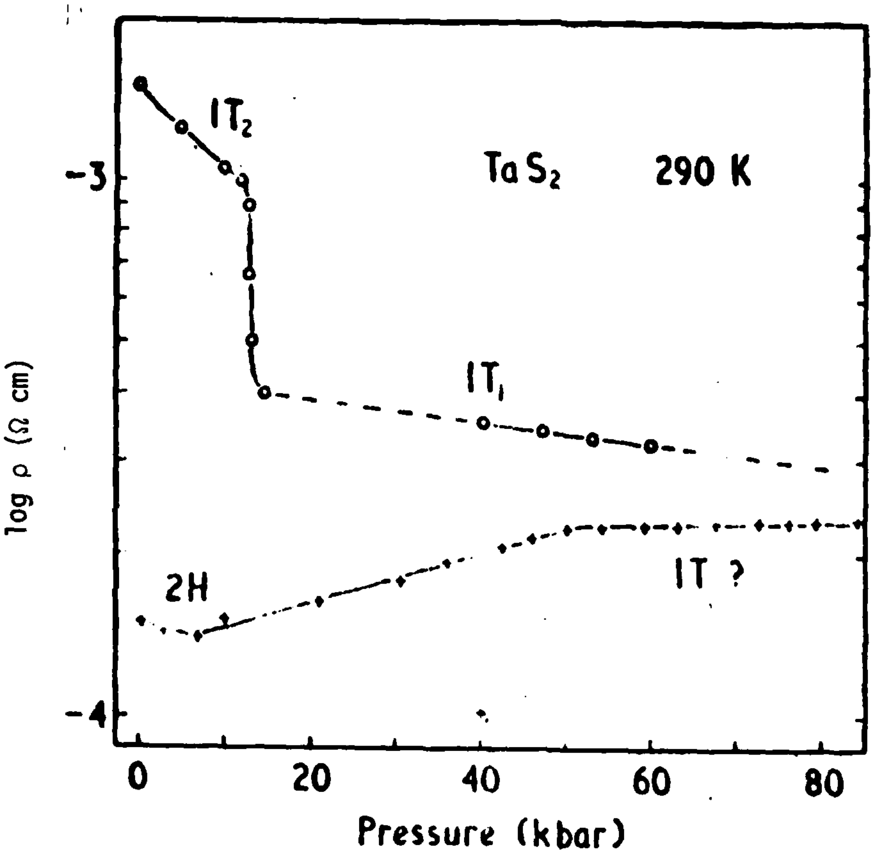

Figure 4. Effect of pressure on the resistivity of 2H and $1T_2$ TaS_2.

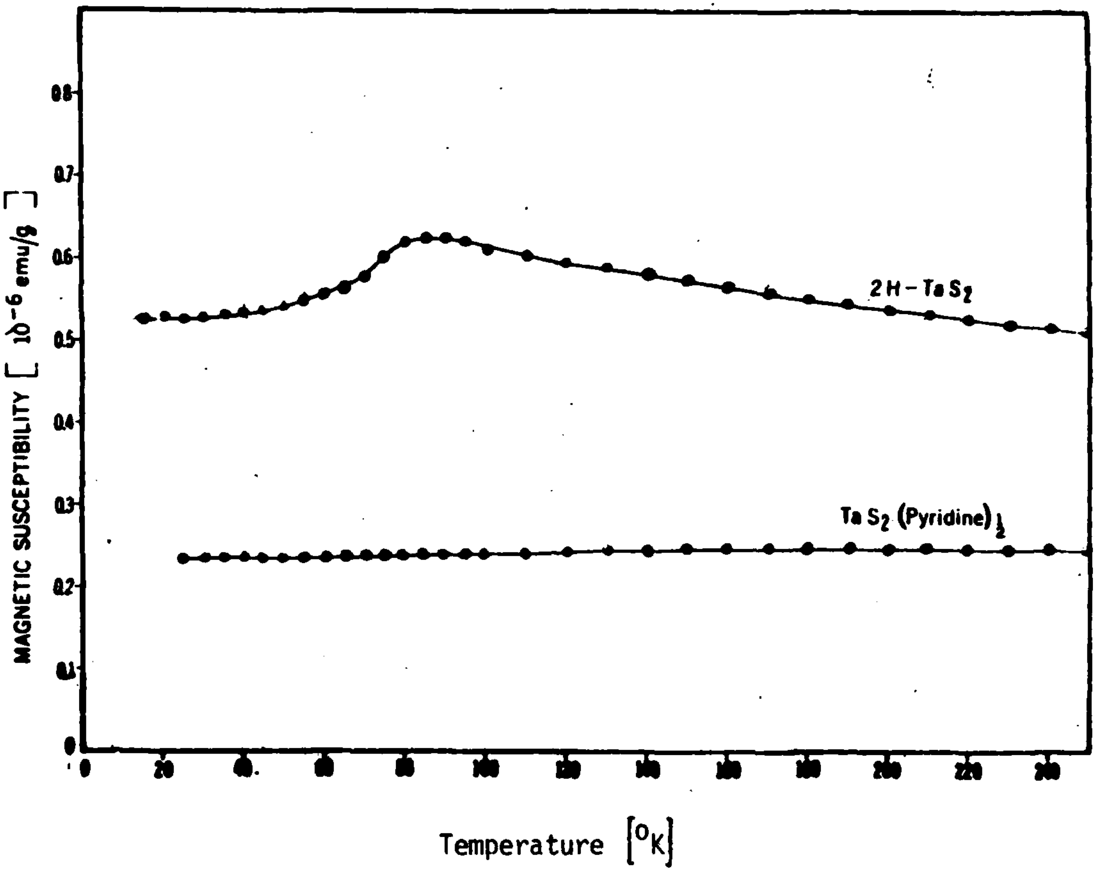

Figure 5. Magnetic susceptibility vs. temperature for 2H-TaS$_2$ and TaS$_2$(py)$_{\frac{1}{2}}$. No correction has been made for the diamagnetism of the cores or of the py molecule.

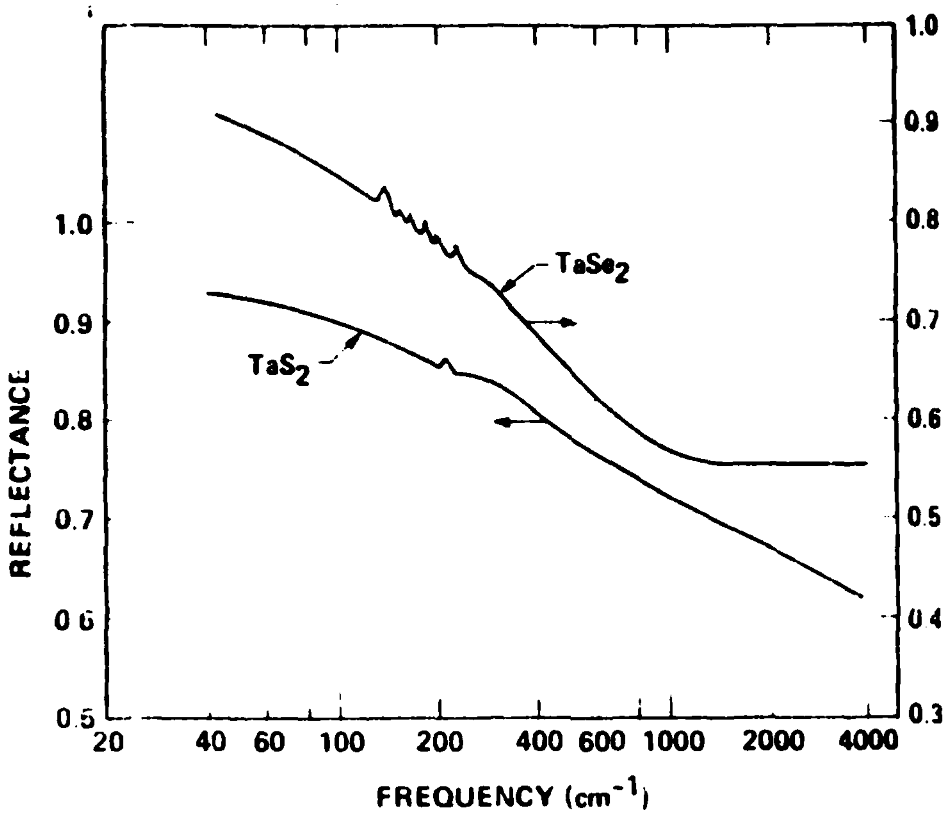

Figure 6. Room-temperature reflectance spectra for TaS$_2$ and TaSe$_2$.

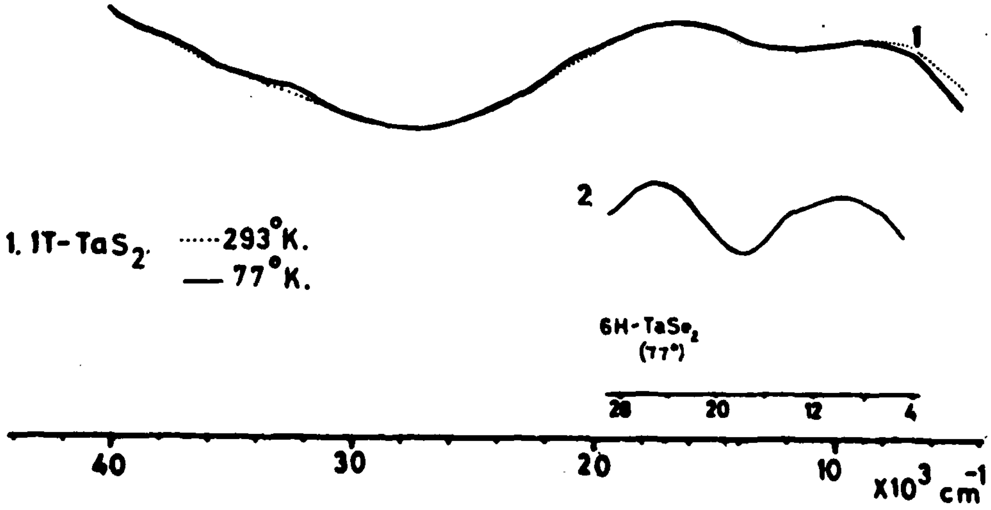

Figure 7. Variation of transmittance of TaS$_2$ at two temperatures.

REFERENCES TaS_2 (CONT.)

7. W. Geertoma, et.al., Solid State Commun. 10, 75 (1972).

8. C. Chu, S. Huang, and P. Hamburger, Phys. Lett., 36, 93 (1971).

9. A. Thompson, et.al., Phys. Rev. B5, 2811 (1972).

10. J.A. Wilson, et.al., Phys. Rev. Lett., 32, 882 (1974).

11. J. Wilson and A. Yoffe, Adv. Phys., 18, 193 (1969).

TaS_3
Tantalum Trisulfide

TaS_3 or tantalum trisulfide is a transition metal trichalcogenide. A general feature of its structure is that it consists of a linear stacking of trigonal prisms of chalcogen atoms parallel to the chain axis with the transition metal atom located at about the center of the prism.[1] TaS_3 possesses an orthorombic structure.[2] Samples of TaS_3 can be prepared by direct reaction of S and Ta in stoichiometric proportions under high temperature (about 650°C) in a quartz tube under a vacuum. TaS_3 also exists in a different polytype with a monoclinic structure.[3] This phase is isotopic to $NbSe_3$. Under preparation, both phases (the orthorombic and monoclinic) are formed in the form of films and small hexagonal plates. The orthorombic structure of TaS_3 has not yet been determined.[4] It is known that the unit cell is huge and is formed from 24 chains. Table 1 gives the lattice parameters and symmetry for the two crystal classes. Figure 1 shows schematically how the crystal structure behaves for many transition metal trichalcogenides.[5] The spacing of metal atoms along the b-axis is much shorter than the inter-prism distances; this is analogous to a bundle of metallic chains each with an insulating sheath. The interaction between chains is weak and, therefore, one-dimensional behavior is expected from the structure.

TABLE 1
LATTICE PARAMETERS OF TAS_3

TaS_3 (Orthorombic)[2]	TaS_3 (Monoclinic)[3]
a = 36.804 Å	a = 9.515 (2) Å
b = 15.173 Å	b = 3.3412 (4) Å
c = 3.340 Å	c = 14.912 (2) Å
V = 1865.15 Å^3	β = 109.99° (2)
Z = 24	V = 445.5 Å
space group C 222_1	Z = 6
	space group $P2_1/m$

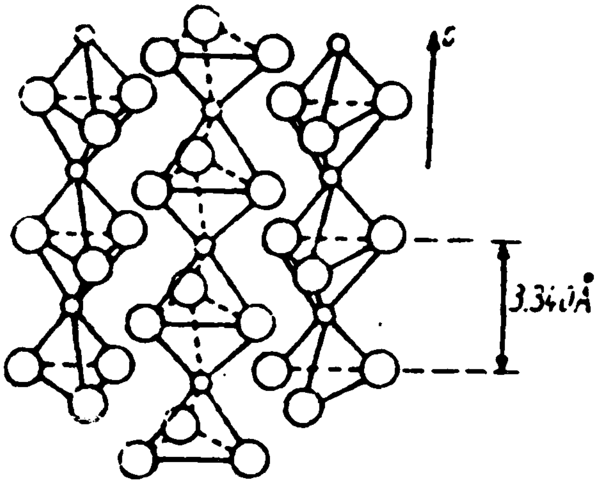

Figure 1. Schematic representation of the structural features of a number of transition metal trichalcogenides.

For orthorombic TaS_3 the resistivity increases slowly down to around 230°K beyond which it starts to increase sharply. Figures 2 and 3 show the resistivity behavior for both TaS_3 classes.[4] At about 210°K there is sharp change in the electrical resistivity - this is believed to be due to a phenomena known as the Peierls transition.[6] Beyond 350°K a metallic variation of the resistance is observed whereby the resistance increases with increasing temperature. For the monoclinic class of TaS_3 there is a minimum in the resistivity around 270°K, then a sharp increase down to about 220°K. It is believed that for this crystal class that there exist two phase transitions: one at 240°K and one at 160°K. Further substantiating evidence of these phase transitions can be made using electron diffraction measurements.[4] It is possible that the two crystal classes may become somewhat mixed during the preparation phase, and that this could lead to anomalies in the measurement and subsequent interpretation of the resistivity curves. The resistivity was measured using the conventional four-probe technique. No temperature hysteresis effects have been observed.[6] For the orthorombic structure of TaS_3, the temperature dependence of the resistivity can be described in the form of

$$\exp(E/2kT) ,$$

with $E = 0.15eV$ in the limited range of 120°K to 200°K. At the lower temperature the resistivity tends to approach a constant value about 10^6 times larger than the room temperature value.

A decrease in the magnetic susceptibility below 300°K has been observed; this can be explained in terms of a substantial vanishing of the Fermi surface.[2]

The Peierls transition is a phenomena which is believed to be due to "charge density waves" along essentially one dimensional crystal strands. Known also as the "Peierls distortion", it has only been observed in a very limited number of materials, such as the one-dimensional organo-metallic substances like KDP. Such transitions may occur in other trichalcogenides like $TaSe_3$, $ZrSe_3$ and $NbSe_3$.

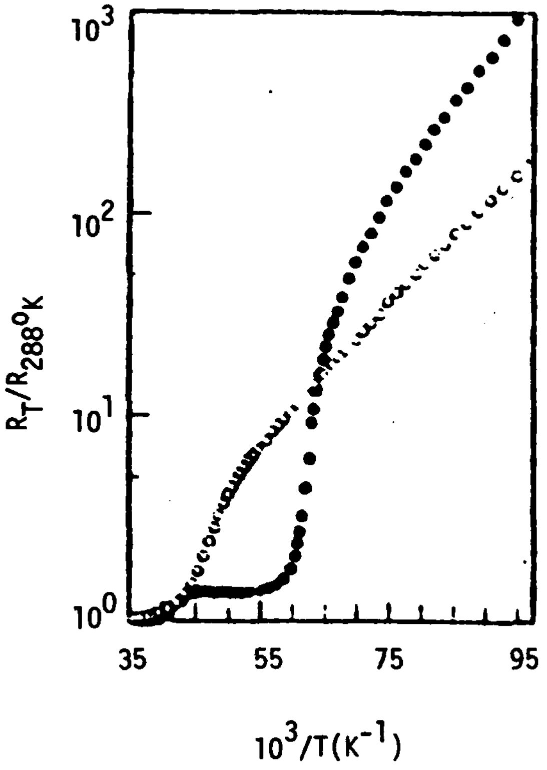

Figure 2. Semilogarithmic plot of the resistance of TaS_3 (normalized to the resistance at 288 K) as a function of $10^3/T$ for the monoclinic and orthorhombic structure. The transition temperatures are defined when d log R/dT is maximum; ● monoclinic and o orthorhombic structure.

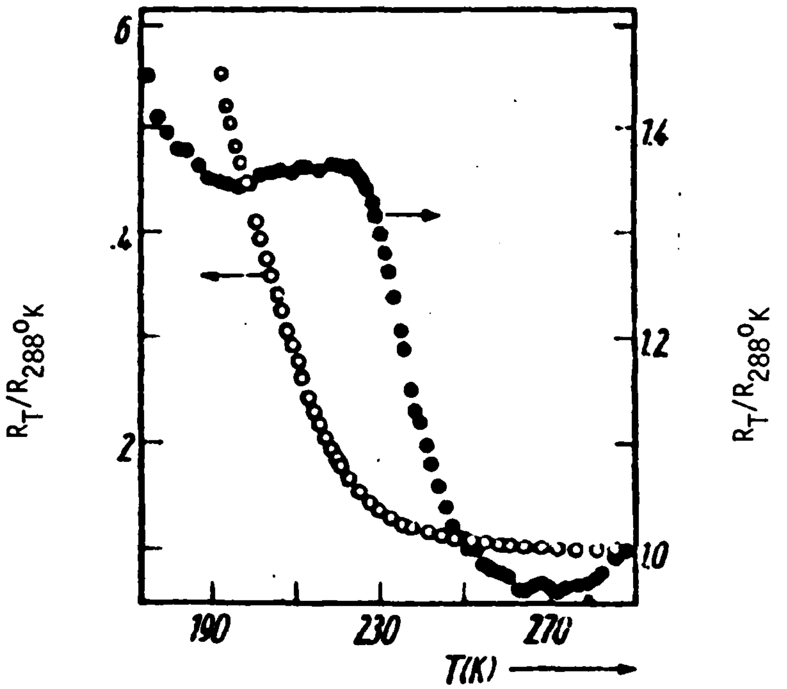

Figure 3. Variation of the resistance of TaS_3 (normalized to the resistance at 288 K) as a function of temperature for the monoclinic (●) and orthorhombic (o) structures.

We have not uncovered any literature on the optical properties of TaS_3, primarily because TaS_3 is of only recent interest. It seems likely that some interesting (perhaps anisotropic) behavior should exist.

REFERENCES (TaS_3)

1. A. Meerschant and J. Rouxel, J. kers-Common Metals, 39 197 (1975).
2. E. Bjerkelund and A. Kjekshus, Z. Anorg. Allg. Chem., 328, 235 (1964).
3. A. Meerschant, et.al., J. Physique, 40, L-157 (1979).
4. C. Roucau, et.al., Phys. Stat. Sol. (a) 62, 483 (1980).
5. G. van Tenbeloo, et.al., Phys. State. Sol. (a) 43, K137 (1977).
6. T. Sombongi, et.al., Solid State Commun., 22, 729 (1977).

TiS_2
Titanium Disulfide

TiS_2 is grown as a single crystal using iodine transport.[1] Its color is golden yellow and its density is 3.28 gm/cm^3. By heating to high temperatures it is possible to obtain the nonstoichiometric compound $Ti_{1+x}S_2$.[2,3] TiS_2 has the hexagonal CdI_2 type structure with a = 3.40Å (Figure 1) and c = 5.698Å. TiS_2 is a Pauli paramagnet and has an optical gap of 0.9eV with a plasma edge below 0.5eV. At 298°K the electrical resistivity is $\rho = 10^{-3}$ ohm-cm, the charge carrier concentration is 10^{21} cm^{-3}.[3,4] There is a controversy concerning the nature of TiS_2: Is it a semi-metal or a semiconductor? Much of the research done on TiS_2 was performed with the intent of arriving at a definitive answer to this question. Quantities that are important to establishing the nature of TiS_2 include the electrical resistivity, Hall coefficient, and the c-axis lattice parameter. The most recent study indicates that TiS_2 is an extrinsic semiconductor.[5]

In Reference 5 the electron concentration is reported to be $2.2 \times 10^{20}/cm^3$ for stoichiometric TiS_2 samples. This level of extrinsic carrier density indicates that TiS_2 is metallic, and the source of these carriers is still unknown. There also is an anomalous temperature dependence for ρ. Below 40°K, ρ varies as T^3 regardless of sample stoichiometry whereas ρ varies as T^2 above 40°K to about 400°K for stoichiometric TiS_2. Otherwise, ρ varies as T^γ from 100°K to 700°K where γ ranges from 1.85 to 22, depending on stoichiometry. No known scattering mechanism amongst carriers can explain this behavior.[5]

The properties of $Ti_{1+x}S_2$ vary strongly with the stoichiometry parameter x. In Table 1, several samples are shown along with the growth conditions, c-axis lattice parameter, and electron concentration. This latter quantity varies from $1.3 \times 10^{20}/cm^3$ to $7.5 \times 10^{20}/cm^3$. These samples will be referred to in several of the diagrams included in this text. Detailed discussion concerning the preparation of each of these samples can be found in reference 5.

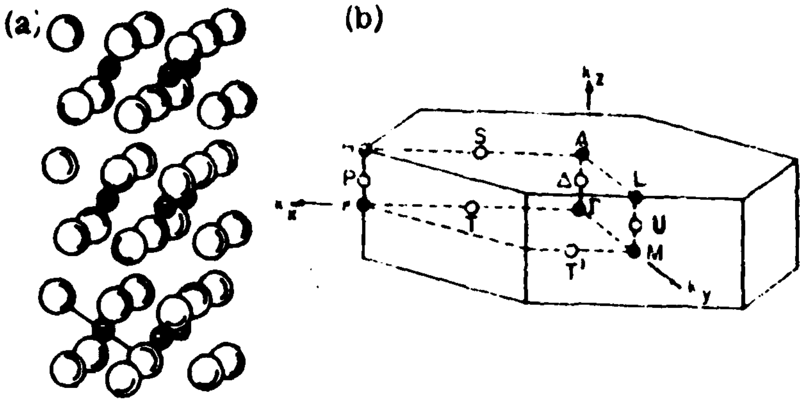

Figure 1. (a) CdI_2 structure. The black circles are the metal atoms and the light circles are the chalcogen atoms. (b) Brillouin zone of the hexagonal Bravais lattice.

In Table 2 we see the values for the measured electrical resistivity for the various samples at three different temperatures. Other data including the Hall coefficient and thermoelectric power are given. In Figure 2 the resistivity as a function of temperature is shown. The resistivity changes

TABLE 1

GROWTH CONDITIONS C-AXIS LATTICE PARAMETER AND CARRIER CONCENTRATION OF $TI_{1+x}S_2$ SINGLE CRYSTALS

Single-crystal batch no.	Growth conditions	c-axis lattice parameter	Electron concencentration[b] (10^{20} cm^{-3})
164	Powder from elements sulfur transport growth temp. = 650°C	5.6982 ± 6 5.6993 ± 13[a]	2.2
9	Powder from elements sulfur transport growth temp. = 600°C	5.6984 ± 6	2.2
6	Powder from elements sulfur transport growth temp. = 700°C	5.6986 ± 8	3.0
3	Commerical powder iodine transfer growth temp. = 700°C	5.7001 ± 9	7.5
7	Powder from elements iodine transfer growth temp. = 700°C	5.6991 ± 7	7.5
8	Commerical powder iodine transfer growth temp. = 800°C	5.7008 ± 6	1.3
1	Commercial powder iodine transport growth temp. = 900°C	5.7043 ± 8	3.4
Exxon		5.6978 ± 6	2.4

a = Measured on powder from crushed single crystal.

b = Calculated from the room temperature Hall coefficient

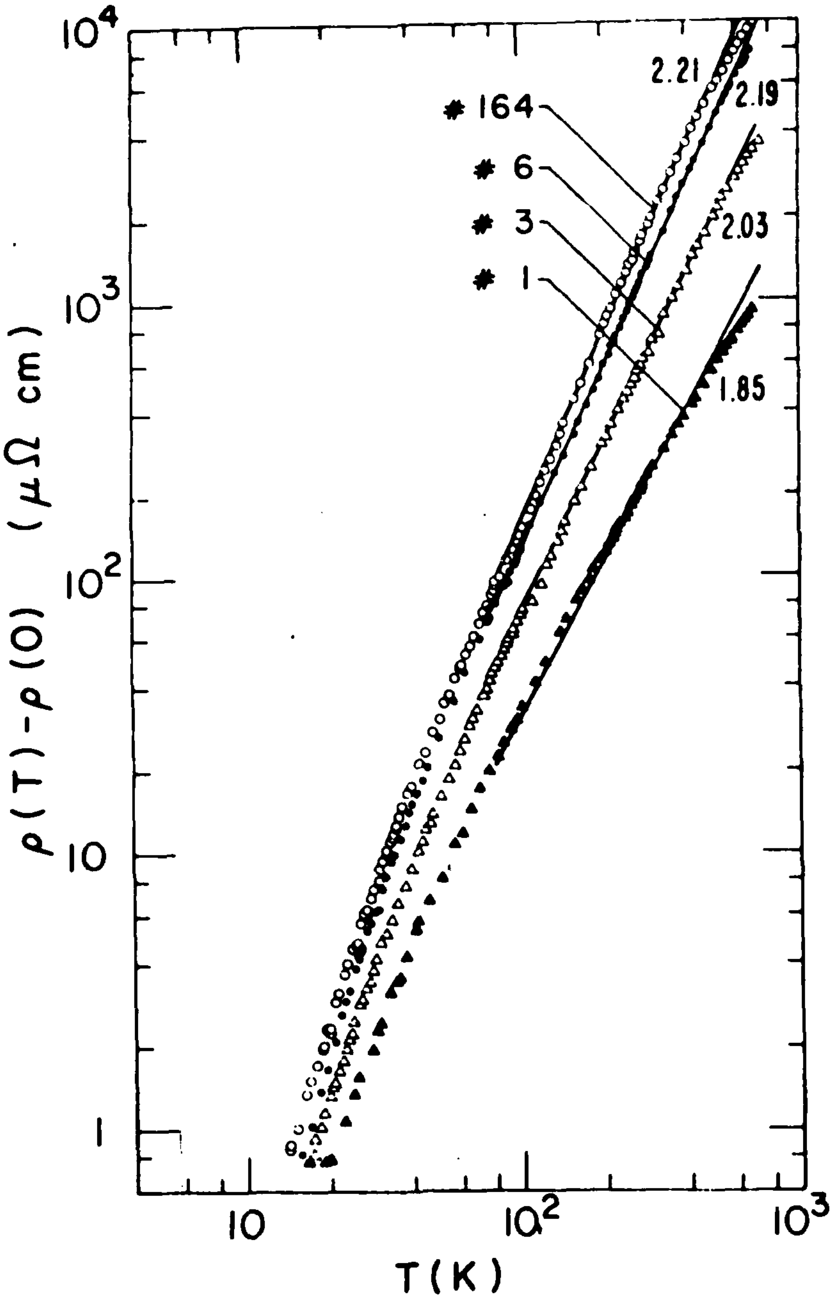

Figure 2. Log-log plot of the temperature-dependent electrical resistivity of four samples of titanium disulfide $Ti_{1+x}S_2$ for varying degrees of nonstoichiometry.

TABLE 2

EXPERIMENTAL RESULTS OF RESISTIVITY, HALL COEFFICIENT AND THERMOELECTRIC POWER OF $Ti_{1+x}S_2$

Single-crystal batch number	Resistivity (μΩcm)			Hall Coeff. ($10^{-2}cm^3/C$) and carrier concentration ($10^{20}cm^{-3}$) (in parenthesis)		Thermoelectric power (μV/K)
	4.2K	77K	300K	77K	300K	300K
164	165	250	2110	2.5 (2.5)	2.9 (2.2)	240
9	102	190	1950	2.5 (2.5)	2.8 (2.2)	
6	99	170	1500	1.9 (3.3)	2.1 (3.0)	203
7	88	131	805	0.71 (8.8)	0.84 (7.4)	
3	93	135	790	0.75 (8.3)	0.83 (7.5)	131
8	99	134	560	0.46 (14.0)	0.49 (13.0)	101
1	133	156	377	0.17 (37.0)	0.19 (34.0)	56
Exxon	166	270	1990	2.4 (2.6)	2.6 (2.4)	245

continuously -- for the range of stoichiometries considered here, there is no evidence of an abrupt change in ρ that may accompany a first order structural phase transition from, say, an insulating to a semiconducting state. Rather, these curves suggest that TiS_2 may have temperature "controlled" optical properties.

The carrier concentration of TiS_2 varies with temperature as approximately:

$$n \approx n_0 - cT,$$

where c is a constant, over the temperature range of 0°K to 80°K. The variation in concentration is illustrated in Figure 3. The variation of ρ and concentration of carriers with stoichiometry and temperature has also been studied in Reference 6. Several publications have appeared which treat the electron structure of TiS_2 and $TiSe_2$, and the reflectivity properties.[7-9]

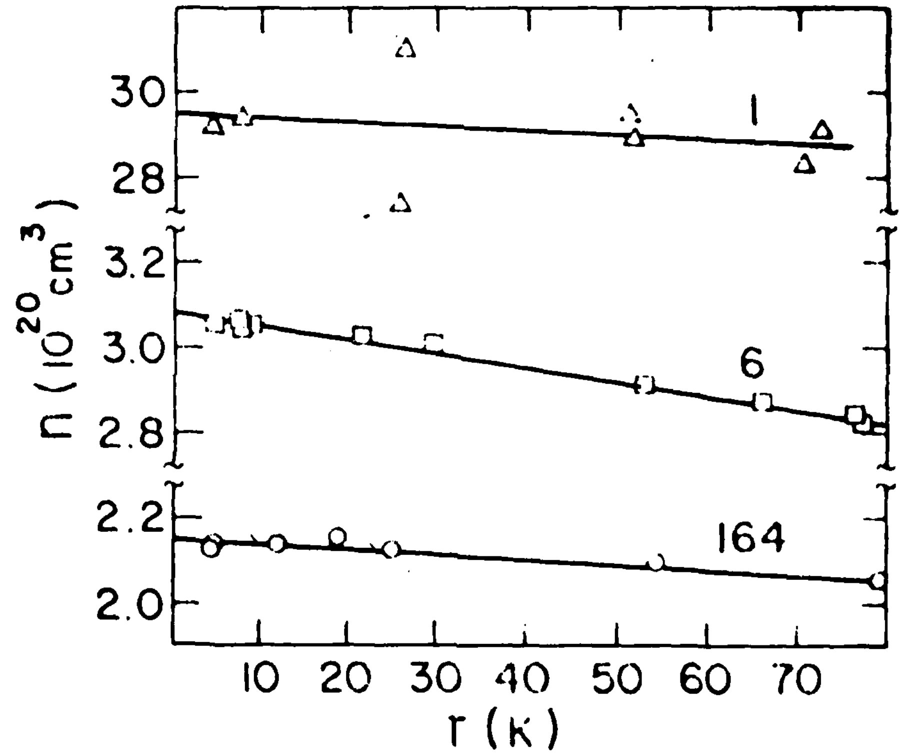

Figure 3. Temperature dependence of the carrier concentration n calculated from the Hall coefficient R_H *in the* range 0-80K for some titanium disulfide samples with varying degrees of nonstoichiometry. n decreases approximately linearly with increasing T.

In Figure 4 a band model of TiS_2 is presented,[10] which reconciles known optical and electrical data. The absorption edge is associated with the transition from the top of the partially filled d band (which in this model overlaps the valence band) to the conduction band.

In Figure 5 the optical absorption spectrum of a typical TiS_2 sample is given in the 0.3eV to 3.5eV energy range, for two temperatures (625°C and 700°C).[10] For the sample measured to give the results of Figure 5, the c-axis was measured to be 5.701Å, corresponding to $x = 1.018$ in $Ti_{1+x}S_2$. As the Ti/S ratio increases, free-carrier absorption tends to play a more important role.

In Figure 6 the infrared reflectivity is presented for the various samples given in Table 1. Here the actual reflectivity values obtained by measurement are compared to the predictions yielded by the simple free-electron Drude theory.[5] For these measurements a Perkin-Elmer IR521 spectrometer was used. These values were measured at room temperature, T = 300°K.

From the curves shown in Figure 6, the first conclusion is that free-carrier absorption is strongly suggested. Each spectrum shows a well-defined plasma edge that shifts to higher frequencies with increasing degree of nonstoichiometry. The data is very well fit with a single-carrier (three parameter) Drude model where the reflectiivty is (at near normal incidence):

$$R = \frac{(n-1)^2 + k^2}{(n+1)^2 + k^2} ,$$

where n is the index of refraction and k is the extinction coefficient. Here we can express n and k in terms of the real and imaginary parts of the complex dielectric function $\hat{\varepsilon} = \varepsilon_1 + i\varepsilon_2$, where:

$$n = \frac{1}{\sqrt{2}} \left[(\varepsilon_1{}^2 + \varepsilon_2{}^2)^{1/2} + \varepsilon_1 \right]^{1/2} ,$$

and

$$k = \frac{1}{\sqrt{2}} \left[(\varepsilon_1{}^2 - \varepsilon_2{}^2)^{1/2} - \varepsilon_1 \right]^{1/2} .$$

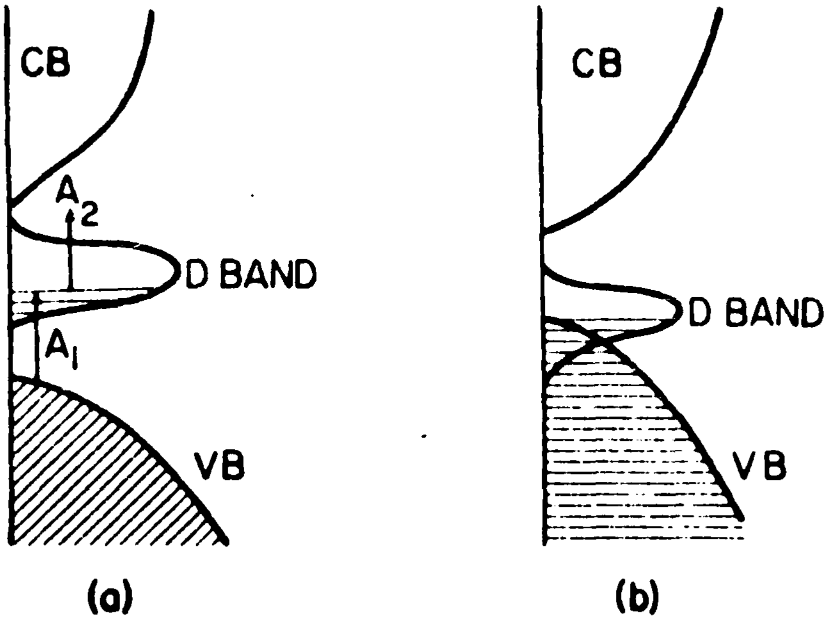

Figure 4. (a) Wilson-Yoffe band model; (b) semimetal band model.

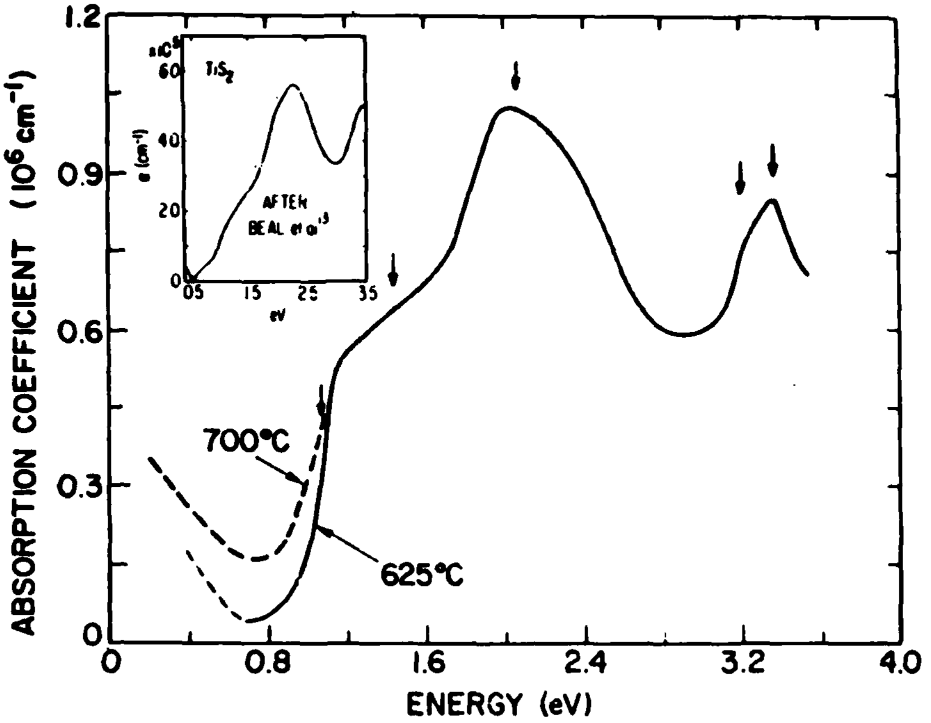

Figure 5. Optical absorption spectrum of a typical H_2S-reacted sample prepared at 625°C, and the band-edge absorption of a 700°C sample. Insert: The 0.5-3.5 eV absorption spectrum of a highly nonstoichiometric sample.

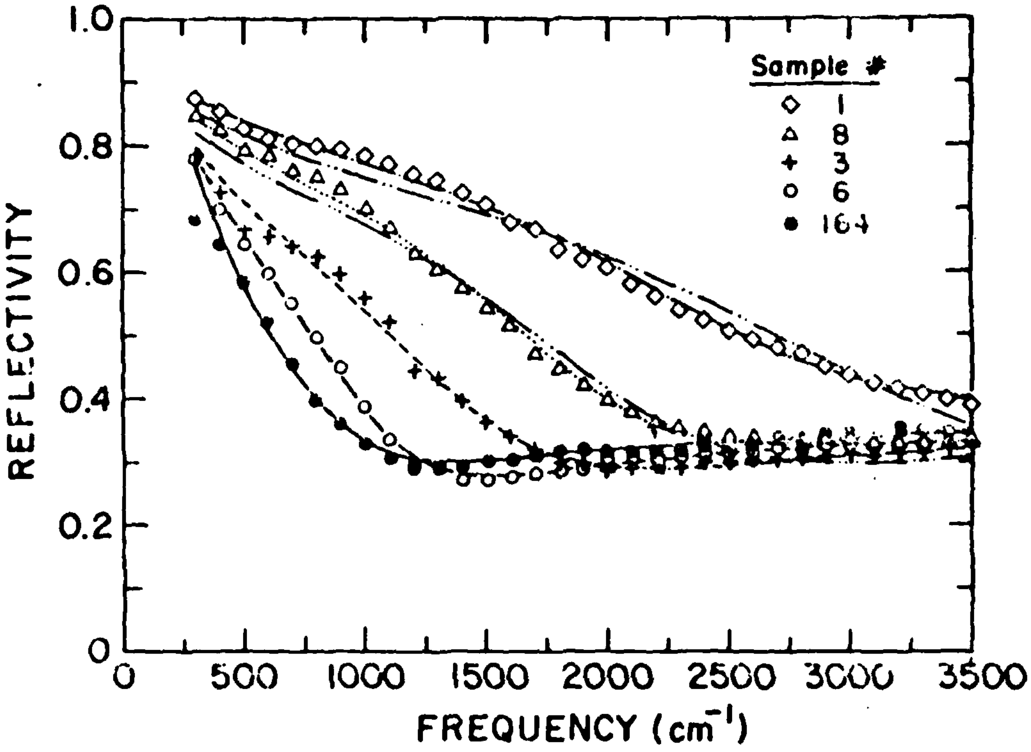

Figure 6. Infrared reflectivity at room temperature of freshly cleaved single crystals of titanium disulfide with various degrees of nonstoichiometry. The plasma edge shifts to higher energy as the crystals become more nonstoichiometric.

According to the Drude model, we can write:

$$\varepsilon_1 = \varepsilon_\infty - \frac{\omega_p^2\ \tau_{opt}^2}{1 + \omega^2\ \tau_{opt}^2} ,$$

$$\varepsilon_2 = \frac{\omega_p^2\ \tau^2_{opt}}{\omega(1+\omega^2\tau^2_{opt})} ,$$

where ω_p is the plasma frequency and:

$$\omega_p = \frac{4\pi\ e^2 n}{m_{opt}} .$$

Here n is the carrier concentration, τ_{opt} the optical relaxation time, m_{opt} the optical (carrier) mass, and ε_∞ the high frequency dielectric constant. We should point out that the Drude model works quite well for free-electron metals, but not for most semiconductors and insulators. Since it works well for TiS_2, it would seem to indicate that TiS_2 is a metal. That other data indicates TiS_2 is not a metal, it is remarkable, indeed, to see that the free-electron (or other carrier) Drude model works so well. The three variable parameters are ε_∞, ω_p, and τ_{opt} -- they will change with the degree of nonstoichiometry of the sample.

In Figure 7 the infrared reflectivity for freshly cleaved samples of titanium disulfide are shown. The reflectivity data in Figures 6 and 7 have been used to model $Ti_{1+x}S_2$ with a two carrier model, each carrier having a different mobility. By ultimately investigating the properties of these carriers and the Hall coefficient, the investigators in Reference 5 have concluded that TiS_2 must be a semiconductor. We should point out that the presence of two types of carriers may refer to electrons in two distinct conduction bands. (We should also, for completeness, mention that the total mobility for a carrier is related to the conductivity by $\sigma = \frac{ne^2\tau}{m} = ne\mu$. In Figure 8 we see a plot of μ vs. the carrier concentration.[5])

There appears to be some uncertainty concerning the possibility of a phase transition in $Ti_{1+x}S_2$. Since TiS_2 appears to possess, experimentally,

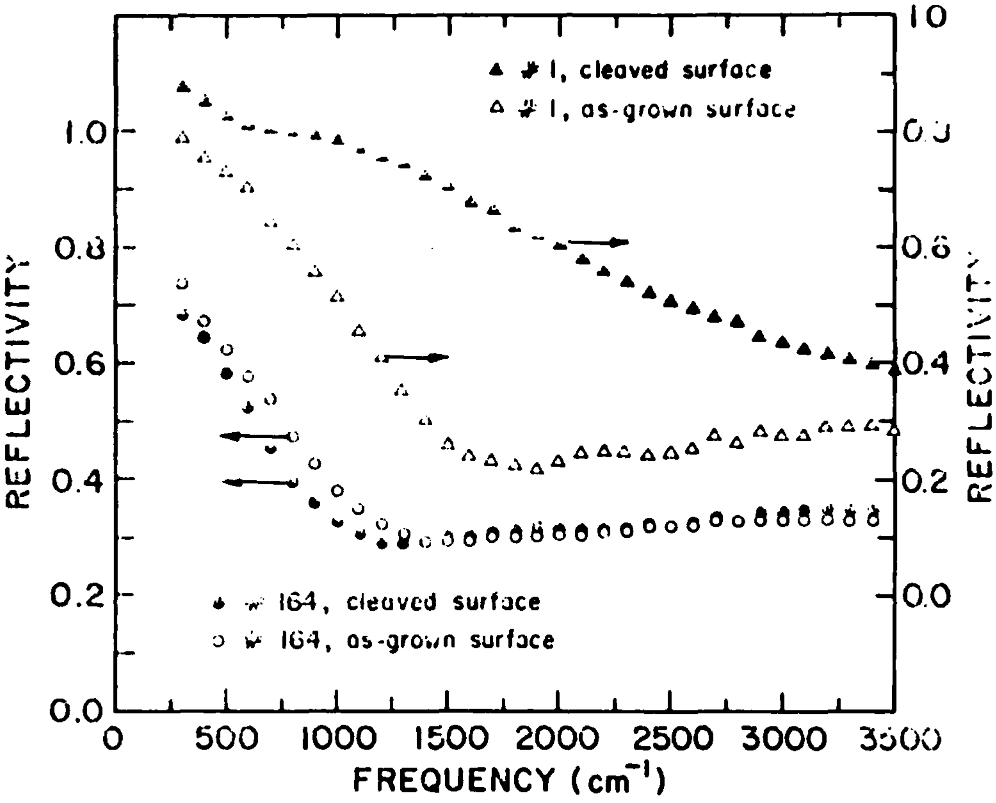

Figure 7. Infrared reflectivity of freshly cleaved and as-grown surfaces of titanium disulfide.

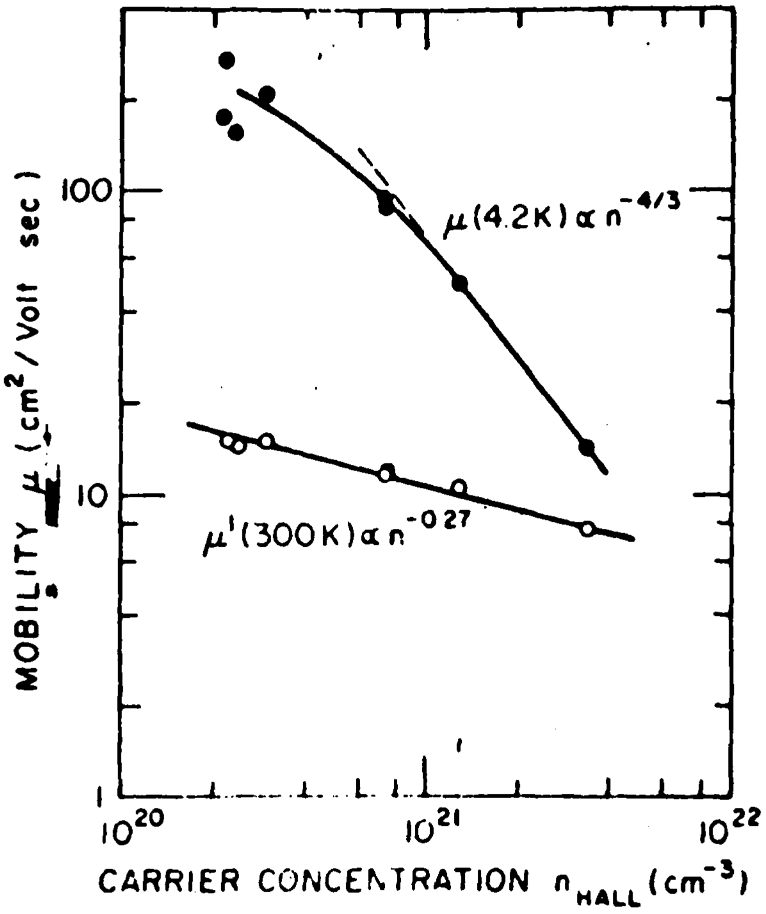

Figure 8. Carrier concentration dependence of the mobility at 4.2 K and the partial mobility $\mu^1(T)$.

properties that are similar to those found in a highly doped semiconductor such as Si or Ge doped with phosphorous, arsenic, or antimony, and they exhibit phase transitions, one may expect similar effects in TiS_2.[11] We have located only one paper that appears to be primarly concerned with the phase transition of TiS_2.[12] However, no quantitative data is presented. As the above may suggest, TiS_2 is a well studied and interesting substance, but to date no strong evidence for a phase transition has been uncovered.

REFERENCES (TiS_2)

1. G.A. Wieger and F. Jellinek, J. Solid State Chem. 1, 519 (1970).
2. L.E. Conroy and K.C. Park, Inorg. Chem. 7, 459 (1968).
3. J. Bernard and Y. Jeannin, Adv. Chem. Ser. 39, 191 (1963).
4. A.H. Thompson, et.al., Phys. Rev. Lett. 29, 163 (1972).
5. C.A. Kukklonen, et.al., Phys. Rev. B24, 1691 (1981).
6. P.C. Klipstein, et.al., J. Phys. C, 14, 4067 (1981).
7. H.W. Myron and A.J. Freeman, Phys. Rev. B9, 481 (1974).
8. D. Fischer, Phys. Rev. B8, 3576 (1973).
9. C. Lucovsky, et.al., Solid State Commun., 19, 303 (1976).
10. P.B. Perry, Phys. Rev. B13, 5211 (1976).
11. M.J. Katz, et.al., Phys. Rev. Lett., 15, 828 (1965).
12. A.P. Silin, Sov. Phys. Solid State, 20, 1963 (1978).

$ZrSe_3$
Zirconium Triselenide

$ZrSe_3$ is a transition metal trichalcogenide with a structure that can be regarded as a series of one-dimensional chains.[1] The unit cells are monoclinic. Figure 1 shows the unit cell dimensions of $ZrSe_3$. For the unit cell the various spacings are: a = 5.41Å, b = 3.77Å, c = 9.45Å, and $\beta = 97.5°$. The intrachain Zr-Se distance is 2.74Å while the interchain Zr-Se distance is 2.87Å. The structural unit is an irregular trigonal prism with its axis along the b direction. Consideration of the interchain distance implies that Van der Waals bonding is not as apparent as for the transition metal dichalcogenides, although easy cleavage planes exist parallel to the direction of the chains.[2] $ZrSe_3$ possesses a slightly different structure than $ZrTe_3$.[3] Single crystals of $ZrSe_3$, can be grown via the vapor transport method with iodine as the transport agent. The crystals are generally grown at high temperatures (in excess of 600°C). $ZrSe_3$ has a monoclinic unit cell; stoichiometry of better than 10% can be typically achieved.

Figure 2 shows the polarization dependent reflectivity for $ZrSe_3$. Note that there is a very slight difference between the 77°K and room temperature measurements - this is most likely due to the distortion of the lattice with temperature. Fairly broad exciton structure is evident near 2eV. There is no evidence for a significant phase transition in this material.

REFERENCES ($ZrSe_3$)

1. W. Kröert and K. Plieth, Z. Anorg. Allg. Chem., 336, 207 (1965).
2. S. Bayliss and W. Liang, J. Phys. C,, submitted for pub. (1982).
3. S. Bayliss and W. Liang, J. Phys. C.,14 L803 (1981).

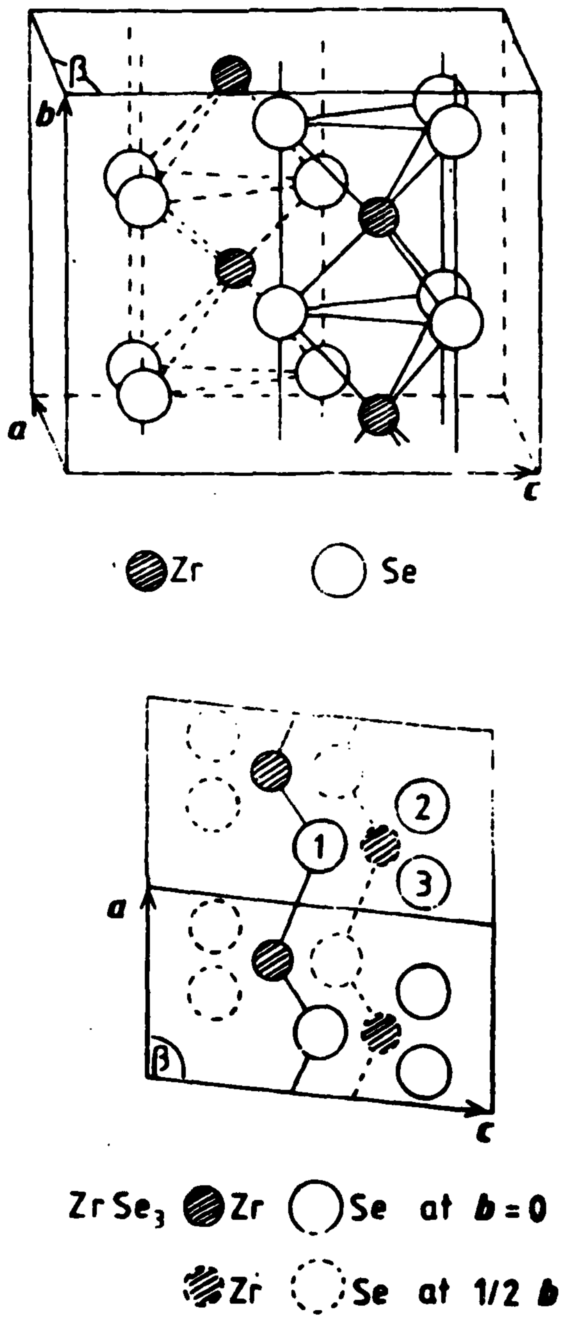

Figure 1 - Schematic structural diagram of ZrSe$_3$

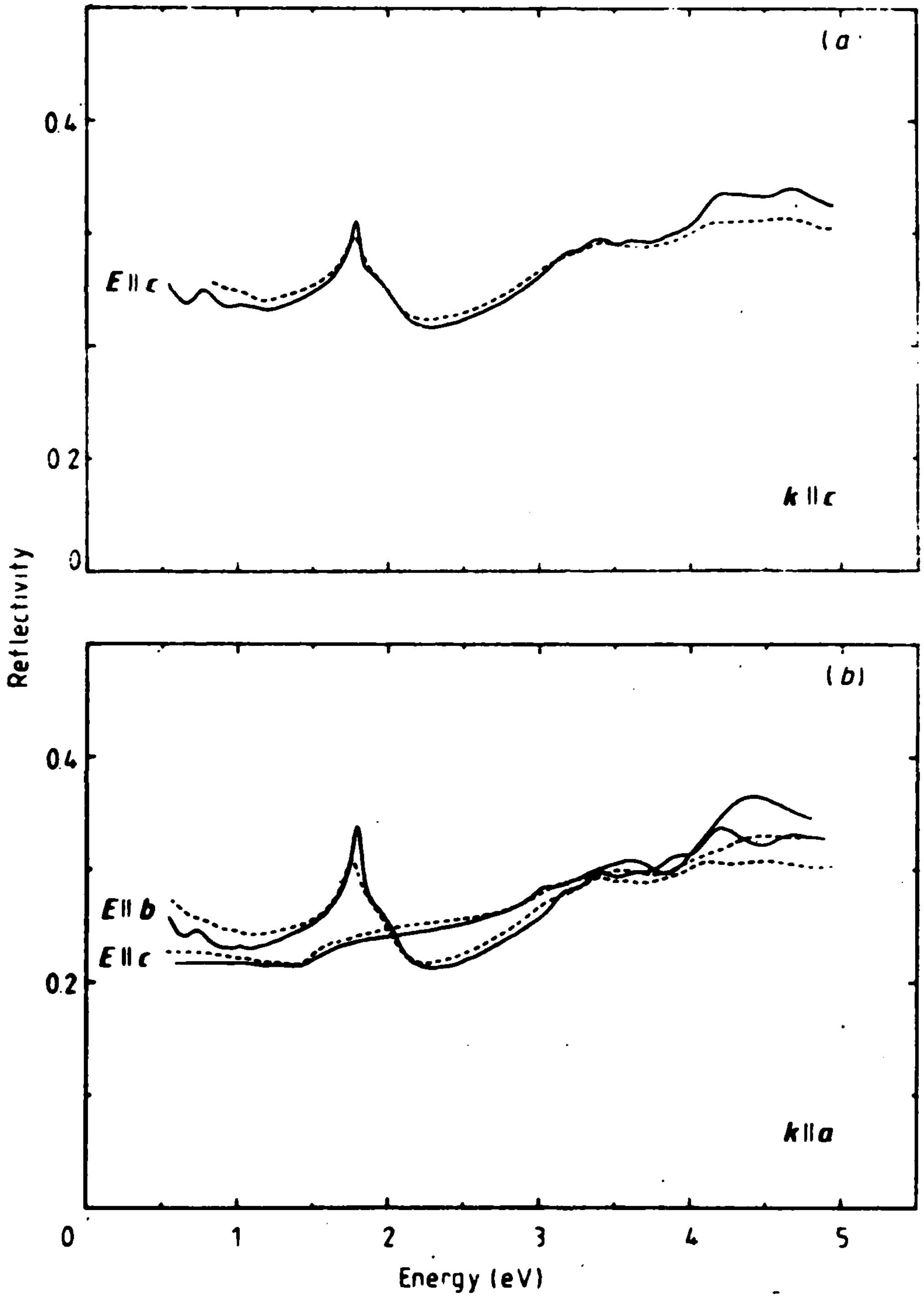

Figure 2 - Reflectivity of $ZrSe_3$. Full curves, 77K; broken curves, room temperature.

THE TACTICAL WEAPON GUIDANCE AND CONTROL INFORMATION ANALYSIS CENTER (GACIAC)

GACIAC is a DoD Information Analysis Center operated by IIT Research Institute under the technical sponsorship of the Joint Service Guidance and Control Committee with members for OUSDRE, Army, Navy, Air Force, and DARPA. The U.S. Army Missile Command provides the Contracting Officer's Technical Representative. Its mission is to assist the tactical weapon guidance and control community by encouraging and facilitating the exchange and dissemination of technical data and information for the purpose of effecting coordination of research, exploratory development, and advanced technology demonstrations. To accomplish this, GACIAC's functions are to:

1. *Develop a machine-readable bibliographic data base--currently containing over 30,000 entries;*
2. *Collect, review, and store pertinent documents in its field of interest--the library contains over 9,000 reports;*
3. *Analyze, appraise and summarize information and data on selected subjects;*
4. *Disseminate information through the GACIAC Bulletin, bibliographies, state-of-the-art summaries, technology assessments, handbooks, special reports, and conferences;*
5. *Respond to technical inquiries related to tactical weapon guidance and control; and*
6. *Provide technical and administrative support to the Joint Service Guidance and Control Committee (JSGCC).*

The products and services of GACIAC are available to qualified industrial users through a subscription plan or individual sales. Government personnel are eligible for products and services under block funding provided by the Army, Navy, Air Force and DARPA. A written request on government stationery is required to receive all the products as a government subscriber.

Further information regarding GACIAC services, products, participation plan, or additional copies of this Handbook may be obtained by writing or calling: GACIAC, IIT Research Institute, 10 West 35th Street, Chicago, Illinois 60616, Area Code 312, 567-4519 or 567-4544.